

**Universität
Rostock**



Traditio et Innovatio

Department of Waste and Resource Management

Rostock University

**Generation of biogenic silica from biomass residues
for sustainable industrial material applications**

Cumulative Dissertation

Submitted in the fulfilment of the requirements of

The Academic Board of Rostock University

Faculty of Agriculture and Environmental Sciences

For the Degree of DOCTOR of Engineering (Dr.-Ing.)

M. Eng. Clement Owusu Prempeh

Born in Kumasi, Ghana

Rostock, 2024

https://doi.org/10.18453/rosdok_id00004559

Reviewers:

Prof. Dr. mont. Michael Nelles, Universität Rostock, Germany

Prof. Dr. John Babafemi, Stellenbosch University, South Africa

Dr. Ing. Volker Lenz, Deutsches Biomasseforschungszentrum gGmbH, Germany

Submission Date: 08.09.2023

Defense Date: 26.01.2024

You cannot protect the environment unless you empower people, inform them, and help them understand that these resources are their own and that they must protect them.

-Wangari Maathai

Dedicated to God, my family, mentors, friends and Katharina

Declaration of Independency

I affirm that I have authored this dissertation without any external assistance and no portion of the work referred to in the thesis has been submitted in support of an application for another degree or qualification of this or any other university or other institute of learning. I have cited all the resources used in this work and appropriately acknowledged any quotes or content borrowed from other works.

Clement Owusu Prempeh

Rostock,

Executive Summary

The heightened demand for sustainable energy and materials has grown considerably worldwide owing to apprehensions about climate change and the exhaustion of non-renewable resources. In this regard, there is a burgeoning interest in using biomass residues from agricultural food production as a renewable energy source and a means to generate value-added materials. Biomass residues, such as cornhusks, corncobs, yam peelings, cassava peelings, and coconut husks, which are widely available in Africa, can be utilized to produce amorphous biogenic silica (SiO_2) for potential applications in industrial and scientific areas such as catalysis, glass making, ceramics, pharmaceuticals, plastics, and refractories.

Conventionally, silica is synthesized from non-renewable sources such as quartz and sand. However, due to the exhaustion and scarcity of these resources, researchers have been exploring alternative methods for synthesizing silica. Additionally, the industrial synthesis of synthetic amorphous silica via phase-separated sodium borosilicate glass precursors is often characterized by significant environmental impacts, including CO_2 and NO_x emissions, deviating from sustainability and environmental protection. One promising approach is silica extraction from agricultural biogenic residues via a thermochemical conversion route. This innovative approach transforms agricultural residues into useful materials, such as biogenic silica, for advanced applications, improving the efficiency of the entire biomass supply chain and promoting climate neutrality.

This PhD dissertation investigates the extraction and characterization of biogenic silica from locally available raw in Africa materials (cornhusk, corncob, yam peelings, cassava peelings, and coconut husks) containing high silicon content for advanced material applications. The dissertation consists of three separate investigations that examined the synthesis and characterization of biogenic silica from biomass residues using generalized, low-cost, sustainable, and environmentally benign procedures. The study also evaluated the practical application of synthesized biogenic silica as catalyst support for catalytic nanoparticles employed in methane combustion operations.

The first study explored the mechanisms of mesoporous biogenic silica generation from selected biomass fuels using a two-stage silica extraction process. In the first stage, the raw materials were chemically pretreated in citric acid solutions at two concentrations (1 and

5% w/v). In the second stage, the pretreated biomass residues were combusted at 600 °C for 2 h to obtain silica-rich ash. The ashes from the combustion process were characterized using various analytic characterizations to evaluate their SiO₂ contents, crystalline phases, and porosities. Inductively coupled plasma-optical emission spectrometry (ICP-OES) results revealed that the SiO₂ content in the generated ashes varies between 42.2 to 81.5 wt.% db and 53.4 to 90.8 wt.% db after acidic pretreatment with 1 and 5 w/v% acid, respectively. Additionally, X-ray diffraction (XRD) analysis revealed dominant crystalline phases of arcanite (K₂SO₄), sylvite (KCl) and calcite (CaCO₃) in ashes of the biomass fuels pretreated with 1 w/v% citric acid due to the presence of impurities¹ such as K₂O and CaO which could limit wide industrial applications. Conversely, the 5 w/v% citric acid pretreatment produced amorphous biogenic silica in the corn husk, with a specific surface area and pore volume of 91 m²/g and 0.21 cm³/g, respectively. The results of this study highlighted a significant end-value to these residues by the extraction of high-quality amorphous silica. However, further improvement of the physicochemical properties of the extracted silica was required before considering it for advanced applications such as catalyst support.

The second study developed processes for modifying and enhancing the physicochemical properties of the biogenic silica obtained in the first study by employing a novel sol-gel polymeric process. This process allowed for the ‘engineering’ of high-quality biogenic silica with improved textural properties compared to the original material. In the sol-gel method, the unmodified ash was dissolved in NaOH to form sodium silicate, which was subsequently hydrolyzed with citric acid to produce a silica xerogel. The engineered silica xerogel was extensively characterized using various techniques to determine their elemental constituents, functional groups, crystalline phases, thermal stability, and porosity. The study revealed that the synthesized silica xerogel exhibited higher specific surface areas and mesopore volumes of 384 m²/g and 0.35 cm³/g, respectively, compared to the unmodified silica ash. Additionally, there was a complete transformation of the pore network structures of the unmodified ash from monomodal to bimodal pore systems, with micro- and mesopore peaks centered around 1.5 and 3.8 nm, respectively. These findings indicate that the synthesized porous silica xerogel possesses the necessary properties to serve as a substrate or support system for anchoring metal oxides during catalytic operations.

¹ In this thesis, "impurities" refer to all ash-forming elements (typically metal ions), excluding Si.

Finally, the practical application of the synthesized sol-gel-derived cornhusk biogenic silica as catalyst support was examined for low-temperature catalytic methane combustion (LTCMC) operations in the third study. The cornhusk support synthesized from the sol-gel process was impregnated with palladium and cerium oxide (Pd/CeO₂) via the classical incipient wetness method. The resulting catalyst was characterized using various techniques to determine its catalytic performance for methane combustion and was compared with that of a commercial catalyst. The results showed that the Pd/CeO₂ dispersed on SiO₂ from the cornhusk ash support (Pd/CeO₂/CHSiO₂) catalyst exhibited excellent catalytic activity for methane combustion, with a lower conversion temperature than that of the commercial silica catalyst (Pd/CeO₂/commercial). Moreover, the Pd/CeO₂/CHSiO₂ catalyst displayed higher catalytic stability after 10 h on stream, with a 7 percentage points of marginal loss in catalytic activity compared with 11 percentage points recorded for the Pd/CeO₂/commercial catalyst. The N₂ physisorption and hydrogen temperature-programmed reduction (H₂-TPR) results indicated that the cornhusk SiO₂ support possessed a higher surface area and reducibility than the synthesized commercial catalyst, contributing to the enhanced catalytic activity of the Pd/CeO₂/SiO₂ catalyst. Overall, the SiO₂ generated from cornhusk ash exhibited promising potential as a low-cost and environmentally friendly support for LTCMC catalysts.

The findings in this dissertation hold considerable significance for incorporating agricultural residues in catalytic operations and developing sustainable materials. More importantly, this study sheds light on the potential of biomass residues as valuable resources and offers insights into sustainable solutions for their utilization in Africa and beyond.

Zusammenfassung

Die gestiegene Nachfrage nach nachhaltiger Energie und Materialien hat weltweit aufgrund von Bedenken bezüglich des Klimawandels und der Erschöpfung nicht erneuerbarer Ressourcen erheblich zugenommen. In diesem Zusammenhang besteht ein wachsendes Interesse an der Verwendung von Biomasse-Reststoffen aus der landwirtschaftlichen Lebensmittelproduktion als erneuerbare Energiequelle und als Rohstoff zur Erzeugung von Wertstoffen. Biomasse-Reststoffe wie Maisblätter, Maiskolben, Yamschalen, Maniokschalen und Kokosnusshülsen, die in Afrika weit verbreitet sind, können zur Herstellung von amorphem biogenem Siliziumdioxid (SiO_2) für potenzielle Anwendungen in industriellen und wissenschaftlichen Bereichen wie Katalyse, Glasherstellung, Keramik, Pharmazie, Kunststoffe und Feuerfestprodukte verwendet werden.

Herkömmlicherweise wird Siliziumdioxid aus nicht erneuerbaren Quellen wie Quarz und Sand hergestellt. Aufgrund der Erschöpfung und Knappheit dieser Ressourcen erforschen Wissenschaftende jedoch alternative Methoden zur Siliziumdioxidherstellung. Darüber hinaus ist die industrielle Synthese von synthetischem amorphem Siliziumdioxid über phasentrennte Natriumborosilikatglasvorläufer häufig mit erheblichen Umweltauswirkungen verbunden, einschließlich CO_2 - und NO_x -Emissionen, wodurch Ziele der Nachhaltigkeit und des Umweltschutzes nicht erreicht werden können. Ein vielversprechender Ansatz ist die Siliziumdioxidextraktion aus landwirtschaftlichen biogenen Reststoffen über einen thermochemischen Umwandlungsweg. Dieser innovative Ansatz wandelt landwirtschaftliche Reststoffe in nützliche Materialien wie biogenes Siliziumdioxid für technische Anwendungen um, verbessert die Effizienz der gesamten Biomasse-Wertschöpfungskette und fördert die Klimaneutralität.

Diese Doktorarbeit untersucht die Extraktion und Charakterisierung von biogenem Siliziumdioxid aus lokal verfügbaren Rohstoffen in Afrika (Maisblätter, Maiskolben, Yamschalen, Maniokschalen und Kokosnusshülsen), die einen hohen Siliziumgehalt für fortschrittliche Materialanwendungen aufweisen. Die Dissertation besteht aus drei Teilen, welche die Synthese und Charakterisierung von biogenem Siliziumdioxid aus Biomasse-Reststoffen unter Verwendung von verallgemeinerten, kostengünstigen, nachhaltigen und umweltfreundlichen Verfahren untersuchten. Die Forschungsarbeit evaluierte auch die

praktische Anwendung des synthetisierten biogenen Siliziumdioxids als Katalysatorträger für metalloxidische Nanopartikel, die bei Methanverbrennungsprozessen eingesetzt werden.

Der erste Teil behandelt die Mechanismen der Generierung von mesoporösem biogenen Siliziumdioxid aus ausgewählten Biomassebrennstoffen unter Verwendung eines zweistufigen Siliziumextraktionsprozesses. In der ersten Aufbereitungsstufe wurden die Rohstoffe chemisch in Zitronensäurelösungen bei zwei Konzentrationen (1 und 5 %) behandelt. In der zweiten Aufbereitungsstufe wurden die behandelten Biomasse-Reststoffe bei 600 °C für 2 Stunden verbrannt, um siliziumdioxidreiche Asche zu erhalten. Die Aschen aus dem Verbrennungsprozess wurden mit verschiedenen analytischen Methoden charakterisiert, um den SiO₂-Gehalt, die kristallinen Phasen und die Porositäten zu ermitteln. Die Ergebnisse der Untersuchungen mittels induktiv gekoppelter Emissionsspektrometrie (ICP-OES) zeigten, dass der SiO₂-Gehalt in den erzeugten Aschen je nach saurer Vorbehandlung mit 1 und 5 % Säure zwischen 42,2 bis 81,5 Ma.-% (trocken) bzw. 53,4 bis 90,8 Ma.-% db variierte. Zusätzlich zeigte die Röntgenbeugungsanalyse (XRD) dominante kristalline Phasen von Arcanit (K₂SO₄), Sylvit (KCl) und Calcit (CaCO₃) in Aschen von Biomassebrennstoffen, die mit 1 % Zitronensäure vorbehandelt wurden. Dies resultiert aus Verunreinigungen¹ wie K₂O und CaO, welche die breite industrielle Anwendung begrenzen könnten. Im Gegensatz dazu produzierte die 5 % Zitronensäurevorbehandlung amorphes biogenes Siliziumdioxid aus Maisschalen mit einer spezifischen Oberfläche und einem Porenvolumen von 91 m²/g bzw. 0,21 cm³/g. Die Ergebnisse dieser Studie zeigen, dass aus diesen Reststoffen durch Extraktion hochwertiges amorphes Siliziumdioxid gewonnen werden kann. Allerdings waren weitere Verbesserungen der physikalisch-chemischen Eigenschaften des extrahierten Siliziumdioxids erforderlich, bevor es für hochwertige Anwendungen wie Katalysatoren in Betracht gezogen werden konnte.

Die zweite Teilarbeit beinhaltete die Entwicklung eines Verfahrens zur Modifizierung und Verbesserung der physikalisch-chemischen Eigenschaften des im ersten Studienteil gewonnenen biogenen Siliziumdioxids unter Verwendung eines neuartigen Sol-Gel-Polymerprozesses. Dieser Prozess ermöglichte die Herstellung von hochwertigem biogenen Siliziumdioxids mit verbesserten texturalen Eigenschaften im Vergleich zum Originalmaterial. In der Sol-Gel-Methode wurde die unmodifizierte Asche in NaOH gelöst, um Natriumsilikat zu bilden, das anschließend mit Zitronensäure hydrolysiert wurde, um ein

¹ In dieser Dissertation bezieht sich der Begriff "Verunreinigungen" auf alle aschebildenden Elemente (typischerweise Metallionen), mit Ausnahme von Si.

Silizium-Xerogel zu produzieren. Das entwickelte Silizium-Xerogel wurde umfassend mit verschiedenen Techniken charakterisiert, um seine elementaren Bestandteile, funktionellen Gruppen, kristallinen Phasen, thermische Stabilität und Porosität zu bestimmen. Die Studie ergab, dass das synthetisierte Silizium-Xerogel im Vergleich zur unmodifizierten Siliziumdioxidasche höhere spezifische Oberflächen und Mesoporenvolumina von $384 \text{ m}^2/\text{g}$ bzw. $0,35 \text{ cm}^3/\text{g}$ aufwies. Darüber hinaus erfolgte eine vollständige Umwandlung der Porennetzwerkstrukturen der unmodifizierten Asche von monomodalen zu bimodalen Porensystemen mit Mikro- und Mesoporensitzen im Bereich von etwa 1,5 und 3,8 nm. Diese Ergebnisse deuten darauf hin, dass das synthetisierte poröse Silizium-Xerogel die notwendigen Eigenschaften besitzt, um als Trägersystem für Metalloxide bei katalytischen Anwendungen zu dienen.

Schließlich wurde in der dritten Studie die praktische Anwendung des synthetisierten Siliziumdioxids als Katalysatorträger für die katalytische Methanverbrennung bei Niedertemperatur (LTCMC) untersucht. Der durch den Sol-Gel-Prozess gewonnene Katalysatorträger wurde mit Palladium und Ceriumoxid (Pd/CeO_2) über die klassische Methode der Incipient Wetness-Beschichtung imprägniert. Der resultierende Katalysator wurde mit verschiedenen Techniken charakterisiert, um seine katalytische Aktivität für die Methanverbrennung zu bestimmen und mit der eines kommerziellen Katalysators zu vergleichen. Die Ergebnisse zeigten, dass der auf SiO_2 aus Maisschalenasche dispergierte $\text{Pd}/\text{CeO}_2/\text{CHSiO}_2$ -Katalysator eine ausgezeichnete katalytische Aktivität für die Methanverbrennung aufwies und eine niedrigere Umwandlungstemperatur als der kommerzielle Katalysator ($\text{Pd}/\text{CeO}_2/\text{commercial}$) zeigte. Darüber hinaus zeigte der $\text{Pd}/\text{CeO}_2/\text{CHSiO}_2$ -Katalysator nach 10 Stunden Betrieb mit einem geringen Verlust von 7 % eine höhere katalytische Stabilität. Im Vergleich dazu betrug der Verlust 11 % des $\text{Pd}/\text{CeO}_2/\text{commercial}$ -Katalysators. Die N_2 -Physisorption und die Ergebnisse der Wasserstoff-Temperaturprogramm-Reduktion (H_2 -TPR) deuteten darauf hin, dass der Katalysator auf SiO_2 -Träger aus Maisschalen eine höhere Oberfläche und Reduzierbarkeit besaß als der synthetisierte kommerzielle Katalysator, was zur verbesserten katalytischen Aktivität des $\text{Pd}/\text{CeO}_2/\text{SiO}_2$ -Katalysators beitrug. Insgesamt zeigte das aus Maisschalenasche gewonnene SiO_2 vielversprechendes Potenzial als kostengünstiger und umweltfreundlicher Träger für LTCMC-Katalysatoren.

Die Erkenntnisse dieser Dissertation sind von erheblicher Bedeutung für die Integration landwirtschaftlicher Reststoffe in katalytische Prozesse und die Entwicklung

nachhaltiger Materialien. Vor allem gibt diese Studie Einblicke in das Potenzial von Biomasse-Reststoffen als wertvolle Ressourcen und bietet Einblicke in nachhaltige Lösungen für ihre Nutzung in Afrika und darüber hinaus.

Table of Contents

Declaration of Independency	i
Executive Summary	ii
Zusammenfassung.....	v
Table of Contents	ix
Acknowledgements	xiii
List of Publications	xv
List of Tables.....	xvii
List of Figures	xviii
Nomenclature	xx
List of Symbols	xxiv
Chapter 1	1
1 Introduction	1
1.1 Background	1
1.2 Motivation for the Study	3
1.3 Research Aim, Objectives and Approach	5
1.4 Structure of the Dissertation	7
CHAPTER 2	8
2 Literature review	8
2.1 Biomass Conversion Processes	8
2.2 Structure and Composition of Biomass	9
2.3 Extraction of Silica from Biomass and Effects of Process Parameters.....	11
2.4 Modification and Improvement of the Textural Properties of Biogenic Silica....	15
2.5 Catalyst and Catalyst Support System	17
2.5.1 Catalyst.....	17
2.5.2 Catalyst support.....	18
2.5.3 Catalyst deactivation in catalytic converters.....	19

2.6	Methane Emissions and Combustion Processes	21
2.6.1	Methane emissions	21
2.6.2	Mechanism of low-temperature catalytic methane combustion.....	22
2.7	Summary of Literature, Recommendations and Future Perspectives	24
CHAPTER 3		27
3	Methodology	27
3.1	Fuels	27
3.2	Acid Leaching	27
3.3	Combustion Processes.....	27
3.4	Textural Improvement and Modification of the Biogenic Silica	28
3.5	Synthesis of Supported Catalysts	28
3.6	Catalytic Activity Tests for Methane Combustion.....	29
3.7	Analysis of Physical and Chemical Properties of Fuels, Ashes and Catalysts	30
References of Chapters 1-3		34
CHAPTER 4		51
4	Extraction and Characterization of Biogenic Silica Obtained from Selected Agro-Waste in Africa.	51
Published Research Article I.....		51
Abstract		54
4.1	Introduction	55
4.2	Materials and Methods	59
4.2.1	Material used and sample preparation.....	59
4.2.2	Analysis of physical and chemical properties	60
4.2.3	Thermal analysis of biomass fuels	61
4.3	Results and Discussion.....	61
4.3.1	Solid fuel analysis	61
4.3.2	TGA analysis of biomass fuels	63
4.3.3	FTIR analysis	65

4.4	Ash Analysis	68
4.4.1	Impact of the pretreatment process on the chemical composition of the inorganic fraction of biomass fuels	68
4.5	Comparative Study of Physical Morphology, Textural Properties, and Phase Analysis of Ashes.....	71
4.5.1	Physical morphology of ashes from untreated and acid-treated biomass	71
4.5.2	Nitrogen gas adsorption-desorption measurements	73
4.5.3	Phase analysis of the biomass ash samples	75
4.6	Conclusions	79
	References of Chapter 4	80
	CHAPTER 5	93
5	An Improved Method for The Production of Biogenic Silica from Cornhusk Using Sol-Gel Polymeric Route	93
	Published Research Article II.....	93
	Abstract	96
5.1	Introduction	97
5.2	Materials and Method	100
5.2.1	Ash preparation	100
5.2.2	Synthesis of silica xerogel.....	101
5.2.3	Analysis of physical and chemical properties	102
5.3	Results and Discussion.....	103
5.3.1	Characterizations of unmodified ash and silica xerogel	103
5.3.2	Influence of the sol-gel polymeric route on the textural properties	107
5.4	Conclusions	112
	References of Chapter 5	112
	CHAPTER 6	120
6	Comparative Study of Commercial Silica and Sol-Gel-Derived Porous Silica from Cornhusk for Low-Temperature Catalytic Methane Combustion	120

Published research Article III.....	120
Abstract	123
6.1 Introduction	124
6.2 Materials and Methods	127
6.2.1 Materials.....	127
6.2.2 Preparation of sol–gel-derived cornhusk support	128
6.2.3 Preparation of supported catalysts	128
6.2.4 Characterization techniques	129
6.2.5 Catalytic activity tests for methane combustion	130
6.3 Results and Discussion.....	131
6.3.1 Structure and properties of synthesized catalysts.....	131
6.3.2 Methane catalytic combustion tests in dry and wet conditions over as-synthesized samples	139
6.3.3 Kinetic studies.....	141
6.3.4 Long-term catalytic tests	144
6.4 Conclusions	145
References of Chapter 6	146
Chapter 7	155
7 Summary, Conclusions, and Future Work	155
Appendix A: Supplementary Data	159
Appendix B: Procedures and Standards	166
Appendix B: Curriculum Vitae	168

Acknowledgements

I would like to express my heartfelt gratitude to all those who have played a significant role in making this thesis possible:

First and foremost, I am deeply thankful to God for His grace and kindness, without which this thesis would not have been conceivable. His unwavering support has been a source of strength and inspiration throughout this journey.

To my esteemed advisors, Prof. Dr. Michael Nelles, Prof. Dr. Ingo Hartmann, and Dr. Steffi Formann, I extend my sincerest appreciation for their unwavering guidance, support, and encouragement throughout my PhD journey. Your profound knowledge and constant feedback have been invaluable in shaping the direction and scope of this thesis. I am truly grateful for your mentorship, patience, and dedication to my academic and personal growth.

I would also like to express my gratitude to my colleagues and friends at the DBFZ, Dr. Hossein Beidaghy, Katharina Görtz, Manfred Eiden, Thomas Schliermann, Daniela Pomsel, Mario König, René Bindig, Dr. Mirjam Müller, Dr. Bettina Stolze, Dr. Konstantin Wink, Dr. Volker Lenz, Dr. Dennis Krüger, Dr. Özge Mutlu, Virginie Bellman, Lukas Richter and Rafiandy Putra at the Thermochemical Department of DBFZ. Your camaraderie, support, and constructive discussions have played a pivotal role in improving the quality of this thesis and shaping my intellectual ideas.

A special word of appreciation to the DBFZ Technical and Analytical team for their exceptional patience and support throughout the sample analyses during this study. I extend my heartfelt thanks to Kehinde Bamgboye, Ralf Schoch, Marc Bohnet, Igor Adolf, Christoph Kröhl, Raphael Duerrse, and Jan Kossack for their commitment to the analyses of the biomass fuels, which was crucial to the success of this study. I would like to acknowledge the contributions of Dr. Sebastian Wohlrab and his esteemed team of scientists at the Leibniz Institute for Catalysis, Rostock, who helped make a significant part of this thesis possible. I am grateful for the unwavering support and welcoming hospitality during my multiple visits to your research institution.

To my cherished Ghanaian community and dear friends beyond the confines of my research environment, I want to extend my sincere gratitude. Your dedication to organizing delightful social events has been nothing short of priceless, providing a much-needed respite and preserving my sanity amid the challenges of this journey. I am incredibly thankful to my dear friends, Joana Serwaa Ampofo, Mavis Opoku Agyemang, Henry Reynolds Enninful,

Diana Addae, Regina Christina Andoh, and Emin Açikkalp for their unwavering camaraderie and uplifting encouragement throughout this remarkable odyssey. Your presence infused each step with joy, making the highs brighter and the lows easier to bear.

To my dear Katharina, the Görtz family and Martin Burgartz, I want to express my heartfelt appreciation for being a pillar of strength and a beacon of unwavering support. Your presence made this expedition unforgettable, and I am truly grateful for your constant encouragement and love.

Last but certainly not least, I extend my deepest thanks to my parents, Mr. Clifford Owusu Prempeh and Mrs. Georgina Appiah, siblings, the German Federal Ministry of Food and Agriculture (BMEL) for their financial support and the entire team at DBFZ. Your unwavering commitment to providing an exceptional academic environment, abundant resources, and state-of-the-art facilities has been instrumental in empowering me to pursue my academic aspirations and successfully complete this thesis. I am deeply grateful for the opportunities you have bestowed upon me, which have been pivotal in shaping my academic growth and achievements. I stand proudly at the threshold of a new chapter in my academic and personal journey, ready to embrace the challenges and accomplishments that lie ahead. Thank you all for being an integral part of this significant milestone in my life.

List of Publications

Journal publications:

1. Owusu Prempeh, C.; Formann, S.; Schliermann, T.; Dizaji, H.B.; Nelles, M. Extraction and Characterization of Biogenic Silica Obtained from Selected Agro-Waste in Africa. *Appl. Sci.* 2021, 11, 10363. <https://doi.org/10.3390/app112110363>.
2. Owusu Prempeh, C., Formann, S., Hartmann, I. and Michael Nelles. An improved method for the production of biogenic silica from cornhusk using sol–gel polymeric route. *Biomass Conv. Bioref.* (2022). <https://doi.org/10.1007/s13399-022-03615-6>.
3. Owusu Prempeh, C.; Hartmann, I.; Formann, S.; Eiden, M.; Neubauer, K.; Atia, H.; Wotzka, A.; Wohlrab, S.; Nelles, M. Comparative Study of Commercial Silica and Sol-Gel-Derived Porous Silica from Cornhusk for Low-Temperature Catalytic Methane Combustion. *Nanomaterials* 2023, 13, 1450. <https://doi.org/10.3390/nano13091450>.

Presentations and conferences:

1. Owusu Prempeh, C. (2021). Generation of Silicon dioxide (silica) from agricultural residues for advanced applications. Presentation: BMEL Doctorate & Postdoc Meeting, [online], 09.02.2021.
2. Owusu Prempeh, C., (2021). The generation of a functional catalytic support system from silicon rich biomass residues for low-temperature methane oxidation operations. ASW-Doctoral Colloquium (2021), Universität Rostock, Rostock, 15.-16.07.2021.
3. Owusu Prempeh, C.; Formann, S.; Hartmann, I.; Nelles, M. (2021). Generation of Silicon Dioxide from Biomass for Industrial Applications. Poster presentation: 4th Doctoral Colloquium Bioenergy, Karlsruhe, 13.-14.09.2021.
4. Hartmann, I.; Formann, S.; Müller, M.; Schliermann, T.; Owusu Prempeh, C.; Bindig, R. (2021). Porous SiO₂ generated from solid biomass combustion as a suitable support for catalyst: biosilica. Presentation: 2nd Workshop Solid Fuels Task in preparation for the 43rd Task Leaders Meeting (TLM), [online], 13.09.2021.
5. Hartmann, I.; Formann, S.; Müller, M.; Schliermann, T.; Owusu Prempeh, C.; Bindig, R. (2021). Low-emission combustion of silicon-rich biogenic residues for the coupled generation of materials and energy. Presentation: EERA Bioenergy SP4 Workshop "Stationary Bioenergy", [online], 16.11.2021.

6. Owusu Prempeh, C., Generation of Silicon dioxide (silica) from agricultural residues for advanced applications: PhD Progress. Presentation: ASW-Doctoral Colloquium (2022), Universität Rostock, Rostock, 07.-08.07.2022.
7. Owusu Prempeh, C.; Formann, S.; Schliermann, T.; Beidaghy Dizaji, H.; Nelles, M. (2022). Extraction and Characterization of Biogenic Silica Obtained from Selected Agro-Waste in Africa. Presentation: 5th Doctoral Colloquium Bioenergy, Leipzig, 13.-14.09.2022.
8. Formann, S.; Schliermann, T.; Owusu Prempeh, C.; Hartmann, I. (2022). Combined substantial and energetic use of biomass in closed-loop systems of elements in the air-soil-organism interface: 20th Symposium on remediation "Jenaer Sanierungskolloquium", Presentation, Jena, 29.-30.09.2022.
9. Owusu Prempeh, C., Formann S, Hartmann I, Nelles M. An improved method for the production of biogenic silica from cornhusk using sol-gel polymeric route. Poster presentation – 7th Mitteleuropäische Biomassekonferenz CEBC 2023, 18. - 20.01.2023, Messe Congress Graz, Austria.
10. Owusu Prempeh, C., Hartmann I, Formann S, Neubauer K, Atia H, Wohlrab S, Nelles M. Low-temperature catalytic methane combustion using Pd/CeO₂ dispersed on Sol-gel-derived cornhusk support, Poster presentation: 12th DGAW-Wissenschaftskongress 08.03.2023, Technische Universität (TU) Hamburg.
11. Owusu Prempeh C., Hartmann I, Formann S, Neubauer K, Atia H, Wohlrab S, Nelles M. Generation of Silicon dioxide (silica) from agricultural residues for Low-temperature catalytic methane combustion, Poster presentation: 31st European Biomass Conference and Exhibition, 05-08.06.2023, Bologna.
12. Owusu Prempeh C., Hartmann I, Formann S, Nelles M. Generation of biogenic silica from biomass residues for sustainable industrial material applications, Presentation: International Conference on Circular Economy, Renewable Energies and Green Hydrogen in Africa. 18-21.08.2023, Kumasi, Ghana.

List of Tables

Table 2.1. Comparison of the major thermochemical conversion processes.	9
Table 3.1. Summary of analysis methods employed in Articles I-III	33
Table 4.1. Potential of crop residues in Ghana.	57
Table 4.2. Fuel and fuel ash properties of untreated (U) and acid leached (L), cassava (CasP), yam (YamP), coconut (CocH), corncob (CorC) and corn husk (CorH).	62
Table 4.3. The main functional groups of the three main components of the biomass fuels and the ashes produced at 600 °C during combustion characterized by FTIR.....	67
Table 4.4. Comparison of the structural characteristics (S_{BET} and pore volume V_p) of ashes.	74
Table 4.5. Crystalline phases identified with XRD in the ash samples after the combustion of 1 w/v% acid-treated biomass fuels at 600 °C.....	78
Table 5.1. Reported Fuel ash composition of selected biomass fuels.....	99
Table 5.2. Chemical compositions of corn husk ashes prepared by different extraction methods	104
Table 5.3. Textural properties of biogenic silica derived from cornhusk before (unmodified ash) and after sol-gel transformation (silica xerogel).	107
Table 6.1. Elemental compositions of catalyst samples measured by ICP-OES analysis (oxygen neglected).	131
Table 6.2. Textural properties of the silica support and synthesized catalysts.	136

List of Figures

Figure 1.1. Outline and novel contribution of work packages.....	7
Figure 2.1. Effects of chemical fuel-pretreatment on the structure of lignocellulosic biomass.	10
Figure 2.2. Schematic of the silica network modifications by the metal (M: Na ⁺ , K ⁺ , Ca ²⁺ , Mg ²⁺) cations.....	13
Figure 2.3. Catalytic methane lean combustion proceeding according to the Mars-van Krevelen (MvK) mechanism.....	23
Figure 3.1. Experimental set-up for methane catalytic activity.	29
Figure 4.1. Extraction of biogenic silica from agricultural biomass residues to produce silica- rich ash.	59
Figure 4.2. TG (black curve and y-axis on the left side) and DTG (red curve and y-axis on the right side) profiles of untreated (a) cassava, (b) yam, (c) coconut, (d) corncob, and (e) cornhusk.	63
Figure 4.3. The evolution of the main functional groups in raw biomass (upper) and ashes of 1 w/v% biomass fuels (bottom).	66
Figure 4.4. Chemical composition of the inorganic fraction (=100 wt.% db) of ashes obtained from the thermal treatment of the untreated and acid-leached samples with citric acid.....	68
Figure 4.5. Visual appearances of thermally produced ashes of the raw and the acid-leached biomass fuels at 600 °C.....	71
Figure 4.6. Adsorption–desorption isotherms of ashes from untreated and treated cornhusk.	73
Figure 4.7. X-ray diffraction pattern of the ash samples resulting from the combustion of 1 w/v% acid-treated biomass fuels at 600 °C.....	76
Figure 4.8. EDX spectrum (30kV) of the ash sample (wt.% db = 100) resulting from the combustion of CorH-A-1%.	77
Figure 4.9. Comparison of the FTIR patterns of CorH-A-1% and CorH-A-5% with commercially available silica.....	79
Figure 5.1. Flow diagram of the procedures used for the preparation of silica xerogel from unmodified ash.	101
Figure 5.2. Visual images of the direct thermochemical conversion and sol-gel products during the extraction of biogenic silica from cornhusk	105
Figure 5.3. FTIR spectrum of unmodified ash and synthesized silica xerogel cornhusk. .	106

Figure 5.4. N ₂ adsorption-desorption isotherms and pore size distribution of unmodified ash and modified silica xerogel.	108
Figure 5.5. Thermogravimetric profiles of unmodified ash and silica xerogel.....	110
Figure 5.6. XRD patterns of unmodified ash and extracted silica xerogel	111
Figure 6.1. SEM/EDX mapping and spatial distributions of the Pd and Ce nanoparticles on supports. (Top row): cornhusk support; (Bottom row): commercial silica supports.	132
Figure 6.2. SEM micrographs of synthesized catalysts prepared from cornhusk (a,c) and commercial (b,d) silica supports.	133
Figure 6.3. FTIR spectra of cornhusk support material, Pd/CeO ₂ /CHSiO ₂ , and Pd/CeO ₂ /commercial catalysts.	134
Figure 6.4. N ₂ adsorption and desorption isotherms of (a) cornhusk support and Pd/CeO ₂ /CHSiO ₂ ; (b) commercial support and Pd/CeO ₂ /commercial.	135
Figure 6.5. X-ray diffraction pattern for the synthesized Pd/CeO ₂ /CHSiO ₂ and Pd/CeO ₂ /commercial catalysts.	137
Figure 6.6. H ₂ -TPR profiles of Pd/CeO ₂ /CHSiO ₂ and Pd/CeO ₂ /commercial catalysts.	138
Figure 6.7. Light-off curves for CH ₄ combustion in stoichiometric conditions	140
Figure 6.8. Arrhenius plots over Pd/CeO ₂ /CHSiO ₂ and Pd/CeO ₂ /commercial catalysts at 600 °C. Conditions:.....	142
Figure 6.9. Methane conversion versus reaction time of the catalysts after reaction for 10 h.	144

Nomenclature

Abbreviations

Abbreviation	Description
AC	Ash content
AU	African Union
BET	Brunauer-Emmett-Teller
BJH	Barrett-Joyner-Halenda method
BO	Bridging oxygen
CA	Citric acid
CasP	Cassava peelings
CasP-A-1%	Ash of 1 w/v% acid-leached cassava peelings
CasP-A-5%	Ash of 5 w/v% acid-leached cassava peelings
CasP-U	Untreated cassava peelings
CasP-U-A	Ash of untreated cassava peelings
CocH	Coconut husk
CocH-1%	Coconut husk leached in 1 w/v% citric acid
CocH-A-1%	Ash of 1 w/v% acid-leached coconut husk
CocH-A-5%	Ash of 5 w/v% acid-leached coconut husk
CocH-U	Untreated coconut husk
CocH-U-A	Ash of untreated coconut husk
CorC	Corncob

Abbreviation	Description
CorC-1%	Corncob leached in 1 w/v% citric acid
CorC-A-1%	Ash of 1 w/v% acid-leached corncob
CorC-A-5%	Ash of 5 w/v% acid-leached corncob
CorC-U	Untreated corncob
CorC-U-A	Ash of untreated corncob
CorH	Cornhusk
CorH-1%	Cornhusk leached in 1 w/v% citric acid
CorH-A-1%	Ash of 1 w/v% acid-leached cornhusk
CorH-A-5%	Ash of 5 w/v% acid-leached cornhusk
CorH-U	Untreated cornhusk
CorH-U-A	Ash of untreated cornhusk
CPG	Controlled porous glass
CSR	Coherent scattering region
db	Dry basis
DFT	Density Functional Theory
DIN	Deutsches Institut für Normung
EA	Effective activation energy
EDX	Energy dispersive X-ray spectrometer
EU	European Union
FTIR	Fourier-transform infrared spectroscopy

Abbreviation	Description
H.V.	Heating value [MJ/kg]
H ₂ -TPR	Hydrogen temperature programmed reduction
ICP-OES	Inductively coupled plasma with optical emission spectrometer
ISO	International Organization for Standardization
IUPAC	International Union of Pure and Applied Chemistry
JRC	Joint research centre
LHV	Lower heating value
LOI	Loss on ignition [wt.% db]
LTCMC	Low-temperature catalytic methane combustion
M	Molarity of the solution,
MC	Moisture content
MFC	Mass flow controller
MvK	Mars-van Krevelen
n.d.	Not detected
PM _{2.5}	particulate matter that are 2.5 microns or less in diameter
PM ₁₀	particulate matter that are 10 microns in diameter
Pt	Platinum
PSD	Pore size distribution
RT	Room Temperature
SEM	Scanning electron microscope

Abbreviation	Description
Si	Silicon
STA	Simultaneous thermal analysis
TCD	Thermal conductivity detector
TEOS	Tetraethyl orthosilicate
TGA	Thermogravimetric analysis
TMO _x	Transition metal oxides
VM	Volatile matter
wb	Wet basis
WP	Work Package
wt. %	Weight percentage
XRD	X-ray diffraction
XRF	X-ray fluorescence spectrometer
YamP	Yam peelings
YamP-1%	Yam peelings leached in 1 w/v% citric acid
YamP-A-1%	Ash of 1 w/v% acid-leached yam peelings
YamP-A-5%	Ash of 5 w/v% acid-leached yam peelings
YamP-U	Untreated yam peelings
YamP-U-A	Ash of untreated yam peelings

List of Symbols

Symbol	Description
(w/v) %	Weight per volume percentage
(X_{CH_4}) %	Methane conversion percentage
A	Pre-exponential
$CH_{4,t=0}$	Initial moles or amount of methane
$CH_{4,t}$	Moles of methane at any time during the reaction
D_p	Pore size mode
E_A	Activation energy
$^{\circ}C$	Degrees Celsius
k	Rate constant
e	Natural logarithm (approximately 2.71828).
R	Gas constant (8.314 J/mol·K)
T	Temperature in Kelvin (K)
S_{BET}	Specific surface area
V_p	Pore volume
d_p	Pore width mode
V_{micro}	Micropore volume
S_{micro}	Micropore surface area
S_{ext}	External surface area

Chapter 1

1 Introduction

1.1 Background

The global energy sector, encompassing coal, oil, and natural gas emissions, is the second-largest source of anthropogenic methane (CH_4) emissions, accounting for approximately a quarter of all emissions (135 million tonnes of CH_4 emissions in 2022) [1]. Methane possesses 25 times more global warming potential than carbon dioxide (CO_2), and the release of unburned CH_4 into the environment contributes significantly to global warming [2]. In the context of energy resources, natural gas, primarily composed of CH_4 , is considered a cleaner-burning fossil fuel with several advantages over conventional fuels, including gasoline or diesel [3]. The higher knock resistance of methane makes it particularly more desirable for automotive applications to lower polluting emissions [4]. Its combustion for energy purposes yields lower CO_2 emissions and other harmful air pollutants, such as nitrogen oxides (NO_x), compared to traditional fossil fuels [5]. However, amid these favourable attributes, it is necessary to avoid the emission of unburned CH_4 due to its potent heat-trapping capabilities [2].

Although specific natural processes in soil, such as methanotrophy—where methane-consuming bacteria convert CH_4 into CO_2 —and a series of chemical reactions in the atmosphere aid in removing emitted CH_4 , it remains crucial to reduce all anthropogenic methane emissions to the atmosphere [6,7]. Of greater importance, innovative pathways that foster the advancement and adoption of renewable energy sources hold the promise of ushering in a cleaner energy future, thereby reducing dependence on fossil fuels [8]. Consequently, various strategies to mitigate CH_4 emissions have been proposed, from capturing and utilizing CH_4 to transforming emitted CH_4 into less potent gases, such as CO_2 [9,10].

However, due to the highly stable carbon-hydrogen (CH) bond in the CH_4 organic compound, the typical decomposition temperature for homogeneous combustion occurs at 1200 °C, resulting in high energy consumption and increased NO_x and particulate emissions [11]. Accordingly, achieving CH_4 combustion at elevated temperatures requires significant energy input [12]. These factors negatively affect operational efficiency and increase the cost of implementing homogeneous methane combustion technology [13]. An important step in this direction has been the introduction of 'low-temperature catalytic methane combustion'

(LTCMC) technology, which has been integrated into developing three-way catalytic converters for natural gas engines [14]. This innovative approach involves the incorporation of suitable catalysts to lower the activation energy (E_A) and provide an alternative reaction pathway for the conversion of CH_4 at much lower temperatures ($< 500\text{ }^\circ\text{C}$) than the homogeneous combustion process [15]. Potential candidates for such operations are supported catalysts containing palladium (Pd) and platinum (Pt), which exhibit the highest activity for CH_4 oxidation [16]. Given its significant potential, the LTCMC process warrants careful consideration in policy and industry initiatives to reduce greenhouse gas emissions. Embracing the LTCMC technology could drive significant progress in mitigating methane-related environmental impacts and promoting sustainable practices in energy use.

While catalytic converters effectively reduce pollutants such as carbon monoxide (CO), hydrocarbon (HC), and NO_x in motor engine exhaust, they are less efficient in mitigating CH_4 emissions [17]. Consequently, the development of a functional catalytic system for LTCMC has garnered significant interest due to the lack of an efficient system optimizing the LTCMC process for high catalytic efficiency and CH_4 combustion [15,18]. Efforts to address this gap have led to considerable interest in functional catalytic systems tailored for LTCMC [19]. However, the activity of the heterogeneous catalysts (Pd and Pt) is mainly promoted by the oxidation states of these metal oxides on a suitable accessible material surface, termed the *catalyst support* [20]. The support, serving as a carrier, plays a vital role by providing high surface area, enhancing metal oxide dispersion, and ensuring thermal, mechanical stability, and catalyst longevity [21]. Nevertheless, existing support systems (e.g., alumina, zeolite, and carbon materials) exhibit operational deficiencies, including inadequate thermal conductivity, chemical reactivity, and mass transfer limitations, affecting their optimal performance as catalyst systems during operations [22,23].

To address these structural and operational deficiencies, alternative porous materials have been introduced as support structures for the catalysts, including controlled porous glass (CPG) and commercial silica (e.g. fumed silica) [24,25]. However, the traditional processes of synthesizing CPG via phase-separated sodium borosilicate glass precursors are energy-intensive and costly [26]. Similarly, commercial silica nanoparticles are typically produced by thermal decomposition or hydrolysis of Si-containing molecular precursors such as Tetraethyl orthosilicate (TEOS) or flame pyrolysis of SiCl_4 , SiH_4 and cyclic siloxanes at $\sim 1500\text{ }^\circ\text{C}$, in gas or spray flames [27], plasma [28], or wall-heated reactors [29].

These conventional routes have significant environmental impacts, including CO₂ and NO_x emissions, and generate substantial wastewater (27 tons), making the entire process environmentally unfriendly and expensive [30]. For example, the traditional production of 1 ton of silica using sodium carbonate powder with quartz sand generates approximately 0.23 tons of CO₂, 0.74 tons of sodium sulfate and 20 tons of wastewater, violating the principle of sustainable processes [31]. As a result, CPG and commercial silica have limited appeal due to environmental and cost considerations, hindering their widespread industrial applications [26]. Consequently, it is imperative to explore more environmentally friendly and sustainable ways to produce silica nanoparticles, with the essential properties and attributes for use as a catalyst support in LTCMC operations. Efforts towards incorporating renewable alternatives promise a greener and more environmentally conscious future.

1.2 Motivation for the Study

The concept of sustainability has received considerable attention in recent years, driving the need to develop environmentally friendly technologies for sustainable processes. One of the pivotal challenges is the efficient utilization of biomass residues from agricultural and industrial operations. Biomass residues are abundant and renewable, with immense potential for synthesizing value-added products, including biofuels, biochemicals, and biomaterials. However, the lack of value-addition pathways to these sustainable resources often leads to indiscriminate disposal in landfills or open combustion, engendering environmental pollution [32].

Silicon (Si)-accumulating plants have emerged as valuable resources for silica extraction, offering a sustainable and environmentally friendly alternative. These residues have minimal processing requirements and low emission profile [26,33]. Several plant species, including cereals, horsetail, and sugarcane, accumulate silicon (>1.5% Si) by absorbing monosilicic acid from the soil solution as a response to biotic and abiotic stresses, such as droughts [34–37]. The extraction of silica microparticles from plant tissues via thermochemical conversion has been the subject of numerous investigations owing to its significant advantages, such as net-zero emissions and cost-effective options over mineral-derived silica [38,39]. After the combustion of biomass residues, the ash generated (10–20 wt. % of the initial fuel) is rich in silica (i.e., “biogenic silica”) [35]. The extracted silica presents numerous potential applications across industries, serving as precursors for water

glass synthesis, supplementary cementitious materials, rubber fillers, adsorbents for effluent treatment, and energy storage [40–43].

For advanced applications, high-purity silica with an amorphous structure and significant surface area is essential [44,45]. However, large-scale biomass combustion often falls short in producing porous biogenic silica with the required purity, exhibiting partial crystallinity and inadequate textural properties in the resulting ashes [46]. The low quality of ashes is partly due to the high amounts of water-soluble alkali, acid-leachable metallic impurities, chlorine, and sulphur compounds embedded in the biomass matrix [47]. These compounds induce slagging tendencies, forming crystalline ashes containing quartz, unburned carbon, and low purity, restricting their use in high-value sectors [48]. To enhance the vital properties of biomass and resulting ashes, various conversion pathways, including thermal, chemical, and pre-and post-treatment procedures, are necessary. These steps ensure the biogenic silica attains the requisite quality (purity, amorphicity, and porosity) for advanced applications, such as synthesizing catalyst supports for low-temperature catalytic methane combustion [31].

In Africa, abundant agricultural residues, including cassava peelings, yam peelings, coconut husk, corncob, and cornhusk, lack established treatment protocols or value-addition pathways [49]. Increased agricultural productivity, driven by advancements in farming technology, has led to the inevitable generation of substantial agricultural waste [49]. Managing these residues has been a persistent challenge, with prevalent disposal methods relegated to open-filled burning and landfill disposal. Along with the evident pollution of air and nearby water bodies, uncontrolled burning releases hazardous gases (CH_4 , NO_x) and fine particles ($\text{PM}_{2.5}$ and PM_{10}), posing health risks such as lung carcinogenesis and silicosis from exposure to crystalline silica [50,51]. In addition, the uncontrolled burning results in ash often lacking the prerequisite quality and characteristics for advanced applications [46]. Consequently, researchers are poised for solutions in developing sustainable technologies for silica extraction from agricultural residues. These include optimizing the synthesis process and implementing efficient and cost-effective methods for extracting and purifying silica from various sustainable sources with broad industrial applicability. This study represents a concerted effort to embrace renewable alternatives, contributing to a greener and more environmentally conscious future and supporting the global transition toward sustainability.

1.3 Research Aim, Objectives and Approach

This dissertation investigates the extraction of high-quality biogenic silica from biomass residues for sustainable industrial material applications. Specifically, the present study is focused on exploring possible alternatives for preparing catalyst supports from silicon-rich agricultural residues that can exhibit enhanced and stable catalytic activity at conditions relevant to LTCMC. Due to biomass fuel heterogeneity and complex structure, extracting high-quality biogenic silica to meet the essential properties prerequisite for advanced applications requires the development of stringent technologies and innovative approaches that manipulate their inherent characteristics or the resulting ashes after the thermochemical conversion processes. Specifically, the following objectives were addressed in this study:

1. Introduce sustainable procedures for extracting and characterizing biogenic silica from selected African biomass residues through systematic experimental investigations (i.e., chemical pretreatment and combustion).
2. Improve the textural properties of the extracted biogenic silica from the direct combustion through post-treatment methods, such as the wet-chemistry-based synthesis routes.
3. Investigate the catalytic effectiveness of metal catalysts supported on biogenic silica for the LTCMC.

Approach

To synthesize appropriate heterogeneous catalyst support materials from agricultural resources, the outlined objectives of this dissertation were categorized into the following work packages (WP):

WP 1: Biomass screening, combustion, and characterization

Suitable and non-competitive biomass resources available on the African continent with no further usage or competition were located and selected for investigation (see **Chapter 4**). Predominant biomass residues of these feedstocks were sourced, including cassava peelings, yam peelings, coconut husk, corn cob, and corn husk. These biomass residues cover about 90% of the main food chain consumed daily, generating considerable waste. Accordingly, the characteristics of silica derived from these residues as a new possible

alternative source for silica-based materials were investigated. Within the boundaries of literature and data reported for the combustion of other biogenic agricultural materials, the selected biomass residues were subjected to various pretreatments (water washing and acidic leaching) before combustion experiments. The generated ashes were examined and compared with commercial silica using different spectroscopic and diffractometric techniques regarding their ash characteristics.

WP 2: Modification and improvement of the textural properties of the generated biogenic silica

Due to the heterogeneous qualities (e.g. silica purity and ash porosity) of the biogenic silica extracted via the direct combustion process in the preliminary study of **WP 1**, the most promising biogenic silica from the generation route was selected for further textural enhancement and modification. This phase aimed to improve the quality of the obtained silica, specifically from cornhusk residue, via a wet-chemistry synthesis route, the sol-gel polymeric process, focusing on factors such as silica purity and ash porosity (see **Chapter 5**). The work package also employed comprehensive characterization techniques to explore the morphological structures of the synthesized silica support and confirm its suitability as a catalyst support system.

WP 3: Development of a synthesis concept for the catalyst support system

The synthesized biogenic silica from **WP 2** was examined for its practical applicability in methane conversion as catalyst support. Methods for synthesizing and testing catalyst support from biogenic silica for low-temperature catalytic methane combustion processes were developed in **WP 3** (see **Chapter 6**). Comprehensive characterization techniques were used to explore the morphological structures of the synthesized silica support and evaluate its effectiveness as catalyst support in LTCMC operations. Furthermore, comparative studies between catalysts (containing Pd and CeO₂ as active metals) synthesized on both biogenic silica from cornhusk and industrially produced silica supports were conducted to assess their feasibility and operational efficiencies in LTCMC operations under realistic experimental conditions simulating exhaust gas conditions.

1.4 Structure of the Dissertation

This thesis is a compendium of three original paper publications, compiled into three separate chapters. Following the introduction established in **Chapter 1**, the subsequent literature review in **Chapter 2** provides the fundamental principles of biogenic silica extraction from agricultural residues via pretreatment and thermochemical conversion pathways. Additionally, the review delves into the catalysts, catalyst supports and the mechanism of LTCMC. **Chapter 3** outlines the methodology adopted in this dissertation. **Chapter 4–6** contains the individual studies presented as distinct scientific publications. Finally, **Chapter 7** discusses the main research findings and presents an outlook for using agricultural residues and developing sustainable value-added materials in Africa. Figure 1.1 shows the relationship between the objectives and the corresponding work chapters, highlighting the novelty of each chapter contribution to the scientific body.

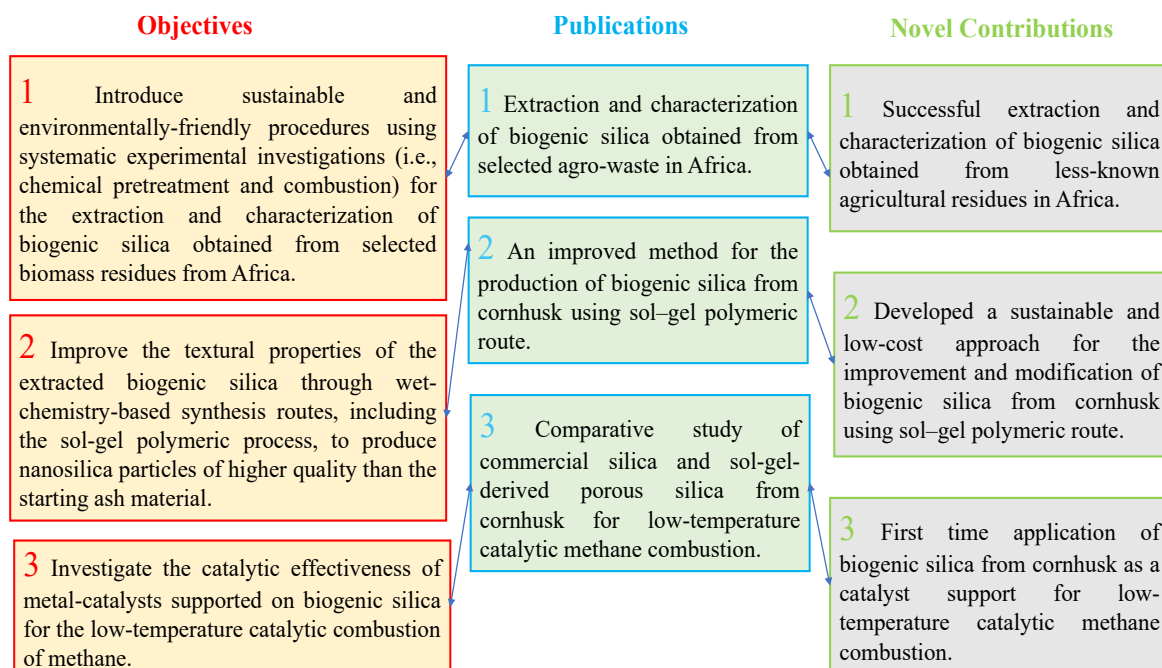


Figure 1.1. Outline and novel contribution of work packages.

CHAPTER 2

2 Literature review

The published manuscripts in this dissertation extensively cover silica production from biomass, textural modification, and its application as a catalyst support. To avoid redundancy, this chapter succinctly summarizes the foundational knowledge and concepts supporting the original contributions of this study while providing insights into future directions.

2.1 Biomass Conversion Processes

Crucial for addressing future energy and sustainability challenges, biomass conversion processes involve transforming organic matter from plants, agricultural residues, and waste materials into valuable resources for energy production [52]. Biomass, derived from organic matter such as plants, agricultural residues, and waste materials, can be a valuable resource for energy production and other applications [53]. Technologies such as combustion, pyrolysis, and gasification play a key role in this transformation, offering diverse energy forms such as heat, electricity, and biofuels [54,55]. Utilizing biomass helps reduce reliance on fossil fuels, thereby mitigating greenhouse gas emissions and fostering a sustainable and circular economy for a greener future [56].

Thermochemical conversion is a conventional approach for converting biomass residues into valuable materials [36,57]. This process encompasses combustion, pyrolysis, and gasification, with extensive research conducted over the years into these significant areas [58].

Table 2.1 compares these processes, highlighting their respective technical and operational conditions during the combustion of biomass fuels. The optimal conversion pathway depends on inherent biomass fuel characteristics, heterogeneity, and desired final products. In comparison to gasification and pyrolysis, combustion stands out as a relatively feasible method for converting lignocellulosic biomass into valuable products such as biogenic silica [58].

Table 2.1. Comparison of the major thermochemical conversion processes. Adapted from the works of Park et al. [58], with permission from Energy Environ. Sci., Copyright (2017). (Abbreviation: H.V, heating value).

	Combustion	Gasification	Pyrolysis
Purpose	Converting biomass to heat and electricity	Converting biomass to high HV gas	Converting biomass to biochar
Atmosphere	Oxidizing atmosphere	Partial oxidizing atmosphere	No oxidant
Temperature	700–1400 °C	500–1300 °C	380–830 °C
Gas products	CO ₂ , H ₂ O	CO, H ₂ , CO ₂ , H ₂ O, CH ₄	CO, H ₂ , CH ₄ , other hydrocarbons
Pollutants	SO _x , NO _x , polycyclic aromatic hydrocarbons (PAHs), dust	H ₂ S, NH ₃ , tar, dust	H ₂ S, NH ₃ , tar, dust
Advantages	Process is relatively simple. Co-combustion of biomass and coal do not need changes to current power plants	Production of a variety of chemical products	Liquid fuels are directly produced, which after appropriate treatment maybe directly treated in conventional refineries
Disadvantages	NO _x , SO _x , particulates formed during combustion	Tar formation, which lowers gasification efficiency.	High energy consumption due to its endothermic nature.

2.2 Structure and Composition of Biomass

Lignocellulosic biomass constitutes cellulose, hemicellulose and lignin, forming the organic structure, with considerable amounts of alkali and alkaline earth metallic species

(AAEMs), constituting the inorganic fraction of the biomass [47,59]. The inorganic fraction, excluding silicon, mainly contains sodium, potassium, calcium, magnesium, and iron, with varying concentrations among biomass fuels [60]. Cellulose (Figure 2.1) is a complex carbohydrate and the main structural component of plant biomass consisting of repeating units of glucose molecules linked together through β -1,4 glycosidic bonds. The chemical structure of cellulose gives it unique properties, such as high tensile strength, providing rigidity and support to plant cells. Cellulose undergoes thermal degradation at temperatures exceeding 300 °C, attributed to its high molecular weight with a long chain formed of D-glycosyl groups [61,62]. Hemicellulose, constituting about 20-35 wt% of the dry weight of the plant biomass, plays a crucial role in cell wall structure and properties, offering flexibility and water-holding capacity. It is a heterogeneous polysaccharide group containing various sugar units like xylose, arabinose, mannose, and galactose, with lower polymerization and thermal stability than cellulose. Dhyani et al. [63] reported the decomposition temperature for hemicellulose at 220–315 °C. Lignin is the third constituent of biomass, comprising a heterogeneous polymer that accounts for 15-30 wt% of the dry weight of plant biomass. It is an amorphous polymeric resin with cross-linked phenolic monomers [64]. The specific structure of lignin varies and functions as a connector between hemicellulose and cellulose in the cell wall, influencing the stiffness and porosity of plant cell walls [65]. Silica is uniformly inter-twinned between the lignin, enabling an extraction by using various thermo chemical and pre/post-treatments methods to produce high-quality silica [66,67].

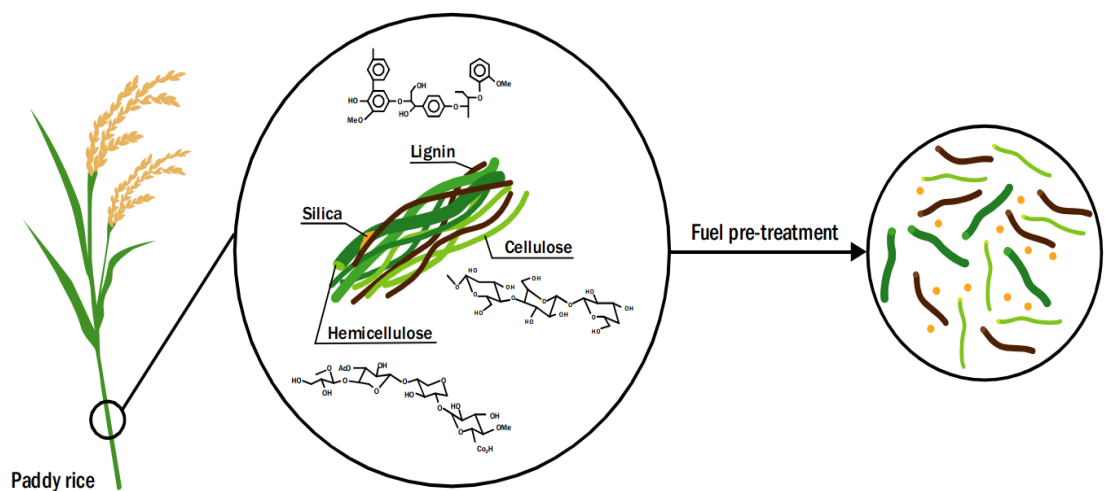


Figure 2.1. Effects of chemical fuel-pretreatment on the structure of lignocellulosic biomass. Reported from Beidaghy Dizaji [68].

2.3 Extraction of Silica from Biomass and Effects of Process Parameters

Silicon (Si) is a naturally occurring element in the soil and plant system. Depending on the species, plants absorb Si as monosilicic acid, $\text{Si}(\text{OH})_4$, from the soil [69]. Phytoliths, or silicified structures consisting of biogenic silica, are formed through deposition in the inter- and intracellular gaps of leaf and stem a plant [70]. The silica accumulation by plants is a response to adverse biotic and abiotic stressors, such as drought [71]. The absorbed silicic acid is polymerized into silica gel in the xylem sap of the plants, promoting mechanical strength and light interception [72]. The uptake, transport and accumulation process of silica in higher plants has been widely reviewed in the scientific literature [67,73]. Guo-Chao et al. [67] provide a comprehensive account of the various mechanisms involved in the absorption of silica, transportation and storage in plants, highlighting its crucial role in enhancing plant growth and survival under biotic and abiotic stress conditions.

The extraction of the biogenic silica from the inter- and intracellular gaps of leaf and stem a plant involves two main processes: fuel pretreatment and combustion [74]. As shown in Figure 2.1, the biomass fuel undergoes chemical pretreatment in an acidic or basic solution to remove the embedded inorganic compounds, followed by controlled combustion. The resulting ash particles, rich in siliceous content, are termed biogenic silica [35]. The properties of the extracted biogenic silica are entirely dependent on various parameters, including the concentration of metallic compounds embedded in the biomass matrix, pretreatment conditions, combustion temperature, heating rate and residence time [75]. These parameters influence the combustion characteristics, ash distribution and quality of the final silica product [35].

Various studies highlight the complexity of the combustion process and the importance of selecting appropriate conditions for extracting biogenic silica from agricultural residues [74]. Ash particles generated at low combustion temperatures are carbonaceous, while higher temperatures and longer combustion times lead to crystalline structures or phases in biogenic silica [76]. For instance, in the case of rice husk, a temperature range of 700 to 800 °C resulted in partial crystalline formation. Complete crystalline phases formed at temperatures above 600 °C and residence times exceeding 2 h in rice husk and rice straw ashes [48]. These phenomena impact the textural properties of the biogenic silica, influencing its suitability for various applications. For instance, in optical applications, white silica is preferred for a filler, as the essential optical properties, such as brightness and whiteness of the silica, are used to quantify the colour of materials [77]. In catalysis operations with biogenic silica as

a support system, considerable surface area and pore volume are essential to impregnate the active metals onto the surface [78]. Therefore, stringent technologies and innovative pathways that can manipulate the inherent characteristics of the biomass or the extracted biogenic silica particles are desired to achieve the prerequisite structural and textural properties for advanced application [79].

Untreated biomass fuels are particularly susceptible to forming ash-related problems due to the high share of alkali metal and alkaline earth metal impurities, such as K_2O , CaO , and MgO , embedded in the biomass matrix [80]. The presence of these contaminants affects the efficiency of the combustion process, resulting in low purity and textural properties of the extracted biogenic silica [81,82]. Thus, pre-treating the biomass fuel before combustion aims to hydrolyse the cell walls, allowing easy contact of the leaching agent to the alkali metal impurities. These impurities differ in concentrations for various biomass fuels [83]. Their influence on the ash characteristics and ash transformation reactions has been fully elucidated in the study of Beidaghy Dizaji et al. [48]. According to their reports, ash transformation reactions occur due to complex interactions of the ash-forming elements with the SiO_2 component during the rice husk and straw combustion. These interactions lead to the formation of eutectic mixtures and crystalline phases such as arcanite (K_2SO_4), albite [$Na(AlSi_3O_8)$] and calcite ($CaCO_3$), reducing the purity of the extracted silica [81]. In addition, the presence of alkali metals during combustion facilitates the phase transformation of silica to cristobalite and tridymite at higher temperatures, reducing the amorphicity of the silica [84].

According to Krishnarao et al. [76], a simultaneous decomposition of the organic matter of biomass fuels and oxidation of the metallic impurities occurs during the combustion process from room temperature (RT) to high temperatures. Before all the carbon is oxidized, if these alkali metal ions are present, surface melting or sintering occurs at high temperatures, resulting in ions trapped inside the organic matrix. This phenomenon leads to the formation of black particles in the biogenic silica, reducing the overall purity of the extracted silica [85–87]. For untreated biomass fuels, ash-related problems that lead to black particle formation or sintering are higher than treated fuels due to the high share of ash-forming elements. Thus, the ash-forming compounds readily form complex associations with the SiO_2 during combustion, as shown in Figure 2.2 [76].

In Figure 2.2, the structural changes of the silica network occur due to the strong affinity of the silica unit to attract positively charged metal ions (M^{2+} and M^{+1}). This affinity

displaces charged cations in the silica matrix, resulting in the formation of new crystal structures such as Albite [$\text{Na}(\text{AlSi}_3\text{O}_8)$] and Sanidine (KAlSi_3O_8), with lower stability than pure silica. These newly formed structures have comparatively low melting temperatures, causing ash slagging and agglomeration tendencies [48]. Thus, demineralizing the biomass before combustion is necessary to mitigate these occurrences and enhance the physicochemical properties of the ash and combustion efficiency.

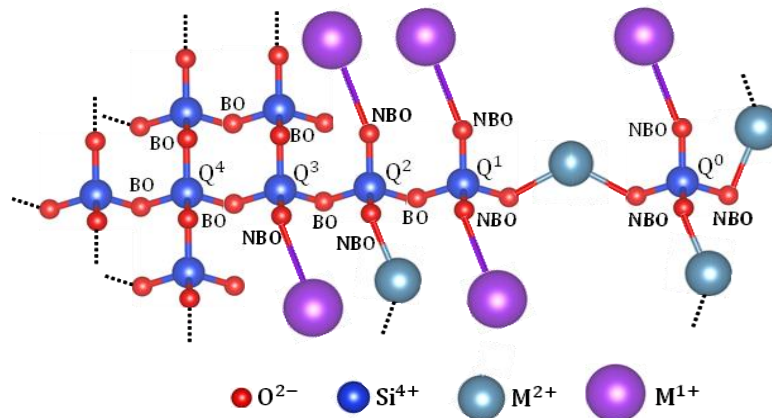


Figure 2.2. Schematic of the silica network modifications by the metal (M: Na^+ , K^+ , Ca^{2+} , Mg^{2+}) cations. BO indicates the bridging oxygen atom found between two silica atoms together (Si-O-Si), whereas the oxygen that binds a metal-cation to a silicon atom is referred to as non-binding oxygen (NBO). Reproduced from the works of Beidaghy Dizaji [48], with permission from Elsevier, Copyright (2021).

Different demineralization or pretreatment techniques influence the physicochemical structure and thermal degradation profile of biomass [88]. For instance, removing alkali and alkaline earth metals decreases ash content in the biomass, resulting in improved fuel properties such as increased calorific value and reduced slagging and fouling tendencies [89,90]. In addition, different demineralization treatments can affect the thermal degradation behaviour of biomass and enhance the overall thermal efficiency of biomass conversion processes [91]. However, the influence of demineralization treatments on biomass is multifaceted and can vary depending on several critical factors, including the specific type of biomass feedstock, the strength and nature of the leaching agent employed, as well as the duration and temperature of the hydrolysis process [92].

Predominant pretreatment procedures include water, strong and weak acid leaching [85]. Water washing removes the adhered soil particles from the biomass fuels while concurrently dissolving intrinsic water-soluble metals on biomass, such as Na^+ , K^+ , Ca^{2+} , and Mg^{2+} [48,93]. The process of acid leaching entails using either organic acid, such as citric acid or inorganic acids (HCl , HNO_3 and H_2SO_4) for the removal of inorganic compounds. However, the use of organic acid is recommended over inorganic acids due to environmental concerns, along with the limited disposal options [94–96].

Umeda et al. [97] have reported on the efficiency of carboxylic acid in producing high-purity and amorphous silica from rice husks. In their report, citric acid effectively removed metallic impurities or inorganic compounds through a chelate reaction between the carboxyl groups and the ions present. Consequently, the propensity of black particle formation in the silica particles (carbon trapping) was mitigated, improving the ash properties and combustion behaviour of the biomass. Nevertheless, they reported that the efficacy of the pretreatment process depended on various factors, including the hydrolysis temperature, time, and acid concentration. Beidaghy Dizaji et al. [35] reported that optimal conditions for leaching rice husk and straw in citric acid solution were found at a hydrolysis temperature and time corresponding to 50 °C and 2 h, respectively. Beidaghy Dizaji [19] also proved that a suitable pretreatment prevents carbon trapping in Si-rich biomass ashes during thermochemical conversion.

Following the acid-leaching procedures, the biomass undergoes a washing step to remove remnants of the acidic solution. Subsequently, the biomass is subjected to a drying process to reduce moisture. Moisture content is one of the parameters that affect the quality of the thermochemical conversion process. According to the literature, some biomasses may have a moisture content as high as 45-55% (wet basis), as in the case of sugarcane bagasse [98]. To enhance the conversion efficiency, subjecting the wet biomass to a drying process before combustion is recommended. In industrial settings, hot air, steam or spray dryers are employed, whereas convective ovens are used in the laboratory to reduce the moisture content. Numerous studies have recommended that the moisture content of the biomass material is reduced below 10 wt% (wet basis) before the biomass materials are either compacted for storage or subjected to a thermal treatment [98].

Several fibrous biomasses, including rice straw, rice husk, corncob, and corn husk, have low bulk density and volumetric energy densities [80]. To increase their energy densities, such as high heating value (HHV), compacting methods like briquetting and

pelletizing are adopted [91]. Briquetting compresses the biomass under high pressure without any binder, allowing the lignin of the biomass to serve as a binder [99]. On the other hand, the pelletizing process involves pressing the raw biomass with a definite binder to produce pellets, typically ranging from 3-50 mm in length and up to 25 mm in diameter. It improves the ash content of biomasses with low ash content and enhances the fuel properties of the biomass feedstock. The high density and reduced moisture content of pellets result in improved energy density and calorific value. This means smaller pellets can provide the same energy output as larger volumes of loose biomass. The standardization of the size of pellets and uniformity also contribute to better combustion efficiency, reduced emissions, and more controlled heat release during thermochemical processes [91]. Other preparation procedures performed on biomass before combustion include cutting, milling, or shredding. Shredding and milling biomass fuels reduce the size and attain a homogeneous size distribution of the starting materials [100].

2.4 Modification and Improvement of the Textural Properties of Biogenic Silica

The textural properties of biogenic silica play a crucial role in its functional applications. Several methods are employed to modify and improve the textural properties of biogenic silica for various purposes. Advanced applications, such as catalyst support, require biogenic silica to have high purity levels, amorphicity, and porosity. However, the ashes from combustion processes often lack these properties and, therefore, require transformation techniques to improve their physicochemical attributes before their intended use in advanced applications. Suitable catalyst supports should have a high specific surface area and pore volume for optimal catalytic activity and efficient mass transfer. However, unmodified biogenic silica from the direct combustion process typically has low textural properties and requires various transformation techniques to modify and improve its morphological and physicochemical attributes [88].

One approach to modifying the textural properties of biogenic silica is through post-processing techniques. These techniques involve calcination, acid leaching, and thermal annealing. Calcination can enhance the porosity and surface area of biogenic silica by removing organic components and inducing structural changes [93]. Acid leaching helps in selectively removing impurities and fine-tuning the pore size distribution. Thermal

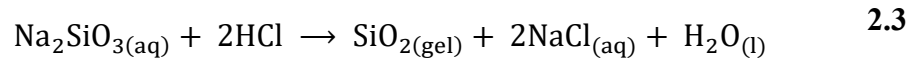
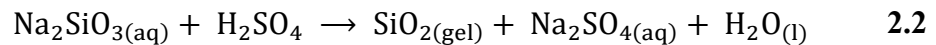
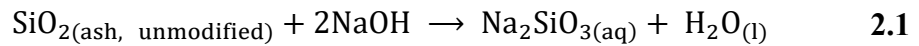
annealing can control the crystallinity and surface chemistry of biogenic silica, leading to modifications in its textural properties [101].

Techniques for surface functionalization, such as the grafting of organic groups or the incorporation of inorganic moieties, offer the capacity to modify the surface chemistry and hydrophobicity of the biogenic silica [102]. These modifications can enhance its compatibility with different matrices, enabling tailored interactions with target substances. Additionally, surface modifications can facilitate the immobilization of functional groups, nanoparticles, or catalysts onto the biogenic silica surface, allowing the development of advanced hybrid materials with improved textural properties and tailored functionalities [103,104].

A post-processing technique for synthesizing controllable mesoporous silica materials exhibiting both micropores and mesopores properties has been reported in the literature [105]. Alyosef et al. [106] reported on transforming pre-shaped mesoporous rice husk ash (RSA) into MCM-41 and MFI-type zeolite using a two-step pseudomorphic transformation. The process of pseudomorphic transformation entails the utilization of a mesoporous template, such as a monoproprylamine (PA)-containing alkaline solution (NaOH), under hydrothermal conditions to modify the morphology and the properties of the silica into various types of zeolites, including MFI-type and ZSM-5. The obtained MFI-type zeolite exhibits unique micro/macroporous characteristics with bimodal pore structure (micro/macro, meso/macro) often required in adsorption, separation and catalysis operations. The latter attributes are mostly lacking in the unmodified or original silica samples before undergoing the transformation process. However, this process requires a substantial energy input and entails a complex transformational procedure.

Various reports have shown the degree of limitation on the manipulability of silica properties, including shape, particle size, uniformity, and pore size configuration, by adjusting only the combustion conditions. Therefore, processes based on the bottom-up method have also been examined, allowing for the precise control of the morphological properties of the silica particles [107,108]. Recently, there have been reports of the morphological evolution of silica nanoparticles based on the sol-gel polymeric process [109,110]. The sol-gel process is a low thermal process involving the dissolution of the unmodified ash in a NaOH solution at 100 ± 10 °C and the formation of sodium silicate solution according to Equation 2.1. This reaction is a classic example of a base-catalyzed hydrolysis reaction, in which the hydroxide ions (OH^-) from the sodium hydroxide molecules

act as a catalyst to break the Si–O–Si bonds in the silicon dioxide molecule, forming dissolved sodium silicate (Na_2SiO_3) and H_2O [111,112]. A chemical reaction of the sodium silicate (Na_2SiO_3) with H_2SO_4 or HCl , as shown in Equations 2.2 and 2.3, result in neutralization processes that create SiO_2 gels.



The effectiveness of the sol-gel technique depends on various factors such as the initial precursors, gelation time, and catalyst employed during gelation [113]. Traditionally, inorganic acids such as H_2SO_4 and HCl are adopted in the pH-controlling step. However, citric acid can be used to achieve similar product quality coupled with environmental benefits. A recent study by Kalapathy et al. [114], using citric or oxalic acid, demonstrated an enhanced morphological structure of sol-gel synthesized silica particles derived from rice husk.

The sol-gel polymeric route is an effective method for synthesizing hybrid organic-inorganic materials with diverse properties required for numerous industrial applications. These include adsorption and separation processes, catalysis, drug delivery systems, sensors, and composite materials. Tailoring the textural properties of biogenic silica provides opportunities to enhance its performance, optimize its interactions with target substances, and maximize its efficiency in various functional applications. [115].

2.5 Catalyst and Catalyst Support System

2.5.1 Catalyst

Catalysts are substances that increase the rate of a chemical reaction without being consumed [116]. They are widely used in various industries, including petrochemicals,

pharmaceuticals, and environmental applications, to enhance reaction efficiency and selectivity. Catalysis may be defined as homogeneous or heterogeneous depending on whether the reactants and the catalysts are in the same or different phases [117]. Noble metals, including Au, Ag, Pt, Pd, Pt and Rh, are widely used as catalysts due to their resistance to oxidation and ability to achieve high activity and selectivity [118]. However, the performance of these catalysts is optimized by a suitable support that functions as a substrate or base for the catalysts.

In chemistry, catalysts play a vital role in facilitating chemical reactions by lowering the activation energy required for the reaction to proceed [119]. The Arrhenius equation in Equation 2.4 is used to estimate the activation energies and the pre-exponential (A) terms, showing the dependence of the rate constant (k) on the temperature of the reaction (T) [120].

$$k = K \exp[-E_A/RT] \quad 2.4$$

In Equation 2.4, K is the pre-exponential factor, E_A is the activation energy, and R is the gas constant (8.314 J/mol·K). The activation energy is the minimum energy that reactant molecules must possess to overcome the energy barrier and transform into products. It is a measure of the sensitivity of the reaction to temperature changes. Reactions with higher activation energies generally have slower reaction rates. The pre-exponential factor represents the frequency of successful collisions between two reactant molecules to form the activated complex. It reflects the probability of reactant molecules having the correct orientation and sufficient energy to undergo a reaction [121].

2.5.2 Catalyst support

A *catalyst support* is a material that provides a structural framework or surface area on which the catalyst is deposited or immobilized. The support material should possess specific characteristics to ensure effective catalyst performance [21]. As such, it can be inferred that the role of these structures in heterogeneous catalysis is of utmost importance [122]. Catalyst support materials are chosen based on chemical stability, high surface area, thermal stability, and mechanical strength. Commonly used support materials include

activated carbon, alumina (Al_2O_3) [23], porous silica [123], SnO_2 [124], zeolite [125], titanium oxide (TiO_2) [126], CeO_2 [127] and carbon-based materials (activated carbon, carbon nanotubes) [128]. The selection of a suitable support material depends on the specific catalytic application and the desired properties of the catalyst.

The catalyst support system offers several advantages:

1. It provides a larger surface area for catalyst deposition, allowing for increased contact between the reactants and the catalyst. This leads to enhanced reaction rates and improved efficiency [21].
2. The support helps to maintain the stability and integrity of the catalyst, preventing its aggregation or deactivation during the reaction.
3. It can assist in controlling the size and dispersion of the catalyst particles, influencing their catalytic activity and selectivity. In some cases, catalyst support systems can also impart additional functionalities to the catalyst. For example, certain support materials can act as adsorbents, contributing to removing impurities or by-products from the reaction mixture.
4. They can also influence the diffusion properties of the reactants, affecting the mass transfer limitations of the catalytic system.

The choice of catalyst support system must be carefully considered to ensure compatibility with the reaction conditions and the catalyst. The physical and chemical properties of the support material should be compatible with the catalytic process, and its interaction with the catalyst should not negatively impact the desired reaction. More importantly, it must be synthesized from low-cost materials to reduce the overall cost of the catalyst. Controlled porous glass (CPG) is a widely used catalyst support material, but its synthesis is complex, expensive, and time-consuming [24]. Current research goals include discovering substitute support materials that utilize renewable resources. This would decrease the overall cost of the catalyst and enhance its catalytic effectiveness.

2.5.3 Catalyst deactivation in catalytic converters

The automobile exhaust control catalyst can be affected by various process parameters, including the type of catalyst support, thermal degradation, sintering, coking, poisoning, and

mechanical damage and water vapour [129,130]. During operation, the presence of water vapour can react with active sites to form hydroxyl compounds, rendering the active phase of the catalyst inactive and reducing its performance [131]. In the case of the Pd catalyst, the presence of water vapour results in the hydroxylation of the support, causing the active phase (PdO_x) to transform into an inactive phase, namely $\text{Pd}(\text{OH})_2$. This blocks the active sites, reducing the catalytic performance of the catalyst [132,133]. Hydroxylation of the support is often reduced by the introduction of Pt, forming a bi-metallic phase of Pd-Pt to slow down the rate of PdO sintering [133].

Secondly, catalysts are susceptible to deactivation attributed to various factors, including thermal degradation, sintering, coking, poisoning, and mechanical damage [134]. The phenomenon of thermal degradation is attributed to the exposure of catalysts to elevated temperatures, resulting in the deterioration of their structural integrity, leading to a decline in their efficiency and activity. The effect of sintering occurs when the catalyst melts into tiny particles, impeding the diffusion of oxygen for coke decomposition. These scenarios above may reduce active surfaces, affecting the number of active sites available for reaction and degradation of catalyst performance [133].

Lastly, the preparation or synthesis method of a catalyst also affects its catalytic activity by influencing the distribution and types of active sites on the catalyst surface [135]. Different preparation methods can result in different levels of crystallinity, active surface area availability, surface species mobility, and catalyst microstructure [136]. A more homogeneous distribution of active sites can result in higher catalytic activity, while a higher concentration of active sites can lead to localized inhibitors that can reduce activity. So far, the most reported methods in the literature include wet or incipient impregnation, coprecipitation, physical mixing, and the sol-gel process [10]. Wet or incipient impregnation is commonly used to prepare heterogeneous catalysts used in various industrial processes. This method allows for precise control over the loading of the catalytic material on the support, leading to well-defined catalyst properties. The resulting catalytic material exhibits a significantly enhanced surface area, facilitating the kinetics of the catalytic reaction [110].

2.6 Methane Emissions and Combustion Processes

2.6.1 Methane emissions

Methane (CH_4) is a potent greenhouse gas with a much higher global warming potential than carbon dioxide (CO_2) over a relatively short time frame [17]. The CO_2 equivalent for methane is 25 for a time horizon of 100 years. Within the first 100 years after release, 1 kg of CH_4 thus contributes 25 times as much to the greenhouse effect as comparable 1 kg of CO_2 [137]. It is released through natural processes and human activities, and its emissions contribute significantly to climate change. Natural sources of methane emissions include wetlands, termites, and certain natural processes in the oceans and geological formations [138]. However, human activities responsible for the majority of methane emissions include:

1. Energy production and use: The production, transport, and use of fossil fuels, such as coal, oil, and natural gas, release methane into the atmosphere. Methane can leak during extraction, storage, and distribution processes, including coal mining, oil drilling, and natural gas extraction [139].
2. Agriculture: Livestock produce methane during digestion, particularly ruminant animals such as cows and sheep [140].
3. Waste management: Landfills and wastewater treatment plants are significant sources of methane emissions. Organic waste decomposes under anaerobic conditions, producing biomethane as a by-product [141].
4. Exhaust emissions: Methane emissions from the automotive industry primarily originate from two primary sources: vehicle fuel systems and exhaust emissions. CH_4 is emitted during the combustion process in internal combustion engines, although the levels are typically lower than CO_2 emissions. Incomplete combustion and unburned hydrocarbons can contribute to methane emissions from motor exhaust [17].

Mitigating methane emissions is crucial for addressing climate change. Governments and regulatory bodies are implementing standards and regulations to address motor methane emissions. These measures include emission limits, testing protocols, and promoting cleaner technologies to capture and utilize methane emissions from vehicle fuel systems or exhaust.

Some key methane capture technologies include vapour recovery units and flare systems, landfill gas collection systems and coal mine methane capture. These technologies are often expensive [142]. In cases where methane emission reduction is a priority, the low-temperature catalytic methane combustion (LTCMC) process offers a promising approach to burning methane at a lower temperature, reducing emissions efficiently.

2.6.2 Mechanism of low-temperature catalytic methane combustion

Catalyst systems for CH₄ combustion are commonly used in catalytic converters to regulate emissions from natural gas engines through LTCMC processes [143]. The underlying principle of LTCMC revolves around promoting CH₄ combustion to yield CO₂ and H₂O utilizing catalysts [144]. Compared to the conventional thermal combustion of methane, LTCMC processes reduce the formation of harmful pollutants such as NO_x and particulate matter, as it occurs at much lower temperatures (< 500 °C) [145]. The efficiency of the catalyst used in promoting the oxidation of CH₄ is promoted by using an appropriate catalyst support [146]. The carrier material provides a stable and porous structure that helps to disperse the catalyst particles.

The Mars-van Krevelen (MvK) mechanism describes the interaction pathway between CH₄, O₂, and the catalyst surface during LTCMC operation. The mechanism involves several steps, as explained in literature [143,147] and simplified in Figure 2.3:

1. Adsorption of oxygen: O₂ molecules from the gas phase are adsorbed onto the catalyst surface. This adsorption step typically occurs on the surface of the catalyst (e.g. Pd).
2. Oxygen dissociation: The adsorbed oxygen molecules undergo dissociation on the catalyst surface, forming reactive oxygen species (O^{*}). These reactive oxygen species play a crucial role in the combustion process.
3. Methane adsorption: CH₄ molecules from the gas phase are adsorbed onto the catalyst surface adjacent to the reactive oxygen species.
4. Surface reaction: The adsorbed CH₄ and reactive oxygen species interact on the catalyst surface, forming surface intermediates. These intermediates can include species such as methoxy (CH₃O^{*}) and formaldehyde (HCHO^{*}).

5. Oxygen transfer: The oxygen species (O^*) obtained from step 2 can react with the surface intermediates (such as methoxy) to regenerate the reactive oxygen species (O^*) and produce water (H_2O). This step involves oxygen transfer between the reactive species and the surface intermediates.
6. Desorption: The combustion products, such as H_2O and CO_2 , are desorbed from the catalyst surface into the gas phase. Steps 1 to 6 occur repeatedly, allowing for the continuous catalytic combustion of CH_4 .

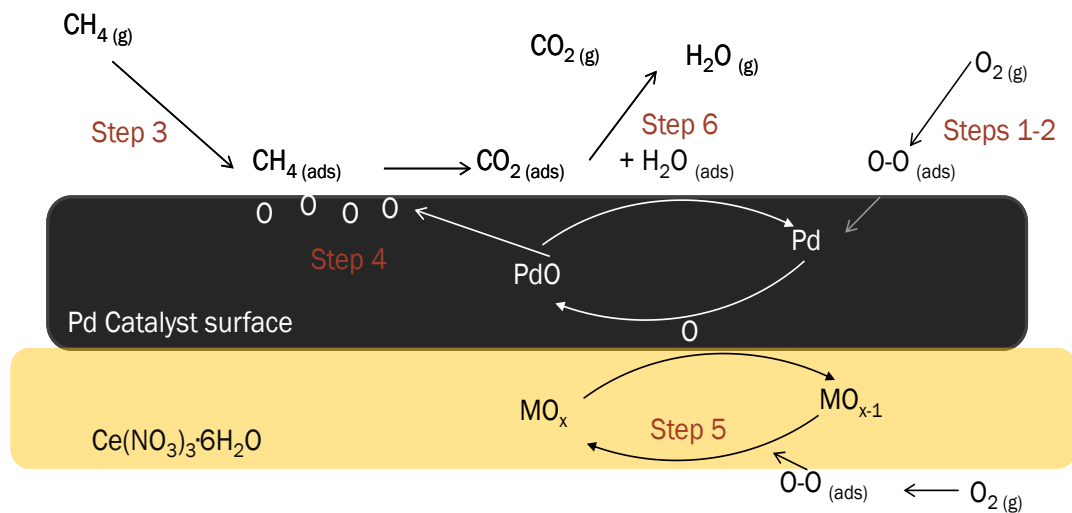


Figure 2.3. Catalytic methane lean combustion proceeding according to the Mars-van Krevelen (MvK) mechanism. Adapted from the works of Seeburg [147] and Keller [143].

During CH_4 combustion, Pd catalysts can exist in multiple oxidation states, Pd(II) and Pd(IV) oxides, namely and in the reduced form Pd^0 [9]. The active PdO_x phase can efficiently oxidize CH_4 to form CO_2 and H_2O at lower temperatures in the presence of oxygen. According to Peng et al. [134], the active PdO_x species decompose into the less active nanometric Pd^0 species at high temperatures, resulting in a loss of catalytic efficiency. Similarly, the presence of H_2O molecules that are evolved during the combustion of the hydrocarbons can reduce the catalytic activity. The reduction is attributed to the formation of hydroxyl compounds on the surface of PdO_x active sites. To overcome H_2O -induced deactivation, high oxygen mobility precursors such as ceria (CeO_2) are often incorporated into the support material to influence the re-oxidation of PdO particles to sustain a high

catalytic activity [148,149]. Additionally, the hydrophobic or hydrophilic nature of the support has been reported to influence the behaviour of the catalysts significantly. Hydrophobic support governs the long-term catalytic activity of CH₄ oxidation catalysts by stabilizing the well-dispersed PdO particles in a low-temperature regime and water presence [150]. Thus, understanding the metal–support interaction in Pd/CeO₂ catalysts is crucial to improving its effectiveness in LTCMC operations [151].

2.7 Summary of Literature, Recommendations and Future Perspectives

Within the scope of this review, the structure components of biomass and its use in the synthesis of biogenic silica have been covered. In particular, the extraction process and the significance of chemical pretreatment procedures in attaining high-quality biogenic silica have been discussed. In addition, transformational processes based on the bottom-up approach to precisely modify the unique properties of the unmodified or as-received ash into morphologically controlled and ordered porous silica particles have been dealt with in detail. Lastly, the catalyst and its support system in methane combustion operation via LTCMC were reviewed. Based on the presented literature review, the following observations and conclusions can be drawn:

- The main components of biomass are cellulose, hemicellulose and lignin with inorganic elements oxides of silica (SiO₂), phosphorus (P₂O₅), potassium (K₂O), calcium (CaO), and trace elements such as Fe₂O₃, ZnO and CuO [47,59].
- Combustion is an economical process compared to gasification and pyrolysis in extracting biogenic silica from agricultural residues with the required properties [58].
- Using strong acids such as HCl and H₂SO₄ in acid leaching effectively reduces the levels of inorganic elements and metallic impurities. However, citric acid offers a safer and more environmentally friendly alternative [97].
- Advanced applications, including catalysis, require specific structural and textural properties of biogenic silica, such as high surface area and pore volume.

- The characteristics and textural properties of the extracted biogenic silica, such as surface area and pore volume, are narrowly impacted by changing the combustion conditions. However, transformational processes such as the sol-gel polymeric route can be adopted to modify and improve the morphological structures of the biogenic silica [88].
- CPG and commercial silica are widely used as catalyst support materials with well-defined and controlled pore structures. However, the synthesis processes are expensive and not sustainable, limiting its vast industrial applications [24].
- Low-temperature catalytic methane combustion (LTCMC) technology reduces methane emissions by operating at lower temperatures than homogeneous combustion [12].
- PdO_x efficiently oxidizes CH₄ to CO₂ and H₂O in the presence of oxygen.
- Water molecules evolved during hydrocarbon combustion can reduce catalytic activity due to the formation of hydroxyl compounds on PdO_x active sites [132].
- Incorporating high oxygen mobility precursors like ceria (CeO₂) into the support material helps re-oxidize PdO particles and sustain high catalytic activity [152].
- The hydrophobic or hydrophilic nature of the support significantly influences catalyst behaviour. Hydrophobic supports stabilize PdO particles in the presence of water, enhancing long-term catalytic activity [153].

Based on the literature report on catalyst and catalyst support systems, the following outlook can be made:

- Catalyst support optimization: One must consider the specific requirements of the reaction when selecting a catalyst support material by focusing on properties such as chemical stability, high surface area, efficient mass and heat transfer and, in addition, exploring the use of the sol-gel polymeric route for precise control over the pore structure and size of the biogenic silica nanoparticles.

- Water vapour inhibition: Development of strategies to mitigate the adverse effects of water vapour on catalyst activity by exploring support materials that exhibit hydrophobic properties. This helps mitigate the hydroxylation of active sites and prevent catalyst deactivation by water.
- Catalyst stability enhancement: Investigate methods to improve catalyst stability and prevent deactivation. Address factors such as thermal degradation, sintering, coking, poisoning, and mechanical damage through proper catalyst design, material selection, and operating conditions.
- Long-term stability testing: Conduct thorough long-term stability tests of catalysts under realistic operating conditions. Assess catalyst durability and reliability by subjecting them to extended periods of continuous operation at constant temperatures. This will help to identify any degradation or performance issues that may arise over time.
- Cost considerations: One must consider the economic aspect when selecting catalyst support materials and preparation methods and strive to minimize the overall cost of catalyst systems without compromising performance and efficiency.

In conclusion, developing sustainable and eco-friendly methods for synthesizing biomass-derived silica can contribute to a more sustainable future by reducing the environmental impact of traditional methods.

CHAPTER 3

3 Methodology

3.1 Fuels

The biomass fuels selected for investigation in this dissertation included the cornhusk, corncob (*Zea mays*), yam peelings (*Dioscorea spec.*), cassava peelings (*Manihot esculenta*), and coconut shell (*Cocos nucifera*), obtained from local farmers in the Ashanti region of Ghana. Five round bales, weighing approximately 50 kg, resulting in a total biomass of 250 kg, were acquired from local farmers and shipped to Deutsches Biomasseforschungszentrum (DBFZ), Germany. Upon collection, the biomass fuels were thoroughly washed using tap water to remove any adhered soil particles. Subsequently, they were dried in an air oven at 105 °C and ground into smaller particles (<1 mm) using a hammer mill (Netzsch-Condux, Hanau, Germany). The dried biomass fuels were stored in airtight plastic containers for further experimentation.

3.2 Acid Leaching

To prepare the biomass fuels for chemical pretreatment, a solid-to-liquid ratio of 1:20 (g/mL) was established using 3000 mL of tap water and 150 g of the solid residues. Leaching was carried out by submerging the biomass fuels into the leaching solution containing citric acid (Sigma-Aldrich, Steinheim, Germany) at two different concentrations (1 and 5 w/v% citric acid) at a hydrolysis temperature of 50 °C for 2 h. This leaching protocol allowed the comparison of the leaching efficiency of citric acid at two different concentrations. Following leaching, the samples were rinsed with tap water and dried overnight at 105 °C in a convective oven. Untreated biomass was also set up as a control experiment.

3.3 Combustion Processes

Lab-scale muffle furnace (Nabertherm 1185H66EA, Lilienthal, Germany) under air atmosphere was used for all the combustion processes in Articles I-III. 50 g of untreated and acid-leached biomass fuels (1 and 5 w/v%) were put in crucibles, placed in the furnace and

heated from room temperature (RT) to 600 °C at a heating rate of 6 °C/min for 2 h. The resulting ashes were allowed to cool to RT within the furnace before they were transferred into glass bottles with closed lids for further analysis characterizations.

3.4 Textural Improvement and Modification of the Biogenic Silica

The sol-gel polymeric approach was carried out in **Article II** with corn husk due to its high silica content and desirable properties. The methodology followed the procedures outlined by Falk et al. [39] and Pijarn et al. [42], albeit with minor adjustments. Specifically, 12 g of unmodified ash from the direct combustion process was boiled in a 500 ml Erlenmeyer flask containing 350 ml of 1 M NaOH solution at 100 °C, accompanied by constant stirring. This process aimed to yield a sodium silicate solution. The resulting solution was filtrated using a vacuum-filtration unit with a Unifil C41 filter paper. Subsequently, the filtrate was allowed to cool to room temperature before titrating it with a 2.5 w/v % citric acid solution (Sigma-Aldrich, Steinheim, Germany, with a purity exceeding 99.99%) until the pH reached 7. Gel formation started at pH levels below 10. The solution was then left undisturbed to facilitate gel formation. After 24 h, the formed gels were washed in distilled water and subsequently subjected to centrifugation (Eppendorf centrifuge 5430, Hamburg, Germany) at a speed of 4000 rpm for 5 minutes. The washing procedure was repeated multiple times to ensure the removal of any remaining traces of the citric acid solution and impurities. The resulting gels, identified as silica xerogels, were dried at 80 °C for 12 h before subsequently crushed into powder using an agate mortar and pestle. The dried xerogels were stored in desiccators and labelled accordingly for future characterization.

3.5 Synthesis of Supported Catalysts

The synthesis of the supported catalysts is presented in **Article III** using the final silica product from **Article II**. Commercial silica was used as a benchmarked support to allow catalytic activity and performance comparability. Supported catalysts were prepared via incipient wetness impregnation, as reported in the study by Liu et al. [26]. Molten $\text{Ce}(\text{NO}_3)_3 \cdot 6\text{H}_2\text{O}$ was first impregnated into the supports (cornhusk-derived-silica and commercial silica) at 235 °C and dried at 90 °C overnight. The impregnated supports containing CeO_2 were subsequently calcined at 450 °C at a heating rate of 5 °C/min for 2 h.

Hereafter, the resultant $\text{CeO}_2/\text{SiO}_2$ mixture was impregnated with an aqueous solution of $\text{Pd}(\text{NO}_3)_2 \cdot 2\text{H}_2\text{O}$. The Pd loading on the supports was controlled to yield 1 wt.% of Pd in the final catalysts. Finally, the catalyst precursors were dried at 120 °C for 12 h and calcined at 500 °C for 1 h at 10 °C /min heating ramp. Synthesized catalysts were designated as Pd/CeO₂/CHSiO₂ and Pd/CeO₂/commercial to represent the catalysts impregnated on cornhusk and commercial silica, respectively.

3.6 Catalytic Activity Tests for Methane Combustion

The catalytic performance of the synthesized catalysts was tested in a temperature-controlled catalytic flow reactor (stainless steel V4A, Ø12 mm), as shown in Figure 3.1.

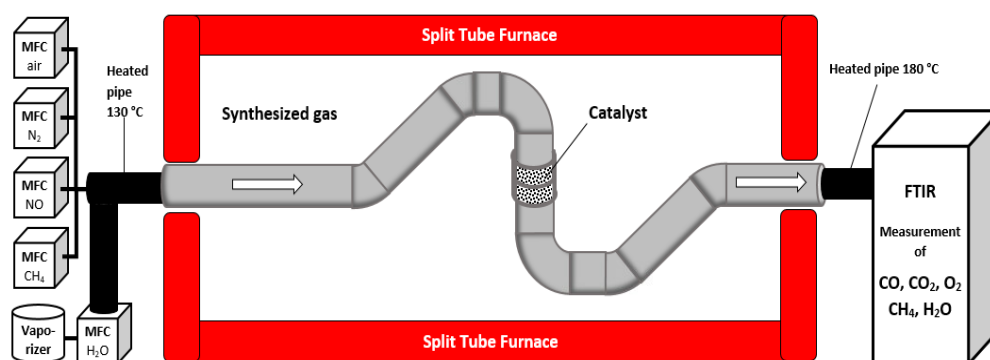


Figure 3.1. Experimental set-up for methane catalytic activity. Modified from König [154].
MFC: Mass Flow Controller

A total of 0.2 g of the synthesized catalysts was mixed with 1.2 g of corundum (inert material) and packed into the reactor tube supported on a quartz wool bed. The amount of inert material mixed with the catalyst was chosen to fill a 7 cm length in the catalyst bed. Light-off tests were carried out by heating the catalyst stepwise from RT to 600 °C (10 °C /min heating ramp) under 70 mL/min flow of a simulated synthetic flue gas mixture containing 800–1000 ppm CH₄, 1528 ppm CO, 207 ppm NO, 10 vol.% CO₂, 6 vol.% O₂ balanced with N₂ (dry condition), or a mixture of above compositions + 12 vol.% H₂O (wet

condition). For each activity run, a gas hourly space velocity (GSHV) of $87,000 \text{ mLg}^{-1} \text{ h}^{-1}$ was used. The conversion of methane (X_{CH_4}) was calculated using Equation 3.1:

$$X_{CH_4}(\%) = \frac{[CH_4]_{t=0} - [CH_4]_t}{[CH_4]_{t=0}} \times 100 \quad 3.1$$

Where $[CH_4]_{t=0}$ and $[CH_4]_t$ refer to the CH_4 concentrations during the start and end of the combustion process, respectively.

The catalytic activities of the catalysts were evaluated based on the temperature at which 50% conversion of methane was achieved ($T_{50\%}$). Kinetic studies were conducted with methane conversion values $\leq 10\%$ to exclude the effects of mass and heat transfer limitations. The stability tests or time-on-stream of the catalysts were performed by maintaining the samples at $500 \text{ }^\circ\text{C}$ for 10 h on stream in the catalytic flow reactor.

3.7 Analysis of Physical and Chemical Properties of Fuels, Ashes and Catalysts

According to the standard analytic characterizations for solid biofuels [155], untreated and acid-leached fuels were analyzed by measuring moisture content (MC), ash content (AC), volatile matter (VM), and elemental composition of the fuel. The elemental composition of the fuel ashes was also determined using inductively coupled plasma-optical emission spectroscopy (ICP-OES) in accordance with DIN EN ISO 16967;2015-07, DIN EN ISO 1 [156]. Each analysis was conducted in duplicate to ensure accuracy, and the mean results were reported. In brief, the fuels were digested in a mixture of 8 ml of nitric acid (65%), 2 ml of HF (48%), and 6 ml of hydrogen peroxide (30%). Then, the solution was diluted with ultra-pure water in the ratio of 1:10 prior to the analysis. The chemical composition spectrum of the ash samples was also analyzed using energy-dispersive X-ray fluorescence spectroscopy (EDX) (Bruker, Massachusetts, USA) to complement the results of the ICP-OES. The carbon content (CC) of the samples was estimated indirectly from the Loss of ignition (LOI) data by combusting the biomass fuels or ash samples at $550 \text{ }^\circ\text{C}$ per DIN EN 15935.

Fourier-transform infrared spectroscopy (FTIR) is an analytical method that measures light absorption by matter over a range of frequencies using an FTIR-spectrometer (Spectrum Two, PerkinElmer, Solingen, Germany). This technique was employed in **Articles I-II** to identify the primary organic compounds and various functional groups present in the ashes and raw biomass fuels. The spectrum scope was 400–4000 cm^{-1} with a resolution factor of 1 cm^{-1} .

Gas sorption technique is used to measure surface area, porosity, and other properties of a material by exerting a pressure of a gas on the material. The sample is exposed to a stream of a known gas, such as nitrogen, while measuring the amount of gas that is absorbed by the material at various pressures and temperatures. The amount of gas absorbed by the material can be used to calculate the surface area, pore size distribution, and other characteristics of the material. Brunauer-Emmett-Teller (BET) can also be used to determine the surface area of more extensive materials, including powders, catalysts and fibrous materials. The isotherm data allow for the calculation using the Barrett-Joyner-Hallenda method (BJH) and the Density Functional Theory (DFT) to determine pore volumes of the biogenic silica. Previously, the BJH was widely used for the determination of the pore volume of materials based on the Kelvin equation. However, recent publications have revealed the limitations associated with this method as it underestimates pores by 20-30% for pore widths less than 10 nm. Thus, the DFT method is currently adopted to estimate the pore volume of materials to overcome this limitation in this dissertation [157].

In **Articles I-III**, the textural properties of the samples (ashes and the catalysts) were examined using an autosorb iQ-MP/XR apparatus (Quantachrome, USA). The samples (0.1–0.3 g) were subjected to degassing by heating at 250 °C under vacuum (ca. 0.4 kPa) for 10 h to eliminate non-dissociative, physically adsorbed water molecules from the sample surface and within the pores. The BET surface area was determined by fitting the adsorption data to the BET equation within the relative pressure range of $(p/p_0) = 0.05–0.30$. Nitrogen gas was used as the adsorptive gas at 77 K, with a standard value of 0.162 nm^2 for the molecular cross-section of nitrogen. The total pore volume was determined at a relative pressure $(p/p_0) = 0.98$. Pore characteristics were calculated using indirect molecular adsorption methods such as nonlocal density functional theory (NLDFT).

In **Articles I-III**, X-ray diffraction (XRD) was employed to analyze the amorphous or crystalline phases in the ash and silica particles. This analysis was conducted using a Malvern Panalytical GmbH XRD instrument equipped with Ni-filtered Cu-K_α radiation ($\lambda =$

1.54 Å). To prepare the samples for measurement, they were coated onto glass substrates and assessed using a Rigaku XRD instrument (Rigaku, Japan) operating at a voltage of 40 kV and a current of 30 mA, with a nickel monochromator filtering wave at a tube voltage of 40 kV and a tube current of 30 mA.

Visual documentation of the ashes and silica nanoparticles was captured in **Articles I-II** after the combustion and sol-gel processes using a Canon EOS 250D camera (Canon Ltd., Krefeld, Germany). All images were taken simultaneously under natural light conditions without using flash.

Thermogravimetric Analysis (TGA) is a type of thermal analysis used to study the physical and chemical properties of materials subjected to a controlled temperature program. TGA measures the change in mass of a material as a function of temperature or time. The data can then be analyzed to determine the weight changes in the sample over the temperature range and the derivatives of those changes, such as the rate of weight change and the total weight change. In **Article I-II**, thermal degradation procedures were conducted using a simultaneous thermal analysis (STA 449 F3 Jupiter®, NETZSCH, Selb, Germany) in a synthetic air flow atmosphere with a flow rate of 100 mL/min, employing a heating rate of 10 K/min. Alumina crucibles were used to hold approximately 10–20 mg of the samples, heated from room temperature to 600 °C. To ensure uniformity in the starting material for the STA analysis, each biomass fuel was ground to a particle size of less than 0.5 mm using a cutting mill (IKATM MF 10 basic Mikrofeinmühle) and vigorously mixed in a plastic box. The thermogravimetric (TG) and derivative thermogravimetric (DTG) curves were simultaneously recorded as the temperature increased.

In **Article III**, the redox properties of the catalysts were measured by employing hydrogen temperature programmed reduction (H₂-TPR) experiments with an AC 2920 equipped with a CryColler unit (Mircomertics, Waltham, MA, USA). The experiments were performed after the following protocol: 80 to 100 mg of each sample was preheated to 500 °C for 30 min in synthetic air (50 mL/min, 20 °C /min). The measurement was started after cooling down to -20 °C. Each sample was heated up to 800 °C in a mixture of 5% H₂ in Ar (20 mL/min, 5 °C/min), and the reduction was performed for 30 min. An online thermal conductivity detector was used to measure the hydrogen consumption throughout the experiment. The amount of H₂ consumption was calculated after calibration of the thermal conductivity detector (TCD).

Scanning electron microscopy (SEM) measurements were performed to observe the morphology of the synthesized catalysts in **Article III**. Samples were analyzed by a field emission scanning electron microscope (SEM, MERLIN[®] VP Compact, Co. Zeiss, Oberkochen, Germany) equipped with an energy dispersive X-ray (EDX) detector (XFlash 6/30, Co. Bruker, Berlin, Germany).

Representative areas of samples in **Articles I** and **III** were analyzed and mapped for elemental distribution based on EDX-spectra data by QUANTAX ESPRIT Microanalysis software (version 2.0). Samples were mounted on a heavy metal-free Al-SEM-carrier (co. PLANO, Wetzlar, Germany) with adhesive conductive carbon tape (Spectro Tabs, TED PELLA INC, Redding, CA, USA) and coated with carbon (5.0 nm thickness) under vacuum (CCU 010 HV-Coating Unit, Co. Safematic GmbH, Zizers, Switzerland). SEM images were taken from the selected regions with the conditions of an applied detector, accelerating voltage, and working distance indicated on the SEM micrographs. Table 3.1 summarizes the various analytical methods employed in this dissertation.

Table 3.1. Summary of analysis methods employed in Articles I-III

Article	Article I	Article II	Article III
Sample	Ashes	Silica xerogel	Catalyst
Analysis	<ul style="list-style-type: none"> • ICP-OES • FTIR • Gas sorption • XRD • STA • Visual image • CC (LOI) 	<ul style="list-style-type: none"> • ICP-OES • FTIR • Gas sorption • XRD • STA • Visual image 	<ul style="list-style-type: none"> • ICP-OES • FTIR • SEM/EDX • H₂-TPR

References of Chapters 1-3

- [1] Methane Abatement - Energy System - IEA. [July 25, 2023]; Available from: <https://www.iea.org/energy-system/fossil-fuels/methane-abatement>.
- [2] EPA US, OAR. Importance of Methane | US EPA. [July 21, 2023]; Available from: <https://www.epa.gov/gmi/importancemethane#:~:text=Methane%20is%20more%20than%2025,dueto%20human%2Drelated%20activities>.
- [3] SoCalGas Methane and the Environment <https://www.socalgas.com/stay-safe/methane-emissions/methane-and-the-environment> (accessed on August 29, 2023).
- [4] Bestel D, Bayliff S, Xu H, Marchese A, Olsen D, Windom B. Investigation of the end-gas autoignition process in natural gas engines and evaluation of the methane number index. *Proceedings of the Combustion Institute* 2021;38(4):5839–47. <https://doi.org/10.1016/j.proci.2020.07.106>.
- [5] Lebel ED, Finnegan CJ, Ouyang Z, Jackson RB. Methane and NO_x Emissions from Natural Gas Stoves, Cooktops, and Ovens in Residential Homes. *Environ Sci Technol* 2022;56(4):2529–39. <https://doi.org/10.1021/acs.est.1c04707>.
- [6] Karakurt I, Aydin G, Aydiner K. Sources and mitigation of methane emissions by sectors: A critical review. *Renewable Energy* 2012;39(1):40–8. <https://doi.org/10.1016/j.renene.2011.09.006>.
- [7] Dedysh SN, Knief C, Dunfield PF. *Methylocella* species are facultatively methanotrophic. *J Bacteriol* 2005;187(13):4665–70. <https://doi.org/10.1128/JB.187.13.4665-4670.2005>.
- [8] Månberger A. Reduced Use of Fossil Fuels can Reduce Supply of Critical Resources. *Biophysical Economics and Sustainability* 2021;6(2):6. <https://doi.org/10.1007/s41247-021-00088-5>.
- [9] Baldwin TR, Burch* R. Catalytic combustion of methane over supported palladium catalysts. *Applied Catalysis* 1990;66(1):359–81. [https://doi.org/10.1016/s0166-9834\(00\)81649-8](https://doi.org/10.1016/s0166-9834(00)81649-8).
- [10] Xiao L, Sun K, Xu X, Li X. Low-temperature catalytic combustion of methane over Pd/CeO₂ prepared by deposition–precipitation method. *Catalysis Communications* 2005;6(12):796–801. <https://doi.org/10.1016/j.catcom.2005.07.015>.

- [11] Senanayake SD, Rodriguez JA, Weaver JF. Low Temperature Activation of Methane on Metal-Oxides and Complex Interfaces: Insights from Surface Science. *Acc Chem Res* 2020;53(8):1488–97. <https://doi.org/10.1021/acs.accounts.0c00194>.
- [12] Ismagilov ZR, Kerzhentsev MA, Susharina TL. Catalytic methods for lowering the amount of nitrogen oxides in exhaust gases on combustion of fuel. *Russ. Chem. Rev.* 1990;59(10):973–88. <https://doi.org/10.1070/RC1990v059n10ABEH003570>.
- [13] Tripathi G, Sharma P, Dhar A. Effect of methane augmentations on engine performance and emissions. *Alexandria Engineering Journal* 2020;59(1):429–39. <https://doi.org/10.1016/j.aej.2020.01.012>.
- [14] Yuvaraja R, Nanthakumar K, Dhasahinamoorthi G. Development and Performance Analysis of New Catalytic Converter. *International Journal of Applications in Mechanical and Production Engineering* Volume 2015;1.
- [15] Leman AM, Jajuli A, Feriyanto D, Rahman F, Zakaria S, Hasan A et al. Advanced Catalytic Converter in Gasoline Engine Emission Control: A Review. *MATEC Web Conf.* 2017;87(3):2020. <https://doi.org/10.1051/mateconf/20178702020>.
- [16] Hasnan NSN, Timmiati SN, Lim KL, Yaakob Z, Kamaruddin NHN, Teh LP. Recent developments in methane decomposition over heterogeneous catalysts: An overview. *Mater Renew Sustain Energy* 2020;9(2):1259. <https://doi.org/10.1007/s40243-020-00167-5>.
- [17] Takigawa A, Matsunami A, Arai N. Methane emission from automobile equipped with three-way catalytic converter while driving. *Energy* 2005;30(2):461–73. <https://doi.org/10.1016/j.energy.2004.04.016>.
- [18] Choudhary T, Goodman D. Methane activation on Ni and Ru model catalysts. *Journal of Molecular Catalysis A: Chemical* 2000;163(1-2):9–18. [https://doi.org/10.1016/s1381-1169\(00\)00395-2](https://doi.org/10.1016/s1381-1169(00)00395-2).
- [19] Eguchi K, Arai H. Low temperature oxidation of methane over Pd-based catalysts—effect of support oxide on the combustion activity. *Applied Catalysis A: General* 2001;222(1-2):359–67. [https://doi.org/10.1016/S0926-860X\(01\)00843-2](https://doi.org/10.1016/S0926-860X(01)00843-2).
- [20] Valdebenito G, González-Carvajal M, Santibañez L, Cancino P. Metal–Organic Frameworks (MOFs) and Materials Derived from MOFs as Catalysts for the

- Development of Green Processes. *Catalysts* 2022;12(2):136. <https://doi.org/10.3390/catal12020136>.
- [21] Zheng T, He J, Zhao Y, Xia W, He J. Precious metal-support interaction in automotive exhaust catalysts. *Journal of Rare Earths* 2014;32(2):97–107. [https://doi.org/10.1016/S1002-0721\(14\)60038-7](https://doi.org/10.1016/S1002-0721(14)60038-7).
- [22] Raynes S, Shah MA, Taylor RA. Direct conversion of methane to methanol with zeolites: Towards understanding the role of extra-framework d-block metal and zeolite framework type. *Dalton Trans* 2019;48(28):10364–84. <https://doi.org/10.1039/c9dt00922a>.
- [23] Persson K, Ersson A, Jansson K, Fierro J, Jaras S. Influence of molar ratio on Pd–Pt catalysts for methane combustion. *Journal of Catalysis* 2006;243(1):14–24. <https://doi.org/10.1016/j.jcat.2006.06.019>.
- [24] Hoffmann M, Kreft S, Georgi G, Fulda G, Pohl M-M, Seeburg D et al. Improved catalytic methane combustion of Pd/CeO₂ catalysts via porous glass integration. *Applied Catalysis B: Environmental* 2015;179:313–20. <https://doi.org/10.1016/j.apcatb.2015.05.028>.
- [25] Wang B, Dai B, Zhu M. Application of Fumed Silica as a Support during Oxidative Desulfurization. *ACS Omega* 2020;5(1):378–85. <https://doi.org/10.1021/acsomega.9b02802>.
- [26] Liu D, Seeburg D, Kreft S, Bindig R, Hartmann I, Schneider D et al. Rice Husk Derived Porous Silica as Support for Pd and CeO₂ for Low Temperature Catalytic Methane Combustion. *Catalysts* 2019;9(1):26. <https://doi.org/10.3390/catal9010026>.
- [27] Wegner K, Pratsinis SE. Scale-up of nanoparticle synthesis in diffusion flame reactors. *Chemical Engineering Science* 2003;58(20):4581–9. <https://doi.org/10.1016/j.ces.2003.07.010>.
- [28] Petermann N, Stein N, Schierning G, Theissmann R, Stoib B, Brandt MS et al. Plasma synthesis of nanostructures for improved thermoelectric properties. *J. Phys. D: Appl. Phys.* 2011;44(17):174034. <https://doi.org/10.1088/0022-3727/44/17/174034>.
- [29] Hülser T, Schnurre SM, Wiggers H, Schulz C. Gas-Phase Synthesis of Nanoscale Silicon as an Economical Route towards Sustainable Energy Technology. *KONA* 2011;29(0):191–207. <https://doi.org/10.14356/kona.2011021>.

- [30] Kim KD, Kim HT. Formation of Silica Nanoparticles by Hydrolysis of TEOS Using a Mixed Semi-Batch/Batch Method. *J Sol-Gel Sci Technol* 2002;25(3):183–9. <https://doi.org/10.1023/A:1020217105290>.
- [31] Soltani N, Bahrami A, Pech-Canul MI, González LA. Review on the physicochemical treatments of rice husk for production of advanced materials. *Chemical Engineering Journal* 2015;264:899–935. <https://doi.org/10.1016/j.cej.2014.11.056>.
- [32] Denise Schneider. Biogenic Silica from Regional Feedstocks—Sustainable Synthesis and Characterization.
- [33] Zemnukhova LA, Egorov AG, Fedorishcheva GA, Barinov NN, Sokol'nitskaya TA, Botsul AI. Properties of amorphous silica produced from rice and oat processing waste. *Inorg Mater* 2006;42(1):24–9. <https://doi.org/10.1134/S0020168506010067>.
- [34] Maseko NN, Schneider D, Wassersleben S, Enke D, Iwarere SA, Pocock J et al. The Production of Biogenic Silica from Different South African Agricultural Residues through a Thermo-Chemical Treatment Method. *Sustainability* 2021;13(2):577. <https://doi.org/10.3390/su13020577>.
- [35] Beidaghy Dizaji H, Zeng T, Hartmann I, Enke D, Schliermann T, Lenz V et al. Generation of High Quality Biogenic Silica by Combustion of Rice Husk and Rice Straw Combined with Pre- and Post-Treatment Strategies—A Review. *Applied Sciences* 2019;9(6):1083. <https://doi.org/10.3390/app9061083>.
- [36] Alyosef HA, Eilert A, Welscher J, Ibrahim SS, Denecke R, Schwieger W et al. Characterization of Biogenic Silica Generated by Thermo Chemical Treatment of Rice Husk. *Particulate Science and Technology* 2013;31(5):524–32. <https://doi.org/10.1080/02726351.2013.782931>.
- [37] Pode R. Potential applications of rice husk ash waste from rice husk biomass power plant. *Renewable and Sustainable Energy Reviews* 2016;53(3):1468–85. <https://doi.org/10.1016/j.rser.2015.09.051>.
- [38] Liou T-H. Preparation and characterization of nano-structured silica from rice husk. *Materials Science and Engineering: A* 2004;364(1-2):313–23. <https://doi.org/10.1016/j.msea.2003.08.045>.

- [39] Vaibhav V, Vijayalakshmi U, Roopan SM. Agricultural waste as a source for the production of silica nanoparticles. *Spectrochim Acta A Mol Biomol Spectrosc* 2015;139:515–20. <https://doi.org/10.1016/j.saa.2014.12.083>.
- [40] Kim H, Kim K, Kim H, Lee DJ, Park J. Eco-Friendly Synthesis of Water-Glass-Based Silica Aerogels via Catechol-Based Modifier. *Nanomaterials (Basel)* 2020;10(12). <https://doi.org/10.3390/nano10122406>.
- [41] van Tuan N, Ye G, van Breugel K, Copuroglu O. Hydration and microstructure of ultra-high-performance concrete incorporating rice husk ash. *Cement and Concrete Research* 2011;41(11):1104–11. <https://doi.org/10.1016/j.cemconres.2011.06.009>.
- [42] Ahmed MN, Ram RN. Removal of basic dye from waste-water using silica as adsorbent. *Environ Pollut* 1992;77(1):79–86. [https://doi.org/10.1016/0269-7491\(92\)90161-3](https://doi.org/10.1016/0269-7491(92)90161-3).
- [43] Qiu Y, Yang Y, Yang N, Tong L, Yin S, Wang L et al. Thermochemical energy storage using silica gel: Thermal storage performance and nonisothermal kinetic analysis. *Solar Energy Materials and Solar Cells* 2023;251:112153. <https://doi.org/10.1016/j.solmat.2022.112153>.
- [44] Chandrasekhar S, Pramada PN, Praveen L. Effect of organic acid treatment on the properties of rice husk silica. *J Mater Sci* 2005;40(24):6535–44. <https://doi.org/10.1007/s10853-005-1816-z>.
- [45] Shen Y, Zhao P, Shao Q. Porous silica and carbon derived materials from rice husk pyrolysis char. *Microporous and Mesoporous Materials* 2014;188:46–76. <https://doi.org/10.1016/j.micromeso.2014.01.005>.
- [46] Junko Umeda, Katsuyoshi Kondoh and Yoshisada Michiura. Process Parameters Optimization in Preparing High-Purity Amorphous Silica Originated from Rice Husks.
- [47] Long J, Song H, Jun X, Sheng S, Lun-Shi S, Kai X et al. Release characteristics of alkali and alkaline earth metallic species during biomass pyrolysis and steam gasification process. *Bioresour Technol* 2012; 116:278–84. <https://doi.org/10.1016/j.biortech.2012.03.051>.
- [48] Beidaghy Dizaji H, Zeng T, Hölzig H, Bauer J, Klöß G, Enke D. Ash transformation mechanism during combustion of rice husk and rice straw. *Fuel* 2022;307(1):121768. <https://doi.org/10.1016/j.fuel.2021.121768>.

- [49] Duku MH, Gu S, Hagan EB. A comprehensive review of biomass resources and biofuels potential in Ghana. *Renewable and Sustainable Energy Reviews* 2011;15(1):404–15. <https://doi.org/10.1016/j.rser.2010.09.033>.
- [50] Rice FL, Park R, Stayner L, Smith R, Gilbert S, Checkoway H. Crystalline silica exposure and lung cancer mortality in diatomaceous earth industry workers: a quantitative risk assessment. *Occup Environ Med* 2001;58(1):38–45. <https://doi.org/10.1136/oem.58.1.38>.
- [51] Ricciardolo FLM, Sterk PJ, Gaston B, Folkerts G. Nitric oxide in health and disease of the respiratory system. *Physiol Rev* 2004;84(3):731–65. <https://doi.org/10.1152/physrev.00034.2003>.
- [52] Beidaghy Dizaji H, Zeng T, Lenz V, Enke D. Valorization of Residues from Energy Conversion of Biomass for Advanced and Sustainable Material Applications. *Sustainability* 2022;14(9):4939. <https://doi.org/10.3390/su14094939>.
- [53] Kaltschmitt M, Hartmann H, Hofbauer H (eds.). *Energie aus Biomasse: Grundlagen, Techniken und Verfahren / Martin Kaltschmitt, Hans Hartmann, Hermann Hofbauer, Herausgeber. 3rd ed. Berlin: Springer Vieweg; 2016.*
- [54] Kleemann M, Meliss M. *Regenerative Energiequellen: Mit 75 Tab. 2nd ed. Berlin: Springer; 2003.*
- [55] Lee SH, Lee TH, Jeong SM, Lee JM. Economic analysis of a 600 mwe ultra supercritical circulating fluidized bed power plant based on coal tax and biomass co-combustion plans. *Renewable Energy* 2019;138:121–7. <https://doi.org/10.1016/j.renene.2019.01.074>.
- [56] Zeng T, Mlonka-Mędrala A, Lenz V, Nelles M. Evaluation of bottom ash slagging risk during combustion of herbaceous and woody biomass fuels in a small-scale boiler by principal component analysis. *Biomass Conv. Bioref.* 2021;11(4):1211–29. <https://doi.org/10.1007/s13399-019-00494-2>.
- [57] Fernandes IJ, Calheiro D, Kieling AG, Moraes CA, Rocha TL, Brehm FA et al. Characterization of rice husk ash produced using different biomass combustion techniques for energy. *Fuel* 2016;165:351–9. <https://doi.org/10.1016/j.fuel.2015.10.086>.

- [58] Zhao X, Zhou H, Sikarwar VS, Zhao M, Park A-HA, Fennell PS et al. Biomass-based chemical looping technologies: The good, the bad and the future. *Energy Environ. Sci.* 2017;10(9):1885–910. <https://doi.org/10.1039/C6EE03718F>.
- [59] Rose M. *Catalysis for the Conversion of Biomass and its Derivatives*. (Max Planck Research Library for the History and Development of Knowledge.) Edited by Malte Behrens and Abhaya K. Datye. *Angew. Chem. Int. Ed.* 2013;52(37):9613. <https://doi.org/10.1002/anie.201305619>.
- [60] Mlonka-Mędrala A, Magdziarz A, Gajek M, Nowińska K, Nowak W. Alkali metals association in biomass and their impact on ash melting behaviour. *Fuel* 2020;261:116421. <https://doi.org/10.1016/j.fuel.2019.116421>.
- [61] Lopez-Velazquez MA, Santes V, Balmaseda J, Torres-Garcia E. Pyrolysis of orange waste: A thermo-kinetic study. *Journal of Analytical and Applied Pyrolysis* 2013;99(1):170–7. <https://doi.org/10.1016/j.jaap.2012.09.016>.
- [62] Ma Z, Chen D, Gu J, Bao B, Zhang Q. Determination of pyrolysis characteristics and kinetics of palm kernel shell using TGA–FTIR and model-free integral methods. *Energy Conversion and Management* 2015;89(3):251–9. <https://doi.org/10.1016/j.enconman.2014.09.074>.
- [63] Dhyani V, Bhaskar T. A comprehensive review on the pyrolysis of lignocellulosic biomass. *Renewable Energy* 2018;129:695–716. <https://doi.org/10.1016/j.renene.2017.04.035>.
- [64] Carrier M, Loppinet-Serani A, Denux D, Lasnier J-M, Ham-Pichavant F, Cansell F et al. Thermogravimetric analysis as a new method to determine the lignocellulosic composition of biomass. *Biomass and Bioenergy* 2011;35(1):298–307. <https://doi.org/10.1016/j.biombioe.2010.08.067>.
- [65] Mohan D, Pittman CU, Steele PH. Pyrolysis of Wood/Biomass for Bio-oil: A Critical Review. *Energy Fuels* 2006;20(3):848–89. <https://doi.org/10.1021/ef0502397>.
- [66] Ma JF, Yamaji N. Silicon uptake and accumulation in higher plants. *Trends Plant Sci* 2006;11(8):392–7. <https://doi.org/10.1016/j.tplants.2006.06.007>.
- [67] YAN G, Nikolic M, YE M, XIAO Z, LIANG Y. Silicon acquisition and accumulation in plant and its significance for agriculture. *Journal of Integrative Agriculture* 2018;17(10):2138–50. [https://doi.org/10.1016/S2095-3119\(18\)62037-4](https://doi.org/10.1016/S2095-3119(18)62037-4).

- [68] H. Beidaghy Dizaji. Ash-related aspects during thermochemical conversion of silica-rich biomass assortments: PhD Thesis, Faculty of Chemistry and Mineralogy, Leipzig University 2022.
- [69] Ngoc Nguyen M, Dultz S, Guggenberger G. Effects of pretreatment and solution chemistry on solubility of rice-straw phytoliths. *J. Plant Nutr. Soil Sci.* 2014;177(3):349–59. <https://doi.org/10.1002/jpln.201300056>.
- [70] Parr JF, Sullivan LA. Soil carbon sequestration in phytoliths. *Soil Biology and Biochemistry* 2005;37(1):117–24. <https://doi.org/10.1016/j.soilbio.2004.06.013>.
- [71] Chen W, Yao X, Cai K, Chen J. Silicon alleviates drought stress of rice plants by improving plant water status, photosynthesis and mineral nutrient absorption. *Biol Trace Elem Res* 2011;142(1):67–76. <https://doi.org/10.1007/s12011-010-8742-x>.
- [72] Mandlik R, Thakral V, Raturi G, Shinde S, Nikolić M, Tripathi DK et al. Significance of silicon uptake, transport, and deposition in plants. *J Exp Bot* 2020;71(21):6703–18. <https://doi.org/10.1093/jxb/eraa301>.
- [73] Ma JF, Tamai K, Yamaji N, Mitani N, Konishi S, Katsuhara M et al. A silicon transporter in rice. *Nature* 2006;440(7084):688–91. <https://doi.org/10.1038/nature04590>.
- [74] Schliermann T, Hartmann I, Beidaghy Dizaji H, Zeng T, Schneider D, Wassersleben S et al. High Quality Biogenic Silica from Combined Energetic and Material Utilization of Agricultural Residues; 2018.
- [75] Kan T, Strezov V, Evans TJ. Lignocellulosic biomass pyrolysis: A review of product properties and effects of pyrolysis parameters. *Renewable and Sustainable Energy Reviews* 2016;57:1126–40. <https://doi.org/10.1016/j.rser.2015.12.185>.
- [76] Krishnarao RV, Subrahmanyam J, Jagadish Kumar T. Studies on the formation of black particles in rice husk silica ash. *Journal of the European Ceramic Society* 2001;21(1):99–104. [https://doi.org/10.1016/S0955-2219\(00\)00170-9](https://doi.org/10.1016/S0955-2219(00)00170-9).
- [77] Suthabanditpong W, Takai C, Fuji M, Buntem R, Shirai T. Improved optical properties of silica/UV-cured polymer composite films made of hollow silica nanoparticles with a hierarchical structure for light diffuser film applications. *Phys Chem Chem Phys* 2016;18(24):16293–301. <https://doi.org/10.1039/c6cp01005a>.

- [78] Dagle VL, Flake MD, Lemmon TL, Lopez JS, Kovarik L, Dagle RA. Effect of the SiO₂ support on the catalytic performance of Ag/ZrO₂/SiO₂ catalysts for the single-bed production of butadiene from ethanol. *Applied Catalysis B: Environmental* 2018;236:576–87. <https://doi.org/10.1016/j.apcatb.2018.05.055>.
- [79] Shen Y. Rice husk silica derived nanomaterials for sustainable applications. *Renewable and Sustainable Energy Reviews* 2017;80:453–66. <https://doi.org/10.1016/j.rser.2017.05.115>.
- [80] Heidenreich S, Müller M, Foscolo PU. Biomass Pretreatment. In: *Advanced Biomass Gasification*. Elsevier; 2016, p. 11–17.
- [81] Beidaghy Dizaji H, Zeng T, Enke D. New fuel indexes to predict ash behavior for biogenic silica production. *Fuel* 2022;310:122345. <https://doi.org/10.1016/j.fuel.2021.122345>.
- [82] Zareihassangheshlaghi A, Beidaghy Dizaji H, Zeng T, Huth P, Ruf T, Denecke R et al. Behavior of Metal Impurities on Surface and Bulk of Biogenic Silica from Rice Husk Combustion and the Impact on Ash-Melting Tendency. *ACS Sustainable Chem. Eng.* 2020;8(28):10369–79. <https://doi.org/10.1021/acssuschemeng.0c01484>.
- [83] Morales-Paredes CA, Rodríguez-Linzán I, Saquete MD, Luque R, Osman SM, Boluda-Botella N et al. Silica-derived materials from agro-industrial waste biomass: Characterization and comparative studies. *Environmental Research* 2023;231:116002. <https://doi.org/10.1016/j.envres.2023.116002>.
- [84] Moroz IK, Maslennikova GN. Thermal transformations of silica (review). *Glass Ceram* 1985;42(12):559–64. <https://doi.org/10.1007/BF00697696>.
- [85] Lee JH, Kwon JH, Lee J-W, Lee H, Chang JH, Sang B-I. Preparation of high purity silica originated from rice husks by chemically removing metallic impurities. *Journal of Industrial and Engineering Chemistry* 2017;50(2):79–85. <https://doi.org/10.1016/j.jiec.2017.01.033>.
- [86] Kamath SR, Proctor A. Silica Gel from Rice Hull Ash: Preparation and Characterization. *Cereal Chemistry Journal* 1998;75(4):484–7. <https://doi.org/10.1094/CCHEM.1998.75.4.484>.

- [87] Chakraverty A, Mishra P, Banerjee HD. Investigation of combustion of raw and acid-leached rice husk for production of pure amorphous white silica. *J Mater Sci* 1988;23(1):21–4. <https://doi.org/10.1007/BF01174029>.
- [88] Jiang L, Hu S, Sun L-S, Su S, Xu K, He L-M et al. Influence of different demineralization treatments on physicochemical structure and thermal degradation of biomass. *Bioresour Technol* 2013;146:254–60. <https://doi.org/10.1016/j.biortech.2013.07.063>.
- [89] Zhu H, Liao Q, Hu L, Xie L, Qu B, Gao R. Effect of removal of alkali and alkaline earth metals in cornstalk on slagging/fouling and co-combustion characteristics of cornstalk/coal blends for biomass applications. *Renewable Energy* 2023;207:275–85. <https://doi.org/10.1016/j.renene.2023.03.022>.
- [90] Das P, Ganesh A, Wangikar P. Influence of pretreatment for deashing of sugarcane bagasse on pyrolysis products. *Biomass and Bioenergy* 2004;27(5):445–57. <https://doi.org/10.1016/j.biombioe.2004.04.002>.
- [91] Karimi K, Taherzadeh MJ. A critical review of analytical methods in pretreatment of lignocelluloses: Composition, imaging, and crystallinity. *Bioresour Technol* 2016;200:1008–18. <https://doi.org/10.1016/j.biortech.2015.11.022>.
- [92] Baruah J, Nath BK, Sharma R, Kumar S, Deka RC, Baruah DC et al. Recent Trends in the Pretreatment of Lignocellulosic Biomass for Value-Added Products. *Front. Energy Res.* 2018;6. <https://doi.org/10.3389/fenrg.2018.00141>.
- [93] Shen J, Liu X, Zhu S, Zhang H, Tan J. Effects of calcination parameters on the silica phase of original and leached rice husk ash. *Materials Letters* 2011;65(8):1179–83. <https://doi.org/10.1016/j.matlet.2011.01.034>.
- [94] Liou T-H, Yang C-C. Synthesis and surface characteristics of nanosilica produced from alkali-extracted rice husk ash. *Materials Science and Engineering: B* 2011;176(7):521–9. <https://doi.org/10.1016/j.mseb.2011.01.007>.
- [95] Gholizadeh Vayghan A, Khaloo AR, Rajabipour F. The effects of a hydrochloric acid pre-treatment on the physicochemical properties and pozzolanic performance of rice husk ash. *Cement and Concrete Composites* 2013;39:131–40. <https://doi.org/10.1016/j.cemconcomp.2013.03.022>.

- [96] Ajeel Sa, Sukkar KA, Zedin NK. Extraction of high purity amorphous silica from rice husk by chemical process. *IOP Conf. Ser.: Mater. Sci. Eng.* 2020;881(1):12096. <https://doi.org/10.1088/1757-899X/881/1/012096>.
- [97] Umeda J, Kondoh K. High-purity amorphous silica originated in rice husks via carboxylic acid leaching process. *J Mater Sci* 2008;43(22):7084–90. <https://doi.org/10.1007/s10853-008-3060-9>.
- [98] Hartmann H, Strehler A. Die Stellung der Biomasse: Im Vergleich zu anderen erneuerbaren Energieträgern aus ökologischer, ökonomischer und technischer Sicht ; Abschlußbericht für das Bundesministerium für Ernährung, Landwirtschaft und Forsten (BML) ; Abschlußbericht für das Bundesministerium für Ernährung, Landwirtschaft und Forsten (BML). Münster: Landwirtschaftsverl; 1995.
- [99] Kristoferson LA, Bokalders V. Briquetting of biomass. In: Kristoferson LA, Bokalders V, editors. *Renewable Energy Technologies*. Pergamon; 1986, p. 43–51.
- [100] Nunes LJR, Oliveira Matias JC de, Da Silva Catalão JP. Chapter 4 - Additional Processes. In: Nunes LJR, Oliveira Matias JC de, Da Silva Catalão JP, editors. *Torrefaction of Biomass for Energy Applications*. Academic Press; 2018, p. 125–141.
- [101] Schneider D, Kircheis R, Wassersleben S, Einicke W-D, Gläser R, Enke D. Low-Cost Microwave-Assisted Partial Pseudomorphic Transformation of Biogenic Silica. *Front Chem* 2019;7:575. <https://doi.org/10.3389/fchem.2019.00575>.
- [102] Ahmad F, Salem-Bekhit MM, Khan F, Alshehri S, Khan A, Ghoneim MM et al. Unique Properties of Surface-Functionalized Nanoparticles for Bio-Application: Functionalization Mechanisms and Importance in Application. *Nanomaterials (Basel)* 2022;12(8). <https://doi.org/10.3390/nano12081333>.
- [103] Sun S-N, Wei C, Zhu Z-Z, Hou Y-L, Venkatraman SS, Xu Z-C. Magnetic iron oxide nanoparticles: Synthesis and surface coating techniques for biomedical applications. *Chinese Phys. B* 2014;23(3):37503. <https://doi.org/10.1088/1674-1056/23/3/037503>.
- [104] McNamara K, Tofail SAM. Nanosystems: the use of nanoalloys, metallic, bimetallic, and magnetic nanoparticles in biomedical applications. *Phys Chem Chem Phys* 2015;17(42):27981–95. <https://doi.org/10.1039/c5cp00831j>.

- [105] Dai H, Yang J, Ma J, Chen F, Fei Z, Zhong M. A green process for the synthesis of controllable mesoporous silica materials. *Microporous and Mesoporous Materials* 2012;147(1):281–5. <https://doi.org/10.1016/j.micromeso.2011.06.029>.
- [106] Alyosef HA, Roggendorf H, Schneider D, Inayat A, Welscher J, Schwieger W et al. Comparative Study between Direct and Pseudomorphic Transformation of Rice Husk Ash into MFI-Type Zeolite. *Molecules* 2017;23(1). <https://doi.org/10.3390/molecules23010001>.
- [107] Hench LL, West JK. The sol-gel process. *Chem. Rev.* 1990;90(1):33–72. <https://doi.org/10.1021/cr00099a003>.
- [108] Mackenzie JD, Bescher EP. Chemical routes in the synthesis of nanomaterials using the sol-gel process. *Acc Chem Res* 2007;40(9):810–8. <https://doi.org/10.1021/ar7000149>.
- [109] Dubey RS, Rajesh Y, More MA. Synthesis and Characterization of SiO₂ Nanoparticles via Sol-gel Method for Industrial Applications. *Materials Today: Proceedings* 2015;2(4-5):3575–9. <https://doi.org/10.1016/j.matpr.2015.07.098>.
- [110] Moncada E, Quijada R, Retuert J. Nanoparticles prepared by the sol–gel method and their use in the formation of nanocomposites with polypropylene. *Nanotechnology* 2007;18(33):335606. <https://doi.org/10.1088/0957-4484/18/33/335606>.
- [111] Falk G, Shinhe GP, Teixeira LB, Moraes EG, Oliveira AN de. Synthesis of silica nanoparticles from sugarcane bagasse ash and nano-silicon via magnesiothermic reactions. *Ceramics International* 2019;45(17):21618–24. <https://doi.org/10.1016/j.ceramint.2019.07.157>.
- [112] Saravanan K, Yuvakkumar R, Rajendran V, Paramasivam P. Influence of sintering temperature and pH on the phase transformation, particle size and anti-reflective properties of RHA nano silica powders. *Phase Transitions* 2012;85(12):1109–24. <https://doi.org/10.1080/01411594.2012.671322>.
- [113] Shim J, Velmurugan P, Oh B-T. Extraction and physical characterization of amorphous silica made from corn cob ash at variable pH conditions via sol gel processing. *Journal of Industrial and Engineering Chemistry* 2015;30:249–53. <https://doi.org/10.1016/j.jiec.2015.05.029>.

- [114] Kalapathy U. A simple method for production of pure silica from rice hull ash. *Bioresour Technol* 2000;73(3):257–62. [https://doi.org/10.1016/S0960-8524\(99\)00127-3](https://doi.org/10.1016/S0960-8524(99)00127-3).
- [115] Owens GJ, Singh RK, Foroutan F, Alqaysi M, Han C-M, Mahapatra C et al. Sol–gel based materials for biomedical applications. *Progress in Materials Science* 2016;77(Suppl. 2):1–79. <https://doi.org/10.1016/j.pmatsci.2015.12.001>.
- [116] Schlögl R. Heterogeneous catalysis. *Angew Chem Int Ed Engl* 2015;54(11):3465–520. <https://doi.org/10.1002/anie.201410738>.
- [117] Gold V (ed.). *The IUPAC Compendium of Chemical Terminology*. Research Triangle Park, NC: International Union of Pure and Applied Chemistry (IUPAC); 2019.
- [118] Li C, Baek J-B. Recent Advances in Noble Metal (Pt, Ru, and Ir)-Based Electrocatalysts for Efficient Hydrogen Evolution Reaction. *ACS Omega* 2020;5(1):31–40. <https://doi.org/10.1021/acsomega.9b03550>.
- [119] Fu G, Xu X, Lu X, Wan H. Mechanisms of methane activation and transformation on molybdenum oxide based catalysts. *J Am Chem Soc* 2005;127(11):3989–96. <https://doi.org/10.1021/ja0441099>.
- [120] van Giezen JC, van den Berg FR, Kleinen JL, van Dillen AJ, Geus JW. The effect of water on the activity of supported palladium catalysts in the catalytic combustion of methane. *Catalysis Today* 1999;47(1-4):287–93. [https://doi.org/10.1016/S0920-5861\(98\)00309-5](https://doi.org/10.1016/S0920-5861(98)00309-5).
- [121] Atkins PW, Ratcliffe RG, Wormald MR, Paula J de. *Physical chemistry for the life sciences*. New York NY: Oxford University Press; 2023.
- [122] Vassalini I, Alessandri I. Switchable Stimuli-Responsive Heterogeneous Catalysis. *Catalysts* 2018;8(12):569. <https://doi.org/10.3390/catal8120569>.
- [123] Enke D, Gläser R, Tallarek U. Sol-Gel and Porous Glass-Based Silica Monoliths with Hierarchical Pore Structure for Solid-Liquid Catalysis. *Chemie Ingenieur Technik* 2016;88(11):1561–85. <https://doi.org/10.1002/cite.201600049>.
- [124] Sekizawa K, Widjaja H, Maeda S, Ozawa Y, Eguchi K. Low temperature oxidation of methane over Pd/SnO₂ catalyst. *Applied Catalysis A: General* 2000;200(1-2):211–7. [https://doi.org/10.1016/S0926-860X\(00\)00634-7](https://doi.org/10.1016/S0926-860X(00)00634-7).

- [125] Martins A, Nunes N, Carvalho AP, Martins LMDRS. Zeolites and Related Materials as Catalyst Supports for Hydrocarbon Oxidation Reactions. *Catalysts* 2022;12(2):154. <https://doi.org/10.3390/catal12020154>.
- [126] Dey S, Mehta NS. Synthesis and applications of titanium oxide catalysts for lower temperature CO oxidation. *Current Research in Green and Sustainable Chemistry* 2020;3:100022. <https://doi.org/10.1016/j.crgsc.2020.100022>.
- [127] Li L, Liu Y, Wang Q, Zhou X, Li J, Song S et al. CeO₂ supported low-loading Au as an enhanced catalyst for low temperature oxidation of carbon monoxide. *CrystEngComm* 2019;21(46):7108–13. <https://doi.org/10.1039/C9CE01301F>.
- [128] Pérez-Mayoral E, Calvino-Casilda V, Soriano E. Metal-supported carbon-based materials: opportunities and challenges in the synthesis of valuable products. *Catal. Sci. Technol.* 2016;6(5):1265–91. <https://doi.org/10.1039/C5CY01437A>.
- [129] Marafi M, Stanislaus A, Furimsky E. Catalyst Deactivation. In: *Handbook of Spent Hydroprocessing Catalysts*. Elsevier; 2017, p. 67–140.
- [130] Sajiv Kumar R, Hayes RE, Semagina N. Effect of support on Pd-catalyzed methane-lean combustion in the presence of water: Review. *Catalysis Today* 2021;382:82–95. <https://doi.org/10.1016/j.cattod.2021.07.024>.
- [131] Lin L, Ge Y, Zhang H, Wang M, Xiao D, Ma D. Heterogeneous Catalysis in Water. *JACS Au* 2021;1(11):1834–48. <https://doi.org/10.1021/jacsau.1c00319>.
- [132] Burch R, Urbano F, Loader P. Methane combustion over palladium catalysts: The effect of carbon dioxide and water on activity. *Applied Catalysis A: General* 1995;123(1):173–84. [https://doi.org/10.1016/0926-860X\(94\)00251-7](https://doi.org/10.1016/0926-860X(94)00251-7).
- [133] Nomura K, Noro K, Nakamura Y, Yazawa Y, Yoshida H, Satsuma A et al. Pd–Pt bimetallic catalyst supported on SAPO-5 for catalytic combustion of diluted methane in the presence of water vapor. *Catalysis Letters* 1998;53(3/4):167–9. <https://doi.org/10.1023/A:1019082611978>.
- [134] Peng R, Li S, Sun X, Ren Q, Chen L, Fu M et al. Size effect of Pt nanoparticles on the catalytic oxidation of toluene over Pt/CeO₂ catalysts. *Applied Catalysis B: Environmental* 2018;220:462–70. <https://doi.org/10.1016/j.apcatb.2017.07.048>.
- [135] Odoom-Wubah T, Li Q, Chen M, Fang H, Asare Bediako BB, Adilov I et al. Influence of Preparation Methods on the Catalytic Activity of Pd–Cu/Mn₂O₃ Catalyst

- in the Hydrogenation of 1,3-Butadiene. *ACS Omega* 2019;4(1):1300–10. <https://doi.org/10.1021/acsomega.8b03216>.
- [136] Kolli NE, Delannoy L, Louis C. Bimetallic Au–Pd catalysts for selective hydrogenation of butadiene: Influence of the preparation method on catalytic properties. *Journal of Catalysis* 2013;297:79–92. <https://doi.org/10.1016/j.jcat.2012.09.022>.
- [137] Stocker T (ed.). *Climate change 2013: The physical science basis Working Group I contribution to the Fifth assessment report of the Intergovernmental Panel on Climate Change / edited by Thomas F. Stocker, Working Group I co-chair, University of Bern [and nine others]*. New York: Cambridge University Press; 2014.
- [138] Zhang Z, Zimmermann NE, Stenke A, Li X, Hodson EL, Zhu G et al. Emerging role of wetland methane emissions in driving 21st century climate change. *Proc Natl Acad Sci U S A* 2017;114(36):9647–52. <https://doi.org/10.1073/pnas.1618765114>.
- [139] Tavakoli S, Jensen MV, Pedersen E, Schramm J. Unburned hydrocarbon formation in a natural gas engine under sea wave load conditions. *J Mar Sci Technol* 2021;26(1):128–40. <https://doi.org/10.1007/s00773-020-00726-5>.
- [140] Moss AR, Jouany J-P, Newbold J. Methane production by ruminants: its contribution to global warming. *Ann. Zootech.* 2000;49(3):231–53. <https://doi.org/10.1051/animres:2000119>.
- [141] IEA. *An introduction to biogas and biomethane –Outlook for biogas and biomethane: Prospects for organic growth analysis*. <https://www.iea.org/reports/outlook-for-biogas-and-biomethane-prospects-for-organic-growth/an-introduction-to-biogas-and-biomethane> (accessed August 17,2023).
- [142] IEA. *Energy Sector Methane Recovery and Use 2009: The Importance of Policy*. <https://www.osti.gov/etdeweb/servlets/purl/21233584> (accessed August 17,2023).
- [143] Keller K, Lott P, Tischer S, Casapu M, Grunwaldt J-D, Deutschmann O. Methane Oxidation over PdO: Towards a Better Understanding of the Influence of the Support Material. *ChemCatChem* 2023;15(11). <https://doi.org/10.1002/cctc.202300366>.
- [144] Velin P, Florén C-R, Skoglundh M, Raj A, Thompsett D, Smedler G et al. Palladium dispersion effects on wet methane oxidation kinetics. *Catal. Sci. Technol.* 2020;10(16):5460–9. <https://doi.org/10.1039/D0CY00734J>.

- [145] Gélin P, Primet M. Complete oxidation of methane at low temperature over noble metal based catalysts: a review. *Applied Catalysis B: Environmental* 2002;39(1):1–37. [https://doi.org/10.1016/S0926-3373\(02\)00076-0](https://doi.org/10.1016/S0926-3373(02)00076-0).
- [146] Chen J, Zhong J, Wu Y, Hu W, Qu P, Xiao X et al. Particle Size Effects in Stoichiometric Methane Combustion: Structure–Activity Relationship of Pd Catalyst Supported on Gamma-Alumina. *ACS Catal.* 2020;10(18):10339–49. <https://doi.org/10.1021/acscatal.0c03111>.
- [147] Seeburg D, Liu D, Radnik J, Atia H, Pohl M-M, Schneider M et al. Structural Changes of Highly Active Pd/MeOx (Me = Fe, Co, Ni) during Catalytic Methane Combustion. *Catalysts* 2018;8(2):42. <https://doi.org/10.3390/catal8020042>.
- [148] Gigola CE, Moreno MS, Costilla I, Sánchez MD. Characterization of Pd–CeOx interaction on α -Al₂O₃ support. *Applied Surface Science* 2007;254(1):325–9. <https://doi.org/10.1016/j.apsusc.2007.07.062>.
- [149] Lee J, Lim TH, Lee E, Kim DH. Promoting the Methane Oxidation on Pd/CeO₂ Catalyst by Increasing the Surface Oxygen Mobility via Defect Engineering. *ChemCatChem* 2021;13(16):3706–12. <https://doi.org/10.1002/cctc.202100653>.
- [150] Araya P, Guerrero S, Robertson J, Gracia FJ. Methane combustion over Pd/SiO₂ catalysts with different degrees of hydrophobicity. *Applied Catalysis A: General* 2005;283(1-2):225–33. <https://doi.org/10.1016/j.apcata.2005.01.009>.
- [151] Binet C, Jadi A, Lavalley J-C, Boutonnet-Kizling M. Metal–support interaction in Pd/CeO₂ catalysts: Fourier-transform infrared studies of the effects of the reduction temperature and metal loading. Part 1.—Catalysts prepared by the microemulsion technique. *J. Chem. Soc., Faraday Trans.* 1992;88(14):2079–84. <https://doi.org/10.1039/FT9928802079>.
- [152] AlMohamadi H, Smith KJ. The Impact of CeO₂ Loading on the Activity and Stability of PdO/ γ -AlOOH/ γ -Al₂O₃ Monolith Catalysts for CH₄ Oxidation. *Catalysts* 2019;9(6):557. <https://doi.org/10.3390/catal9060557>.
- [153] El Rassy H, Pierre AC. NMR and IR spectroscopy of silica aerogels with different hydrophobic characteristics. *Journal of Non-Crystalline Solids* 2005;351(19-20):1603–10. <https://doi.org/10.1016/j.jnoncrysol.2005.03.048>.

- [154] Mario König (ed.): Development and application of novel scr catalysts. 3rd Doctorial Colloquium bioenergy 17th/18th September 2020, Leipzig for the low-temperature denitrification of exhaust gases from the thermo-chemical conversion of biogenic solid fuels.
- [155] Deutsches Institut für Normung. DIN EN ISO 17225-1:2014-09, Biogene Festbrennstoffe_ - Brennstoffspezifikationen und -klassen_ - Teil_1: Allgemeine Anforderungen (ISO_17225-1:2014); Deutsche Fassung EN_ISO_17225-1:2014. Berlin: Beuth Verlag GmbH. <https://doi.org/10.31030/2073606>.
- [156] Deutsches Institut für Normung. DIN EN ISO 16967:2015-07, Biogene Festbrennstoffe_ - Bestimmung von Hauptelementen_ - Al, Ca, Fe, Mg, P, K, Si, Na und Ti (ISO_16967:2015); Deutsche Fassung EN_ISO_16967:2015. Berlin: Beuth Verlag GmbH. <https://doi.org/10.31030/2266314>.
- [157] Johansson EM. Controlling the Pore Size and Morphology of Mesoporous Silica 2010.

CHAPTER 4

4 Extraction and Characterization of Biogenic Silica Obtained from Selected Agro-Waste in Africa.

Published Research Article I

Prempeh, C. O., Formann, S., Schliermann, T., Dizaji, H. B., & Nelles, M. (2021). Extraction and Characterization of Biogenic Silica Obtained from Selected Agro-Waste in Africa. *Applied Sciences*, 11(21), 10363. <https://doi.org/10.3390/app112110363>.

Short Summary

The first objective of this PhD thesis was to locate suitable and accessible biomass resources available in the African continent with no further usage or competition. Thus, predominant biomass materials were sourced, including cassava, yam, coconut husk, corncob and cornhusk. These feedstocks constitute approximately 90% of the predominant food chain in Africa and generate a significant amount of waste. Following a thorough review of relevant literature and data on the combustion of similar biogenic agricultural materials, the selected biomass residues were subjected to various pretreatment steps, such as water washing and leaching at 1 and 5 w/v% citric acid concentrations, before being subjected to combustion processes. The resulting biogenic silica powder was then characterized with a comprehensive analysis of its chemical compositions, morphological and thermal behaviour, textural properties, and X-ray diffraction. These systematic characterizations were carried out to gain a deeper understanding of the attributes and morphology of the silica derived from these residues and to explore their potential as a novel alternative source for silica-based materials. The key finding of this study was that, among the investigated biomass resources, the cornhusk residue showed that the highest silica potential. Thus, the extracted biogenic silica exhibited the prerequisite quality (e.g. silica purity, amorphicity and porosity) needed for any advanced application. Consequently, the rest of the investigations was continued with only the cornhusk residues. The novel result of this study widens the fundamental knowledge for the preparation of value-added materials

from primary but less-known African residues, opening up new value chains for the recovery of silica from the chosen biomasses.

Proof of individual contribution:

The nature and contributions of various authors towards the completion of Chapter 4 are as follows:

	Authors	Contribution	Extent of contribution (%)
<u>Author</u>	<u>Clement Owusu Prempeh</u>	Conceptualization, methodology, formal analysis, investigations, resources, data curation, writing—original draft preparation, writing—review and editing, and visualization.	80
Co-author (1)	Steffi Formann	Conceptualization, methodology, resources, writing—review and editing, supervision, and project administration.	6
Co-author (2)	Thomas Schliermann	Investigations, data curation, writing—review and editing and visualization	6
Co-author (3)	Hossein Beidaghy Dizaji	Investigations data curation, writing—review and editing, and visualization	6
Co-author (4)	Michael Nelles	Conceptualization, methodology, supervision, and project administration	2

Signature of candidate:.....

Date:.....

Declaration by co-authors: The undersigned hereby confirm that

1. the declaration above accurately reflects the nature and extent of the contributions of the candidate and the co-authors to **Chapter 4**,

2. no other authors contributed to **Chapter 4**, pg. 53 - 91, besides those specified above, and
3. potential conflicts of interest have been revealed to all interested parties and that the necessary arrangements have been made to use the material in **Chapter 4**, pg. 53 - 91, of this dissertation.

Extraction and Characterization of Biogenic Silica Obtained from Selected Agro-Waste in Africa

Clement Owusu Prempeh^{1,2,*}, Steffi Formann¹, Thomas Schliermann¹, Hossein Beidaghy Dizaji^{1,3}, Michael Nelles^{1,2}

¹Department of Thermochemical Conversion, DBFZ Deutsches Biomasseforschungszentrum gemeinnützige GmbH, Torgauer Straße 116, 04347 Leipzig, Germany; Steffi.Formann@dbfz.de (S.F.); Thomas.Schliermann@dbfz.de (T.S); Hossein.Beidaghy@dbfz.de (H.B); Michael.Nelles@dbfz.de (M.N)

²Department of Agriculture and Environmental Science, University of Rostock, Justus-von-Liebig-Weg 6, 18059 Rostock, Germany

³Institute of Chemical Technology, Universität Leipzig, Linnéstr. 3, 04103 Leipzig, Germany

*Correspondence: Clement.OwusuPrempeh@dbfz.de, phone: +49-(0)341-2434-523

Abstract

Increased amounts of available biomass residues from agricultural food production are present widely around the globe. These biomass residues can find essential applications as bioenergy feedstock and precursors to produce other value-added materials. This study assessed the production of biogenic silica (SiO₂) from different biomass residues in Africa, including cornhusk, corncob, yam peelings, cassava peelings and coconut husks. Two processes were performed to synthesize the biogenic silica. First, the biomass fuels were chemically pretreated with 1 and 5% w/v citric acid solutions. In the second stage, combustion at 600 °C for 2 h in a muffle oven was applied. The characterization of the untreated biomasses was conducted using Inductively coupled plasma - optical emission spectrometry (ICP-OES), thermal analysis (TG-DTA) and Fourier-transform infrared spectroscopy (FTIR). The resulting ashes from the combustion step were subjected to ICP, nitrogen physisorption, Energy dispersive X-ray spectroscopy (EDX) as well as X-Ray diffraction (XRD). ICP results revealed that the SiO₂ content in the ashes varies between 42.2 to 81.5 wt.% db and 53.4 to 90.8 wt.% db after acidic pretreatment with 1 or 5 w/v% acid, respectively. The relative reductions of K₂O by the citric acid in yam peel was the lowest (79 wt.% db) in comparison to 92, 97, 98 and 97 wt.% db calculated for corncob, cassava peel, coconut husk and cornhusk, respectively. XRD analysis revealed dominant

crystalline phases of arcanite (K_2SO_4), sylvite (KCl) and calcite ($CaCO_3$) in ashes of the biomass fuels pretreated with 1 w/v% citric acid due to potassium and calcium ions present. In comparison, the 5 w/v% citric acid pretreatment produced amorphous, biogenic silica with specific surface areas of up to $91 \text{ m}^2/\text{g}$ and pore volumes up to $0.21 \text{ cm}^3/\text{g}$. The examined biomass residues are common wastes from food production in Africa without competition in usage with focus application. Our studies have highlighted a significant end-value to these wastes by the extraction of high quality, amorphous silica, which can be considered in applications such as catalyst support, construction material, concrete and backing material.

Keywords: Biogenic silica; African biomass fuels; Thermochemical conversion; Ash characterization; Combustion

4.1 Introduction

Lignocellulosic residues, also known as biomass, have a pivotal role in the context of sustainable development due to their unique properties. They offer biodegradability, which contributes to a healthy ecosystem, as it can drastically reduce greenhouse gas emissions compared to fossil fuels [1,2]. The combustion of biomass fuels is perceived as carbon-neutral in many perspectives as it results in no net increase of greenhouse (GHG) emissions on a life-cycle basis. Plants are able to capture the same amount of CO_2 through photosynthesis during the different stages of plant growth. Thus, the same amount of CO_2 is released into the atmosphere from the combustion process, which is reabsorbed by the plants for photosynthesis [3]. Furthermore, since the combustion operation is performed in sufficient air atmosphere, it is assumed that the entirety of the CO released during this reaction is converted to CO_2 .

In developing countries, biomass supplies most energy services, but in inefficient implementations, mainly for cooking and heating space [4]. Major negative environmental impacts of biomass reliance and usage include increased air pollution and carcinogenic health problems to users [5]. However, more resourceful biomass applications are expected in the future, such as the production of biogas and liquid fuels for cooking, value-added materials, and power generation [6]. In addition, with climate protection policies intensified by the EU [7] and AU [8] to achieve CO_2 neutrality by 2050 [9], the utilization of biomass waste is seen as a promising strategy to reduce the effects of climate change because of its

potentials as a domestic and environmentally sound renewable fuel. The additional motivation that has spurred renewed interest in biomass residues, especially for developing countries, includes being part of the global industry as manufacturers of value-added materials, promising increased revenues, and job creation [10].

Against this background, numerous efforts have been undertaken to assess and characterize lignocellulosic residues of Africa origin individually [4,11–14] or as part of a composite investigation [15–19] to find an improved utilization. Dasappa [18] investigated the potential of biomass energy for electricity generation in Sub-Saharan Africa, whereas Duku et al. [4] conducted a comprehensive review of the biomass resources and biofuels potential in Ghana. In addition, Kemausuor et al. [6] assessed the biomass residues availability in Ghana and their potential in meeting the energy demand using crop residues of the country. While there is a wealth of information on the material properties of a range of lignocellulosic fibres, including several studies on rice husk and rice straw, miscanthus, and sugarcane bagasse in Europe [20,21], the characterization studies of predominant and accessible residues in Africa (such as cassava, yam, coconut, corncob, and cornhusk) are still underrepresented. These foodstuffs provide over 90% of the continent's food needs and predominantly for Western and Central Africa [4]. However, extensive reviews reported in the literature so far on these biomass fuels are on their potential, and only a few are exclusively presented as a systematic study on material properties or the prospect of value-addition [22,23]. As a result, a thorough investigation is required, while also providing information on value addition processes for these residues. Such efforts are expected to result in better utilization, opening a wide range of possibilities for many developing countries.

As a case study in Ghana, Table 4.1 depicts the theoretical and technical potential of primary residues of Ghana in 2011 [6]. Other minor agricultural residues in Ghana include rice husk, oilseed cake, sugarcane bagasse and oil palm empty fruit bunch. The study of Kemausuor et al. [6] highlighted the vast potential regarding residues availability and shed light on the government's intervention and commitments to promote the cultivation of agricultural produce. For example, through the Special Initiative of the President on cassava production, the FAO statistics reported a significant increase in production figures from 2001 to 2007 [24]. Thus, approximately 9.95 million tonnes of the crop were harvested from an area of 800,000 hectares. In addition, about 1.10 million tonnes of maize were harvested from 750,000 hectares within the same production year [3]. Jekayinfa et al. [16] estimated the residue to product ratio values of cassava peelings, corncob, and corn husk at 0.25, 0.27

and 0.20 g/g, and residue amount at 9.54, 1.30 and 0.96 metric tonnes (Mt), respectively. These values show a huge biomass residue potential with minimal end-use due to the lack of study or available options for value addition.

Table 4.1. Potential of crop residues in Ghana. Modified from Resources, Conservation and Recycling, 86, F. Kemausuor, A. Kamp, S. Tjalfe Thomsen, E. Cudjoe Bensah, H. Østergård, Assessment of biomass residue availability and bioenergy yields in Ghana [6], 28–37, Copyright (2014), with permission from Elsevier.

Crop	Theoretical Potential of Residue (Mt/Year)	Technical Potential of Residue (Mt/Year)
Cassava peeling ^P	3.6	0.72
Yam straw ^F	3.2	2.5
Coconut husk ^P	0.12	0.12
Corn cob ^P	0.49	0.49
Corn husk ^P	0.34	0.34

^Fdenotes a field-based residue, whereas ^P indicates a processing residue.

Silicon dioxide (silica) is one of the most valuable inorganic materials with a range of industrial applications such as an alternative to ordinary Portland cement [25], a precursor for the synthesis of water glass [26], a rubber filler [27], an adsorbent for the treatment of effluents [28], silica mesoporous material [29], a support system in catalysis operations [30] and coatings in epoxy paints [31]. However, the conventional synthesis of silica from a mineral-based precursor, tetraethyl orthosilicate (TEOS), involves a high thermal hydrolysis process. This process is energy-consuming and cost-intensive. In addition, secondary products (CO₂ and voluminous amount of wastewater) that are environmentally unfriendly are generated [32–35]. Therefore, these downsides along the silica production route have hindered their wide applications.

Over the last decades, there have been renewed interest in silica extraction from naturally occurring silica plants, including rice husk and straw, wheat straw and cereal remnant, oat husk and spelt husk [36–39]. Si-accumulating plants present a viable alternative that can be harnessed for producing silicon-based materials [35–41]. Vaibhav et al. [42] investigated the use of agricultural wastes to produce silica nanoparticles. Through thermochemical conversion and leaching procedures, pure silica can be generated from the

residues as the bottom ash [43] or fly ash [44] contains a significant amount of silica. The high silica content in fly and bottom ashes can find applications in the production of zeolites and admixtures in cement [25,44].

Lignocellulosic biomass constitutes cellulose, hemicellulose, and lignin [45] with considerable amounts of alkali and alkaline earth metallic species (AAEMs), such as sodium, potassium, calcium, magnesium, and iron, etc. [46]. The high presence of AAEMs can influence the physicochemical properties of the resulting biogenic silica during combustion, and thus, needs to be removed from the organic matrix before thermal treatment [47]. The use of organic acid such as citric acid to remove the content of AAEMs from the biomass is recommended over inorganic acids due to environmental considerations [48]. The effectiveness of carboxylic acid in producing high-purity amorphous silica from rice husk has been reported by Umeda et al. [49]. More importantly, for high-end applications such as catalyst support, the generated biogenic silica must attain specific purity, crystallinity, and porosity [50]. So far, the use of agricultural waste products is economically and commercially successful in many applications. Utsev et al. [51] investigated coconut shell ash as a partial substitute of ordinary portland cement in concrete production. Other efforts have been made to understand the role of major constituents of coconut fibres and yam peels in the absorption of ionic dyes [52] and removal of Cd(II) ions from an aqueous solution [53], respectively. Interestingly, limited studies (Adepoju et al. [15], Biswas et al. [38], Utsev et al. [51] and Anuar et al. [54]) have been conducted on residues from cassava, yam, coconut, corncob, and cornhusk as potential silica sources.

Therefore, this study critically examines some biomass resources accessible in Africa and presents a systematic characterization of their chemical compositions, morphological and thermal behaviour, aspects of textural properties and X-ray diffraction in respect of the five lignocellulosic residues. Hence, the characteristics of silica derived from these residues as a new possible alternative source for silica-based materials are investigated. With the agricultural potential of the continent and considering the voluminous quantity of wastes generated, these agricultural residues can be converted into the fabrication of valuable resources. Therefore, it is envisaged that such efforts will lead to better usage of crop residues, opening a new and wide array of options for many developing countries while tackling the challenges associated with waste management in Africa.

4.2 Materials and Methods

4.2.1 Material used and sample preparation

Biomass fuels/residues of cornhusk, corncob (*Zea mays*), yam peelings (*Dioscorea spec.*), cassava peelings (*Manihot esculenta*) and coconut shell (*Cocos nucifera*) were obtained from farmers in the Ashanti region, Ghana. Upon collection, they were washed in tap water to remove adhered soil particles and dried in an air oven at 105 °C. The biomass fuels were cut into smaller particles (<1 mm) using the hammer mill (Netzsch-Condux, Hanau, Germany) and then stored in airtight plastic containers until further use. Figure 4.1 illustrates the sample preparation and the extraction process to prepare the silica-rich ashes.

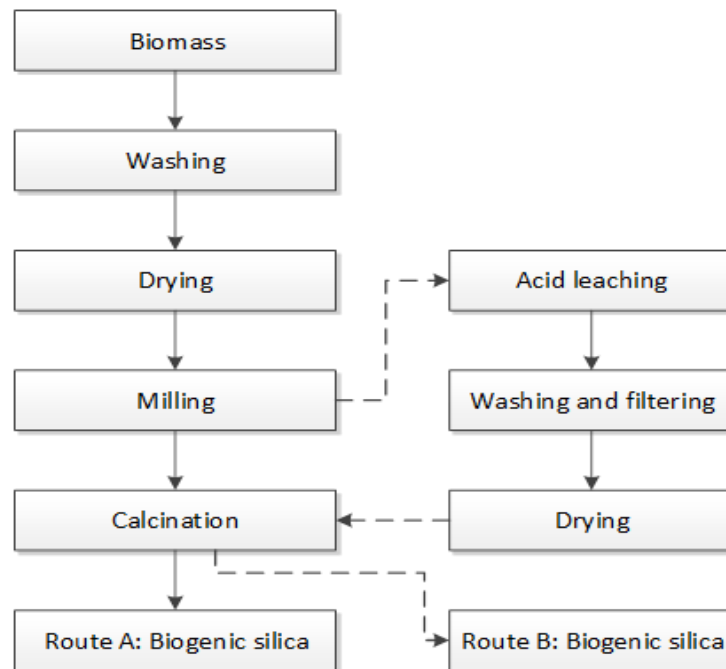


Figure 4.1. Extraction of biogenic silica from agricultural biomass residues to produce silica-rich ash.

Using 3000 mL of tap water and 150 g of the solid residues, a solid-(dry mass) to-liquid ratio of 1:20 (g/mL), the biomass fuels were leached in tap water dissolved in 1 or 5 wt.% citric acid (CA) (Sigma-Aldrich, Steinheim, Germany, purity of >99.99%) at 50 °C for 2h. The leaching conditions follow the experimental protocol of Schliermann et al. [55], and this allowed the comparison of the behaviour of the resulting ashes (biogenic silica powders)

regarding purity and textural properties at different citric acid concentrations. The leached samples were rinsed with tap water and dried overnight at 105 °C.

For the combustion process, weighed amount of the untreated and acid-leached biomass fuels were combusted at 600 °C in a lab-scale muffle furnace (Nabertherm 1185H66EA, Lilienthal, Germany) under air atmosphere for 2h at a heating rate of 6 °C/min. The resulting ashes were then cooled to room temperature in the furnace. The combustion temperature was chosen based on literature data [14].

The biomass fuels were abbreviated as CasP, YamP, CocH, CorC, and CorH to represent cassava peelings, yam peelings, coconut husks, corncobs, and cornhusks, respectively. Furthermore, the resulting ashes of the biomass fuels were identified as X-U-A-Y, where X is the name of the biomass fuels, U is untreated, A represents the ashes, and Y is the acid concentration used for leaching (1 and 5 w/v%).

4.2.2 Analysis of physical and chemical properties

To fully characterize the biomass fuels, elemental analysis of the raw, leached biomass fuels and the generated ashes were carried out by inductively coupled plasma-optical emission spectroscopy (ICP-OES) according to the DIN EN ISO 16967;2015-07, DIN EN ISO 1. ICP-OES analysis provided information on the distribution of fundamental organic elements and ash forming elements embedded in the raw and leached biomass fuels.

FTIR analysis of the biomass fuels and the ashes from the combustion was performed using an FTIR-spectrometer (PerkinElmer, Solingen, Germany) to identify the main organic compounds and various functional groups within the ashes and raw biomass fuels. The spectrum scope was in the range of 400–4000 cm^{-1} with a resolution factor of 1 cm^{-1} .

The phases in the resulting ashes were determined by X-ray diffraction (XRD) apparatus (Malvern Panalytical GmbH, Kassel, Germany) equipped with Ni-filtered, Cu-K α radiation ($\lambda = 1.54 \text{ \AA}$). The chemical composition spectrum of the ash samples was calculated using the Energy-dispersive X-ray fluorescence spectroscopy (EDX) (Bruker, Massachusetts, USA).

The textural properties of the ashes were determined using autosorb iQ-MP/XR apparatus, Quantachrome, USA. The samples (~0.1–0.3g) were degassed by heating at 250 °C under vacuum (ca. 0.4 kpa) for 10 h to remove non-dissociative, physically adsorbed

water molecules from the sample surface and within the pores. The Brunauer, Emmett and Teller (BET) surface area was determined by fitting the adsorption data to the BET equation in the relative pressure range of $(p/p_0) = 0.05\text{--}0.3$. Nitrogen was used as the adsorptive gas at 77 K, with a standard value of 0.162 nm^2 for the molecular cross-section of nitrogen. The total pore volume was obtained at a relative pressure $(p/p_0) = 0.98$. The pore characteristics were calculated using indirect molecular adsorption methods such as nonlocal density functional theory (NLDFT).

Canon EOS 250D (Canon Ltd., Krefeld, Germany) was used to capture the visual appearances of the ashes after the combustion process. All the images were recorded at the same time under natural light with no flashing light.

4.2.3 Thermal analysis of biomass fuels

To assess the rate of thermal degradation of the biomass fuels, the weight loss caused by changing temperature was measured according to the experimental method of Hilbers et al. [56]. The thermal degradations were carried out in a simultaneous thermal analysis (STA 449 F3 Jupiter[®], NETZSCH, Selb, Germany) in a synthetic air flow atmosphere with a 100 mL/min flow rate under a heating rate of 10 K/min. Approximately 10–20 mg of biomass fuels were placed in alumina crucibles and the samples were heated from room temperature to 600 °C. To create homogeneous starting material for the STA analysis, each biomass fuel was ground to a particle size of less than 0.5 mm with a cutting mill (IKATM MF 10 basic Mikrofeinmühle) and vigorously mixed in a plastic box. The TG and DTG curves were recorded simultaneously along the temperature increase.

4.3 Results and Discussion

4.3.1 Solid fuel analysis

Table 4.2 presents the fuel analysis results, including proximate and ultimate analysis, the lower heating value of the biomass fuels, and the chemical composition of the fuel ash. According to Table 4.2, all the untreated biomass fuels are characterized by an ash content (AC) of 1.85–5.04 wt.% db. The moisture content (MC) of all tested samples is in the range of approximately 2.71–10.7 wt.% wb. The fuel ash analysis results show predominant ash

forming elements being compounds of K, Ca, Al, Mg, Na, P, S, and Si. The K concentration was high in the untreated biomass fuels but reduced significantly along with other impurities after the chemical pretreatment. Observed silica content in the untreated and chemically pretreated biomass fuel ash increased from 11.53–44.13 to 38.62–70.74 wt.% db, respectively. Similar silica enrichment after acidic pretreatment of biomass fuels has been reported elsewhere [35,36]. The high carbon and oxygen contents of 44.4–50.10 wt.% db suggest the presence of oxygen-containing functional groups on the biomass fuels' surface and the lignocellulosic nature of samples [57]. The lower heating values (LHV) define the amount of heat released during the combustion ranged between 16.36–18.8 MJ/kg db as indicated in Table 4.2.

Table 4.2. Fuel and fuel ash properties of untreated (U) and acid leached (L), cassava (CasP), yam (YamP), coconut (CocH), corncob (CorC) and corn husk (CorH). Inorganic species are specified on fuel ash basis. Abbreviations wb, db, and n.d. stand for wet basis, dry basis and not detected. Oxygen is calculated by difference. VM: volatile matter; AC: ash content; MC: moisture content; and LHV: lower heating value.

Parameter	Unit	CasP		YamP		CocH		CorC		CorH	
		U	L	U	L	U	L	U	L	U	L
VM	wt.% db	77.1	79.7	79	82.4	68.6	79.2	79.9	86.6	82	87.4
AC	wt.% db	5.5	3.59	4.57	2.38	5.04	0.93	2.32	0.74	1.85	1.04
MC	wt.% wb	9.96	4.23	13.6	2.71	10.7	1.73	5.34	3.53	9.9	5.18
LHV	MJ/kg db	16.52	17.3	16.36	16.64	18.12	18.8	17.49	17.68	17.14	17.41
C	wt.% db	45	47.3	44.4	45.3	49.3	50.1	47.7	47.6	47.4	46.6
H	wt.% db	5.76	5.93	5.82	6.23	5.24	5.92	5.91	5.86	5.87	5.81
N	wt.% db	1.09	1.04	1.01	1.02	0.54	0.4	0.66	0.58	0.26	0.23
O	wt.% db	49.12	46.77	49.69	48.37	45.36	43.98	46.39	46.54	46.73	47.59
S	wt.% db	0.12	n.d	0.09	0.1	0.1	n.d	n.d	n.d	n.d	n.d
Fuel ash analysis											
Al ₂ O ₃	wt.% db	5.67	8.46	1.76	2.87	0.84	1.57	0.51	0.79	0.91	0.68
CaO	wt.% db	14.80	30.31	3.91	8.07	4.96	16.76	2.23	9.82	6.02	10.69
Fe ₂ O ₃	wt.% db	2.23	3.03	0.65	2.11	0.92	2.07	0.87	2.98	1.04	0.84
K ₂ O	wt.% db	40.84	1.83	46.66	17.67	61.98	4.24	62.44	8.21	30.41	1.61
MgO	wt.% db	3.96	2.62	2.22	1.97	4.67	3.07	2.97	2.49	9.88	2.67
MnO	wt.% db	0.14	0.08	0.08	0.12	0.06	0.04	0.10	0.05	0.15	0.05
Na ₂ O	wt.% db	0.36	1.10	0.43	1.04	4.45	2.96	0.09	2.23	0.09	1.72
P ₂ O ₅	wt.% db	4.35	2.94	11.15	8.88	4.48	5.81	3.98	4.64	6.25	1.16
SiO ₂	wt.% db	20.01	38.62	26.70	45.22	11.53	44.57	20.82	49.53	39.94	70.74
SO ₃	wt.% db	6.82	9.68	5.98	11.23	5.86	18.17	5.67	18.52	4.77	9.37
Others *	wt.% db	0.82	1.33	0.45	0.82	0.25	0.74	0.31	0.75	0.54	0.47

*Others ** include trace minerals such as BaO, Cr₂O₃, CuO, Li₂O, NiO, SrO, TiO₂, ZnO.

4.3.2 TGA analysis of biomass fuels

According to Ma et al. [58], TGA is a useful tool to examine the mass-loss characteristics and kinetics parameters of the thermal breakdown process. The results of the TGA and DTG analysis during the combustion process of the biomass fuels are shown in Figure 4.2.

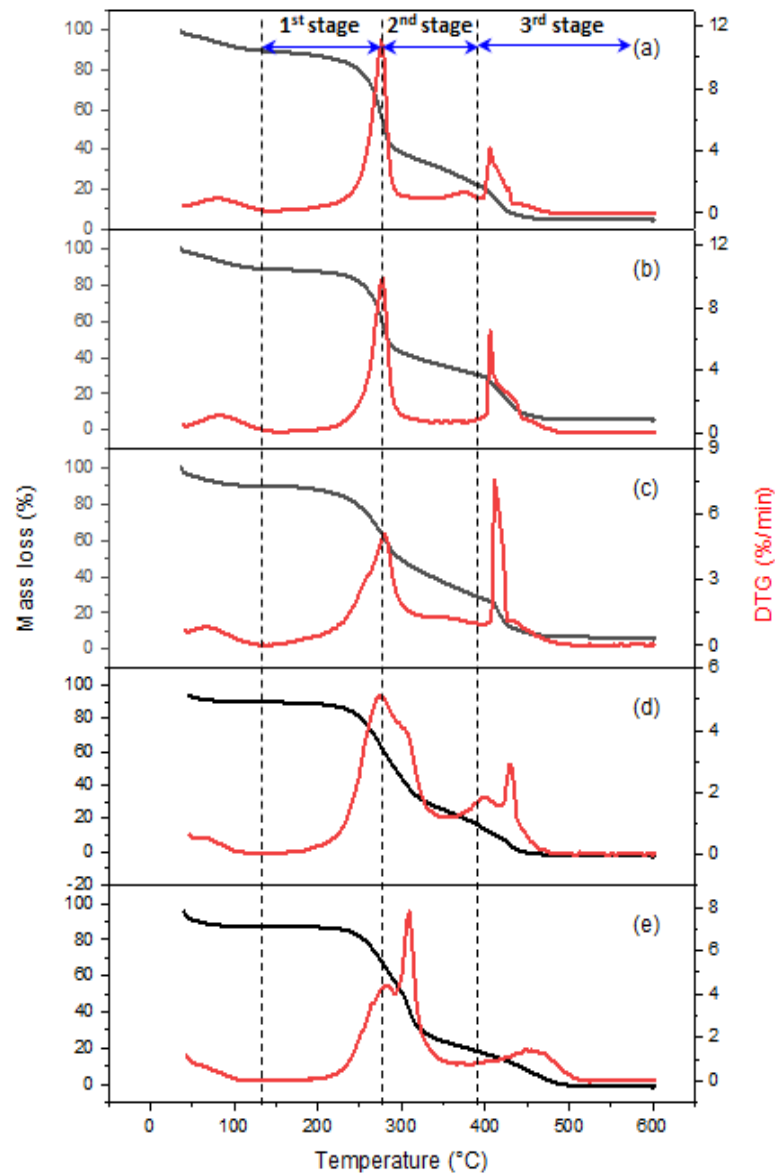


Figure 4.2. TG (black curve and y-axis on the left side) and DTG (red curve and y-axis on the right side) profiles of untreated (a) cassava, (b) yam, (c) coconut, (d) corncob, and (e) cornhusk.

The combustion process occurred in three stages: 68–281 °C, 307–381 °C and 408–454 °C. The first two stages were characterized by rapid devolatilization. A considerable amount of the sample's weight was lost (25.43–45.15 wt.% db), with two distinct mass-loss peaks indicated in the DTG curves. Conversely, the third stage depicted a slow degradation process.

In the first phase of the first stage (25–105 °C), there was a small percentage of mass loss (3.13–5.75 wt.% db), which corresponds to water evaporation in the samples [58]. The second phase of the first stage, where the maximum decomposition rate occurred, is mainly attributed to the decomposition of hemicellulose. Since hemicellulose is a mixture of several polymerized monosaccharides (xylose, mannose, glucose, galactose, and arabinose, among others) with a lower degree of polymerization, its thermal stability is lower than that of cellulose [58-60], and this occurred at a temperature between 268.1 to 281.3 °C. Ma et al. [58] reported that the predominant temperature for hemicellulose breakdown appears between 139–323 °C for palm kernel shell, whereas Dhyani et al. [61] reported the decomposition temperature for hemicellulose in the range of 220–315 °C.

In the second stage (307–381 °C), a simultaneous degradation process was seen, owing primarily to the presence of cellulose [58], which accounts for approximately 20.25–30.69 wt.% of mass loss. In yam and coconut biofuels, the second devolatilization stage (i.e., decomposition of cellulose) was not observed. The decomposition of the organic compounds occurred in parallel, in a super-compositional manner, as shown in the DTG curves. However, cellulose decomposition was observed in cassava, corncob, and cornhusk with the maximum decomposition rate at a temperature between 307–381 °C. Because cellulose is a high-molecular-weight substance with a long linear chain formed of D-glucosyl groups [62], and a portion of cellulose has a crystal structure composed of organized microfibrils, it degrades more slowly than hemicellulose [63].

The third stage only accounts for a minor portion of mass loss (6.14–7.81 wt.% db) with a maximum decomposition rate at a temperature range of 408.3–454.7 °C. This stage might be attributed to the degradation of lignin, which is the most stable component of lignocellulosic biomass. It is difficult to decompose and requires higher decomposition temperatures, as the decomposition occurs slowly along the whole combustion temperature range [61]. From Figure 4.2, the distinct weight loss peaks in the DTG curves of cassava, yam and coconut were considerably different from corncob and cornhusk, which presented only one distinct peak and an additional “shoulder” peak. This could be a result of a low

lignin content compared to cassava, yam and coconut. Lignin is an amorphous substrate that resides in the minute spaces between cellulose microfibrils. It is covalently bonded to hemicellulose and crosslinked to polysaccharides and contributes to the crystallinity of biomass fuels [58–60]. It is conceivable that there is a higher lignin content in cassava, yam, and coconut. Thus, they were thermally degraded more slowly than the other biomass residues, corncob and cornhusk, resulting in distinct mass losses of hemicellulose and cellulose [64]. Ceylan et al. [65] observed a similar result of two discrete mass-loss maxima in hazelnut husk with a high lignin concentration (39%). Similar observations for other biomasses that showed only one distinct peak in the DTG curve (such as pinewood [66], bamboo [67] and corn stover [68] or with a minor “shoulder” (e.g., wheat straw [68]) have been reported in the literature. In addition, charring of the biomass fuels has been reported to occur at this stage due to lignin breakdown [69, 70].

Therefore, it can be concluded that the overall decomposition behaviour of cassava, yam, coconut, corncob, and cornhusk is due to the decomposition of the primary organic materials: cellulose, hemicellulose, and lignin, with the extent of complexity of the TGA curves depending on the definite compositions of the individual components of the lignocellulosic biomasses [61]. Similar decomposition behaviours of cellulose, hemicellulose and lignin have been reported in the study of Yang et al. [60]. They noted that the degradation of hemicellulose and cellulose showed the highest mass loss rate at 268 °C and 355 °C, respectively, and lignin was the most difficult of the three to disintegrate [60,61]. According to Mansaray et al. [71], the hemicellulose and cellulose constituents are the primary contributors to the evolution of volatile compounds, whereas the degradation of lignin leaves behind char particles as the direct product.

4.3.3 FTIR analysis

The evolution of the functional groups during the combustion of the raw biomass fuels and the ashes produced at 600 °C was examined by employing a Fourier Transformation Infrared (FTIR) analysis. The characteristic peaks and functional groups are presented in Figure 4.3 and Table 4.3, respectively. According to the FTIR analysis, the major volatile components change in the spectra relates to the vibration generated by the O–H bonds (3000–3600 cm^{-1}), C–H groups (2900–3000 cm^{-1}), stretching vibration of C=C and C–O. These bands generally disappear during combustion as the significant share of organic

compounds (i.e., cellulose, hemicellulose, and lignin) is decomposed as observed in Figure 4.3 (bottom). The bands at approximately 1065, 972, and 1415 cm^{-1} are corresponding to the stretching vibration of CO_3^{2-} , which corresponds to the content of calcite (CaCO_3) in the ashes. The positions of the bands agree with the reference calcite in Figure 4.3 (bottom).

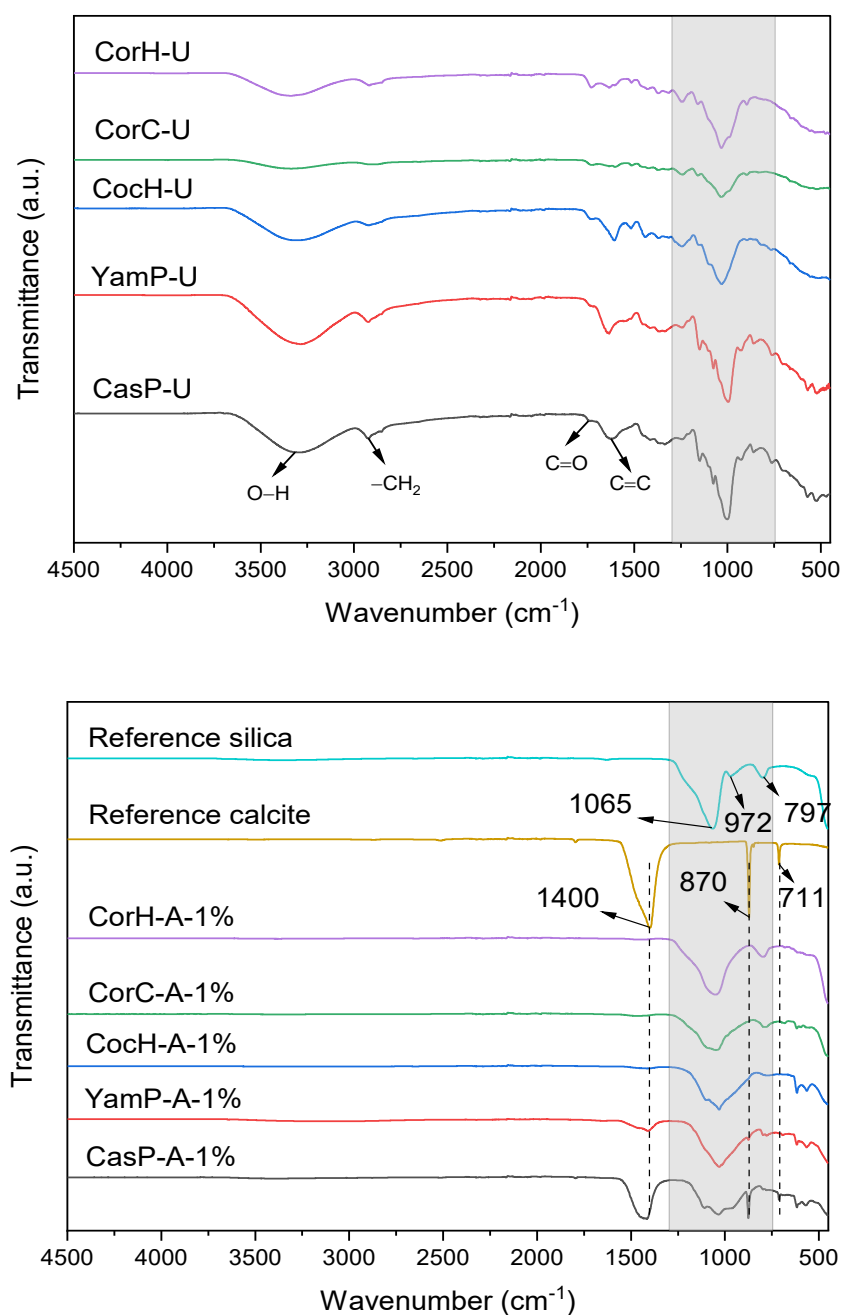


Figure 4.3. The evolution of the main functional groups in raw biomass (upper) and ashes of 1 w/v% biomass fuels (bottom). Ashes were generated at 600 °C and compared with commercial calcite and silica powders.

Table 4.3. The main functional groups of the three main components of the biomass fuels and the ashes produced at 600 °C during combustion characterized by FTIR.

Wavenumber (cm ⁻¹)	Functional Groups	Compounds	Reported Values (cm ⁻¹)	References
3600–3000	O-H stretching	Acid, methanol	3600–3000	Yang et al. [60]
2900–3000	C-H stretching	Alkyl, aliphatic, aromatic	2860–2970	Yang et al. [60]
1402–1415	OH bending, CO ₃ ²⁻ , CH bending	Acid and CaCO ₃	1440–1400, 1400–1460, 1417–1425	Magdziarz et al. [77] Nieves et al. [78] Ceylan et al. [65] Yang et al. [60]
1159–1108; 1027–1051	C–O–C stretching vibration	Pyranose ring skeletal	1170, 1082	Yang et al. [60]
1035–1125	C–O stretching, C–O deformation, OH association and Si–O–Si	C–OH (ethanol), SO ₄ ²⁻ and SiO ₂	1035–1065, 1108	Nana et al. [79] Ma et al. [80] Nieves et al. [78] Yang et al. [60]
956–972	Si–O–Si	SiO ₂	956–972	Bathla et al. [81] Morrow et al. [82] Mohanraj et al. [83]
	C–H and stretching vibration of CO ₃ ²⁻	Aromatic hydrogen and CaCO ₃	700–900	Ennaciri et al. [84] Bonfim et al. [26] Medina et al. [85] Liou et al. [86]
778–799	Si–O–Si	SiO ₂	796, 798	Frías et al. [87]
711	Stretching vibration of C–O	CaCO ₃	713, 709	Leng et al. [88] Ennaciri et al. [84]
400–600	C–C stretching	Aromatic hydrogen	700–400	Yang et al., 2007 [60]

Beidaghy Dizaji et al. [50] also detected the formation of CaCO₃ in the silica-rich ashes obtained from rice husk and rice straw using a diffractometry technique (i.e., quantitative Rietveld refinement of XRD data). They reported that the formation of this phase could result from a reaction between CaO in the ash and the ambient CO and CO₂ gaseous species after the combustion. It is probably because some of the ashes were regularly exposed to the ambient air for different analyses after production considering their production time.

The infrared spectra at the ranges 400–600, 778–799, and 1035–1125 cm^{-1} could be attributed to bending, stretching, and asymmetrical stretching vibration of Si–O–Si, which are in line with the literature reports and the detected bands (i.e., 797 and 1065 cm^{-1}) in the reference silica sample (CWK Köstropur[®] 021012). Typically, the asymmetrical stretching vibration of Si–O–Si in the wavenumber region 1035–1125 cm^{-1} obscures with several different bands such as the SO_4^{2-} bands in the region 1138–1155 cm^{-1} , R–OH groups in 1051 cm^{-1} , stretching band of aliphatic ether C–O and alcohol C–O in cellulose and hemicellulose in 1050 cm^{-1} , β -(1–4) glycosidic bonds in cellulose such as C–O–C stretching and pyranose ring skeleton vibration in the region 1159–1108 and 1027–1051 cm^{-1} [72–76].

4.4 Ash Analysis

4.4.1 Impact of the pretreatment process on the chemical composition of the inorganic fraction of biomass fuels

The changes in elemental composition upon treatments [1 and 5 w/v% citric acid (CA)] of the biomass fuels are shown in Figure 4.4.

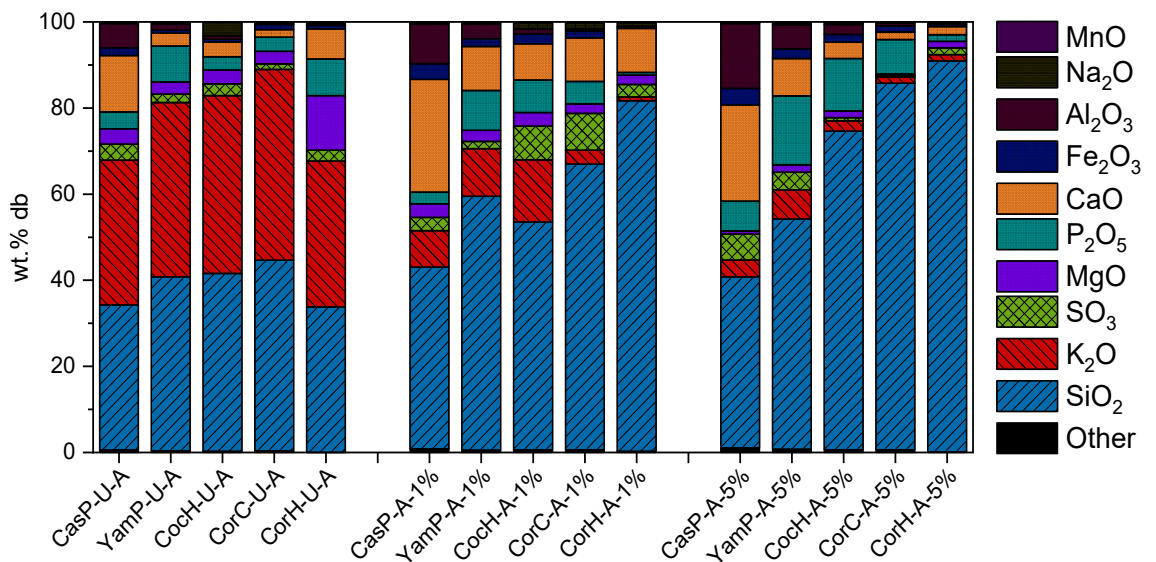


Figure 4.4. Chemical composition of the inorganic fraction (=100 wt.% db) of ashes obtained from the thermal treatment of the untreated and acid-leached samples with citric acid.

The results indicated that in untreated ash samples (U-A), the share of oxides of silica, potassium, sodium and calcium are in higher proportion compared to other ash forming elements (such as Al_2O_3 , CaO , K_2O , MnO , etc.). Acidification of the biomass fuels proved to be effective in removing the above metals to substantially lower levels, as the main component of the samples was SiO_2 . The reduction in the metal impurities after the pretreatment process could be attributed to the dissolution of weakly and strongly bonded metals within the organic matrix of the biomass fuels [89], and the volatilization of metals that occurred during the thermal decomposition process [90]. Nevertheless, the ashes of some of the samples contained a considerable amount of potassium and oxides of Al constituents relative to silica even after the acidic pretreatment. These observed effects align with similar observations made by Alyosef et al. [89] during their investigations on Egyptian diatomite.

According to the analyses, the removal efficiency of K_2O by the citric acid in yam peel was the lowest (79 wt.% db) in comparison to 92, 97, 98 and 97 wt.% db calculated for corncob, cassava peel, coconut husk and cornhusk, respectively. Chen et al. [91] have reported a K_2O removal in the proximity of 98 wt.% db after acetic acid pretreatment of rice husk. According to Dunlop [92], hydrolysis of cellulose and hemicellulose to produce monosaccharides occurs during the leaching of biomass fuels. Consequently, the monosaccharides were assumed to block access of the leaching agent to the inorganic impurities [92]. Thus, the volatilization of K^+ ions is hindered due to their attachment to the organic matrix at temperatures below 400 °C [93].

In this study, further removal of metals from the biomass fuels occurred in diminutive amounts with increasing concentration of the citric acid (5 w/v%). Nonetheless, the amounts of some metallic oxide (such as Al_2O_3) in 5 w/v% CA treated ashes of yam and cassava residues were more than those of 1 w/v% citric acid samples. This confirmed that the treatment of yam and cassava biomass fuels with citric acid for silica extraction or removal of Al_2O_3 might not be suitable at higher citric acid concentrations. Probably, the use of inorganic acids including HCl and HNO_3 or inorganic bases such as NH_4OH and NaOH as adopted by several researchers (Hunt et al. [94]; Amick [95]; Umeda et al. [96]) could be used in pre-treating cassava and yam biofuels. Adepoju et al. [15] reported a 61.5% silica yield from cassava periderm after leaching with HCl.

This study found higher silica content in the ashes of the acid-treated biomass fuels compared to the other ash-forming elements such as K^+ ions. The silica contents of all the

studied samples under each pretreatment (1 and 5 w/v% citric acid) increased in the following order: CorH-A-5% (90.87 wt.% db) > CorC-A-5% (85.12 wt.% db) > CorH-A-1% (81.45 wt.% db) > CocH-A-5% (73.97 wt.% db) > CorC-A-1% (66.13 wt.% db) > YamP-A-1% (58.94 wt.% db) > YamP-A-5% (53.47 wt.% db) > CasP-A-1% (42.15 wt.% db) > CasP-A-5% (39.72 wt.% db). The observed variability of silica contents across the ashes of the various biomass fuels might be due to the diverse Si-accumulation mechanism used by plants [40]. The role of silica in plants is to offer some protection against certain biotic and abiotic stressors [41]. As a result, depending on their requirements and the quantity of silica in the soil, various plants uptake varying concentrations of silica particles in the form of silicic acid $[\text{Si}(\text{OH})_4]$ from the soil [97].

Ma et al. [98] reported that the SiO_2 concentrations in plants vary owing to unequal silica deposition in tissues, variations in origin and growth circumstances (soil, humidity, sun exposure), and genotypic variations. On a dry weight basis, the silica in plant shoots can naturally fluctuate between 0.1 and 10% dry weight depending on the plant species [98, 99]. In rice (*Oryza sativa*), cultivars usually showed a reduced silica concentration than japonica cultivars [98]. Alyosef et al. [100] found above 7 wt.% db deviation in the silica concentration of various batches of raw rice husk from different regions in Egypt. In addition, 5 wt.% db SiO_2 variations have been reported in the results of rice husk ash in India [101]. According to Ma et al. [102] and Takahashi et al. [103], silica is less deposited in most *Angiosperme*, *Gymnospermae*, *Filicopsidae*, and *Pteridophyta*. However, some plants, such as rice (*Oryza sativa*) and sugarcane (*Saccharum officinarum*), may accumulate as much as 39 mg [104] and 10.2 mg [105] of silica per gram, respectively. Thus, the affinity for silica by the plants may influence the total concentration stored inside their shoots and roots [97], which might explain the differences in silica contents as observed in the case of *Zea mays* examined in this study. Two different parts of the plant (cob and husk) were examined, explaining the variability in silica contents. For the rest of the examined biomass fuels, the variability in silica contents may be due to differences in origin or genotypic differences, as explained above.

The variations of carbon content (not directly determined but indirectly estimated from the LOI values of the ashes) decrease from 7.80, 5.83, 4.67, 5.3 and 34.47 wt.% db in the untreated ashes of cassava, yam, coconut, corncob, and cornhusk, respectively to undetectable levels in the ashes of the 5 wt.% acid-leached biomass fuels.

4.5 Comparative Study of Physical Morphology, Textural Properties, and Phase Analysis of Ashes

4.5.1 Physical morphology of ashes from untreated and acid-treated biomass

Figure 4.5 shows the effects of the pretreatment step on the physical appearance of the ashes of the untreated and the acid-leached biomass fuels.

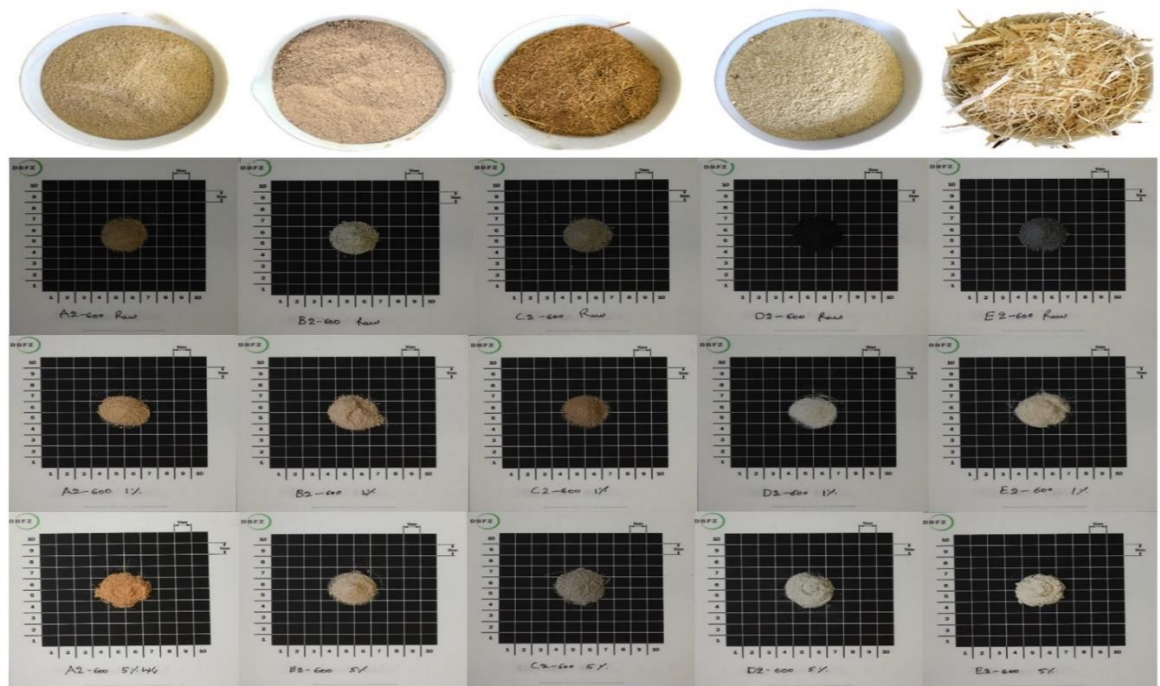


Figure 4.5. Visual appearances of thermally produced ashes of the raw and the acid-leached biomass fuels at 600 °C. First row from the top: untreated biomass fuels; second row: ashes of untreated biomass fuels; third row: ashes of 1 w/v% biomass fuels, and; last row: ashes of 5 w/v% biomass fuels. From left to right, biomass fuels and ashes of cassava peelings (CasP), yam peelings (YamP), coconut husk (CocH), corncobs (CorC) and cornhusk (CorH) generated at 600 °C for 2h.

The results indicated that white biogenic silica could be generated by pre-treating the biomass in a hot citric acid solution. According to Alyosef et al. [99] and Beidaghy Dizaji et al. [36], the colouration of the ashes is an indication of completeness of a combustion process and low concentration of remaining impurities. The metallic oxides in the untreated biomass

fuels result in the formation of black particles in the ashes [106]. Furthermore, in silica-rich biomass ashes, impurities increase the risk of slag formation during the combustion process [50,124]. The role of different impurities on the slag formation in silica-rich biomass ashes have been discussed by Beidaghy Dizaji et al. [50].

From Figure 4.5, the ashes of the untreated biomass fuels indicated the presence of black particles (fixed carbon). A plausible explanation for the formation of black particles, as explained by Krishnarao et al. [106], is that, during the combustion of biomass fuels from room temperature to high temperature, there is a simultaneous decomposition and oxidation of the organic matter into carbon. Prior to the removal of all the carbon, if the temperature rise is higher than the melting temperature of potassium oxide (350 °C), surface melting or sintering of the ash occurs, and the K^+ ions trap the carbon inside the organic matrix. This phenomenon inhibits carbon removal and results in the formation of black particles at high temperatures [106-108]. This explains the basis for the higher LOI values (indirect carbon content) measured in the untreated samples compared to the acid-treated biomass samples. Since the potassium oxide concentration is higher in the untreated biomass fuels than the acid-treated biomass, there was a high propensity for black particles formation in the ashes [106].

Furthermore, chemical pretreatment hydrolyses the organic (i.e., cellulose, hemicellulose and lignin) compounds and break their structures down [109–111]. Therefore, the evolution of volatile matter in the pretreated samples could easily occur, decreasing the amount of residual carbon in ashes [112]. Comparatively, the ashes at 1 w/v% CA had few remnants of black particles than the ashes of 5 w/v% CA for the same reasons explained above. Analysis of the metallic impurities shown in Figure 4.4 confirms a higher concentration of K^+ ions in the 1 w/v% CA than the ashes of 5 w/v% CA. Hence, the tendency to form black particles was more pronounced than the ashes from 5 w/v% CA treated samples. Chakraverty et al. [113] obtained ash completely white in colour after leaching rice husk in dilute 1 N HCl, thus proving the effectiveness of acid pretreatment in mitigating the formation of black particles. The complete white colour of CorC-A-5% and CorH-A-5% indicates total amorphous structured silica [114], as it is proven by the XRD measurements.

4.5.2 Nitrogen gas adsorption-desorption measurements

The isotherms for the CorH-U-A, CorH-A-1% and CorH-A-5% are given in Figure 4.6 as examples since the other samples show similar behaviour; the corresponding textural properties data along with the different samples are summarized in Table 4.4.

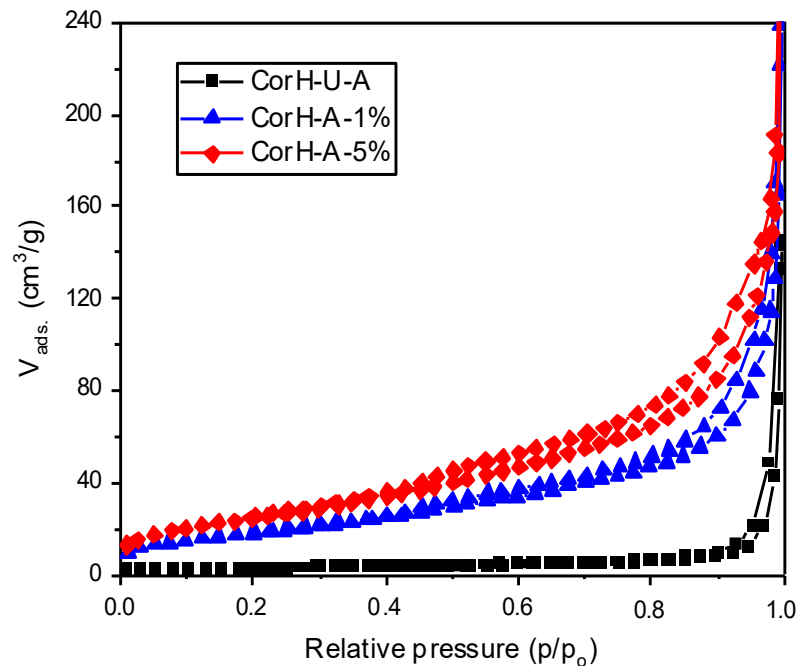


Figure 4.6. Adsorption–desorption isotherms of ashes from untreated and treated cornhusk.

For the treated samples (CorH-A-1% and CorH-A-5%), the isotherms exhibited a common characteristic of type IV(a) isotherm according to the IUPAC classifications [115], with a small knee at $p/p_0 = 0.05$. They showed an H3 apparent hysteresis loop with closure points around $p/p_0 = 0.40$, which is often associated with the effects of capillary condensation in non-uniform pore arrangements [116,117]. In addition, the presence of hysteresis loop in isotherms has been attributed to the presence of larger mesopores in the ash, which can only be accessed through the smaller mesopores [115]. Furthermore, the isotherms followed a similar path at the lower regions, and the amount of nitrogen adsorbed increases when approaching the saturation vapour pressure ($p/p_0 = 1$). The absence of an apparent plateau close to $p/p_0 = 1$ implies the presence of larger meso and macropores, which cannot be fully filled with the nitrogen condensate [47] and/or the presence of interstices between particles.

Conversely, the isotherm for the untreated ash sample (CorH-U-A) exhibited a much lower nitrogen adsorption capacity with no visible hysteresis loop, indicating no or much smaller porosity than the acid-leached ash samples. Agglomeration of ash particles has been reported to be accelerated by the presence of alkali metals [118], which were high in CorH-U-A according to the elemental analysis in Figure 4.4, resulting in diminished porosity [119]. CorH-U-A might contain some microporosity, which might have been formed by possible agglomeration of ash particles [35].

The textural properties, including the specific surface area (BET) and pore volume (NLDFT) from the nitrogen adsorption-desorption isotherms of the untreated and acid leached ashes are given in Table 4.4. Ashes/biogenic silica from cassava and yam biomass fuels exhibited the lowest surface area and pore volume compared to those of the other biomass fuels. According to Soltani et al. [120], a chelate reaction occurs between the carboxyl group (-COOH) of the citric acid and the metal impurities in the biomass fuels. Consequently, hydrolysis of the organic matter cleaves the macromolecules (monosaccharides), thereby removing the embedded impurities and opening the pores within the biomass fuels [121].

Table 4.4. Comparison of the structural characteristics (S_{BET} and pore volume V_p) of ashes. Ashes were generated from biomass fuels leached in 1 w/v% CA and 5 w/v% CA at a combustion temperature of 600 °C and residence time of 2h.

Sample	S_{BET} (m ² /g)	V_p (cm ³ /g)
Untreated		
CasP-U-A	3	0
YamP-U-A	2	0
CocH-U-A	0	0
CorC-U-A	2	0.01
CorH-U-A	9	0.04
1 w/v % CA		
CasP-A-1%	16	0.06
YamP-A-1%	7	0.16
CocH-A-1%	20	0.05
CorC-A-1%	47	0.09
CorH-A-1%	67	0.17
5 w/v % CA		
CasP-A-5%	26	0.10
YamP-A-5%	5	0.02
CocH-A-5%	56	0.14
CorC-A-5%	70	0.14
CorH-A-5%	91	0.21

Table 4.4 shows that the surface area and pore volume of the ashes (biogenic silica) increase with increasing citric acid concentration for all biomass fuels investigated. For example, the specific area of the CorH-U-A was 9 m²/g; however, after being treated with 1 w/v% citric acid, it increases to 67 m²/g and continued up to 91 m²/g at 5 w/v% CA concentration. Similarly, the pore volume of the ashes also increased in the order of preparation: X-A-5 w/v% > X-A-1 w/v% > X-U-A (X represents the name of the sample) within the different biogenic silica samples investigated.

The results obtained agree with similar observations made by Schneider et al. [47]. According to Schneider et al. [47], an increase in the purity of ashes (low presence of carbon and metallic impurities) will increase the surface areas and pore volumes due to pore blocking effects of the impurities present in the ashes. Hence, the purity of the ashes at 5 w/v% CA was higher than those of untreated and 1 w/v%. Moreover, a possible agglomeration of the ash particles of the untreated samples might have resulted in a diminished porosity [119]. It is conceivable that at 1 w/v% citric acid solution, the maximal removal capacity for metal impurities was achieved. Additional impurities could not be removed further to increase the pores/holes between the molecules. Secondly, these pores are developed within the particles by the thermal decomposition process. Since the carbon is easily volatilized in the treated samples during combustion, the pore walls are disintegrated, resulting in a rise in mesopore volume [93,94]. In addition, the textural variation between the individual biomasses is most likely since distinct Si integration mechanisms and varying SiO₂ domains exist among the various plants and plant parts investigated [34].

4.5.3 Phase analysis of the biomass ash samples

Venezia et al. [122] reported that the presence of alkali ions such as K, Mg, and Na in the ashes results in low melting temperature alkali-rich compounds, which drives the transition to different crystalline phases of silica. In addition, Yang et al. [123] reported that these metallic species accelerate the crystallization of amorphous silica above 1000 °C. Thus, eutectic mixtures or silica phases are induced, decreasing the phase transition temperature from amorphous to crystalline silica. These minerals, introduced as fuel contaminants, result in a less active amorphous silica with low textural properties [115] due to the strong correlation between the crystallinity fraction and porosity changes of the silica-

rich ashes [50]. This phenomenon is even more pronounced for untreated biomass fuels, as mentioned in the study of Schneider et al. [35,47] during their investigations with rice husk.

Figure 4.7 shows the XRD patterns and crystalline phases identified in the ash samples of the biomass fuels pretreated with 1 w/v% citric acid.

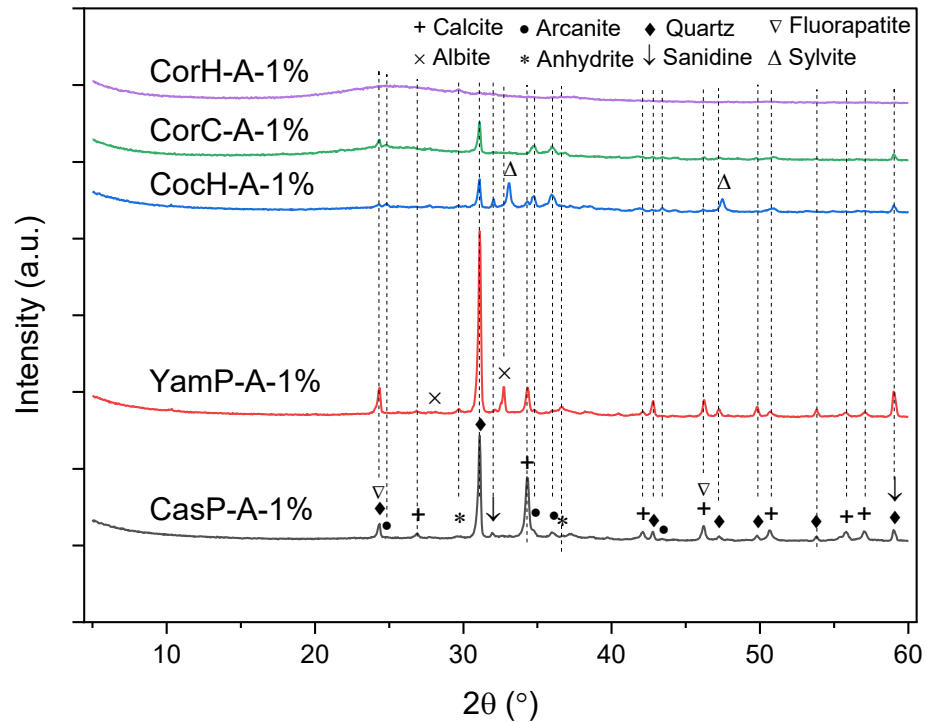


Figure 4.7. X-ray diffraction pattern of the ash samples resulting from the combustion of 1 w/v% acid-treated biomass fuels at 600 °C.

In all the ash samples, the following dominant phases were detected: quartz (SiO_2), calcite (CaCO_3) and anhydrite [$\text{Ca}(\text{SO}_4)$]. The presence of these dominant phases has also been reported during the investigations of wheat straw, miscanthus and cereal remnant pellet, all leached in hot solution of sulfuric acid [20]. Other minor crystalline phases, such as feldspar of the plagioclase series such as albite [$\text{Na}(\text{AlSi}_3\text{O}_8)$], were found in cassava and yam peelings as well as coconut husk in addition to an amorphous fraction. Potassium feldspar, such as sanidine (KAlSi_3O_8) was clearly detected in CocH-A-1%. The formation of sanidine (KAlSi_3O_8), as reported in the study of Alyosef et al. [20] could be as a result of a thermodynamic effect (i.e., “back-formation” of feldspar or arcanite) that reduces part of the amorphous silica particles [10,100]. The major differences in the XRD patterns of the samples were that of the CorC-A-1%, CorH-A-1%, which were characterized by a clear and

dominant amorphous component with traces of arcanite (K_2SO_4) and anhydrite [$Ca(SO_4)$], respectively. These last two phases are because of the remaining low impurities of K_2O and CaO present in the ashes, as confirmed by the EDX spectrum of the CorH-A-1% sample in Figure 4.8.

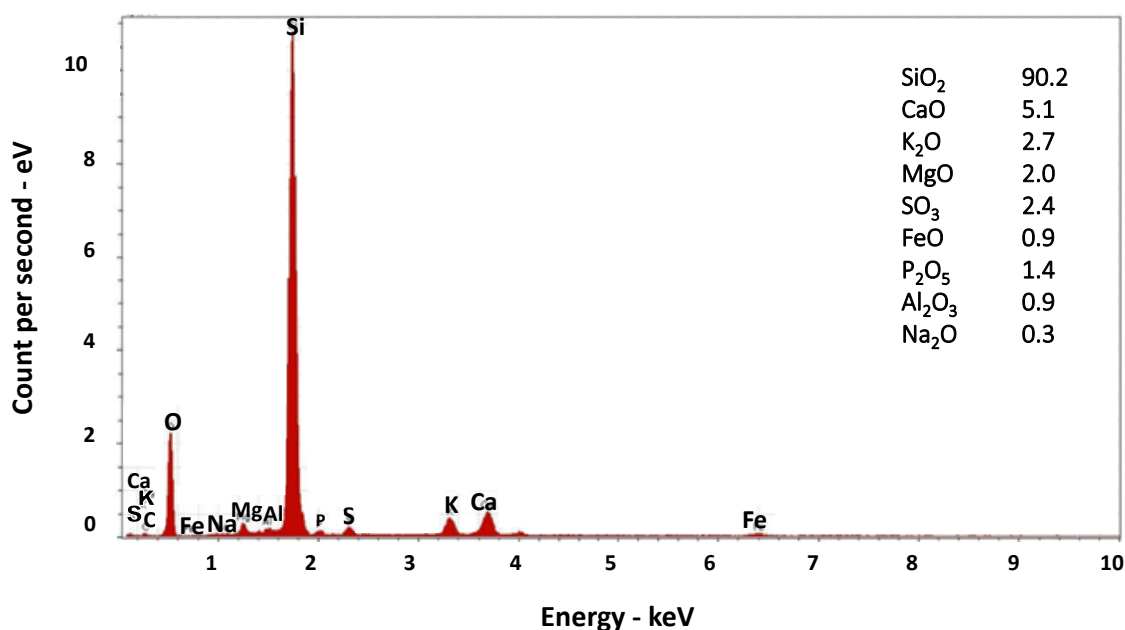


Figure 4.8. EDX spectrum (30kV) of the ash sample (wt.% db = 100) resulting from the combustion of CorH-A-1%.

According to the literature, the phase formations in the ashes can be attributed to the high presence of critical ash forming elements (such as Ca, K and Na) and their interactions with the silica particles [50,124–126]. Comparing the elemental compositions of the ashes of the biomass fuels leached at 1 w/v% citric acid in Table 4.5, all ash samples except for CorC-A-1% and CorH-A-1% had a higher content of potassium and sodium oxide (see “Elemental Composition of ashes in Figure 4.4). Thus, the tendencies for the formation of these minerals (fuel contaminants), i.e., anhydrite $Ca(SO_4)$, quartz (SiO_2), arcanite (K_2SO_4), sylvite (KCl), calcite and albite [$Na(AlSi_3O_8)$] were more evident in those samples as confirmed by the XRD measurements and summarized in Table 4.5. The broad peak in the range of $2\theta = 20\text{--}30^\circ$ found in the cornhusk ash samples was predominantly due to the amorphous silica in the analyzed samples. The thermally unstable phase of calcite ($CaCO_3$) was also observed in some of the samples, especially cassava and yam peels, and this was

due to the high concentration of Ca^{2+} ions in the water used for the leaching. This observation is in line with the results from the FTIR analyses where bands of calcite were dominant. Deng et al. [127] also reported on the formation of calcite on $-\text{OH}$ surfaces in high Ca^{2+} concentration.

Table 4.5. Crystalline phases identified with XRD in the ash samples after the combustion of 1 w/v% acid-treated biomass fuels at 600 °C.

Phase	Ashes				
	CasP-A-1%	YamP-A-1%	CocH-A-1%	CorC-A-1%	CorH-A-1%
Anhydrite [$\text{Ca}(\text{SO}_4)$]	x	x			x
Quartz (SiO_2)	x	x	x	x	x
Arcanite (K_2SO_4)	x		x		
Sylvite (KCl)			x		
Calcite (CaCO_3)	x	x	x		
Albite [$\text{Na}(\text{AlSi}_3\text{O}_8)$]		x			
Sanidine (KAlSi_3O_8)	x	x	x		

“x” denoting the presence of such a phase in the ashes.

A recent study of Beidaghy Dizaji et al. [50] on rice husk and straw ashes showed that once the temperature exceeds 550 towards 700 °C, there is a high tendency to form thermally non-stable compounds such as arcanite, calcite, and sylvite, which were also observed in this study. The result of this study only showed the presence of quartz instead of the other stable polymorphs forms of silica, i.e., cristobalite and tridymite [83,93,123]. The formation of cristobalite and tridymite phases in ashes is reported to occur at temperatures above 800 °C, lower than the temperature at which the selected biomass fuels in this study were combusted. Vassilev et al. [128] also reported the formation of cristobalite in rice husk ashes produced at higher temperatures (900 °C) as the main crystalline silica phase. The absence of cristobalite and tridymite in our ash samples affirms the appropriateness of the selected temperature regime for the combustion of the biomass fuels. This is because a high percentage of cristobalite and tridymite in ashes could negatively impact the textural properties and pose other health risks due to the carcinogenic attribute of crystalline silica [50,129].

Figure 4.9 also shows the improvement of silica content by employing higher citric acid concentration during the pretreatment stage. As observed, the O-Si-O bands at CorH-A-5% are of higher intensity than those of CorH-A-1%. More importantly, they are

comparable to the bands of commercial reference silica (CWK Köstropur[®] 021012) on the market, paving the way for the possibility of a wide variety of applications. The literature also reported silica purity improvement by pretreatment of other silica-rich biomass fuels [20,125].

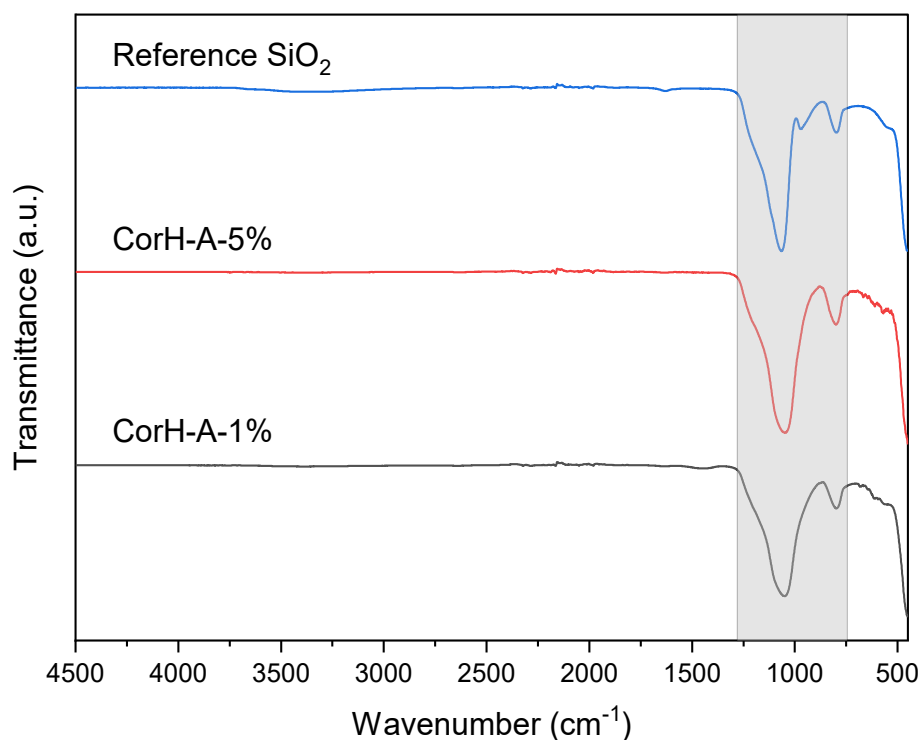


Figure 4.9. Comparison of the FTIR patterns of CorH-A-1% and CorH-A-5% with commercially available silica (CWK Köstropur[®] 021012) in the market (purity > 99.9%).

4.6 Conclusions

This work systematically examined the potential of producing high-quality amorphous silica from African biomass fuels such as cassava, yam, coconut, corncob, and cornhusk. The results showed that the leaching of the biomass fuels effectively removed a significant fraction of metallic impurities, especially K_2O and carbon compounds, from the organic matrix. The relative reductions of K_2O by the citric acid in yam peel was the lowest (79 wt.% db) in comparison to 92, 97, 98 and 97 wt.% db calculated for corncob, cassava peel, coconut husk and cornhusk, respectively. Acid leaching of the biomass in 5 w/v% citric acid resulted in producing ashes with larger surface areas, pore volume and completely white (no traces

of carbon). The colour, surface area and pore volume of the resulting ashes after combustion were highly influenced by the initial composition of the biomass fuels and the concentration of citric acid used in the pretreatment step. Cornhusk ash obtained the highest surface area (91 m²/g) and the highest silica content (>90 wt.% db), which was completely amorphous along with corncob (85 wt.% db SiO₂). However, crystalline phases such as arcanite (K₂SO₄), sylvite (KCl) and calcite (CaCO₃) were found in the ashes of cassava, yam, and coconut due to the influence of potassium and calcium ions. Consequently, the existing pretreatment and combustion methods should be optimized and extensively investigated to avoid phase formations. After these modifications, the production of biogenic silica products, which has already been realized in rice husk ash, should be possible from cassava, yam, and coconut residues. The results of this study widen the fundamental knowledge for the preparation of value-added materials from primary but less-known African residues opening up new value chains for the recovery of silica from cassava, yam, coconut, corncob, and cornhusk.

Acknowledgments: Special gratitude to the analytical laboratory and technical team members of DBFZ for their invaluable support during this study. Special appreciation to Marc Bohnet and Christoph Kröhl for their commitments to the analyses of the biomass fuels.

References of Chapter 4

1. Shah, M.A.; Khan, M.N.S.; Kumar, V. Biomass residue characterization for their potential application as biofuels. *J. Therm. Anal. Calorim.* **2018**, *134*, 2137–2145, doi:10.1007/s10973-018-7560-9.
2. Jiang, L.; Hu, S.; Sun, L.-S.; Su, S.; Xu, K.; He, L.-M.; Xiang, J. Influence of different demineralization treatments on physicochemical structure and thermal degradation of biomass. *Bioresour. Technol.* **2013**, *146*, 254–260, doi:10.1016/j.biortech.2013.07.063.
3. Marland, G. Accounting for Carbon Dioxide Emissions from Bioenergy Systems. *J. Ind. Ecol.* **2010**, *14*, 866–869, doi:10.1111/j.1530-9290.2010.00303.x.
4. Duku, M.H.; Gu, S.; Ben Hagan, E. A comprehensive review of biomass resources and biofuels potential in Ghana. *Renew. Sustain. Energy Rev.* **2011**, *15*, 404–415, doi:10.1016/j.rser.2010.09.033.

5. Lim, J.S.; Manan, Z.A.; Alwi, S.R.W.; Hashim, H. A review on utilisation of biomass from rice industry as a source of renewable energy. *Renew. Sustain. Energy Rev.* **2012**, *16*, 3084–3094, doi:10.1016/j.rser.2012.02.051.
6. Kemausuor, F.; Kamp, A.; Thomsen, S.T.; Bensah, E.; Østergård, H. Assessment of biomass residue availability and bioenergy yields in Ghana. *Resour. Conserv. Recycl.* **2014**, *86*, 28–37, doi:10.1016/j.resconrec.2014.01.007.
7. United Nations Framework Convention on Climate Change. Adoption of the Paris Agreement: Proposal by the President. Paris Climate Change Conference – November 2015, Cop 21, Paris. France.
8. African Climate Policy Centre (ACPC). 2010. Overview of the ClimDev Africa Programme. Available online: <http://www.climdev-africa.org/afrian-climate-policy-center> (accessed on 28 September 2021).
9. Catuti, M.; Elkerbout, M.; Alessi, M.; Egenhofer, C. Biomass and Climate Neutrality: CEPS Policy Insights. No 2020-19. August 2020. Available online: https://www.ceps.eu/wp-content/uploads/2020/08/PI2020-19_Biomass-and-climate-neutrality.pdf (accessed on 28 September 2021).
10. Guimarães, J.; Frollini, E.; da Silva, C.G.; Wypych, F.; Satyanarayana, K. Characterization of banana, sugarcane bagasse and sponge gourd fibers of Brazil. *Ind. Crop. Prod.* **2009**, *30*, 407–415, doi:10.1016/j.indcrop.2009.07.013.
11. Milbrandt, A. *Assessment of Biomass Resources in Liberia*; No. NREL/TP-6A2-44808; National Renewable Energy Lab. (NREL): Golden, CO, USA, 2009.
12. Smith, O.B. Utilization of Crop Residues in the Nutrition of Sheep and Goats in the Humid Tropics of West Africa. In Atta Krah A.N and Reyholds L. Sheep and goat meat production in humid tropics of West Africa. Yamoussoukro, 21–25, September 1987. FAO Animal Production and Health paper. <http://www.fao.org/library/library-home/en/> (accessed on 29 September 2021).
13. Abass, A.; Mlingi, N.; Ranaivoson, R.; Zulu, M.; Mukuka, I.; Abele, S.; Bachwenkizi, B.; Cromme, N. *Potential for Commercial Production and Marketing of Cassava: Experiences from the Small-Scale Cassava Processing Project in East and Southern Africa*; IITA: Ibadan, Nigeria, 2013.
14. Titiloye, J.; Abu Bakar, M.S.; Odetoeye, T. Thermochemical characterisation of agricultural wastes from West Africa. *Ind. Crop. Prod.* **2013**, *47*, 199–203, doi:10.1016/j.indcrop.2013.03.011.

15. Adepoju, A.D.; Adebisi, J.A.; Odusote, J.K.; Ahmed, I.I.; Hassan, S.B. Preparation of Silica from Cassava Periderm. *J. Solid Waste Technol. Manag.* **2016**, *42*, 216–221, doi:10.5276/jswtm.2016.216.
16. Jekayinfa, S.O.; Scholz, V. Potential Availability of Energetically Usable Crop Residues in Nigeria. *Energy Sources Part A Recover. Util. Environ. Eff.* **2009**, *31*, 687–697, doi:10.1080/15567030701750549.
17. Cooper, C.; Laing, C. A macro analysis of crop residue and animal wastes as a potential energy source in Africa. *J. Energy S. Afr.* **2007**, *18*, 10–19, doi:10.17159/2413-3051/2007/v18i1a3339.
18. Dasappa, S. Potential of biomass energy for electricity generation in sub-Saharan Africa. *Energy Sustain. Dev.* **2011**, *15*, 203–213, doi:10.1016/j.esd.2011.07.006.
19. Stecher, K.; Brosowski, A.; Thrän, D. Biomass Potential in Africa. Irena 2013, 44. Available online: https://www.dbfz.de/fileadmin/user_upload/Referenzen/Broschueren/IRENA-DBFZ_Biomass_Potential_in_Africa.pdf (accessed on 4 October 2021).
20. Alyosef, H.A.; Schneider, D.; Wassersleben, S.; Roggendorf, H.; Weiß, M.; Eilert, A.; Denecke, R.; Hartmann, I.; Enke, D. Meso/Macroporous Silica from Miscanthus, Cereal Remnant Pellets, and Wheat Straw. *ACS Sustain. Chem. Eng.* **2015**, *3*, 2012–2021, doi:10.1021/acssuschemeng.5b00275.
21. Nitsch, J.; Krewitt, W.; Langniss, O. Renewable Energy in Europe. *Encycl. Energy* **2004**, *5*, 313–331, doi:10.1016/b0-12-176480-x/00365-x.
22. Adebisi, J.A.; Agunsoye, J.O.; Bello, S.A.; Kolawole, F.O.; Ramakokovhu, M.M.; Daramola, M.O.; Hassan, S.B. Extraction of Silica from Sugarcane Bagasse, Cassava Periderm and Maize Stalk: Proximate Analysis and Physico-Chemical Properties of Wastes. *Waste Biomass Valorization* **2017**, *10*, 617–629, doi:10.1007/s12649-017-0089-5.
23. Omohimi, C.I.; Piccirillo, C.; Roriz, M.; Ferraro, V.; Vasconcelos, M.W.; Sanni, L.; Tomlins, K.; Pintado, M.M.; Abayomi, L.A. Study of the proximate and mineral composition of different Nigerian yam chips, flakes and flours. *J. Food Sci. Technol.* **2017**, *55*, 42–51, doi:10.1007/s13197-017-2761-y.
24. FAOSTAT. *The State of Food and Agriculture*; Food and Agriculture Organisation of the UN: Rome, Italy, 2007. Available online: <http://www.fao.org/3/a1200e/a1200e.pdf> (accessed on 21 August 2021).

25. Bonfim, W.B.; de Paula, H.M. Characterization of different biomass ashes as supplementary cementitious material to produce coating mortar. *J. Clean. Prod.* **2021**, *291*, 125869, doi:10.1016/j.jclepro.2021.125869.
26. Andreola, F.; Martín, M.; Ferrari, A.; Lancellotti, I.; Bondioli, F.; Rincón, J.; Romero, M.; Barbieri, L. Technological properties of glass-ceramic tiles obtained using rice husk ash as silica precursor. *Ceram. Int.* **2013**, *39*, 5427–5435, doi:10.1016/j.ceramint.2012.12.050.
27. Sae-Oui, P.; Rakdee, C.; Thanmathorn, P. Use of rice husk ash as filler in natural rubber vulcanizates: In comparison with other commercial fillers. *J. Appl. Polym. Sci.* **2002**, *83*, 2485–2493, doi:10.1002/app.10249.
28. Ajmal, M.; Rao, R.A.K.; Anwar, S.; Ahmad, J.; Ahmad, R. Adsorption studies on rice husk: Removal and recovery of Cd(II) from wastewater. *Bioresour. Technol.* **2003**, *86*, 147–149, doi:10.1016/s0960-8524(02)00159-1.
29. Niculescu, V.-C.; Miricioiu, M.; Geana, E.-I.; Ionete, R.-E.; Paun, N.; Parvulescu, V. Silica Mesoporous Materials -an Efficient Sorbent for Wine Polyphenols Separation. *Rev. Chim.* **2019**, *70*, 1513–1517, doi:10.37358/rc.19.5.7161.
30. Liu, D.; Seeburg, D.; Kreft, S.; Bindig, R.; Hartmann, I.; Schneider, D.; Enke, D.; Wohlrab, S. Rice Husk Derived Porous Silica as Support for Pd and CeO₂ for Low Temperature Catalytic Methane Combustion. *Catalyst* **2019**, *9*, 26, doi:10.3390/catal9010026.
31. Azadi, M.; Bahrololoom, M.E.; Heidari, F. Enhancing the mechanical properties of an epoxy coating with rice husk ash, a green product. *J. Coat. Technol. Res.* **2010**, *8*, 117–123, doi:10.1007/s11998-010-9284-z.
32. Dai, H.; Yang, J.; Ma, J.; Chen, F.; Fei, Z.; Zhong, M. A green process for the synthesis of controllable mesoporous silica materials. *Microporous Mesoporous Mater.* **2012**, *147*, 281–285, doi:10.1016/j.micromeso.2011.06.029.
33. Adebisi, J.; Agunsoye, J.; Bello, S.; Ahmed, I.; Ojo, O.; Hassan, S. Potential of producing solar grade silicon nanoparticles from selected agro-wastes: A review. *Sol. Energy* **2017**, *142*, 68–86, doi:10.1016/j.solener.2016.12.001.
34. Florek, J.; Guillet-Nicolas, R.; Kleitz, F. Ordered mesoporous silica: Synthesis and applications. In *Functional Materials*; Walter de Gruyter GmbH & Co KG, Berlin, Germany, 2014; pp. 61–100.
35. Schneider, D. Biogenic silica from regional feedstocks—Sustainable synthesis and characterization. Ph.D. Thesis, Universität Leipzig, Leipzig, Germany, 2019.

36. Beidaghy Dizaji, H.; Zeng, T.; Hartmann, I.; Enke, D.; Schliermann, T.; Lenz, V.; Bidabadi, M. Generation of High-quality Biogenic Silica by Combustion of Rice Husk and Rice Straw Combined with Pre- and Post-Treatment Strategies—A Review. *Appl. Sci.* **2019**, *9*, 1083, doi:10.3390/app9061083.
37. Quispe, I.; Navia, R.; Kahhat, R. Energy potential from rice husk through direct combustion and fast pyrolysis: A review. *Waste Manag.* **2017**, *59*, 200–210, doi:10.1016/j.wasman.2016.10.001.
38. Biswas, B.; Pandey, N.; Bisht, Y.; Singh, R.; Kumar, J.; Bhaskar, T. Pyrolysis of agricultural biomass residues: Comparative study of corn cob, wheat straw, rice straw and rice husk. *Bioresour. Technol.* **2017**, *237*, 57–63, doi:10.1016/j.biortech.2017.02.046.
39. Zemnukhova, L.A.; Egorov, A.G.; Fedorishcheva, G.A.; Barinov, N.N.; Sokol’Nitskaya, T.A.; Botsul, A.I. Properties of amorphous silica produced from rice and oat processing waste. *Inorg. Mater.* **2006**, *42*, 24–29, doi:10.1134/s0020168506010067.
40. Ma, J.F.; Yamaji, N. Silicon uptake and accumulation in higher plants. *Trends Plant Sci.* **2006**, *11*, 392–397, doi:10.1016/j.tplants.2006.06.007.
41. Yan, G.; Nikolic, M.; Ye, M.-J.; Xiao, Z.-X.; Liang, Y.-C. Silicon acquisition and accumulation in plant and its significance for agriculture. *J. Integr. Agric.* **2018**, *17*, 2138–2150, doi:10.1016/s2095-3119(18)62037-4.
42. Vaibhav, V.; Vijayalakshmi, U.; Roopan, S.M. Agricultural waste as a source for the production of silica nanoparticles. *Spectrochim. Acta Part A Mol. Biomol. Spectrosc.* **2015**, *139*, 515–520, doi:10.1016/j.saa.2014.12.083.
43. Abu Bakar, R.; Yahya, R.; Gan, S.N. Production of High Purity Amorphous Silica from Rice Husk. *Procedia Chem.* **2016**, *19*, 189–195, doi:10.1016/j.proche.2016.03.092.
44. Miricioiu, M.G.; Niculescu, V.-C. Fly Ash, from Recycling to Potential Raw Material for Mesoporous Silica Synthesis. *Nanomaterials* **2020**, *10*, 474, doi:10.3390/nano10030474.
45. Behrens, M.; Datye, A.K. *Catalysis for the Conversion of Biomass and Its Derivatives*; Max Planck Research Library for History and Development of Knowledge: Berlin, Germany, 2013.
46. Long, J.; Song, H.; Jun, X.; Sheng, S.; Lun-Shi, S.; Kai, X.; Yao, Y. Release characteristics of alkali and alkaline earth metallic species during biomass pyrolysis and

- steam gasification process. *Bioresour. Technol.* **2012**, *116*, 278–284, doi:10.1016/j.biortech.2012.03.051.
47. Schneider, D.; Wassersleben, S.; Weiß, M.; Denecke, R.; Stark, A.; Enke, D. A Generalized Procedure for the Production of High-Grade, Porous Biogenic Silica. *Waste Biomass Valorization* **2020**, *11*, 1–15, doi:10.1007/s12649-018-0415-6.
 48. Umeda, J.; Imai, H.; Kondoh, K. Polysaccharide hydrolysis and metallic impurities removal behaviour of rice husks in citric acid leaching treatment. *Trans. JWRI.* **2009**, *38* (2), 13-18.
 49. Umeda, J.; Kondoh, K. High-purity amorphous silica originated in rice husks via carboxylic acid leaching process. *J. Mater. Sci.* **2008**, *43*, 7084–7090, doi:10.1007/s10853-008-3060-9.
 50. Beidaghy Dizaji, H.; Zeng, T.; Hölzig, H.; Bauer, J.; Klöß, G.; Enke, D. Ash transformation mechanism during combustion of rice husk and rice straw. *Fuel* **2022**, *307*, 121768, doi:10.1016/j.fuel.2021.121768.
 51. Utsev, J.T.; Taku, J.K. Coconut Shell Ash as Partial Replacement of Ordinary Portland Cement In Concrete Production. *Int. J. Sci. Technol. Res.* **2012**, *1*, 86–89.
 52. Samanta, A.K.; Basu, G.; Mishra, L. Role of major constituents of coconut fibres on absorption of ionic dyes. *Ind. Crop. Prod.* **2018**, *117*, 20–27, doi:10.1016/j.indcrop.2018.02.080.
 53. Asuquo, E.D.; Martin, A.D.; Nzerem, P. Evaluation of Cd(II) Ion Removal from Aqueous Solution by a Low-Cost Adsorbent Prepared from White Yam (*Dioscorea rotundata*) Waste Using Batch Sorption. *ChemEngineering* **2018**, *2*, 35, doi:10.3390/chemengineering2030035.
 54. Anuar, M.F.; Fen, Y.W.; Zaid, M.H.M.; Matori, K.A.; Khaidir, R.E.M. Synthesis and structural properties of coconut husk as potential silica source. *Results Phys.* **2018**, *11*, 1–4, doi:10.1016/j.rinp.2018.08.018.
 55. Schliermann, T.; Hartmann, I.; Beidaghy Dizaji, H.; Zeng, T.; Schneider, D.; Wassersleben, S.; Enke, D.; Jobst, T.; Lange, A.; Roelofs, F.; et al. High-quality Biogenic Silica from Combined Energetic and Material Utilization of Agricultural Residues. In Proceedings of the 7th International Symposium on Energy from Biomass and Waste, Venice, Italy. 15-18 October 2018; ISBN 978-8-86-265013-7; 2018.
 56. Hilbers, T.J.; Wang, Z.; Pecha, B.; Westerhof, R.J.; Kersten, S.R.; Pelaez-Samaniego, M.R.; Garcia-Perez, M. Cellulose-Lignin interactions during slow and fast pyrolysis. *J. Anal. Appl. Pyrolysis* **2015**, *114*, 197–207, doi:10.1016/j.jaap.2015.05.020.

57. Chen, D.; Gao, A.; Cen, K.; Zhang, J.; Cao, X.; Ma, Z. Investigation of biomass torrefaction based on three major components: Hemicellulose, cellulose, and lignin. *Energy Convers. Manag.* **2018**, *169*, 228–237, doi:10.1016/j.enconman.2018.05.063.
58. Ma, Z.; Chen, D.; Gu, J.; Bao, B.; Zhang, Q. Determination of pyrolysis characteristics and kinetics of palm kernel shell using TGA–FTIR and model-free integral methods. *Energy Convers. Manag.* **2015**, *89*, 251–259, doi:10.1016/j.enconman.2014.09.074.
59. Zhao, C.; Jiang, E.; Chen, A. Volatile production from pyrolysis of cellulose, hemicellulose and lignin. *J. Energy Inst.* **2017**, *90*, 902–913, doi:10.1016/j.joei.2016.08.004.
60. Yang, H.; Yan, R.; Chen, H.; Lee, D.H.; Zheng, C. Characteristics of hemicellulose, cellulose and lignin pyrolysis. *Fuel* **2007**, *86*, 1781–1788, doi:10.1016/j.fuel.2006.12.013.
61. Dhyani, V.; Bhaskar, T. A comprehensive review on the pyrolysis of lignocellulosic biomass. *Renew. Energy* **2018**, *129*, 695–716, doi:10.1016/j.renene.2017.04.035.
62. Lopez-Velazquez, M.A.; Santes, V.; Balmaseda, J.; Torres-Garcia, E. Pyrolysis of orange waste: A thermo-kinetic study. *J. Anal. Appl. Pyrolysis* **2013**, *99*, 170–177, doi:10.1016/j.jaap.2012.09.016.
63. Yang, H.; Yan, R.; Chin, T.; Liang, D.T.; Chen, A.H.; Zheng, C. Thermogravimetric Analysis–Fourier Transform Infrared Analysis of Palm Oil Waste Pyrolysis. *Energy Fuels* **2004**, *18*, 1814–1821, doi:10.1021/ef030193m.
64. Mendes, C.A.; Adnet, F.A.; Leite, M.C.A.M.; Furtado, C.; Furtado, M. Chemical, physical, mechanical, thermal and morphological characterization of corn husk residue. *Cellul. Chem. Technol.* **2015**, *49*, 727–735.
65. Ceylan, S.; Topçu, Y. Pyrolysis kinetics of hazelnut husk using thermogravimetric analysis. *Bioresour. Technol.* **2014**, *156*, 182–188, doi:10.1016/j.biortech.2014.01.040.
66. Gu, X.; Ma, X.; Li, L.; Liu, C.; Cheng, K.; Li, Z. Pyrolysis of poplar wood sawdust by TG-FTIR and Py-GC/MS. *J. Anal. Appl. Pyrolysis* **2013**, *102*, 16–23, doi:10.1016/j.jaap.2013.04.009.
67. Jiang, Z.; Liu, Z.; Fei, B.; Cai, Z.; Yu, Y.; Liu, X. The pyrolysis characteristics of moso bamboo. *J. Anal. Appl. Pyrolysis* **2012**, *94*, 48–52, doi:10.1016/j.jaap.2011.10.010.
68. Kumar, A.; Wang, L.; Dzenis, Y.A.; Jones, D.D.; Hanna, M.A. Thermogravimetric characterization of corn stover as gasification and pyrolysis feedstock. *Biomass Bioenergy* **2008**, *32*, 460–467, doi:10.1016/j.biombioe.2007.11.004.

69. Chen, D.; Zheng, Y.; Zhu, X. In-depth investigation on the pyrolysis kinetics of raw biomass. Part I: Kinetic analysis for the drying and devolatilization stages. *Bioresour. Technol.* **2013**, *131*, 40–46, doi:10.1016/j.biortech.2012.12.136.
70. Amutio, M.; Lopez, G.; Aguado, R.; Artetxe, M.; Bilbao, J.; Olazar, M. Kinetic study of lignocellulosic biomass oxidative pyrolysis. *Fuel* **2012**, *95*, 305–311, doi:10.1016/j.fuel.2011.10.008.
71. Mansaray, A.E.G.K.G. Kinetics of the Thermal Degradation of Rice Husks in Nitrogen Atmosphere. *Energy Sources* **1999**, *21*, 773–784, doi:10.1080/00908319950014335.
72. Jose, A.; Nivitha, M.; Krishnan, M.; Robinson, R. Characterization of cement stabilized pond ash using FTIR spectroscopy. *Constr. Build. Mater.* **2020**, *263*, 120136, doi:10.1016/j.conbuildmat.2020.120136.
73. Jung, H.; Kwak, H.; Chun, J.; Oh, K. Alkaline Fractionation and Subsequent Production of Nano-Structured Silica and Cellulose Nano-Fibrils for the Comprehensive Utilization of Rice Husk. *Sustainability* **2021**, *13*, 1951, doi:10.3390/su13041951.
74. Nakason, K.; Khemthong, P.; Kraithong, W.; Chukaew, P.; Panyapinyopol, B.; Kitkaew, D.; Pavasant, P. Upgrading properties of biochar fuel derived from cassava rhizome via torrefaction: Effect of sweeping gas atmospheres and its economic feasibility. *Case Stud. Therm. Eng.* **2021**, *23*, 100823, doi:10.1016/j.csite.2020.100823.
75. Pollard, Z.A.; Goldfarb, J.L. Valorization of cherry pits: Great Lakes agro-industrial waste to mediate Great Lakes water quality. *Environ. Pollut.* **2021**, *270*, 116073, doi:10.1016/j.envpol.2020.116073.
76. Volpe, M.; Goldfarb, J.L.; Fiori, L. Hydrothermal carbonization of *Opuntia ficus-indica* cladodes: Role of process parameters on hydrochar properties. *Bioresour. Technol.* **2018**, *247*, 310–318, doi:10.1016/j.biortech.2017.09.072.
77. Magdziarz, A.; Dalai, A.K.; Koziński, J.A. Chemical composition, character and reactivity of renewable fuel ashes. *Fuel* **2016**, *176*, 135–145, doi:10.1016/j.fuel.2016.02.069.
78. Nieves, L.J.J.; Elyseu, F.; Goulart, S.; Pereira, M.D.S.; Valvassori, E.Z.; Bernardin, A.M. Use of fly and bottom ashes from a thermoelectrical plant in the synthesis of geopolymers: Evaluation of reaction efficiency. *Energy Geosci.* **2021**, *2*, 167–173, doi:10.1016/j.engeos.2020.09.004.
79. Nana, A.; Epey, N.; Rodrique, K.C.; Deutou, J.G.N.; Djobo, J.N.Y.; Tomé, S.; Alomayri, T.S.; Ngouné, J.; Kamseu, E.; Leonelli, C. Mechanical strength and microstructure of metakaolin/volcanic ash-based geopolymer composites reinforced

- with reactive silica from rice husk ash (RHA). *Materialia* **2021**, *16*, 101083, doi:10.1016/j.mtla.2021.101083.
80. Ma, X.; Zhou, B.; Gao, W.; Qu, Y.; Wang, L.; Wang, Z.; Zhu, Y. A recyclable method for production of pure silica from rice hull ash. *Powder Technol.* **2012**, *217*, 497–501, doi:10.1016/j.powtec.2011.11.009.
 81. Bathla, A.; Narula, C.; Chauhan, R.P. Hydrothermal synthesis and characterization of silica nanowires using rice husk ash: An agricultural waste. *J. Mater. Sci. Mater. Electron.* **2018**, *29*, 6225–6231, doi:10.1007/s10854-018-8598-y.
 82. Morrow, B.A.; McFarlan, A.J. Surface vibrational modes of silanol groups on silica. *J. Phys. Chem.* **1992**, *96*, 1395–1400, doi:10.1021/j100182a068.
 83. Mohanraj, K.; Kannan, S.; Barathan, S.; Sivakumar, G. Preparation and Characterization of Nano SiO₂ from Corn Cob Ash by Precipitation Method. *Optoelectron. Adv. Mater. Rapid Commun.* **2012**, *6* (3-4), 394–397.
 84. Ennaciri, Y.; El Alaoui-Belghiti, H.; Bettach, M. Comparative study of K₂SO₄ production by wet conversion from phosphogypsum and synthetic gypsum. *J. Mater. Res. Technol.* **2019**, *8*, 2586–2596, doi:10.1016/j.jmrt.2019.02.013.
 85. Medina, J.M.; Del Bosque, I.F.S.; Frías, M.; De Rojas, M.I.S.; Medina, C. Characterisation and valorisation of biomass waste as a possible addition in eco-cement design. *Mater. Struct.* **2017**, *50*, 207, doi:10.1617/s11527-017-1076-9.
 86. Liou, T.-H. Evolution of chemistry and morphology during the carbonization and combustion of rice husk. *Carbon* **2004**, *42*, 785–794, doi:10.1016/j.carbon.2004.01.050.
 87. Frías, M.; Villar-Cociña, E.; Savastano, H. Brazilian sugar cane bagasse ashes from the cogeneration industry as active pozzolans for cement manufacture. *Cem. Concr. Compos.* **2011**, *33*, 490–496, doi:10.1016/j.cemconcomp.2011.02.003.
 88. Leng, L.; Bogush, A.A.; Roy, A.; Stegemann, J.A. Characterisation of ashes from waste biomass power plants and phosphorus recovery. *Sci. Total Environ.* **2019**, *690*, 573–583, doi:10.1016/j.scitotenv.2019.06.312.
 89. Alyosef, H.A.; Ibrahim, S.; Welscher, J.; Inayat, A.; Eilert, A.; Denecke, R.; Schwieger, W.; Münster, T.; Kloess, G.; Einicke, W.-D.; et al. Effect of acid treatment on the chemical composition and the structure of Egyptian diatomite. *Int. J. Miner. Process.* **2014**, *132*, 17–25, doi:10.1016/j.minpro.2014.09.001.
 90. Keown, D.; Favas, G.; Hayashi, J.; Li, C.-Z. Volatilisation of alkali and alkaline earth metallic species during the pyrolysis of biomass: Differences between sugar cane

- bagasse and cane trash. *Bioresour. Technol.* **2005**, *96*, 1570–1577, doi:10.1016/j.biortech.2004.12.014.
91. Chen, H.; Wang, W.; Martin, J.C.; Oliphant, A.J.; Doerr, P.A.; Xu, J.F.; DeBorn, K.M.; Chen, C.; Sun, L. Extraction of Lignocellulose and Synthesis of Porous Silica Nanoparticles from Rice Husks: A Comprehensive Utilization of Rice Husk Biomass. *ACS Sustain. Chem. Eng.* **2012**, *1*, 254–259, doi:10.1021/sc300115r.
 92. Dunlop, A.P. Furfural Formation and Behavior. *Ind. Eng. Chem.* **1948**, *40*, 204–209, doi:10.1021/ie50458a006.
 93. Olsson, J.G.; Jäglid, U.; Pettersson, J.B.C.; Hald, P. Alkali Metal Emission during Pyrolysis of Biomass. *Energy Fuels* **1997**, *11*, 779–784, doi:10.1021/ef960096b.
 94. Hunt, L.P.; Dismukes, J.P.; Amick, J.A.; Schei, A.; Larsen, K. Rice Hulls as a Raw Material for Producing Silicon. *J. Electrochem. Soc.* **1984**, *131*, 1683–1686, doi:10.1149/1.2115937.
 95. Amick, J.A. Purification of Rice Hulls as a Source of Solar Grade Silicon for Solar Cells. *J. Electrochem. Soc.* **1982**, *129*, 864–866, doi:10.1149/1.2123989.
 96. Umeda, J.; Katsuyoshi, K. Process Optimization to Prepare High-Purity Amorphous Silica from Rice Husks via Citric Acid Leaching Treatment. *Trans. JWRI* **2008**, *37*, 13–17.
 97. Currie, H.A.; Perry, C.C. Silica in Plants: Biological, Biochemical and Chemical Studies. *Ann. Bot.* **2007**, *100*, 1383–1389, doi:10.1093/aob/mcm247.
 98. Ma, J.F.; Yamaji, N. Functions and transport of silicon in plants. *Cell. Mol. Life Sci.* **2008**, *65*, 3049–3057, doi:10.1007/s00018-008-7580-x.
 99. Singh, S.P.; Endley, N. Fabrication of nano-silica from agricultural residue and their application. In *Nanomaterials for Agriculture and Forestry Applications*; Elsevier: Amsterdam, The Netherlands, 2020; pp. 107–134.
 100. Alyosef, H.A.; Eilert, A.; Welscher, J.; Ibrahim, S.S.; Denecke, R.; Schwieger, W.; Enke, D. Characterization of Biogenic Silica Generated by Thermo Chemical Treatment of Rice Husk. *Part. Sci. Technol.* **2013**, *31*, 524–532, doi:10.1080/02726351.2013.782931.
 101. Chandrasekhar, S.; Satyanarayana, K.G.; Pramada, P.N.; Raghavan, P.; Gupta, T.N. Review Processing, properties and applications of reactive silica from rice husk—An overview. *J. Mater. Sci.* **2003**, *38*, 3159–3168, doi:10.1023/a:1025157114800.

102. Ma, J.F.; Higashitani, A.; Sato, K.; Takeda, K. Genotypic variation in silicon concentration of barley grain. *Plant Soil* **2003**, *249*, 383–387, doi:10.1023/a:1022842421926.
103. Takahashi, E.; Ma, J.F.; Miyake, Y. The Possibility of Silicon as an Essential Element for Higher Plants. *Comments Agric. Food Chem.* **1990**, *2*, 99–122.
104. Broadley, M.; Brown, P.; Cakmak, I.; Ma, J.F.; Rengel, Z.; Zhao, F. *Beneficial Elements*; Elsevier: Amsterdam, The Netherlands, 2012; pp. 249–269.
105. Deren, C. Chapter 8 Plant genotype, silicon concentration, and silicon-related responses. *Inulin Inulin-Contain. Crop.* **2001**, *8*, 149–158, doi:10.1016/s0928-3420(01)80012-4.
106. Krishnarao, R.; Subrahmanyam, J.; Kumar, T.J. Studies on the formation of black particles in rice husk silica ash. *J. Eur. Ceram. Soc.* **2001**, *21*, 99–104, doi:10.1016/s0955-2219(00)00170-9.
107. Zareihassangheshlaghi, A.; Beidaghy Dizaji, H.; Zeng, T.; Huth, P.; Ruf, T.; Denecke, R.; Enke, D. Behavior of Metal Impurities on Surface and Bulk of Biogenic Silica from Rice Husk Combustion and the Impact on Ash-Melting Tendency. *ACS Sustain. Chem. Eng.* **2020**, *8*, 10369–10379, doi:10.1021/acssuschemeng.0c01484.
108. Chandrasekhar, S.; Pramada, P.N.; Majeed, J. Effect of calcination temperature and heating rate on the optical properties and reactivity of rice husk ash. *J. Mater. Sci.* **2006**, *41*, 7926–7933, doi:10.1007/s10853-006-0859-0.
109. Kumar, P.; Barrett, D.M.; Delwiche, M.J.; Stroeve, P. Methods for Pretreatment of Lignocellulosic Biomass for Efficient Hydrolysis and Biofuel Production. *Ind. Eng. Chem. Res.* **2009**, *48*, 3713–3729, doi:10.1021/ie801542g.
110. Mosier, N.; Wyman, C.; Dale, B.; Elander, R.; Lee, Y.Y.; Holtzapple, M.; Ladisch, M. Features of promising technologies for pretreatment of lignocellulosic biomass. *Bioresour. Technol.* **2005**, *96*, 673–686, doi:10.1016/j.biortech.2004.06.025.
111. Tadesse, H.; Luque, R. Advances on biomass pretreatment using ionic liquids: An overview. *Energy Environ. Sci.* **2011**, *4*, 3913–3929, doi:10.1039/c0ee00667j.
112. Hanna, S.; Farag, L.; Mansour, N. Pyrolysis and combustion of treated and untreated rice hulls. *Thermochim. Acta* **1984**, *81*, 77–86, doi:10.1016/0040-6031(84)85112-6.
113. Chakraverty, A.; Mishra, P.; Banerjee, H.D. Investigation of combustion of raw and acid-leached rice husk for production of pure amorphous white silica. *J. Mater. Sci.* **1988**, *23*, 21–24, doi:10.1007/bf01174029.

114. Shen, Y.; Zhao, P.; Shao, Q. Porous silica and carbon derived materials from rice husk pyrolysis char. *Microporous Mesoporous Mater.* **2014**, *188*, 46–76, doi:10.1016/j.micromeso.2014.01.005.
115. Thommes, M.; Kaneko, K.; Neimark, A.V.; Olivier, J.P.; Rodriguez-Reinoso, F.; Rouquerol, J.; Sing, K.S.W. Physisorption of gases, with special reference to the evaluation of surface area and pore size distribution (IUPAC Technical Report). *Pure Appl. Chem.* **2015**, *87*, 1051–1069, doi:10.1515/pac-2014-1117.
116. Banerjee, S.; Gautam, R.K.; Jaiswal, A.; Chattopadhyaya, M.C.; Sharma, Y.C. Rapid scavenging of methylene blue dye from a liquid phase by adsorption on alumina nanoparticles. *RSC Adv.* **2015**, *5*, 14425–14440, doi:10.1039/c4ra12235f.
117. Li, T.; Shen, J.; Huang, S.; Li, N.; Ye, M. Hydrothermal carbonization synthesis of a novel montmorillonite supported carbon nanosphere adsorbent for removal of Cr (VI) from waste water. *Appl. Clay Sci.* **2014**, *93-94*, 48–55, doi:10.1016/j.clay.2014.02.015.
118. Basu, P. Biomass Characteristics. In *Biomass Gasification, Pyrolysis and Torrefaction*; Elsevier: Amsterdam, The Netherlands, 2018; pp. 49–91.
119. Shen, J.; Liu, X.; Zhu, S.; Zhang, H.; Tan, J. Effects of calcination parameters on the silica phase of original and leached rice husk ash. *Mater. Lett.* **2011**, *65*, 1179–1183, doi:10.1016/j.matlet.2011.01.034.
120. Soltani, N.; Bahrami, A.; Pech-Canul, M.; González, L. Review on the physicochemical treatments of rice husk for production of advanced materials. *Chem. Eng. J.* **2015**, *264*, 899–935, doi:10.1016/j.cej.2014.11.056.
121. Ozdemir, S.; Ozdemir, S.; Yetilmezsoy, K. Poultry abattoir sludge as bio-nutrient source for walnut plantation in low-fertility soil. *Environ. Prog. Sustain. Energy* **2019**, *38*, e13066, doi:10.1002/ep.
122. Venezia, A.M.; La Parola, V.; Longo, A.; Martorana, A. Effect of Alkali Ions on the Amorphous to Crystalline Phase Transition of Silica. *J. Solid State Chem.* **2001**, *161*, 373–378, doi:10.1006/jssc.2001.9345.
123. Yang, H.; Liu, B.; Chen, Y.; Li, B.; Chen, H. Influence of Inherent Silicon and Metals in Rice Husk on the Char Properties and Associated Silica Structure. *Energy Fuels* **2015**, *29*, 7327–7334, doi:10.1021/acs.energyfuels.5b01617.
124. Gilbe, C.; Öhman, M.; Lindström, E.; Boström, D.; Backman, R.; Samuelsson, R.; Burvall, J. Slagging Characteristics during Residential Combustion of Biomass Pellets. *Energy Fuels* **2008**, *22*, 3536–3543, doi:10.1021/ef800087x.

125. Strandberg, A.; Skoglund, N.; Thyrel, M.; Lestander, T.A.; Broström, M.; Backman, R. Time-Resolved Study of Silicate Slag Formation During Combustion of Wheat Straw Pellets. *Energy Fuels* **2019**, *33*, 2308–2318, doi:10.1021/acs.energyfuels.8b04294.
126. Boström, D.; Skoglund, N.; Grimm, A.; Boman, C.; Öhman, M.; Broström, M.; Backman, R. Ash Transformation Chemistry during Combustion of Biomass. *Energy Fuels* **2012**, *26*, 85–93, doi:10.1021/ef201205b.
127. Deng, H.; Wang, X.-M.; Du, C.; Shen, X.-C.; Cui, F.-Z. Combined effect of ion concentration and functional groups on surface chemistry modulated CaCO₃ crystallization. *CrystEngComm* **2012**, *14*, 6647–6653, doi:10.1039/c2ce25731a.
128. Vassilev, S.V.; Baxter, D.; Vassileva, C.G. An overview of the behaviour of biomass during combustion: Part II. Ash fusion and ash formation mechanisms of biomass types. *Fuel* **2014**, *117*, 152–183, doi:10.1016/j.fuel.2013.09.024.129.
129. World Health Organization, 2016. Agents Classified by the IARC Monographs, World Health Organization. International Agency for Research on Cancer. Available online: <https://monographs.iarc.who.int/agents-classified-by-the-iarc/>. (Last assessed on 28 October 2021).

CHAPTER 5

5 An Improved Method for The Production of Biogenic Silica from Cornhusk Using Sol-Gel Polymeric Route

Published Research Article II

Owusu Prempeh, C., Formann, S., Hartmann, I. and Michael Nelles. An improved method for the production of biogenic silica from cornhusk using sol–gel polymeric route. *Biomass Conv. Bioref.* (2022). <https://doi.org/10.1007/s13399-022-03615-6>.

Short Summary

Silica extraction from the direct combustion process of agricultural residues often yield ash particles with low quality (e.g. silica purity and porosity). Based on the preliminary investigation and results presented in **Chapter 4**, the biogenic silica from corn husk residues showed the highest potential with considerable surface area and pore volume of 91 m²/g and pore volume up to 0.21 cm³/g, respectively. However, considerations for suitable catalyst support should possess the following essential attributes: (i) a high specific surface area (>150 m²/g) and a pore volume (> 0.25 m³/g). Thus, the study presented here explores a novel approach to obtaining a high-quality biogenic silica from cornhusk with enhanced textural properties. The study proposes a sol-gel polymeric route as a low-cost method for the extraction and synthesis of silica nanoparticles from this agricultural waste material. The chapter will elaborate on the sol-gel polymeric route employed in the study, discussing the specific steps, parameters, and control over silica formation that lead to enhanced purity, structure, and properties. The novel finding in this study revolves around the development of an improved method that harnesses the potential of cornhusk to produce biogenic silica nanoparticles using a sol-gel polymeric route, with potential catalytic applications. This study offers a sustainable and valuable alternative to traditional silica synthesis methods.

Proof of individual contribution:

The nature and contributions of various authors towards the completion of **Chapter 5** are as follows:

	Authors	Contribution	Extent of contribution (%)
<u>Author</u>	<u>Clement Owusu Prempeh</u>	Conceptualization, methodology, formal analysis, investigations, resources, data curation, writing—original draft preparation, writing—review and editing, and visualization.	85
Co-author (1)	Steffi Formann	Conceptualization, methodology, resources, writing—review and editing, visualization, supervision, and project administration	5
Co-author (2)	Ingo Hartmann	Conceptualization, methodology, resources, writing—review and editing, supervision, and project administration.	5
Co-author (3)	Michael Nelles	Conceptualization, methodology, supervision, and project administration	5

Signature of candidate:.....

Date:.....

Declaration by co-authors: The undersigned hereby confirm that:

1. the declaration above accurately reflects the nature and extent of the contributions of the candidate and the co-authors to **Chapter 5**,
2. no other authors contributed to **Chapter 5**, pg. 95 - 118, besides those specified above,

and

3. potential conflicts of interest have been revealed to all interested parties and that the necessary arrangements have been made to use the material in **Chapter 5**, pg. 95 - 118, of this dissertation.

An Improved Method for The Production of Biogenic Silica from Cornhusk Using Sol-Gel Polymeric Route

Clement Owusu Prempeh^{1,2*}, Steffi Formann¹, Ingo Hartmann¹, and Michael Nelles^{1,2}

¹ DBFZ Deutsches Biomasseforschungszentrum gemeinnützige GmbH, Torgauer Straße 116, 04347 Leipzig, Germany

² Department of Agriculture and Environmental Science, University of Rostock, Justus-von-Liebig-Weg 6, 18059 Rostock, Germany

* Correspondence: Clement.OwusuPrempeh@dbfz.de; Tel.: +49-(0)341-2434-523

Abstract

Porous silica was synthesized from cornhusk using the sol-gel polymeric route and compared with ash obtained from the direct combustion process under laboratory conditions. The unmodified ash from the direct combustion process was dissolved in NaOH for 1 h to form sodium silicate, which was subsequently hydrolyzed with citric acid to yield a silica xerogel. The obtained xerogel was characterized using inductively coupled plasma-optical emission spectrometry (ICP-OES), Fourier transforms infrared (FTIR) spectroscopy, X-ray diffraction (XRD), simultaneous thermal analysis (STA), gas sorption techniques to determine their elemental constituents, functional groups, crystalline phases, thermal stability, and porosity, respectively. The results showed that the synthesized silica xerogel exhibited porous network structures with a high specific surface area and mesopore volume of 384 m²/g and 0.35 cm³/g, respectively. The pore size distribution revealed a complete transformation of the pore network structures of the unmodified ash from a monomodal to a bimodal pore system, with micro- and mesopore peaks centered around 1.5 and 3.8 nm, respectively. The ICP-OES results showed that the silica content significantly increased from 52.93 to 91.96 wt. % db after the sol-gel treatment. XRD diffraction confirmed the amorphicity of the silica particles obtained from the sol-gel extraction method. In addition, the STA data showed that the silica xerogel has high thermal stability compared to the unmodified ash, as the latter exhibited poor thermal stability and low textural properties. The high surface area and narrow pore cavity size distribution of the porous silica xerogel make it an ideal substrate for catalysts and an excellent template for growing other nanoparticles within the pores.

Keywords: biogenic silica, combustion, sol-gel, agricultural waste, cornhusk, sodium silicate

5.1 Introduction

Silica products such as precipitated silica, fumed silica, arc silica, and silica xerogels, are industrially synthesized by: (i) the hydrolysis of mineral precursors such as tetraethyl orthosilicate (TEOS), (ii) the acidification of sodium silicate solutions and (iii) the smelting of quartz sand with sodium carbonate at elevated temperatures ($> 1200\text{ }^{\circ}\text{C}$) [1–3]. Common to these synthesis routes are the energy-intensive attributes and the release of hazardous by-products along with CO_2 emissions [4]. These downsides have rendered industrialized silica products less desirable from cost and environmental considerations, limiting their wide applications in various industrial sectors. Besides, the intensification of global policies enacted by the EU [5] and the AU [6] against greenhouse gas emissions has spurred a renewed interest in finding a comprehensive, tailor-made solution to these exhausted synthesis routes by embracing a more sustainable approach.

As an alternative, biomass has been the subject of several investigations over the years due to its versatility, low cost, and biodegradability attribute [7]. The combustion of biomass fuels for bio-energy production could play a significant role in achieving a healthy ecosystem, as many perspectives perceive it as carbon-neutral [8]. Through photosynthesis, plants can capture the equivalent amount of CO_2 released to the atmosphere during combustion. Thus, there is no net increase in greenhouse gas emissions based on life-cycle analysis [8,9]. Presently, biomass plays a subordinate role to fossils in energy generation. Besides the cogeneration of heat, biomass can be considered for value-added material production, such as the extraction of biogenic silica [10]. High-quality biogenic silica has been extracted from agricultural residues such as rice husk, rice straw, oat and spelt processing wastes, miscanthus and sugarcane bagasse with comparable properties to industrialized silica [11–14]. Consequently, the extracted silica has found applications in several industrial processes ranging from controlled porous glass production [15], catalyst support [16], optoelectronic application [17], ceramics, and in its finest form, as a filler for paints, plastics and rubber [18]. Furthermore, recent developments in the field of biogenic silica have shown the synthesis of n- SiO_2 and C-based nanomaterials as a result of the cost-effective fabrication of modern and smart sensor devices [19].

The main constituents of biomass are cellulose, hemicellulose, lignin and inorganic compounds [20]. Typically, the inorganic compounds consist of alkali and non-alkali metals (e.g., Na, K, Li), which, along with other mineral components (e.g., Si), result in a less active amorphous silica with low textural properties and purity [21]. The silica atoms are uniformly dispersed molecular units inter-twinned between the lignin and need to be liberated using pretreatment methods and thermochemical conversion processes such as combustion and gasification [11,22]. The generation of high-quality biogenic silica from biomasses involves two main processes. First, the pretreatment of the biomass material is performed to remove the incorporated inorganic metals from the organic matrix, followed by combustion under controlled conditions to oxidize the organic components. The resulting ash is referred to as biogenic silica due to its high siliceous content [23]. During the pretreatment phase, an organic acid such as citric acid is often preferred due to its environmental friendliness compared to mineral acids, e.g., sulfuric acid [24].

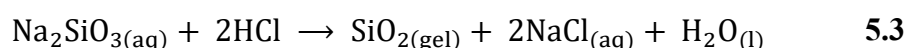
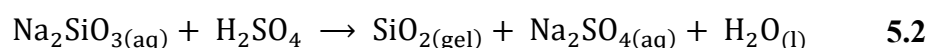
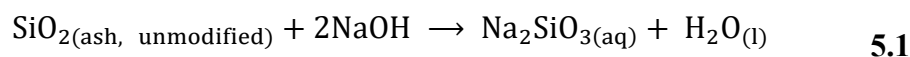
Corn (*Zea mays*) is one of the staple food crops cultivated on the African continent, with global production figures of 1.16 billion tons in 2020 [25]. A known predominant by-product of corn production is the corn husk residues. Invariably, the intensification of production figures leads to a corresponding increase in the available corn husk residues [26]. From the perspective of waste management, the disposal of these vast quantities of residues presents a challenge; accordingly, they are disposed of in landfills or openly burned, causing pollution [27]. A major contributing factor to these preferred waste eradication options is the lack of value-addition pathways, especially for developing countries. In spite of this, recent reports have shown the high silica potential of corn husk residues, making it a cheap resource for amorphous silica extraction [28,29]. However, one of the significant challenges associated with the biogenic silica from agricultural residues is the low purity silica owing to the high impurities (e.g., concentrations of metal oxides) in the ashes after the direct combustion process, as shown in Table 5.1 for various agricultural residues [23,28,30]. These inorganic impurities hinder obtaining the required silica purity with less crystallinity and improved porosity needed for high-end applications such as catalyst support [31]. Thus, the low-purity silica requires additional post-treatment or wet chemical treatments, such as the hot hydrochloric leaching process associated with the solution-gelation ('sol-gel') polymeric method. The sol-gel polymeric method has been used to synthesize numerous nano-/micro structures, which have applications in the biomedical field as drug delivery vectors, optics, electronics, semi-/super-conductors, and biomaterials [32].

Table 5.1. Reported Fuel ash composition of selected biomass fuels. Untreated (U) and leached (L) biomass fuels of cassava (CasP), yam (YamP), coconut (CocH), corncob (CorC) and corn husk (CorH) after direct combustion. Inorganic species are specified on a fuel ash basis [28].

	Unit	CasP		YamP		CocH		CorC		CorH	
		U	L	U	L	U	L	U	L	U	L
Fuel ash analysis											
Al ₂ O ₃	wt.% db	5.67	8.46	1.76	2.87	0.84	1.57	0.51	0.79	1	0.68
CaO	wt.% db	14.8	30.3	3.91	8.07	4.96	16.76	2.23	9.82	6.65	10.6
Fe ₂ O ₃	wt.% db	2.23	3.03	0.65	2.11	0.92	2.07	0.87	2.98	0.02	0.84
K ₂ O	wt.% db	40.84	1.83	46.66	17.67	61.98	4.24	62.44	8.21	33.6	1.61
MgO	wt.% db	3.96	2.62	2.22	1.97	4.67	3.07	2.97	2.49	0	2.67
MnO	wt.% db	0.14	0.08	0.08	0.12	0.06	0.04	0.1	0.05	8.5	0.05
Na ₂ O	wt.% db	0.36	1.1	0.43	1.04	4.45	2.96	0.09	2.23	0.18	1.72
P ₂ O ₅	wt.% db	4.35	2.94	11.15	8.88	4.48	5.81	3.98	4.64	0.02	1.16
SiO ₂	wt.% db	20.01	38.6	26.7	45.22	11.53	44.57	20.82	49.53	44.13	70.7
SO ₃	wt.% db	6.82	9.68	5.98	11.23	5.86	18.17	5.67	18.52	5.27	9.37
Others*	wt.% db	0.82	1.33	0.45	0.82	0.25	0.74	0.31	0.75	0.61	0.47

*Others ** include trace minerals such as BaO, Cr₂O₃, CuO, Li₂O, NiO, SrO, TiO₂, ZnO.

The chemistry of the sol-gel involves the isolation of the silica particles from the impure silica (usually, ash from the direct combustion process; herein, unmodified ash) in an alkaline medium to yield a sodium silicate solution, followed by a gelation period via a controlled pH process [33,34]. The dissolution process is a low-temperature process usually performed in a boiling NaOH at 100 ±10 °C for 1 h with continuous stirring, according to Equation 5.1. The gelation starts during the acid precipitation process, and the pH is adjusted below 7 or as low as 4, according to Equations 5.2 and 5.3. The solution is allowed to gel for 24 h, after which the gel is centrifuged to separate the silica from the mixture and thereafter dried [35–37].



One advantage of the sol-gel process is the ability to control the morphology, shape, mechanical, and pore structure of the synthesized silica xerogel, allowing an impressive range of applications [32]. Accordingly, the sol-gel method has been used to investigate the effects of nanostructuring on the crystal sizes of the silica obtained from corn cob, as well as the synthesis of nanosilica particles with average sizes from cassava periderm [4]. In addition, the development of sol-gel and porous glass-based silica monoliths with hierarchical pore structures for solid-liquid catalysis has been reported [38]. Previous studies have also shown the use of mineral acids, including HCl and H₂SO₄, in the neutralization reaction to promote gelation [39]. Nevertheless, these mineral acids are not only environmentally unfriendly but introduce into the structure of the synthesized nanosilica particles other ions (Cl⁻ ions, as in the case of HCl as a gelation catalyst) (see Equation 5.3) [24]. For further application of the extracted silica xerogels as a catalyst support system for encapsulating or anchoring noble metals such as Pd, Rh and Pt, Cl⁻ ions have been reported to have a poisoning effect on the catalyst operation [40]. Therefore, this study adopted citric acid (C₆H₈O₇) over the standard HCl usually adopted in the gelation step.

Against this background, this study explores the reuse of agricultural residue, with a particular focus on cornhusks, for synthesizing biogenic silica nanoparticles using the sol-gel polymeric method. The sol-gel product, the silica xerogel, was compared to biogenic silica produced from the direct combustion of cornhusk in the laboratory. The extracted silica particles were fully characterized using various techniques, including ICP-OES and gas sorption techniques, TGA/STA, XRD, and FTIR, to obtain information about their elemental compositions, micro-structural properties, and physicochemical characteristics. The results of this study would be relevant for effectively utilizing biomass resources and fabricating valuable nanosilica powder for essential applications.

5.2 Materials and Method

5.2.1 Ash preparation

Cornhusks were purchased from farmers in the Ashanti region, Ghana, in the form of five round bales, each approximately 50 kg and a total of 250 kg. Upon collection, they were washed in an extractor (STAHL ATOLL 290 E, Gottlob Stahl Wäschereimaschinen GmbH, Sindelfingen, Germany) at 50 °C for 2 hours to remove dirt and soil particles. The water-

washing procedure has been reported to remove some water-soluble inorganic metals embedded in the biomass matrix [11]. The washed residues were dried overnight at 105 °C and stored in airtight plastic containers for further experimentation. 250 g of the biomass were directly combusted in a chamber furnace (Nabertherm 1185H66EA, Lilienthal, Germany) under an air atmosphere at 600 °C for 2 hours using a heating rate of 10 K/min to obtain unmodified ash. The unmodified ash was then stored in airtight plastic containers until further use and characterization. The combustion temperature was chosen based on literature data [41].

5.2.2 Synthesis of silica xerogel

In a separate experiment, the sol-gel polymeric route was performed using the ashes from the direct combustion process following the experimental procedures of Falk et al. [39] and Pijarn et al. [42], with minor modifications. Figure 5.1 shows the schematic flow diagram for the sol-gel synthesis route of biogenic silica extracted from the cornhusk ash.

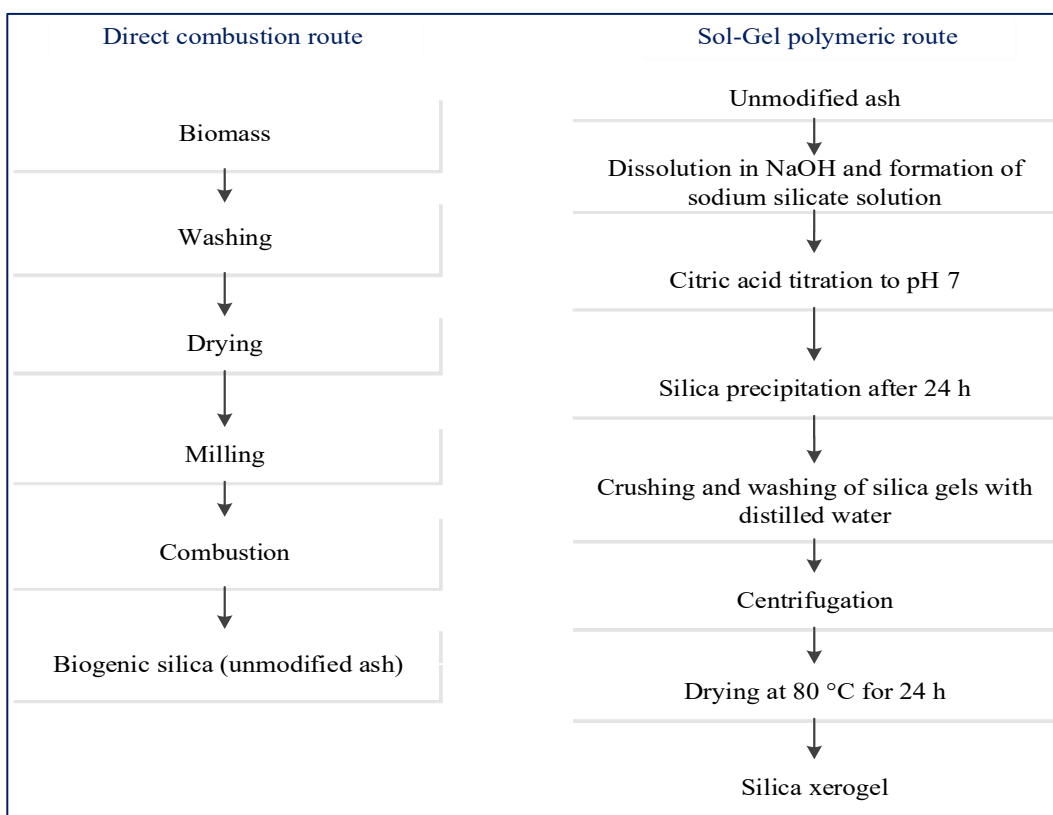


Figure 5.1. Flow diagram of the procedures used for the preparation of silica xerogel from unmodified ash.

12 g of the prepared unmodified ash was boiled at 100 °C in 350 ml of 1 M NaOH in a 500 ml Erlenmeyer flask with constant stirring to yield a sodium silicate solution. The sodium silicate solution was filtered using a vacuum-filtration unit containing a Unifil C41 filter paper. The filtrate was allowed to cool to room temperature before titrating with 2.5 w/v % citric acid solution (Sigma-Aldrich, Steinheim, Germany, purity of >99.99%) until the pH reached 7. Gels started to form below a pH of 10. The solution was left to allow gel formation. After 24 h, distilled water was added to the formed gels and centrifuged (Eppendorf centrifuge 5430, Hamburg, German) at 4000 rpm for 5 minutes. This process was repeated several times to remove remnants of the citric acid solution and impurities. The obtained gels (silica xerogels) were dried at 80 °C for 12 h, after which they were crushed in an agate mortar and pestle. The dried xerogels were stored in desiccators and labelled as silica xerogel for further characterization.

5.2.3 Analysis of physical and chemical properties

The elemental constituents of the prepared silica samples from the unmodified ash and silica xerogel were assessed by the inductively coupled plasma-optical emission spectrometry (ICP-OES, CETAC, ASX-520, Omaha, Nebraska, USA) using HF digestion and according to the DIN EN ISO 16967;2015-07, DIN EN ISO 1 standard method.

FTIR-spectrometer (PerkinElmer, Solingen, Germany) was used to identify the types of functional groups present in the synthesized silica xerogel and unmodified ash from the direct combustion process. The spectrum scope was in the range of 400–4000 cm^{-1} with a resolution factor of 1 cm^{-1} .

The textural properties were measured by gas sorption techniques using autosorb iQ-MP/XR apparatus, Quantachrome, USA. The samples were first degassed for 12 h at 250 °C under a vacuum to remove adsorbed water particles on the surface and within the pores. The specific surface area was determined by multipoint Brunauer-Emmett-Teller (BET) surface area analysis in the pressure range of $p/p_0 = 0.05-0.30$ at 77 K and considering the cross-section area of N_2 molecules of 16.2 Å [43]. The pore volume was determined using the nonlocal density functional theory (NDLFT) method as it is advantageous over the classical macroscopic method such as Barrett-Joyner-Halenda (BJH). NDLFT considers the adsorption mechanism over the complete micropore and mesopore range and can reliably estimate the pore size distribution from the adsorption and desorption branch of the isotherm

data by considering the delay in condensation as a result of metastable adsorption films in mesopores [44].

The thermal stability of the silica xerogel was studied in a simultaneous thermal analysis (STA 449 F3 Jupiter®, NETZSCH, Selb, Germany) in a synthetic air flow atmosphere with a 100 mL/min flow rate at a heating rate of 10 K/min. The sample was first ground to a particle size of less than 0.5 mm using a cutting mill (IKATM MF 10 basic Mikrofeinmühle, Germany) and vigorously mixed in a plastic box to create homogeneous starting material for the STA analysis. 10 mg of the samples were placed in alumina crucibles, and the samples were heated from room temperature to 1000 °C. The rate of mass loss was recorded simultaneously with the rise in temperature.

The amorphous phases in the silica particles were analyzed by X-ray diffraction (XRD, Malvern Panalytical GmbH, Kassel, Germany) equipped with Ni-filtered, Cu-K α radiation ($\lambda = 1.54 \text{ \AA}$). The samples were first coated with a glass substrate and measured in an instrument (Rigaku XRD; Rigaku, Japan) operating at a voltage of 40 kV and a current of 30 mA and nickel monochromator filtering wave at a tube voltage of 40 kV and tube current of 30 mA.

5.3 Results and Discussion

5.3.1 Characterizations of unmodified ash and silica xerogel

Table 5.2 shows the chemical compositions of the ashes produced from the various extraction methods and analyzed using ICP-OES. After the direct combustion process, the contents of principal ash-forming elements or impurities (CaO, MgO, SO₃ and K₂O) in the unmodified ash were predominant. However, CaO, MgO, and SO₃ contents were effectively removed, whereas diminutive concentrations of K₂O and Al₂O₃ remained (< 1 wt. % db) after the sol-gel treatment. Consequently, the silica content significantly increased from 52.93 to 91.96 wt. % db, with the content of Na₂O, also increasing to 7 wt.% db in the silica xerogel. The additional Na⁺ ions in the modified silica xerogel might have originated from the NaOH solution, as it was the principal surface modification agent. The addition of the citric acid (C₆H₈O₇) promoted the formation of high-purity silica due to the Na⁺ ions exchange from the structure of the sodium silicate to the acid. According to Umeda et al. [45], dilute acids are effective in accelerating the hydrolysis process of organics and, more

importantly, the removal of metallic impurities. The enrichment in silica content demonstrates the effectiveness of the selected post-treatment protocol in obtaining high purity silica. Similar improvements in the silica purity have been reported in other studies after the sol-gel extraction process [29,39]. The unmodified and synthesized silica xerogel moisture contents were 2.65 and 11.4 wt. % db (dry-basis), respectively. The high moisture content of the silica xerogel is probably caused by the presence of water-attractive structures such as phyllosilicate minerals which contains hydroxyl ion, OH⁻ [46].

Table 5.2. Chemical compositions of corn husk ashes prepared by different extraction methods determined by ICP-OES analysis (expressed in oxides wt.%); n.d.: not detected.

Element	Direct	Sol-gel
	Unmodified Ash	Silica xerogel
SiO ₂	52.93	91.96
CaO	26.36	n.d.
MgO	7.43	n.d.
SO ₃	5.84	n.d.
K ₂ O	2.63	0.49
Na ₂ O	1.64	7.46
P ₂ O ₅	1.33	n.d.
Fe ₂ O ₃	0.88	n.d.
ZnO	0.38	n.d.
Al ₂ O ₃	0.22	0.09
others	0.36	n.d.

'Others' include SrO, MnO, CuO, TiO₂, BaO, Li₂O and Cr₂O₃.

The visual images of the unmodified ash, wet and dried xerogels are shown in Figure 5.2. As observed in the unmodified ash produced by direct combustion, there were few remnants of black particles due to high impurities, such as K⁺ ions, which could trap carbon within the organic matrix during the combustion process. The formation of black particles has been fully elucidated in the study of Krishnarao et al. [47]. In brief, black particle formation in the ashes affects the purity and the quality of the biogenic silica [47], and similar observations were also reported by Chandrasekhar et al. [48] during their investigations on rice husk ash.

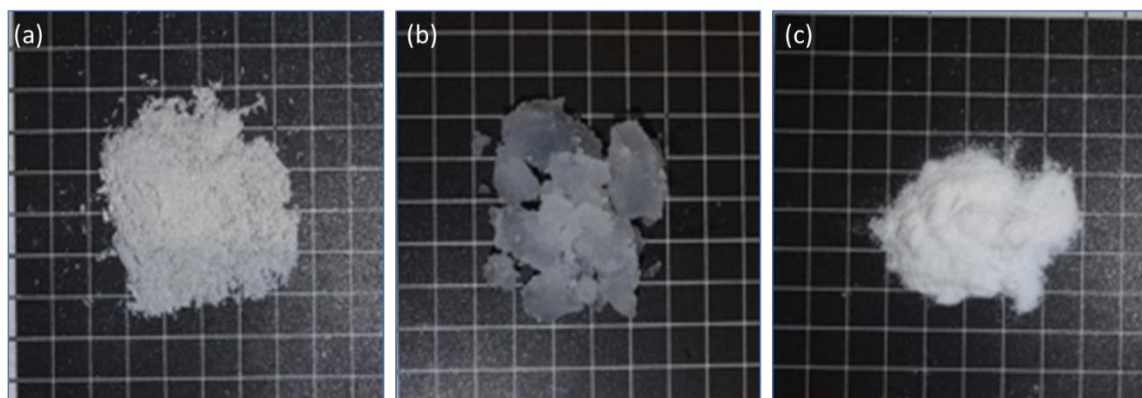
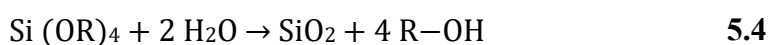


Figure 5.2. Visual images of the direct thermochemical conversion and sol-gel products during the extraction of biogenic silica from cornhusk: (a) ash from direct combustion (unmodified ash), (b) wet silica xerogel, and (c) dried silica xerogel.

With the sol-gel polymeric process, the silica in the unmodified ash is dissolved as sodium silicate according to Equation 5.1, and ion pairing between alkali cations and anions (silicates or sodium silicates) decreases the repulsion between anions and accordingly enhances their condensation to form a gel [49]. Depending on the amount of hydrolysis catalyst (herein, $C_6H_8O_7$ or H_2O), the hydrolysis process may proceed to the completion of silica xerogel, as shown in Equation 5.4. Equally, there is a possibility of the formation of intermediate species such as $[(OR)_2-Si-(OH)_2]$ or $[(OR)_3-Si-(OH)]$ in the formed silica xerogel as observed in Equation 5.5, in which the functional groups were identified in the FTIR diagram [50,51]. R represents an organic chain of the formula, C_xH_{2x+1} .



The FTIR spectra of the major functional groups in the unmodified ash from direct combustion (unmodified ash), and the modified silica xerogels are shown in Figure 5.3. The broad peak at $3500-3300\text{ cm}^{-1}$ corresponds to asymmetric stretching and bending of the O-H bond from the silanol group (Si-OH) as a result of adsorbed water molecules on the surface of the silica xerogel or from the intermediate species $[(OR)_3-Si-(OH)]$ formed during the

hydrolysis process [52]. The infrared spectra at $1626\text{--}1573\text{ cm}^{-1}$ are attributed to Si-H₂O flexion as well as the bending of the H-O-H [53]. The bands at approximately $1095\text{--}1100$ and $750\text{--}800\text{ cm}^{-1}$ were assigned to the asymmetric and symmetric vibration of Si-O-Si bonds, respectively [54].

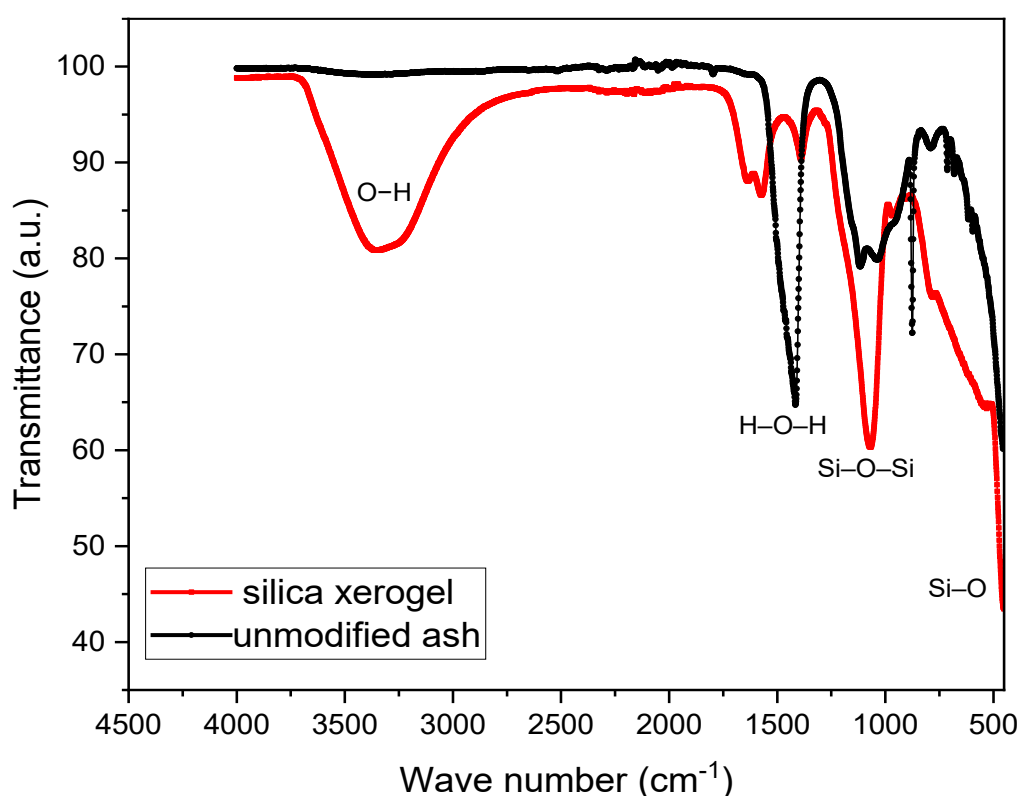


Figure 5.3. FTIR spectrum of unmodified ash and synthesized silica xerogel cornhusk.

The apparent differences between the spectra of the samples were the intensity of the absorbance peaks at $1095\text{--}1100\text{ cm}^{-1}$ attributed to the asymmetrical vibration of Si-O-Si, which was intensive in the silica xerogels compared to the unmodified ashes from the direct combustion. The sol-gel polymeric route has been reported to cause a higher polymerization degree of the Si-O group, thus enabling the formation of a stronger band between the silicon and the oxygen with higher silica concentration and the polymerization of silicate to form a more robust silica network [55]. This confirms that high-quality silica could be obtained by altering the skeleton network of the gel via the sol-gel polymeric route. Additional characteristic peaks of asymmetrical vibration of O-Si-O were also visible at absorption

peaks 456-500 cm^{-1} in both samples, as shown in the FTIR spectra [56]. The observed infrared spectra peaks are comparable to similar studies reported in the literature [56–59].

5.3.2 Influence of the sol-gel polymeric route on the textural properties

The porosity of the unmodified ash and the silica xerogel is shown in Table 5.3. The results showed improvements in the specific surface area and pore volume of the unmodified ash after the sol-gel transformation process.

Table 5.3. Textural properties of biogenic silica derived from cornhusk before (unmodified ash) and after sol-gel transformation (silica xerogel). Specific surface area (S_{BET}), pore volume (V_{p}), pore width mode (d_{p}), (NLDFT, determined by N_2 -sorption), micropore volume (V_{micro}), micropore surface area (S_{micro} , determined by t-plot method) and external surface area (S_{ext} , determined by t-plot method).

	S_{BET} (m^2/g)	V_{p} (cm^3/g)	D_{p} (nm)	V_{micro} (cm^3/g)	S_{micro} (m^2/g)	S_{ext} (m^2/g)
Unmodified Ash	88	0.25	3.3	0	0	0
Silica xerogel	384	0.35	3.8	0.12	211	173

The surface area largely increased from 88 m^2/g in the unmodified ash to 384 m^2/g in the silica xerogel. This increase in the surface area could be ascribed to the effective removal of the principal remaining impurities from the unmodified ash without destroying the structural integrity of the biogenic silica network. During combustion, the silica could interact with the inorganic impurities forming silicate melts, reducing the surface area, as evidenced in the unmodified ash and reported in the literature [60]. In addition, the pore volume was higher in the silica xerogel (0.35 cm^3/g) than in the ashes from direct combustion (0.25 m^3/g), which affirms the advantage of the proposed method on the porosity of the biogenic silica. Two accounts could explain the differences between the reported pore volumes: (i) cavitation effects that result from the differences in the pore structures of the two silica products and (ii) the formation of inaccessible porosity in the unmodified ash [44].

The N_2 adsorption-desorption isotherms of unmodified ash and the modified silica xerogel in Figure 5.4(a) are classified according to the International Union of Pure and

Applied Chemistry (IUPAC) classification. For both samples, type IV(a) with hysteresis was observed. This type of isotherm is generally observed for mesoporous materials where the monolayer-multilayer formation is followed by pore condensations [44]. In Figure 5.4(a), the shapes of the hysteresis loops, H3 in the unmodified ash, and H2(a) in the silica xerogels, indicate different pore structures in the two silica products, in accordance with the pore size distribution (PSD) diagram shown in Figure 5.4(b). The hysteresis loop type H3 indicates slit-shaped mesopores or plate-like particles and is mostly observed in materials comprising aggregates (loose assemblages) [61,62]. The H2 hysteresis loop is exhibited by numerous porous adsorbents (e.g., inorganic oxide gels and porous vycor glasses). It is mainly formed due to delayed condensation during adsorption. A shift in the liquid-vapour phase transition during desorption results in a more complex pore network, often referred to as “ink bottle” pores [44,61]. According to Cychosz et al. [63], the pore-blocking phenomenon also leads to the formation of the H2(a) hysteresis loop.

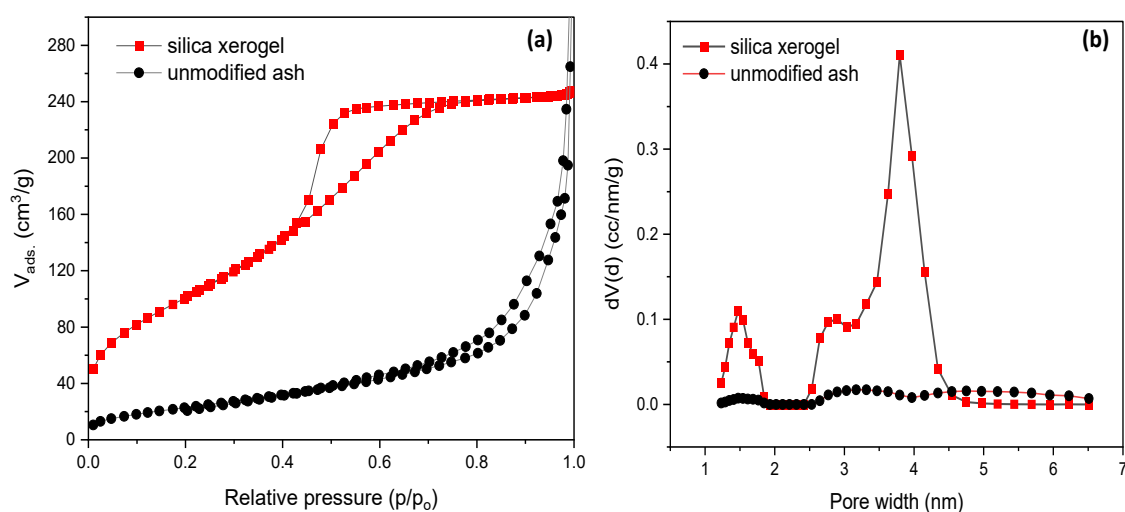


Figure 5.4. N₂ adsorption-desorption isotherms and pore size distribution of unmodified ash and modified silica xerogel. (a) Nitrogen sorption isotherms of the biogenic silica extracted from corn husk using sol-gel polymeric and direct combustion routes; silica xerogel and unmodified ash; (b) Pore size distribution of silica xerogel and unmodified ash determined by applying a dedicated NLDFT adsorption branch kernel on the adsorption branch of the N₂ (77 K) isotherm.

In Figure 5.4(a) of the isotherm of the silica xerogel, the existence of a horizontal plateau in the isotherm near the bulk saturation pressure indicates the complete filling of all pores with the adsorbate (N₂). Conversely, the isotherm of the unmodified ash does not reach

a plateau near $p/p_0 = 1$, indicating the presence of larger meso- and macropores, which cannot be completely filled with nitrogen. In addition, the shape of the isotherm shows a broad distribution of pore width in the mesoporous range. In contrast, the H2(a) hysteresis is typical for materials that show a narrow pore cavity size distribution [63] and useful as a template or as a constrainer when growing nanoparticles inside the pores [62].

The NLDFT pore size distributions obtained for the nitrogen (77 K) isotherm data for the silica xerogels and unmodified ash are shown in Figure 5.4(b). The PSD revealed a complete transformation of the pore network structure of the unmodified ash from a monomodal to a bimodal pore system under the sol-gel polymeric route. For all samples, the shape of the isotherms closer to the regions of lower pressures indicated that little or no micropores were present. However, the silica xerogel exhibited a bimodal pore system with micro- and mesopore peaks centered around 1.5 nm and 3.8 nm, respectively. Further analysis by t-plot showed that the silica xerogel exhibited a micropore volume $V_{\text{micro}} = 0.12 \text{ cm}^3/\text{g}$ and micropore surface area, $S_{\text{micro}} = 211 \text{ m}^2/\text{g}$, which explains the high total surface area of $384 \text{ m}^2/\text{g}$ [$S_{\text{micro}} = 211 \text{ m}^2/\text{g} + \text{external surface area } (S_{\text{ext}}) = 173 \text{ m}^2/\text{g} = 384 \text{ m}^2/\text{g}$] as shown in Table 5.3.

Conversely, the t-plot kernel showed a non-existence micropore volume and surface area (V_{micro} and $S_{\text{micro}} = 0$) within the pore structure of the unmodified ash, although a small indication of closed pores or inaccessible micropores was found. Thus, conclusions about the existence of mesopores can be made on the silica xerogel. The previous report of biogenic silica derived from horse-tail has also shown the presence of micropores [64]. Similar studies into the transformations of silica materials, such as porous glass materials with a monomodal pore system, have been altered into a hierarchical pore system by methods such as sol-gel and pseudomorphic transformation reported in a previous study [65]. More importantly, this study affirms a complete transformation of the pore structure network and the presence of both open micro- and mesopores within the silica xerogel's structure. The pore size mode (D_p) of the modified silica xerogel was slightly higher than the unmodified particles, which is acceptable within the deviation of the method used.

The thermal stability of the synthesized silica xerogels was evaluated in STA by measuring the weight loss caused by changing temperature, and the results are shown in Figure 5.5. The thermogravimetric curves of the silica produced by direct combustion (unmodified ash) showed a total weight loss of 17.74%. In the early stages, there was a sharp

decrease in weight at approximately 200 °C, mainly attributed to the dehydration of physically adsorbed water molecules on the surfaces or in the pores.

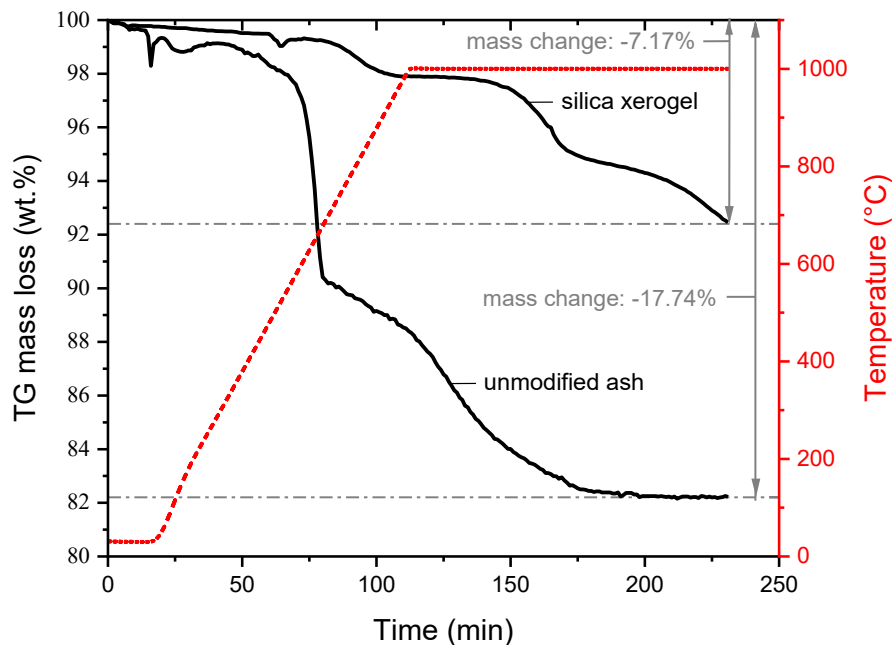


Figure 5.5. Thermogravimetric profiles of unmodified ash and silica xerogel

Above 200 °C to 800 °C, there was an extra weight loss most likely caused by the volatilization of residual carbon in unmodified ash samples. Conversely, as shown in the curve for the modified silica xerogel, the total mass loss above 200 °C was 7.17%, attributed to the evaporation of chemically bound water and surface dehydroxylation of silica [66]. This demonstrates a greater hydrophobicity of the modified silica compared to the unmodified ash and, thus, could influence its capabilities as a potential catalyst or adsorbent. It is probable that due to the surface dehydroxylation of the silica xerogel at high temperatures (above 300 °C), hydrophobic surfaces in the pores were created [62]. Consequently, a strong negative capillary pressure was generated that prevented the entrance of water into the pores. On the other hand, the unmodified ash might contain hydrophilic surfaces that generate positive pressure and direct water into the pores [67]. Above 600 °C, no further weight loss was observed, an explicit confirmation/depiction of the modified xerogel's thermal stability compared to the silica produced from direct combustion. The results of the TGA are entirely in tandem with similar results obtained by Feng et al. [55]

and Pouretedal et al. [57] during the synthesis of high specific surface area silica xerogel from rice husk ash and sodium silicate, respectively.

The amorphicity of the extracted silica xerogel was determined by XRD measurement, as shown in Figure 5.6. The broad hump-shaped diffraction peaks between $2\theta = 15$ and 35° are the characteristics of an amorphous substance [68]. The absence of sharp, defined peaks in the XRD pattern of the silica xerogel shows that the sol-gel polymeric method did not result in the crystallization of the silica particles and was predominantly amorphous. These observations are entirely in tandem with other studies showing peaks at $2\theta = 15$ and 35° , indicating the amorphicity of the extracted samples [69,70]. However, there were weaker crystalline phases at peaks near $2\theta = 30^\circ$ and 38° in the XRD of the unmodified ash, as observed in Figure 5.6. These weaker crystalline phases were identified in our earlier study [28] as quartz (SiO_2) and anhydrite [$\text{Ca}(\text{SO}_4)$] respectively, rendering the unmodified ash less amorphous compared to the silica xerogel. Consequently, it is anticipated that the amorphous property can be utilized in a vast array of applications.

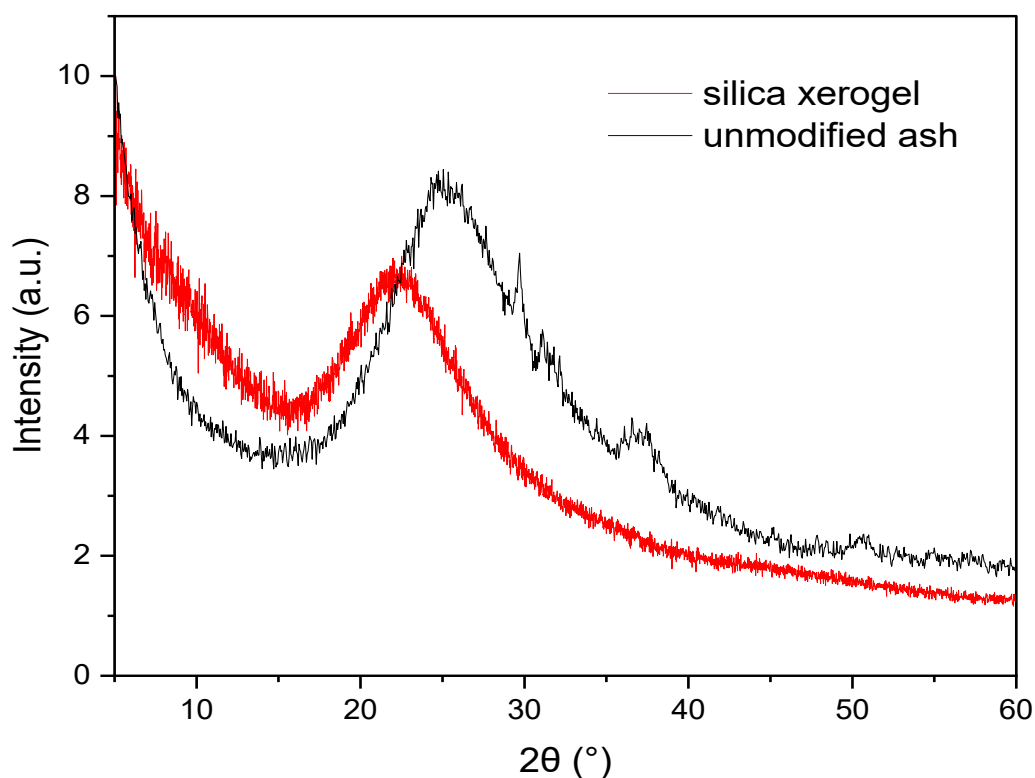


Figure 5.6. XRD patterns of unmodified ash and extracted silica xerogel

5.4 Conclusions

This study investigated the extraction of high-quality biogenic silica from cornhusk using the sol-gel polymeric compared to the direct combustion routes. The study has shown that variations in the silica particles, such as different pore structure networks, physicochemical characteristics and purity, can be achieved by altering the properties of the starting material. Consequently, the extracted silica xerogel exhibited an amorphous attribute with high thermal stability based on the XRD and STA results. A remarkable transformation of the textural properties of the ashes obtained from direct combustion was achieved as the sol-gel polymeric silica particles exhibited improved textural parameters with an opened surface area and pore volume close to 400 m²/g and 0.35 cm³/g, respectively. The disproportionate increase in the specific area and the mesopore volume of the sol-gel silica particles were attributed to additional micro- and mesopores formed during the sol-gel process, which led to the opening up of the pore structure by the elimination of inorganic impurities. Accordingly, there was a change in the pore size distribution system from a monomodal in the unmodified ash to a bimodal pore system in the silica xerogels. The presented sol-gel polymeric route offers a significantly low-cost approach to preparing high-quality biogenic silica particles with improved properties. Future research works should consider the potential application of the extracted sol-gel polymeric silica particles into catalysis or adsorption operations due to the high surface and pore volume. These value-addition pathways are expected to intensify the reuse of underutilized biomass and minimize the waste disposal problems in the agricultural or food production sector.

Acknowledgements

The authors thank Mr. Bamgboye Kehinde & Mr. Manfred Eiden for their technical assistance during the laboratory experiments.

References of Chapter 5

1. Sudirman, Anggaravidya M, Budianto E et al. (2012) Synthesis and Characterization of Polyester-Based Nanocomposite. *Procedia Chemistry* 4(11):107–113. doi: 10.1016/j.proche.2012.06.016

2. He ZW, Liu XQ, Su Q et al. (2006) Improvement of electrical properties of low dielectric constant nanoporous silica films prepared using sol–gel method with catalyst HF. *Appl. Phys. A* 82(2):349–355. doi: 10.1007/s00339-005-3376-0
3. Soltani N, Bahrami A, Pech-Canul MI et al. (2015) Review on the physicochemical treatments of rice husk for production of advanced materials. *Chemical Engineering Journal* 264:899–935. doi: 10.1016/j.cej.2014.11.056
4. Adebisi JA, Agunsoye JO, Bello SA et al. (2017) Potential of producing solar grade silicon nanoparticles from selected agro-wastes: A review. *Solar Energy* 142(6):68–86. doi: 10.1016/j.solener.2016.12.001
5. United Nations Framework Convention on Climate Change. Adoption of the Paris Agreement: Proposal by the President. In *Proceedings of the Paris Climate Change Conference, Paris, France, 30 November–12 December 2015*.
6. African Climate Policy Centre (ACPC). 2010. Overview of the ClimDev Africa Programme. Available online: <https://www.uneca.org/acpc> (accessed on 22 November 2022).
7. Shah MA, Khan MNS, Kumar V (2018) Biomass residue characterization for their potential application as biofuels. *J Therm Anal Calorim* 134(3):2137–2145. doi: 10.1007/s10973-018-7560-9
8. Jiang L, Hu S, Sun L-S et al. (2013) Influence of different demineralization treatments on physicochemical structure and thermal degradation of biomass. *Bioresour Technol* 146:254–260. doi: 10.1016/j.biortech.2013.07.063
9. Marland G (2010) Accounting for Carbon Dioxide Emissions from Bioenergy Systems. *Journal of Industrial Ecology* 14(6):866–869. doi: 10.1111/j.1530-9290.2010.00303.x
10. Pode R (2016) Potential applications of rice husk ash waste from rice husk biomass power plant. *Renewable and Sustainable Energy Reviews* 53(3):1468–1485. doi: 10.1016/j.rser.2015.09.051
11. Beidaghy Dizaji H, Zeng T, Hartmann I et al. (2019) Generation of High-Quality Biogenic Silica by Combustion of Rice Husk and Rice Straw Combined with Pre- and Post-Treatment Strategies—A Review. *Applied Sciences* 9(6):1083. doi: 10.3390/app9061083
12. Quispe I, Navia R, Kahhat R (2017) Energy potential from rice husk through direct combustion and fast pyrolysis: A review. *Waste Manag* 59:200–210. doi: 10.1016/j.wasman.2016.10.001

13. Zemnukhova LA, Egorov AG, Fedorishcheva GA et al. (2006) Properties of amorphous silica produced from rice and oat processing waste. *Inorg Mater* 42(1):24–29. doi: 10.1134/S0020168506010067
14. Biswas B, Pandey N, Bisht Y et al. (2017) Pyrolysis of agricultural biomass residues: Comparative study of corn cob, wheat straw, rice straw and rice husk. *Bioresour Technol* 237:57–63. doi: 10.1016/j.biortech.2017.02.046
15. Andreola F, Martín MI, Ferrari AM et al. (2013) Technological properties of glass-ceramic tiles obtained using rice husk ash as silica precursor. *Ceramics International* 39(5):5427–5435. doi: 10.1016/j.ceramint.2012.12.050
16. Liu D, Seeburg D, Kreft S et al. (2019) Rice Husk Derived Porous Silica as Support for Pd and CeO₂ for Low Temperature Catalytic Methane Combustion. *Catalysts* 9(1):26. doi: 10.3390/catal9010026
17. Ebnalwaled AA, Sadek AH, Ismail SH et al. (2022) Structural, optical, dielectric, and surface properties of polyimide hybrid nanocomposites films embedded mesoporous silica nanoparticles synthesized from rice husk ash for optoelectronic applications. *Opt Quant Electron* 54(11):45502. doi: 10.1007/s11082-022-03976-2
18. Sae-Oui P, Rakdee C, Thanmathorn P (2002) Use of rice husk ash as filler in natural rubber vulcanizates: In comparison with other commercial fillers. *J. Appl. Polym. Sci.* 83(11):2485–2493. doi: 10.1002/app.10249
19. Sharma SK, Sharma G, Sharma A et al. (2022) Synthesis of silica and carbon-based nanomaterials from rice husk ash by ambient fiery and furnace sweltering using a chemical method. *Applied Surface Science Advances* 8:100225. doi: 10.1016/j.apsadv.2022.100225
20. Rose, M. (2013). Catalysis for the conversion of biomass and its derivatives. (Max Planck Research Library for the history and development of knowledge.) edited by Malte Behrens and Abhaya K. Datye. *Angewandte Chemie International Edition*, 52(37), 9613–9613. <https://doi.org/10.1002/anie.201305619>
21. Long J, Song H, Jun X et al. (2012) Release characteristics of alkali and alkaline earth metallic species during biomass pyrolysis and steam gasification process. *Bioresour Technol* 116:278–284. doi: 10.1016/j.biortech.2012.03.051
22. Ma JF, Yamaji N (2006) Silicon uptake and accumulation in higher plants. *Trends Plant Sci* 11(8):392–397. doi: 10.1016/j.tplants.2006.06.007

23. Schneider D, Wassersleben S, Weiß M et al. (2020) A Generalized Procedure for the Production of High-Grade, Porous Biogenic Silica. *Waste Biomass Valor* 11(1):1–15. doi: 10.1007/s12649-018-0415-6
24. Umeda J, Kondoh K (2008) High-purity amorphous silica originated in rice husks via carboxylic acid leaching process. *J Mater Sci* 43(22):7084–7090. doi: 10.1007/s10853-008-3060-9
25. The State of Food and Agriculture 2022. In: FAO. <https://www.fao.org/publications/sofa/2022/en/>. Accessed 22 Nov 2022
26. Kemausuor F, Kamp A, Thomsen ST et al. (2014) Assessment of biomass residue availability and bioenergy yields in Ghana. *Resources, Conservation and Recycling* 86(3):28–37. doi: 10.1016/j.resconrec.2014.01.007
27. Lim JS, Abdul Manan Z, Wan Alwi SR et al. (2012) A review on utilisation of biomass from rice industry as a source of renewable energy. *Renewable and Sustainable Energy Reviews* 16(5):3084–3094. doi: 10.1016/j.rser.2012.02.051
28. Prempeh CO, Formann S, Schliermann T et al. (2021) Extraction and Characterization of Biogenic Silica Obtained from Selected Agro-Waste in Africa. *Applied Sciences* 11(21):10363. doi: 10.3390/app112110363
29. Velmurugan P, Shim J, Lee K-J et al. (2015) Extraction, characterization, and catalytic potential of amorphous silica from corn cobs by sol-gel method. *Journal of Industrial and Engineering Chemistry* 29:298–303. doi: 10.1016/j.jiec.2015.04.009
30. Lee JH, Kwon JH, Lee J-W et al. (2017) Preparation of high purity silica originated from rice husks by chemically removing metallic impurities. *Journal of Industrial and Engineering Chemistry* 50(2):79–85. doi: 10.1016/j.jiec.2017.01.033
31. Beidaghy Dizaji H, Zeng T, Hölzig H et al. (2022) Ash transformation mechanism during combustion of rice husk and rice straw. *Fuel* 307(1):121768. doi: 10.1016/j.fuel.2021.121768
32. Owens GJ, Singh RK, Foroutan F et al. (2016) Sol–gel based materials for biomedical applications. *Progress in Materials Science* 77(Suppl. 2):1–79. doi: 10.1016/j.pmatsci.2015.12.001
33. Liou T-H, Yang C-C (2011) Synthesis and surface characteristics of nanosilica produced from alkali-extracted rice husk ash. *Materials Science and Engineering: B* 176(7):521–529. doi: 10.1016/j.mseb.2011.01.007

34. Affandi S, Setyawan H, Winardi S et al. (2009) A facile method for production of high-purity silica xerogels from bagasse ash. *Advanced Powder Technology* 20(5):468–472. doi: 10.1016/j.appt.2009.03.008
35. Saravanan K, Yuvakkumar R, Rajendran V et al. (2012) Influence of sintering temperature and pH on the phase transformation, particle size and anti-reflective properties of RHA nano silica powders. *Phase Transitions* 85(12):1109–1124. doi: 10.1080/01411594.2012.671322
36. Yuvakkumar R, Elango V, Rajendran V et al. (2012) High-purity nano silica powder from rice husk using a simple chemical method. *Journal of Experimental Nanoscience* 9(3):272–281. doi: 10.1080/17458080.2012.656709
37. Anuar MF, Fen YW, Zaid MHM et al. (2018) Synthesis and structural properties of coconut husk as potential silica source. *Results in Physics* 11:1–4. doi: 10.1016/j.rinp.2018.08.018
38. Enke D, Gläser R, Tallarek U (2016) Sol-Gel and Porous Glass-Based Silica Monoliths with Hierarchical Pore Structure for Solid-Liquid Catalysis. *Chemie Ingenieur Technik* 88(11):1561–1585. doi: 10.1002/cite.201600049
39. Falk G, Shinhe GP, Teixeira LB et al. (2019) Synthesis of silica nanoparticles from sugarcane bagasse ash and nano-silicon via magnesiothermic reactions. *Ceramics International* 45(17):21618–21624. doi: 10.1016/j.ceramint.2019.07.157
40. Chai H, Han W, Zhu H, Liu H. The effect of chloride ion on ruthenium supported catalyst for ammonia synthesis. *Progress in Chemistry*, 2006, 18(10): 1262-1269.
41. Titiloye JO, Abu Bakar MS, Odetoye TE (2013) Thermochemical characterisation of agricultural wastes from West Africa. *Industrial Crops and Products* 47:199–203. doi: 10.1016/j.indcrop.2013.03.011
42. Pijarn N, Galajak P (2014) New Insight Technique for Synthesis of Silica Gel from Rice Husk Ash by Using Microwave Radiation. *AMR* 1025-1026:574–579. doi: 10.4028/www.scientific.net/AMR.1025-1026.574
43. Brunauer S, Emmett PH, Teller E (1938) Adsorption of Gases in Multimolecular Layers. *J. Am. Chem. Soc.* 60(2):309–319. doi: 10.1021/ja01269a023
44. Schlumberger C, Thommes M (2021) Characterization of Hierarchically Ordered Porous Materials by Physisorption and Mercury Porosimetry—A Tutorial Review. *Adv. Mater. Interfaces* 8(4):2002181. doi: 10.1002/admi.202002181

45. Umeda, J., Kondoh, K., & Michiura, Y. (2007). Process parameters optimization in preparing high-purity amorphous silica originated from Rice Husks. *Materials Transactions*, 48(12), 3095–3100. <https://doi.org/10.2320/matertrans.mk200715>
46. Dziewonski AM, Romanowicz BA (2015) *Deep Earth Seismology: An introduction and overview*. Treatise on Geophysics 1–28. doi: 10.1016/b978-0-444-53802-4.00001-4.
47. Krishnarao RV, Subrahmanyam J, Jagadish Kumar T (2001) Studies on the formation of black particles in rice husk silica ash. *Journal of the European Ceramic Society* 21(1):99–104. doi: 10.1016/S0955-2219(00)00170-9
48. Chandrasekhar S, Pramada PN, Majeed J (2006) Effect of calcination temperature and heating rate on the optical properties and reactivity of rice husk ash. *J Mater Sci* 41(23):7926–7933. doi: 10.1007/s10853-006-0859-0
49. Chen X, Mondal P (2020) Effects of NaOH amount on condensation mechanism to form aluminosilicate, case study of geopolymer gel synthesized via sol–gel method. *J Sol-Gel Sci Technol* 96(3):589–603. doi: 10.1007/s10971-020-05360-6
50. Hanaor DAH, Chironi I, Karatchevtseva I et al. (2013) Single and mixed phase TiO₂ powders prepared by excess hydrolysis of titanium alkoxide. *Advances in Applied Ceramics* 111(3):149–158. doi: 10.1179/1743676111Y.0000000059
51. Singh LP, Bhattacharyya SK, Kumar R et al. (2014) Sol-Gel processing of silica nanoparticles and their applications. *Adv Colloid Interface Sci* 214:17–37. doi: 10.1016/j.cis.2014.10.007
52. Moncada E, Quijada R, Retuert J (2007) Nanoparticles prepared by the sol–gel method and their use in the formation of nanocomposites with polypropylene. *Nanotechnology* 18(33):335606. doi: 10.1088/0957-4484/18/33/335606
53. El Rassy H, Pierre AC (2005) NMR and IR spectroscopy of silica aerogels with different hydrophobic characteristics. *Journal of Non-Crystalline Solids* 351(19-20):1603–1610. doi: 10.1016/j.jnoncrysol.2005.03.048
54. Frías M, Villar E, Savastano H (2011) Brazilian sugar cane bagasse ashes from the cogeneration industry as active pozzolans for cement manufacture. *Cement and Concrete Composites* 33(4):490–496. doi: 10.1016/j.cemconcomp.2011.02.003
55. Feng Q, Chen K, Ma D et al. (2018) Synthesis of high specific surface area silica aerogel from rice husk ash via ambient pressure drying. *Colloids and Surfaces A: Physicochemical and Engineering Aspects* 539:399–406. doi: 10.1016/j.colsurfa.2017.12.025

56. Yang H, Yan R, Chen H et al. (2007) Characteristics of hemicellulose, cellulose and lignin pyrolysis. *Fuel* 86(12-13):1781–1788. doi: 10.1016/j.fuel.2006.12.013
57. Pouretedal, H. R., & Kazemi, M. (2012). Characterization of modified silica aerogel using sodium silicate precursor and its application as adsorbent of Cu^{2+} , Cd^{2+} , and Pb^{2+} ions. *International Journal of Industrial Chemistry*, 3(1), 20. <https://doi.org/10.1186/2228-5547-3-20>.
58. Reynolds JG, Coronado PR, Hrubesh LW (2001) Hydrophobic aerogels for oil-spill cleanup – synthesis and characterization. *Journal of Non-Crystalline Solids* 292(1-3):127–137. doi: 10.1016/S0022-3093(01)00882-1
59. Venkateswara Rao A, Kulkarni MM, Amalnerkar DP et al. (2003) Superhydrophobic silica aerogels based on methyltrimethoxysilane precursor. *Journal of Non-Crystalline Solids* 330(1-3):187–195. doi: 10.1016/j.jnoncrysol.2003.08.048
60. Beidaghy Dizaji H, Zeng T, Hölzig H et al. (2022) Ash transformation mechanism during combustion of rice husk and rice straw. *Fuel* 307(1):121768. doi: 10.1016/j.fuel.2021.121768
61. Sapei L (2007) Characterisation of silica in *Equisetum hyemale* and its transformation into biomorphous ceramics. In: KOBV. <http://opus.kobv.de/ubp/volltexte/2007/1588/>. Accessed 22 Nov 2022.
62. Johansson, E. M. (2010). Controlling the pore size and morphology of mesoporous silica (dissertation). Department of Physics, Chemistry and Biology, Linköping University, Linköping.
63. Cychosz KA, Guillet-Nicolas R, García-Martínez J et al. (2017) Recent advances in the textural characterization of hierarchically structured nanoporous materials. *Chem Soc Rev* 46(2):389–414. doi: 10.1039/C6CS00391E
64. Sapei L, Nöske R, Strauch P et al. (2008) Isolation of Mesoporous Biogenic Silica from the Perennial Plant *Equisetum hyemale*. *Chem. Mater.* 20(5):2020–2025. doi: 10.1021/cm702991f
65. Uhlig H, Muenster T, Kloess G et al. (2018) Synthesis of MCM-48 granules with bimodal pore systems via pseudomorphic transformation of porous glass. *Microporous and Mesoporous Materials* 257:185–192. doi: 10.1016/j.micromeso.2017.08.033
66. Dubey RS, Rajesh YBRD, More MA (2015) Synthesis and Characterization of SiO_2 Nanoparticles via Sol-gel Method for Industrial Applications. *Materials Today: Proceedings* 2(4-5):3575–3579. doi: 10.1016/j.matpr.2015.07.098

67. Romero E, Quirantes M, Nogales R (2017) Characterization of biomass ashes produced at different temperatures from olive-oil-industry and greenhouse vegetable wastes. *Fuel* 208:1–9. doi: 10.1016/j.fuel.2017.06.133
68. Proctor A (1990) X-ray diffraction and scanning electron microscope studies of processed rice hull silica. *J Am Oil Chem Soc* 67(9):576–584. doi: 10.1007/BF02540770
69. Kalapathy U (2000) A simple method for production of pure silica from rice hull ash. *Bioresour Technol* 73(3):257–262. doi: 10.1016/S0960-8524(99)00127-3
70. Kamath SR, Proctor A (1998) Silica Gel from Rice Hull Ash: Preparation and Characterization. *Cereal Chemistry Journal* 75(4):484–487. doi: 10.1094/CCHEM.1998.75.4.484.

CHAPTER 6

6 Comparative Study of Commercial Silica and Sol–Gel-Derived Porous Silica from Cornhusk for Low-Temperature Catalytic Methane Combustion

Published research Article III

Owusu Prempeh, C.; Hartmann, I.; Formann, S.; Eiden, M.; Neubauer, K.; Atia, H.; Wotzka, A.; Wohlrab, S.; Nelles, M. Comparative Study of Commercial Silica and Sol-Gel-Derived Porous Silica from Cornhusk for Low-Temperature Catalytic Methane Combustion. *Nanomaterials* 2023, 13, 1450. <https://doi.org/10.3390/nano13091450>.

Short summary

Using green and renewable feedstocks in catalytic processes is a crucial strategy towards achieving sustainability. This study evaluated the sustainability of catalytic processes, focusing on using biomass-derived support as a promising alternative to industrialized synthesized catalyst support. The catalyst systems containing Pd and CeO₂ as active metals on biogenic silica support was tested under real experimental conditions simulating exhaust gas, followed by a series of characterizations to ascertain their feasibility and performance for low-temperature catalytic methane combustion operation. In addition, the effectiveness and suitability of the synthesized catalyst was ultimately compared with the commercial silica support. The key findings here were that the cornhusk-derived support exhibited promising properties as a support material for the Pd/CeO₂ catalyst in LTCMC, with comparable or even better performance than the commercial support catalyst. This was a result of the sol-gel polymeric process altering the surface chemistry and hydrophobicity of biogenic silica thereby improving its catalytic performance and resistance against water. The novel investigations explored here have shown that the utilization of agricultural waste materials as support materials offers a sustainable and cost-effective approach to catalyst synthesis while offering avenues for reducing environmental impacts, promoting circular economy principles, and advancing towards a more sustainable future in the field of catalysis.

Proof of individual contribution:

The nature and contributions of various authors towards the completion of **Chapter 6** are as follows:

	Authors	Contribution	Extent of contribution (%)
<u>Author</u>	<u>Clement Owusu Prempeh</u>	Conceptualization, methodology, formal analysis, investigations, resources, data curation, writing—original draft preparation, writing—review and editing, and visualization.	80
Co-author (1)	Ingo Hartmann	Conceptualization, methodology, resources, writing—review and editing, visualization, supervision, and project administration.	5
Co-author (2)	Steffi Formann	Conceptualization, methodology, resources, writing—review and editing, supervision, and project administration.	3
Co-author (3)	Manfred Eiden	Investigations, data curation, and visualization.	2
Co-author (4)	Katja Neubauer	Investigations data curation, writing—review and editing, and visualization.	2
Co-author (5)	Hanan Atia	Investigations data curation, and writing—review and editing.	2
Co-author (6)	Alexander Wotzka	methodology, and writing—review and editing.	2
Co-author (7)	Sebastian Wohlrab	Methodology, and writing—review and editing.	2
Co-author (8)	Michael Nelles	Conceptualization, methodology, supervision, and project administration.	2

Signature of candidate:.....

Date:.....

Declaration by co-authors: The undersigned hereby confirm that

- the declaration above accurately reflects the nature and extent of the contributions of the candidate and the co-authors to **Chapter 6**,
- no other authors contributed to **Chapter 6**, pg. 122 - 153, besides those specified above,
and
- potential conflicts of interest have been revealed to all interested parties and that the necessary arrangements have been made to use the material in **Chapter 6**, pg. 122 - 153, of this dissertation.

Comparative Study of Commercial Silica and Sol–Gel-Derived Porous Silica from Cornhusk for Low-Temperature Catalytic Methane Combustion

Clement Owusu Prempeh^{1,2,*}, Ingo Hartmann^{1,*}, Steffi Formann¹, Manfred Eiden¹, Katja Neubauer³, Hanan Atia³, Alexander Wotzka³, Sebastian Wohlrab³ and Michael Nelles^{1,2}

¹Department of Thermochemical Conversion, DBFZ—Deutsches Biomasseforschungszentrum

Gemeinnützige GmbH, Torgauer Straße 116, 04347 Leipzig, Germany; steffi.formann@dbfz.de (S.F.); manfred.eiden@dbfz.de (M.E.); michael.nelles@dbfz.de (M.N.)

²Department of Agriculture and Environmental Science, University of Rostock, Justus-von-Liebig-Weg 6, 18059 Rostock, Germany

³Leibniz-Institute for Catalysis e.V. (LIKAT), Albert-Einstein-Str. 29a, 18059 Rostock, Germany; katja.neubauer@catalysis.de (K.N.); hanan.atia@catalysis.de (H.A.); alexander.wotzka@catalysis.de (A.W.); sebastian.wohlab@catalysis.de (S.W.)

*Correspondence: clement.owusuprempeh@dbfz.de (C.O.P.); ingo.hartmann@dbfz.de (I.H.);

Tel.: +49-(0)341-2434-523 (C.O.P.)

Abstract

The synthesis and characterization of sol–gel-derived cornhusk support for low-temperature catalytic methane combustion (LTCMC) were investigated in this study. The prepared cornhusk support was impregnated with palladium and cerium oxide (Pd/CeO₂) via the classical incipient wetness method. The resulting catalyst was characterized using various techniques, including X-ray diffraction (XRD), N₂ physisorption (BET), transmission electron microscopy (TEM), and hydrogen temperature-programmed reduction (H₂-TPR). The catalytic performance of the Pd/CeO₂/CHSiO₂ catalyst was evaluated for methane combustion in the temperature range of 150–600 °C using a temperature-controlled catalytic flow reactor, and its performance was compared with a commercial catalyst. The results showed that the Pd/CeO₂ dispersed on SiO₂ from the cornhusk ash support

(Pd/CeO₂/CHSiO₂) catalyst exhibited excellent catalytic activity for methane combustion, with a conversion of 50% at 394 °C compared with 593 °C for the commercial silica catalyst (Pd/CeO₂/commercial). Moreover, the Pd/CeO₂/CHSiO₂ catalyst displayed better catalytic stability after 10 h on stream, with a 7 percentage points of marginal loss in catalytic activity compared with 11 percentage points recorded for the Pd/CeO₂/commercial catalyst. The N₂ physisorption and H₂-TPR results indicated that the cornhusk SiO₂ support possessed a higher surface area and strong reducibility than the synthesized commercial catalyst, contributing to the enhanced catalytic activity of the Pd/CeO₂/SiO₂ catalyst. Overall, the SiO₂ generated from cornhusk ash exhibited promising potential as a low-cost and environmentally friendly support for LTCMC catalysts.

Keywords: sol–gel; cornhusk; support material; biogenic silica; low-temperature catalytic methane combustion; Pd/CeO₂; characterization.

6.1 Introduction

Energy generation from fossils deviates from the culture of sustainability and environmental protection due to the wide emissions of greenhouse gases such as methane (CH₄), nitrous oxide (N₂O), and carbon dioxide (CO₂) [1,2]. With the daily increase in global dependency on fossils for energy generation due to industrialization, the need for alternative energy sources has become paramount. Although methane has a relatively short life span in the atmosphere, it possesses a global warming potential 28–34 times higher than that of CO₂ [3,4], and its abatement is still not realized in the industrial domain due to the lack of feasible and economical mitigation routes [5]. Consequently, the EU [6] and African Unions [7] have enacted stringent policies that serve as a driving force toward the incorporation of carbon-neutral-based resources such as biomass in energy and advanced materials generation. These measures are expected to serve as a framework for reducing the global emissions of greenhouse gases from various industrial and human activities by 2050 [8]. One such intervention is the conversion of methane to a less potent gas, such as CO₂, via the so-called low-temperature catalytic methane combustion (LTCMC) process [9,10].

LTCMC technology activates methane at low temperatures, forming complex intermediate species that are oxidized to produce energy, CO₂, and H₂O [11]. Compared with traditional high-temperature combustion, LTCMC operates at lower temperatures, reducing the formation of harmful pollutants such as nitrogen oxides (NO_x) and particulate matter

[12]. An example of the LTCMC process is the three-way catalytic converter in natural gas vehicles [13]. While three-way catalytic converters reduce CO, HC, and NO_x emissions, they are less effective at reducing CH₄ emissions [14]. CH₄ is a non-polar molecule and the least kinetically reactive molecule, with a C–H bond strength of 104 kcal/mol [15,16]. This necessitates a high activation energy and decomposition temperature for the homogeneous combustion of methane at approximately 1200 °C [17,18]. Moreover, a typical three-way catalytic converter operates in a nominal temperature range of 100–600 °C [9], which may not be sufficient to achieve the level of methane conversion necessary to significantly reduce emissions. Thus, significant research has been aimed at exploring novel catalyst materials, such as metal-organic frameworks (MOFs), which have tuneable chemical properties to activate and mitigate CH₄ emissions at low temperatures [19,20]. These materials, including transition metals, oxides, sulfides, carbides, and zeolites, are better suited to promoting methane oxidation at lower temperatures, leading to improved conversion rates and lower vehicle emissions [21–23].

In this regard, catalysts with exceptional activity, such as noble metals Pd and Pt, have been reported as the best candidates to promote LTCMC operations [24–26]. Nonetheless, the efficiency of these metal oxides (MO_x) can be fine-tuned by supporting them on alumina (Al₂O₃) [27], sol-gel-based porous silica (SiO₂) [28], ZrO₂ [16], and SnO₂ [29]. These supports act as carriers and play a crucial role in the activity of the metal oxides by providing a high surface area, which enhances the metal oxide dispersion, thermal and mechanical stability, and lifetime of the catalyst [13]. According to Eguchi et al. [30], the performance of a Pd-containing catalyst is related to the nature of the support through Pd dispersion and Pd-support interaction.

Pd supported on alumina (Pd/Al₂O₃) is widely perceived as the ‘standard’ catalyst for LTCMC operations, with various studies providing historical insight into the role and performance in methane catalytic reactions [27,31]. However, Al₂O₃ has been reported to be less efficient due to the inert nature of the support and only being active at medium temperatures above 400 °C [30]. More importantly, it often suffers from severe deactivation in the presence of water vapour (10–15 vol%) during operations in the exhausts due to the hydroxylation of the support [32]. The hydroxylation of the support causes the active sites of the Pd catalyst, PdO_x, to sinter, forming the less active sites, Pd(OH)₂. This slows the exchange of active lattice oxygen replacement, resulting in a loss of the catalytic activity [33]. This process is often mitigated by the introduction of Pt, which forms a bimetallic phase

of Pd–Pt to slow down the rate of PdO sintering [33]. Although the Pd–Pt bimetallic phase enhances the stability of the catalyst system against sintering and hydroxylation by water vapour, the catalytic activity is usually compromised, as the Pd–Pt phase is less active compared with PdO_x under low temperature and oxygen-rich conditions [34,35]. To ensure a high catalytic activity with favorable interactions between the active species and the support, precursors such as ceria (CeO₂) are incorporated as a promoter into the Pd lattice to form Pd/CeO₂ complex [36]. The CeO₂ provides abundant active surface oxygen species, improving the reducibility and thermal stability of the catalyst. However, the effects of high temperature on the catalytic activity cannot be ruled out. According to Peng et al. [37], the active PdO_x species decompose into the less active nanometric Pd⁰ species at high temperatures, resulting in a loss of catalytic efficiency.

For the preparation of novel methane combustion catalysts, the adoption of controlled porous glass (CPG) as a support for the dispersion of the active species was employed [38]. However, the synthesis process of CPG from phase-separated borosilicate glass is expensive and time-consuming, limiting broad industrial applicability [39]. Similarly, the functionalization of Pd on commercial silica supports, such as fused and precipitated silica, synthesized via the hydrolysis process of tetraethyl orthosilicate, provides a feasible alternative to obtain efficient Pd/SiO₂-based catalysts, albeit with energy-intensive and environmentally unfriendly properties [40]. These downsides render commercial silica less desirable from cost and environmental considerations as a catalytic support material, and therefore necessitates research into other sustainable silica sources that may have the potential to offset these deficiencies. Recent research has shown that using biogenic silica as a catalyst support can lead to higher catalytic activity and selectivity in the LTCMC process [39]. Biogenic silica is a low-cost, environmentally friendly alternative to industrial-produced silica and has been shown to improve the performance of catalysts in LTCMC applications. Liu et al. [39] investigated rice husk-derived porous silica to support Pd and CeO₂ for LTCMC operations. Although they reported a high catalytic activity for the gas stream at dry conditions, the catalyst had lower activity when tested in the wet feed gas (10.5 vol%-H₂O).

Cornhusk, as an agricultural residue, is therefore ideal for use in a holistic manner, not only thermally but also materially for the production of porous biogenic silica [41]. As a result, Prempeh et al. [42] synthesized high-quality biogenic silica nanoparticles using the sol–gel polymeric route with high potential in catalysis operations. Sol–gel products benefit

from favorable properties such as high surface area with a bimodal pore size distribution, allowing for adequate surface for the active species immobilization and unimpeded mass transfer of gaseous species (reactants and products) [43]. In addition, they exhibited high thermal stability and hydrophobicity that could reduce hydroxylation and water deactivation during catalysis operations [44]. According to Schwarz et al. [45], sol–gel products have extremely low thermal conductivity, good texture, and excellent stability at high temperatures. Notwithstanding, studies on the incorporation of sol–gel-derived biogenic silica from agricultural residues into the field of catalysis are limited. To the best of the authors' knowledge, no studies have been conducted to that effect, and this present study serves as a baseline to bridge this knowledge gap.

Against this background, investigations were conducted into the catalytic activity of sol–gel-derived porous biogenic silica from cornhusk as a support for the MO_x couple (Pd/CeO₂) for LTCMC. The catalytic activities of Pd and CeO₂ impregnated on the sol–gel-derived porous biogenic silica were discussed and compared with conventional support (CWK Köstropur[®] 021012). Both supports were impregnated with the catalytic materials using the classical incipient wetness impregnation method. The final synthesized catalysts were both characterized, and their catalytic performances of methane combustion were examined under lean methane conditions (800 ppm) in a simulated real and dry exhaust gas in the temperature range of 150–600 °C. Catalytic stability tests of the catalysts were performed by running the reaction at 500 °C for 10 h on stream. This present investigation could offer a sustainable and cost-effective approach to catalyst synthesis, while also contributing to waste reduction.

6.2 Materials and Methods

6.2.1 Materials

Two kinds of supports were used in this study: biogenic silica and commercial silica. Cornhusk (*Zea mays*) residues were obtained from a local farm in the Ashanti region, Ghana, in the form of five round bales, each approximately 50 kg, for a total of 250 kg. Upon collection, they were washed in an extractor (STAHL ATOLL 290 E, Gottlob Stahl Wäschereimaschinen GmbH, Sindelfingen, Germany) at 50 °C for 2 h to remove dirt and soil particles. Commercially available support (99.89 wt.% SiO₂, CWK Köstropur[®] 021012,

Chemiewerk Bad Köstritz GmbH, Bad Köstritz, Germany,) was also purchased and used as a benchmarked catalyst. Metal oxide precursors of $\text{Pd}(\text{NO}_3)_2 \cdot 2\text{H}_2\text{O}$ and $\text{Ce}(\text{NO}_3)_3 \cdot 6\text{H}_2\text{O}$ were purchased from Sigma-Aldrich (Taufkirchen, Germany) to synthesize the Pd/CeO₂ nanoparticles.

6.2.2 Preparation of sol–gel-derived cornhusk support

The cornhusk residues were combusted at 600 °C for 2 h to obtain unmodified ash (53 wt.% silica content, surface area = 88 m²/g, and pore volume = 0.25 cm³/g). The unmodified ash was subjected to a sol–gel polymeric route, as detailed in our earlier publication [43], with slight modification to the washing step. A dissolution process of the unmodified ash in NaOH solution at 100 °C for 1 h yielded a sodium silicate solution, which, after a careful pH-controlled process and vigorous washing steps, promoted the formation of silica gels. The gels were dried at 80 °C for 24 h to obtain a silica xerogel powder with improved properties (99 wt.% silica content, surface area = 384 m²/g, and pore volume = 0.35 cm³/g) compared with those of the unmodified ash. The obtained cornhusk support was characterized and subsequently used as the support for the impregnation of the MO_x in the subsequent catalysis experiments.

6.2.3 Preparation of supported catalysts

Supported catalysts were prepared via incipient wetness impregnation as reported in the study by Liu et al. [39]. Molten $\text{Ce}(\text{NO}_3)_3 \cdot 6\text{H}_2\text{O}$ was first impregnated into the supports (cornhusk and commercial silica) at 235 °C and dried at 90 °C overnight. The impregnated supports containing CeO₂ were subsequently calcined at 450 °C at a heating rate of 5 °C/min for 2 h. Hereafter, the resultant CeO₂/SiO₂ mixture was impregnated with an aqueous solution of $\text{Pd}(\text{NO}_3)_2 \cdot 2\text{H}_2\text{O}$. The Pd loading on the supports was controlled to yield 1 wt.% of Pd in the final catalysts. Finally, the catalyst precursors were dried at 120 °C for 12 h and calcined at 500 °C for 1 h. Synthesized catalysts were designated as Pd/CeO₂/CHSiO₂ and Pd/CeO₂/commercial to represent the catalysts impregnated on cornhusk and commercial silica, respectively.

6.2.4 Characterization techniques

The elemental composition of the supports, actual Pd and Ce loadings on the synthesized catalysts (Pd/CeO₂/CHSiO₂ and Pd/CeO₂/commercial) were measured using inductively coupled plasma-optical emission spectrometry (ICP-OES, CETAC, ASX-520, Omaha, NE, USA).

SEM measurements were performed to observe the morphology of the synthesized catalysts in **Article III**. Samples were analyzed by a field emission scanning electron microscope (SEM, MERLIN[®] VP Compact, Co. Zeiss, Oberkochen, Germany) equipped with an energy dispersive X-ray (EDX) detector (XFlash 6/30, Co. Bruker, Berlin, Germany). Representative areas of the samples were analyzed and mapped for elemental distribution on the basis of EDX-spectra data by QUANTAX ESPRIT Microanalysis software (version 2.0). Samples were mounted on a heavy metal-free Al-SEM-carrier (co. PLANO, Wetzlar, Germany) with adhesive conductive carbon tape (Spectro Tabs, TED PELLA INC, Redding, CA, USA) and coated with carbon (5.0 nm thickness) under vacuum (CCU 010 HV-Coating Unit, Co. Safematic GmbH, Zizers, Switzerland). SEM images were taken from the selected regions with the conditions of an applied detector, accelerating voltage, and working distance indicated on the SEM micrographs.

An FTIR spectrometer (PerkinElmer, Solingen, Germany) was used to identify the types of functional groups present in the synthesized catalysts. The spectrum scope in the range of 400–4000 cm⁻¹ with a resolution factor of 1 cm⁻¹ was recorded after four scans and background subtraction.

The specific surface area and pore size distribution of the catalysts were determined using nitrogen adsorption/desorption measurements (BET method) in the autosorb iQ-MP/XR apparatus, Quantachrome, Boynton Beach, FL, USA. According to the literature, the samples were first degassed for 12 h at 250 °C under a vacuum to remove adsorbed water molecules on the surface and within the pores [46]. The specific surface area was determined by multipoint Brunauer–Emmett–Teller (BET) surface area analysis in the pressure range of $p/p_0 = 0.05–0.30$ at 77 K and considering the cross-section area of N₂ molecules of 16.2 Å [47]. The pore volume and pore size distribution were determined using the nonlocal density functional theory (NDLFT) method and considering the adsorption and desorption branch of the isotherm data.

X-ray diffraction (XRD) was used to determine the crystalline phases and crystal structure of the Pd/CeO₂ nanoparticles and the supported catalysts using an X-ray powder diffraction apparatus (XRD, Malvern Panalytical GmbH, Kassel, Germany) equipped with Ni-filtered, Cu-K α radiation ($\lambda = 1.54 \text{ \AA}$). XRD powder patterns were recorded on a Panalytical 'X'Pert $\theta/2\theta$ -diffractometer equipped with an Xcelerator detector using automatic divergence slits and Cu $k\alpha_{1/2}$ radiation (40 kV, 40 mA; $\lambda = 0.15406 \text{ nm}$, 0.154443 nm). Cu beta-radiation was excluded using a nickel filter foil. The measurements were performed with 0.021 s^{-1} and 0.005 s^{-1} , respectively. Samples were mounted on silicon zero background holders. Obtained intensities were converted from automatic to fixed divergence slits (0.25) for further analysis. The size of the coherent scattering region (CSR) was determined using the Scherrer equation [48] applied to corresponding phase reflections. The diffraction patterns were collected in the 2θ range from 5° to 80° .

The redox properties of the catalysts were measured by employing hydrogen temperature programmed reduction (H₂-TPR) experiments with an AC 2920 equipped with a CryColler-unit (Mircomertics, Waltham, MA, USA). The experiments were performed after the following protocol: 80 up to 100 mg of each sample was preheated to 500°C for 30 min in synthetic air (50 mL/min, $20^\circ\text{C}/\text{min}$). The measurement was started after cooling down to -20°C . Each sample was heated up to 800°C in a mixture of 5% H₂ in Ar (20 mL/min, $5^\circ\text{C}/\text{min}$), and the reduction was performed for 30 min. An online thermal conductivity detector was used to measure the hydrogen consumption throughout the entire experiment. The amount of H₂ consumption was calculated after calibration of the thermal conductivity detector (TCD).

6.2.5 Catalytic activity tests for methane combustion

The catalytic performance of the synthesized catalysts was tested in a temperature-controlled catalytic flow reactor (stainless steel V4A, $\varnothing 12 \text{ mm}$). A total of 0.2 g of the synthesized catalysts was mixed with 1.2 g of corundum (inert material) and packed into the reactor tube supported on a quartz wool bed. The amount of inert material mixed with the catalyst was chosen to fill a 7 cm length in the catalyst bed. Light-off tests were carried out by heating the catalyst stepwise from RT to 600°C ($10^\circ\text{C}/\text{min}$ heating ramp) under 70 mL/min flow of a simulated synthetic flue gas mixture containing 800–1000 ppm CH₄, 1528 ppm CO, 207 ppm NO, 10 vol.% CO₂, 6 vol.% O₂ balanced with N₂ (dry condition), or a

mixture of above compositions + 12 vol.% H₂O (wet condition). For each activity run conducted, a gas hourly space velocity (GSHV) of 87,000 mLg⁻¹ h⁻¹ was used. The conversion of methane (X_{CH_4}) was calculated as:

$$X_{CH_4}(\%) = \frac{[CH_4]_{t=0} - [CH_4]_t}{[CH_4]_{t=0}} \times 100 \quad 6.1$$

The catalytic activities of the catalysts were evaluated based on the temperature at which 50% conversion of methane was achieved ($T_{50\%}$). Kinetic studies were conducted with methane conversions values $\leq 10\%$ to exclude the effects of mass and heat transfer limitations. The stability tests or time-on-stream of the catalysts were performed by maintaining the samples at 500 °C for 10 h on stream.

6.3 Results and Discussion

6.3.1 Structure and properties of synthesized catalysts

Table 6.1 presents the ICP-OES results of the bulk elemental compositions of the prepared silica xerogel (SX) support obtained from the cornhusk ash and commercial silica.

Table 6.1. Elemental compositions of catalyst samples measured by ICP-OES analysis (oxygen neglected).

Catalyst	Elements ^a		
	Si %	Ce %	Pd %
Pd/CeO ₂ /CHSiO ₂	20.1	29.9	0.92
Pd/CeO ₂ /commercial	20.9	32.4	1.0

^aCalculated bulk atomic composition

The cornhusk support was characterized by a high silica content (>99 wt.%) with negligible impurities, as later verified in the EDX spectra of the final catalysts and shown in Figure 6.1. The amount of Pd and Ce loadings on both supports, as measured by ICP-OES, are shown in Table 6.1. Both synthesized catalysts showed approximately equivalent

amounts of the designated concentrations of impregnated Pd, highlighting the effectiveness of the synthesis method in preparing the catalysts.

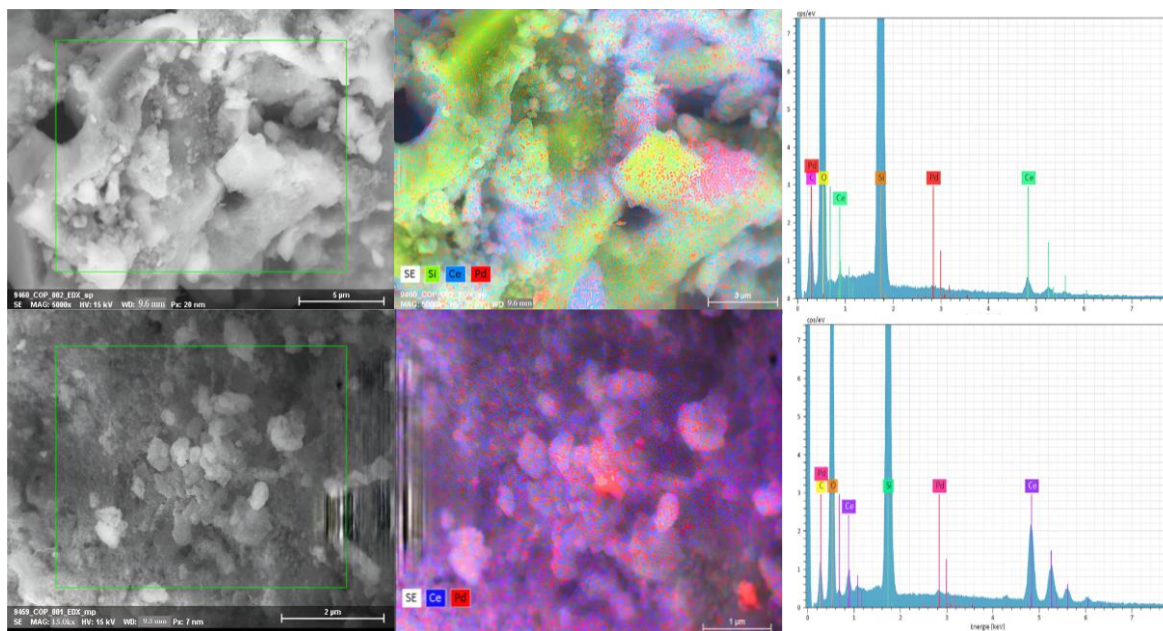


Figure 6.1. SEM/EDX mapping and spatial distributions of the Pd and Ce nanoparticles on supports. (Top row): cornhusk support; (Bottom row): commercial silica supports.

The spatial distributions of the Pd and Ce nanoparticles on the surfaces of the prepared catalysts were observed using different selected areas in the SEM/EDX diagrams, and their corresponding peaks of the various elements in EDX are shown in Figure 6.1. Additional information on the SEM/EDX mappings and spectra values of Pd/CeO₂/CHSiO₂ and Pd/CeO₂/commercial catalysts in atomic wt.% are provided in the supplementary materials (Figures S1 and S2). As observed in the SEM/EDX mapping images in Figure 6.1, the Pd grains were non-uniformly distributed in both catalysts as dispersed crystallites over the CeO₂ granules (red regions on the blue and white surfaces), indicating a successful impregnation of the Pd and Ce species on the supports. Furthermore, apparent proximity between the Pd and Ce can be observed according to the backscattered electrons detector (BSE) and line scan analyses provided in supplementary Figure S3, indicating a successful preparation of the decoupled Pd species from Ce on the samples. Additional elements, such as C (from the sample holder) and O, can also be detected in the EDX spectra diagram in Figure 6.1.

The surface morphologies of the prepared catalysts are examined in Figure 6.2 by comparing their SEM micrographs, and the results revealed different morphological structures of both catalysts. The Pd/CeO₂/CHSiO₂ catalyst exhibited non-uniform shapes and particle sizes (Figure 6.2a) compared with those of the Pd/CeO₂/commercial, which was more analogous in its particle sizes and shapes (Figure 6.2b). In addition, the Pd/CeO₂/CHSiO₂ had rough and irregular surfaces with visible pores and cracks, while the commercial silica support exhibited a smooth and uniform surface with less conspicuous pores. The rough surfaces of the cornhusk support could serve as a scaffold and anchor for the impregnation of the active species [39]. It can also be observed from the SEM image in Figure 6.2c that the Pd/CeO₂/CHSiO₂ catalyst exhibited a compact assemblage with narrow pore cavities compared with Pd/CeO₂/commercial in Figure 6.2d, which could serve as a constrainer for growing nanoparticles inside the pores [49].

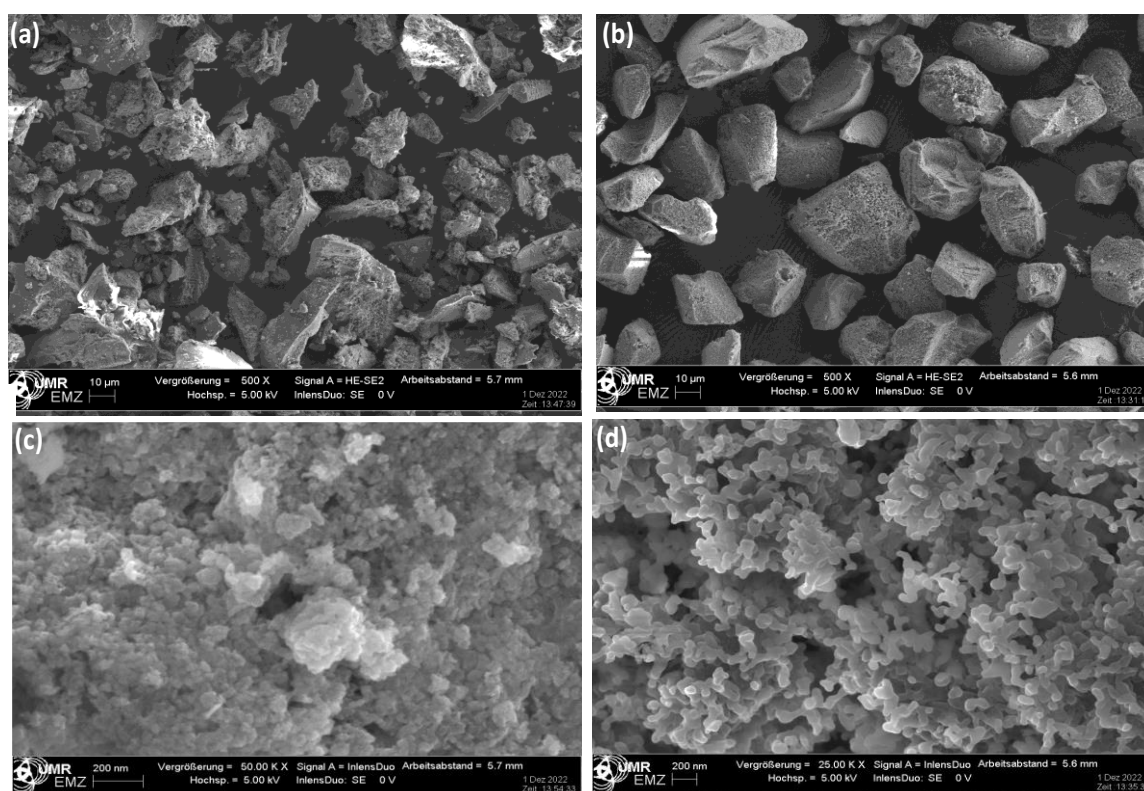


Figure 6.2. SEM micrographs of synthesized catalysts prepared from cornhusk (a,c) and commercial (b,d) silica supports.

The FTIR spectra of corn husk support (silica xerogel), Pd/CeO₂/CHSiO₂, and Pd/CeO₂/commercial catalysts are shown in Figure 6.3. The broad peak between 3500 and

3000 cm^{-1} of the cornhusk support is attributed to the asymmetric stretching of O–H groups from the silanol group [43]. This is formed due to water molecules' adsorption on the silica xerogel's surface and the occlusion of intermediate species $[(\text{OR})_3 - \text{Si} - (\text{OH})]$ within the porous structure during the hydrolysis process of the sol-gel polymeric route [50]. However, this band disappears with the thermal treatment of the catalyst at $500\text{ }^\circ\text{C}$, as seen in the spectrum of the Pd/CeO₂/CHSiO₂ after synthesis. Lopez et al. [51] reported similar observations during their study on preparing high surface area sol-gel Pd/SiO₂ catalysts. Similarly, the infrared spectra between 1644 and 1573 cm^{-1} of the cornhusk support correspond to Si–H₂O flexion and the bending of the H–O–H [52].

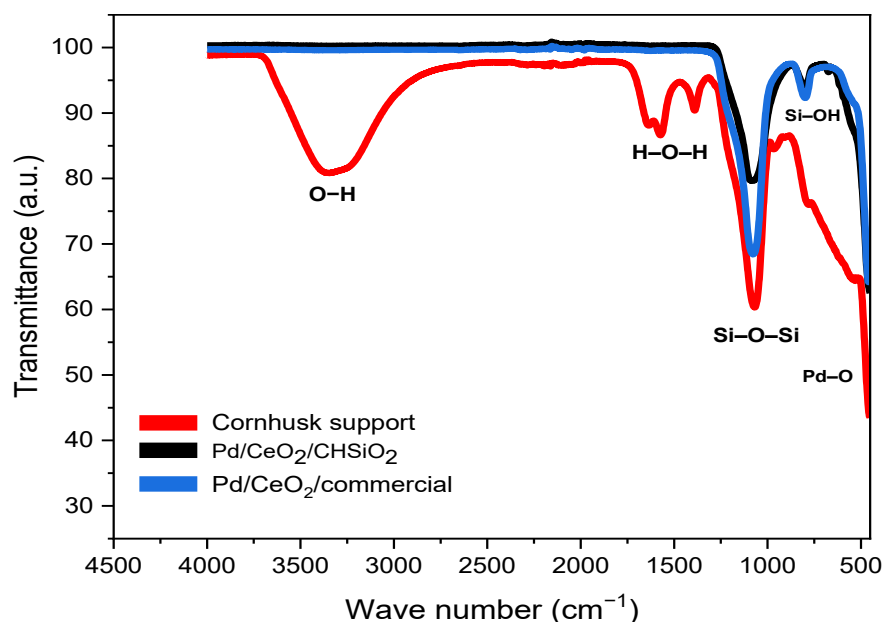


Figure 6.3. FTIR spectra of cornhusk support material, Pd/CeO₂/CHSiO₂, and Pd/CeO₂/commercial catalysts.

The highest energy bands spectrum centered at approximately $1090\text{--}1000\text{ cm}^{-1}$ are assigned to the asymmetric vibration of Si–O–Si bonds [53]. According to Brinker et al. [54], the intensity and symmetry of the high-energy bands could change due to the formation of siloxane bridges. Simultaneously, other characteristic peaks were also visible at $900\text{--}500\text{ cm}^{-1}$, which are features of the asymmetric vibration of O–Si–O formed due to the condensation reaction between neighbouring silanol groups [43,53]. These silanol groups are significant for the structural characterization of solids, as they are involved in changes in

the microcrystallinity of the solids after the post-gelation period [51]. The lower energy bands within the 800 cm^{-1} result from the symmetric vibration of $-\text{Si}-\text{OH}$ [55,56]. More importantly, calcination at/above $450\text{ }^\circ\text{C}$ often leads to the formation of small-energy bands centered at $485\text{--}500\text{ cm}^{-1}$, which are usually assigned to a $\text{Pd}-\text{O}$ bond [57], as observed in Figure 6.3. This indicates the successful formation of metal–oxygen bonds through interactions with the support and the presence of Pd active species on the surface of the catalyst.

The textural properties of the supports and prepared catalysts were measured using nitrogen physisorption experiments, and the results are shown in Figure 6.4a,b and summarized in Table 6.2. Both supports exhibited type IV(a) hysteresis, primarily observed in mesoporous materials [49]. However, the shapes of the hysteresis loops were different, indicating different pore structures in the catalysts.

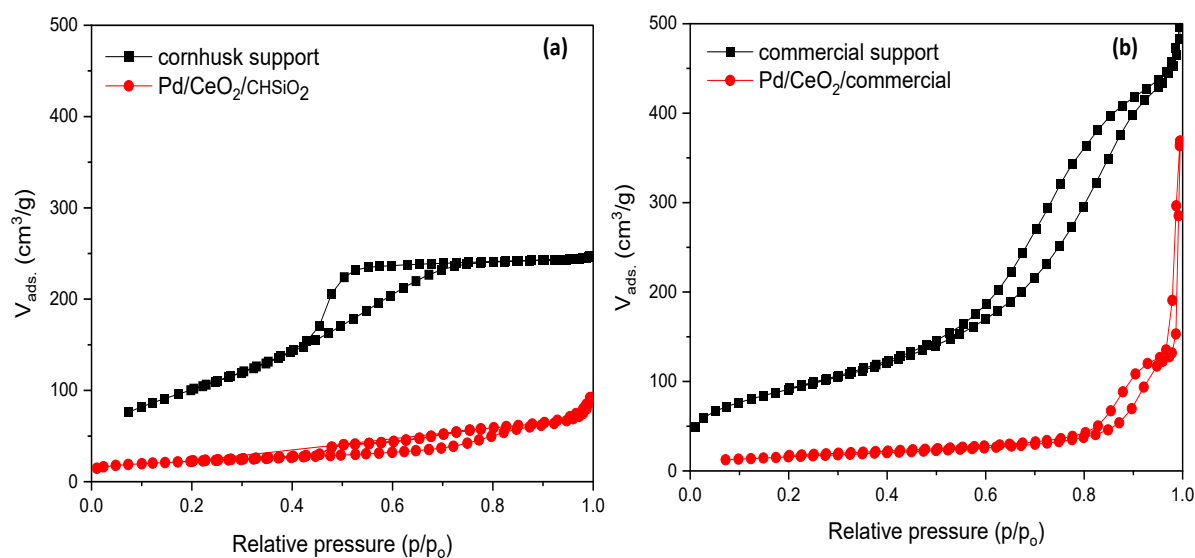


Figure 6.4. N₂ adsorption and desorption isotherms of (a) cornhusk support and Pd/CeO₂/CHSiO₂; (b) commercial support and Pd/CeO₂/commercial.

For the commercial silica support in Figure 6.4b, the type H3 hysteresis loop was observed, in contrast to type H2(a) realized in the cornhusk support (Figure 6.4a). According to Johansson et al. [49], an H3 hysteresis loop is indicative of slit-shaped mesopores or plate-like particles and is mainly observed in materials comprising aggregates (loose assemblage),

as can be observed in the SEM micrograph of the Pd/CeO₂/commercial catalyst in Figure 6.2d. Conversely, the H₂ hysteresis formed in the cornhusk support is due to delayed condensation during adsorption, exhibited by various adsorbents such as inorganic oxide gels and porous vycor glasses, as explained in our earlier study on mesoporous silica materials derived from sol–gel processes [43]. Eventually, the pore volume measured for the Pd/CeO₂/commercial catalyst appeared higher than that of the Pd/CeO₂/CHSiO₂ owing to the loose assemblage of aggregates in the former, as shown in Table 6.2.

Table 6.2 summarizes the Brunauer–Emmett–Teller (BET) surface areas and NDLFT pore volumes measured for the unsupported and as-synthesized catalyst samples.

Table 6.2. Textural properties of the silica support and synthesized catalysts. Specific surface area (S_{BET}), pore volume (NLDFT, determined by N₂-sorption), micropore volume (V_{micro}), micropore surface area (S_{micro} , determined by t-plot method), and external surface area (S_{ext} , determined by t-plot method).

Sample	S_{BET} (m ² /g)	V_{t} (cm ³ /g)	V_{micro} (cm ³ /g)	S_{micro} (m ² /g)	S_{ext} (m ² /g)	C_e^a (nm)
Cornhusk support	384	0.35	0.12	211	173	-
Commercial support	329	0.66	-	-	-	-
Pd/CeO ₂ /CHSiO ₂	77	0.11	0.01	12	65	7.2
Pd/CeO ₂ /commercial	56	0.2	-	-	-	7.7

^a The average crystallite sizes of the CeO₂ phase in the two catalysts estimated from the Debye–Scherrer equation [48] and the representative reflections in the XRD diagram (Figure 6.5) at full-width half maximum.

Unlike the commercial support, the cornhusk support (silica xerogel) exhibited a bimodal pore system consisting of micropores and mesopores with widths centered at 1.5 and 3.8 nm, respectively, as observed in supplementary Figure S4. Further analysis by t-plot showed that the silica xerogel exhibited a micropore volume $V_{\text{micro}} = 0.12 \text{ cm}^3/\text{g}$ and micropore surface area $S_{\text{micro}} = 211 \text{ m}^2/\text{g}$. This allowed for an optimal distribution of the active catalytic species and improved reaction kinetics. The mesopores within the cornhusk silica support can enhance mass transport and accessibility to reaction sites, while the micropores can retain and stabilize catalytic species [58]. On the other hand, the t-plot kernel showed a non-existence micropore volume and surface area (V_{micro} and $S_{\text{micro}} = 0$) within the pore structure of the commercial silica support, although a small indication of closed pores or inaccessible micropores was found. Thus, conclusions about the existence of only

mesopores can be made on the commercial silica support with the mean pore width centered at 5.4 nm in Figure S4.

After the catalyst synthesis, the N₂-desorption capacity observed in the resultant catalysts showed a decrease in the respective surface areas and pore volumes, as seen in Table 6.2. This signifies the successful filling of the metal oxide particles into the supports. The highest surface area of 77 m²/g was achieved in the final as-synthesized Pd/CeO₂/CHSiO₂ catalyst compared with the Pd/CeO₂/commercial catalyst (56 m²/g). The respective reduction in the textural properties of the catalysts was mainly due to the CeO₂ impregnation into the interspaces (mesopores and micropores), as the effects of Pd loading on the supports can be neglected based on its negligible amount compared with the amount of CeO₂, as evidenced in the XRD profiles in Figure 6.5.

X-ray diffraction (XRD) analysis was carried out to investigate the crystalline structures of the prepared Pd/CeO₂/CHSiO₂ catalyst and Pd/CeO₂/commercial support, as shown in Figure 6.5.

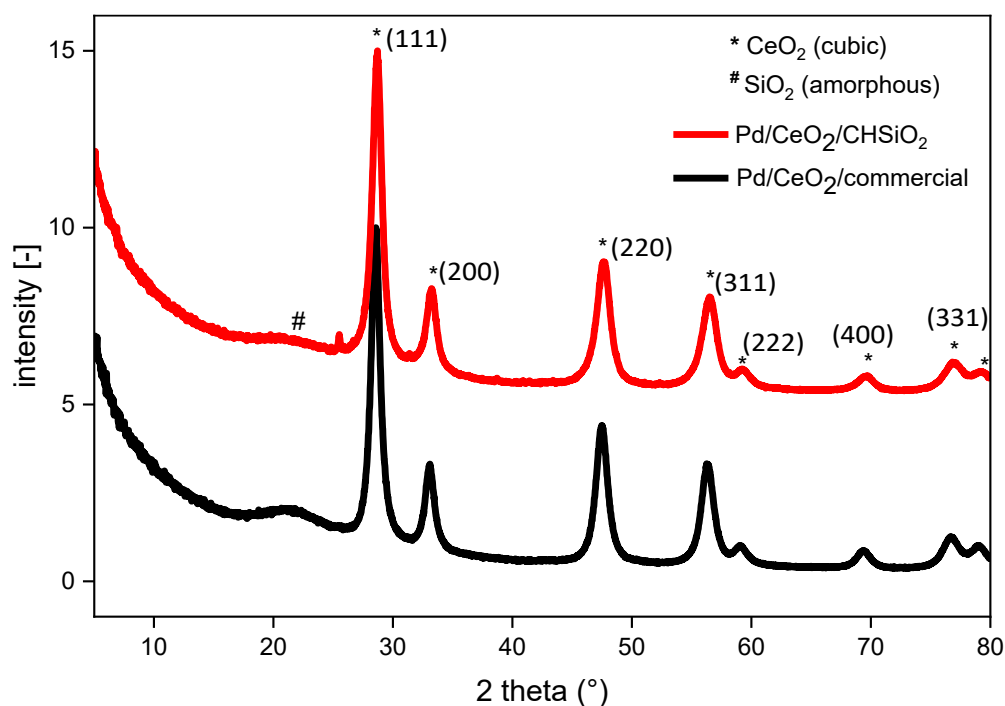


Figure 6.5. X-ray diffraction pattern for the synthesized Pd/CeO₂/CHSiO₂ and Pd/CeO₂/commercial catalysts.

The XRD patterns of both catalysts in Figure 6.5 displayed a series of well-defined peaks with the reflection angles at $2\theta = 28.6, 33.2, 47.6, 56.4, 59.3, 69.6, 77.1,$ and 79.3° , attributed to the reflection of the hexagonal phase of CeO_2 (111), CeO_2 (200), CeO_2 (220), CeO_2 (311), CeO_2 (222), CeO_2 (400), and CeO_2 (311) lattice planes [Joint Committee on Powder Diffraction Standards (JCPDS) card number no. 34-0394], respectively. This indicates that the CeO_2 nanoparticles are well-dispersed in both catalysts without significant aggregation. However, no peaks related to the PdO phase were observed due to its low content in the catalyst. XRD has detection limits for small percentages of nanoparticles [59].

The broad hump-shaped diffraction peaks between $2\theta = 20$ and 25° are the characteristics of amorphous silica [60]. The average crystallite sizes of the CeO_2 phase in the two catalysts were also estimated from the Scherrer equation [48], and the results are summarized in Table 6.2. The Pd/ CeO_2 /CHSiO₂ catalyst showed a smaller crystallite size (7.2 nm) compared with that of the Pd/ CeO_2 /commercial silica support (7.7 nm).

The temperature-programmed reduction with hydrogen (H_2 -TPR) profiles provide information about the reducibility of the catalysts, which is an important factor in their catalytic activity. The TPR plots of the catalysts were obtained by measuring the H_2 consumption as a function of temperature, as illustrated in Figure 6.6.

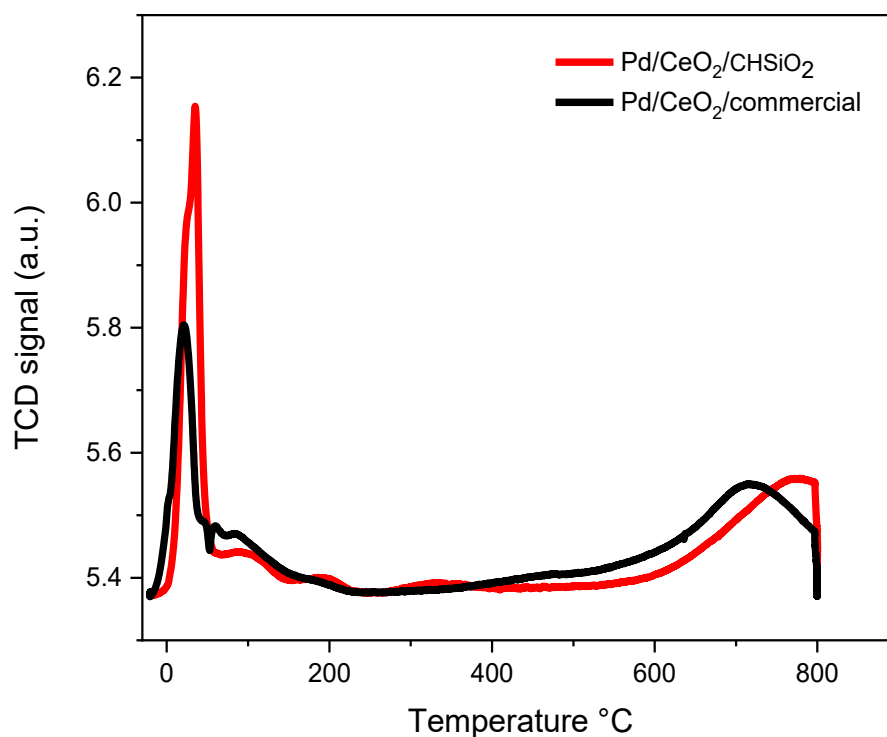


Figure 6.6. H_2 -TPR profiles of Pd/ CeO_2 /CHSiO₂ and Pd/ CeO_2 /commercial catalysts.

The intense peaks of Pd/CeO₂/commercial and Pd/CeO₂/CHSiO₂ at the lowest temperature of ~30 °C are attributed to the reduction of the PdO_x species in contact with CeO₂ [61]. The TPR plot of the Pd/CeO₂/CHSiO₂ catalyst showed two minor peaks, between 200 °C and 400 °C, which corresponded to Pd–O reducibility to Pd and surface reduction of CeO₂ to CeO_{2-x}, respectively [38]. These peaks were rather absent in the Pd/CeO₂/commercial catalyst, indicating that the Pd–O and CeO₂ are not well-dispersed on commercial support compared with the cornhusk silica catalyst. In addition, there were broad peaks between 600 and 800 °C, which corresponded to the reduction of bulk CeO₂ to CeO_{2-x} [62].

The differences in reducibility between the two catalysts can be attributed to the different properties of the support materials. The cornhusk support used in synthesizing the Pd/CeO₂/CHSiO₂ catalyst had a slightly higher surface area with micropores than that of the commercial silica catalyst (Table 6.2), which allowed for more Pd/CeO₂ interaction and a higher metal oxide dispersion on the support, leading to higher catalyst reducibility. Furthermore, by comparing the total amount of H₂ consumption during the duration of the measurements, Pd/CeO₂/CHSiO₂ showed 89% of H₂ consumption, which was higher than that of the Pd/CeO₂/commercial (74.1%), denoting higher reducibility compared with the Pd/CeO₂/commercial [63].

6.3.2 Methane catalytic combustion tests in dry and wet conditions over as-synthesized samples: effect of support on the catalytic activity of Pd/CeO₂ for methane combustion

The catalytic performance of the Pd/CeO₂/CHSiO₂ and Pd/CeO₂/commercial catalysts for methane combustion in the temperature range of 150–600 °C was investigated using light-off curves under dry and wet conditions, as shown in Figure 6.7a,b, respectively. The temperature corresponding to 50% conversion of CH₄ (T_{50%}) is widely used to compare the low-temperature combustion activity of the catalysts [64,65].

The results showed that the Pd/CeO₂/CHSiO₂ catalyst exhibited higher catalytic activity in dry conditions than the Pd/CeO₂/commercial silica catalyst, with a T_{50%} value of 394 °C compared with 593 °C for the commercial catalyst (Figure 6.7a). The activity of the Pd/CeO₂/CHSiO₂ catalyst is comparable to highly efficient catalysts reported in previous

studies [66–68]. Similarly, Chen et al. [69] reported a catalytic activity for methane combustion with a conversion of 50% at 395 °C for 1 wt.% Pd/Ce supported on Al₂O₃.

In addition, the higher catalytic activity exhibited by the Pd/CeO₂/CHSiO₂ catalyst may be ascribed to the unique pore structure and surface chemistry, which may have provided more active sites for the catalytic reaction. Likewise, the lower reduction temperature and higher reduction peak area of the Pd/CeO₂/CHSiO₂ catalyst, as explained earlier in Figure 6.6, showed that the Pd/CeO₂ nanoparticles were more reducible on the cornhusk support, which may have contributed to its enhanced catalytic activity.

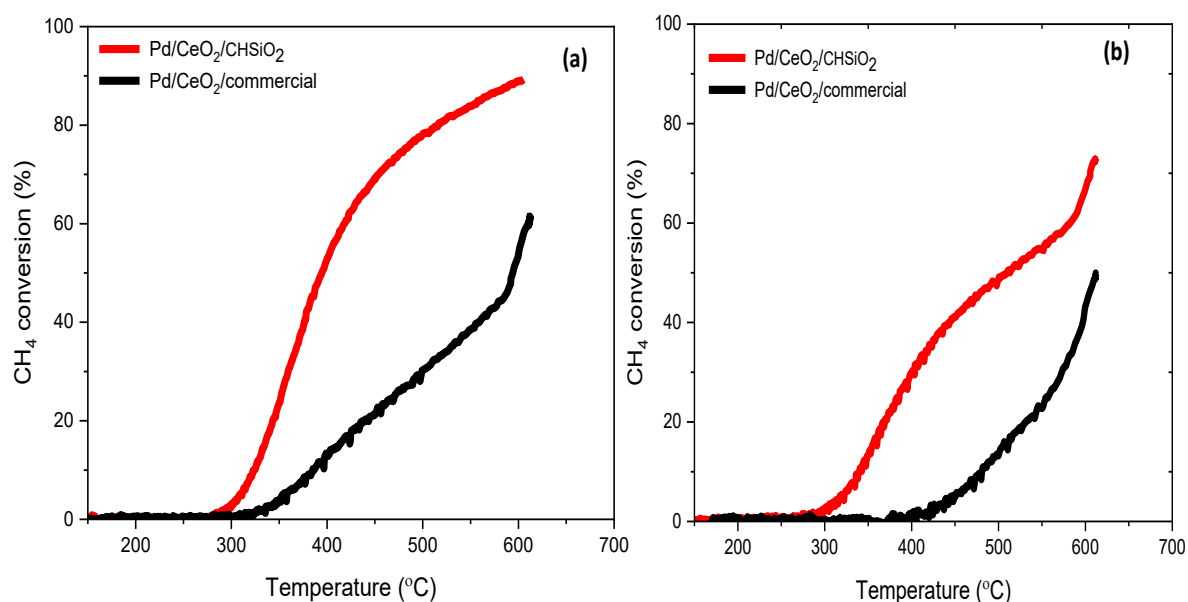


Figure 6.7. Light-off curves for CH₄ combustion in stoichiometric conditions; (a) dry conditions (b) wet conditions. Conditions: Gas mixture containing 800–1000 ppm CH₄, 1528 ppm CO, 207 ppm NO, 10 vol.% CO₂, 6 vol.% O₂ balanced with N₂, or a mixture of above compositions + 12 vol.% H₂O (wet condition) (catalyst mass: 0.2 g mixed with 1.2 g of corundum, a space velocity of 87,000 mLg⁻¹ h⁻¹ in simulated synthetic gas with total flow rate of 70 mL/min).

The effect of water vapour on the catalytic activity and stability of the prepared catalysts was also investigated in the LTCMC reaction. The CH₄ conversion over the Pd/CeO₂/CHSiO₂ and Pd/CeO₂/commercial catalysts were performed under 12 vol.% vapour concentrations at a gas hourly space velocity (GHSV) of 87,000 mLg⁻¹ h⁻¹, and the

results are shown in Figure 6.7b. As observed, the presence of water vapour in the reaction mixture resulted in a significant decrease in the catalytic activities of all the prepared catalysts. Thus, the methane conversion over the catalysts in water vapour decreased from 90 to 73% and 69 to 49% at 600 °C for the Pd/CeO₂/CHSiO₂ and Pd/CeO₂/commercial catalysts, respectively. Similarly, the ignition temperatures of the Pd/CeO₂/commercial catalyst shifted to higher reaction temperatures, from 315 to 415 °C, in the presence of water vapour. In contrast, the Pd/CeO₂/CHSiO₂ catalyst maintained its ignition temperature, albeit with reduced activity.

The reduced catalytic activity for both as-synthesized catalysts can be attributed to the possibility of the water vapour competing with the methane for active sites on the catalyst surface. This competitive adsorption between the methane and water species leads to blocking the active sites by occupying the surface hydroxyl groups, reducing the catalytic activity [32]. From kinetics studies, the reaction rate for methane oxidation is of order -1 with regard to water concentration, as water prevents the desorption of water from the catalyst surface [70,71].

In addition, water vapour can also lead to the sintering of the metal particles and a decrease in the surface area of the catalyst, which can further reduce the catalytic activity [33]. The catalyst prepared from cornhusk support showed better resistance to water vapour than the commercial catalyst. For example, the methane conversion over the prepared catalyst was still above 70%, while the commercial catalyst showed a methane conversion of approximately below 50% in wet conditions at 600 °C. This observation may be due to the hydrophobic nature of the sol–gel support [42], the high dispersion of the active metal particles, and the strong metal-support interactions in the Pd/CeO₂/CHSiO₂ catalyst, which helped to prevent the sintering of the metal particles and maintained the stability of the catalyst under the water vapour atmosphere. Similar adverse effects of water inhibition on catalytic performance have been reported in the literature [32,33].

6.3.3 Kinetic studies

Kinetic studies were performed on both Pd/CeO₂/CHSiO₂ and Pd/CeO₂/commercial silica catalysts to investigate the reaction mechanism of methane combustion in the simulated synthetic gas flue gas mixture. The activation energies were calculated from the

Arrhenius plots, in Equation (2), and estimated within methane conversion values $\leq 10\%$ to exclude the effects of mass and heat transfer limitations [70,72]. In addition, the Arrhenius plots in Figure 6.8 were reasonably linear and, thus, allowed reasonable estimations of the activation energies and pre-exponential terms using the Arrhenius Equation (2), which shows the dependence of the rate constant (k) on the temperature (T) [70].

$$k = K \exp[-E_A/RT] \quad 6.2$$

In Equation 6.2, K is the pre-exponential factor, E_A is the activation energy, and R is the gas constant. According to the results in Figure 6.8, both catalysts followed pseudo first-order kinetics, with the Pd/CeO₂/CHSiO₂ catalyst showing a lower activation energy ($E_A = 130$ kJ/mol) than the Pd/CeO₂/commercial catalyst ($E_A = 137$ kJ/mol).

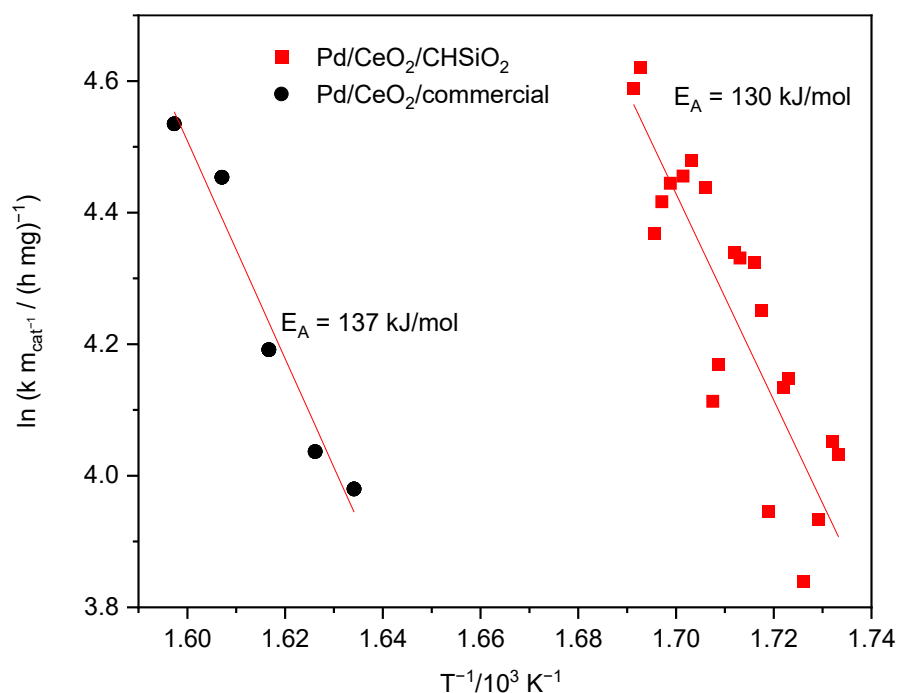


Figure 6.8. Arrhenius plots over Pd/CeO₂/CHSiO₂ and Pd/CeO₂/commercial catalysts at 600 °C. Conditions: Gas mixture containing 800–1000 ppm CH₄, 1528 ppm CO, 207 ppm NO, 10 vol.% CO₂, 6 vol.% O₂ balanced with N₂ (dry condition, catalyst mass: 0.2 g mixed with 1.2 g of corundum, a space velocity of 87,000 mLg⁻¹ h⁻¹ in simulated synthetic gas with total flow rate of 70 mL/min).

The lower activation energy of the Pd/CeO₂/CHSiO₂ catalyst indicates a high possibility of activation of the reaction at a lower temperature, which is beneficial for energy-saving and cost-effective processes [73], and is consistent with the higher catalytic activity for the Pd/CeO₂/CHSiO₂. This lower activation energy of the Pd/CeO₂/CHSiO₂ catalyst could be ascribed to the presence of surface hydroxyl groups, which facilitated the activation of methane molecules [74].

According to the literature [74], the presence of surface hydroxyl groups on transition metal oxides (TMO_x) facilitates methane activation by promoting the dissociation of the C–H bonds. The cornhusk support provides a large surface area and abundant surface hydroxyl groups, as evidenced in the FTIR diagram in Figure 6.3, enhancing the dispersion of Pd particles and promoting active PdO_x species formation. The –OH groups can then act as proton acceptors or donors, creating a favourable environment for the methane reaction. In addition, they can form coordinatively unsaturated metal sites that act as active sites for methane activation. Furthermore, the hydroxyl groups can also promote methane adsorption onto the Pd surface, increasing methane concentration at the reaction sites, and thus enhancing methane activation [74–77].

In chemical kinetics, the pre-exponential factor, also known as the pre-exponential constant or A factor, is a parameter in the Arrhenius equation representing the frequency of successful collisions between two reactant molecules to form the activated complex [9]. The pre-exponential factor is an important parameter to consider when evaluating the catalytic activity of a material. It is related to the rate constant, indicating the rate at which the reaction proceeds [78]. The pre-exponential factor is influenced by various factors, including the nature and concentration of the reactants, the temperature, and the catalyst used in the reaction [79]. In the case of the Pd/CeO₂/CHSiO₂ and Pd/CeO₂/commercial catalysts, the pre-exponential factor can provide insight into their catalytic activity and efficiency.

The results of the studies have shown that the pre-exponential factor of the Pd/CeO₂/CHSiO₂ catalyst is higher ($A = 3.2 \times 10^{13} \text{ h}^{-1}$) than that of the Pd/CeO₂/commercial catalyst ($A = 2.8 \times 10^{13} \text{ h}^{-1}$), suggesting that the latter had a higher frequency of successful collision between the CH₄ and O₂ molecules. This indicates that the Pd/CeO₂/CHSiO₂ catalyst is more efficient at promoting the reaction between methane and oxygen and requires lower activation energy to initiate the reaction. This is consistent with the higher catalytic activity observed for the Pd/CeO₂/cornhusk catalyst, rendering it a more promising candidate for catalyzing the combustion of methane.

6.3.4 Long-term catalytic tests

Long-term catalytic tests are important to assess the durability and reliability of catalysts in real-world applications. This study evaluated the Pd/CeO₂/CHSiO₂ and Pd/CeO₂/commercial catalysts for their long-term catalytic performance during continuous methane combustion for 10 h under reaction conditions of 500 °C and a space velocity of 87,000 mLg⁻¹ h⁻¹.

According to the results illustrated in Figure 6.9, both catalysts exhibited comparable and excellent stabilities. However, the catalytic activity of the Pd/CeO₂/CHSiO₂ and Pd/CeO₂/commercial catalysts degraded gradually with time on stream. For the Pd/CeO₂/CHSiO₂ catalyst, the fresh catalyst showed a methane conversion of 68%, which decreased to 61% after the reaction at 500 °C for 10 h, accounting for a 7% points reduction in catalytic activity.

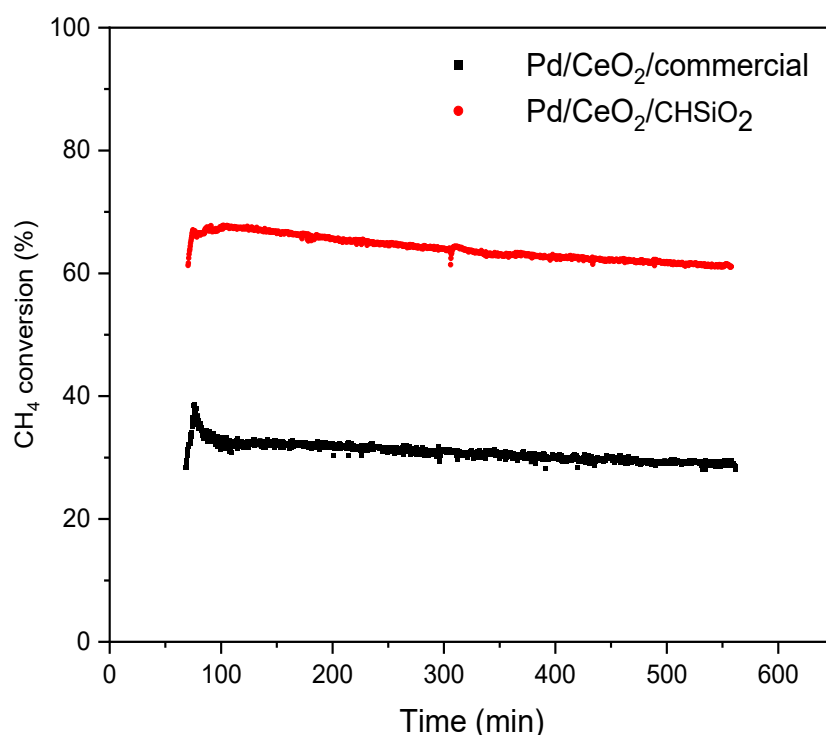


Figure 6.9. Methane conversion versus reaction time of the catalysts after reaction for 10 h. The reactions were conducted at 500 °C with gas mixture containing 800–1000 ppm CH₄, 1528 ppm CO, 207 ppm NO, 10 vol.% CO₂, 6 vol.% O₂ balanced with N₂ (dry condition, catalyst mass: 0.2 g mixed with 1.2 g of corundum, a space velocity of 87,000 mLg⁻¹ h⁻¹ in simulated synthetic gas with total flow rate of 70 mL/min).

Comparatively, there was a decrease in catalytic activity for the Pd/CeO₂/commercial catalyst from 39% to 28%, resulting in an 11% points decrease in activity at the same set of experimental conditions. Thus, the Pd/CeO₂/CHSiO₂ catalyst exhibited superior long-term stability compared with the Pd/CeO₂/commercial catalyst, which may be ascribed to the unique properties of the cornhusk support. The high surface area and surface hydroxyl groups of the cornhusk support may have enhanced the metal-support interaction and stability compared with the commercial silica support, which lacked some of these properties. Hence, it is probable that there was a state transformation of active Pd species and a sintering of Pd particles in the Pd/CeO₂/commercial catalyst during the long-term catalytic tests. Thus, it was tentatively more prone to aggregation and deactivation [80]. For example, the accumulation of reaction intermediates or coke deposition on the catalyst surface could lead to a decrease in the active surface area, resulting in reduced catalytic activity over time. Another possibility could be the deactivation of the catalyst due to changes in the oxidation state or morphology of the Pd nanoparticles during the long-term catalytic reaction. Further characterization techniques, such as in situ spectroscopic or microscopic analysis, could provide insights into the changes occurring at the catalyst surface during the reaction and help elucidate the reasons for the observed phenomenon. Similar results of Pd sintering and deactivation were reported in the study of Yang et al. [80].

6.4 Conclusions

In conclusion, this study investigated the performance and characterization of sol–gel-derived cornhusk silica support for low-temperature catalytic methane combustion (LTCMC). The results showed that the cornhusk-derived support exhibited promising properties as a support material for the Pd/CeO₂ catalyst in LTCMC, with comparable or even better performance than the commercial support. The prepared catalysts were characterized by various techniques, including SEM/EDX, XRD, BET, and H₂-TPR, which showed the successful synthesis of highly dispersed Pd and CeO₂ nanoparticles on the cornhusk support. The observed superior performance of the cornhusk support was attributed to its unique properties, including high surface area, high porosity, and stability. The lower activation energy of the prepared catalysts, as indicated by the Arrhenius plot, suggests that the Pd/CeO₂ catalyst on the cornhusk support facilitated the reaction mechanism of methane combustion. Moreover, the Pd/CeO₂/CHSiO₂ catalyst showed good long-term catalytic

stability. In a gas stream containing water vapour, the Pd/CeO₂/CHSiO₂ catalyst also exhibited better performance than the Pd/CeO₂/commercial silica catalyst. Overall, this study provides valuable insights into the potential of cornhusk-derived support materials for LTCMC applications. The utilization of agricultural waste materials as support materials could offer a sustainable and cost-effective approach to catalyst synthesis while also contributing to a reduction in waste residues. Further studies could investigate optimizing the cornhusk support properties and exploring other metal oxide catalysts for LTCMC on biogenic supports.

Supplementary Materials: The following supporting information can be found in the Appendix A: **Table S1.** Bulk elemental compositions measured by ICP-OES of the prepared silica xerogel support (SX) obtained from cornhusk ash and commercial silica; **Figure S1.** SEM/EDX mappings of Pd/CeO₂/CHSiO₂ (left side) and Pd/CeO₂/commercial catalyst (right side); **Figure S2.** Details of the two EDX spectra values of Pd/CeO₂/CHSiO₂ (top) and Pd/CeO₂/commercial (bottom) catalysts in atomic weight %; **Figure S3:** Analysis with a BSE (back scattered electrons) detector and line scan for Pd/CeO₂/CHSiO₂ (left side) and Pd/CeO₂/commercial (right side) catalysts; **Figure S4.** Pore size distribution of cornhusk support and commercial silica support determined by applying a dedicated NLDFT adsorption branch kernel on the adsorption branch of the N₂ (77 K) isotherms.

Acknowledgments: Special gratitude to Hossein Beidaghy Dizaji, Katharina Görtz, and the technical team members of DBFZ for their invaluable support during this study. Special appreciation to Mr. Bamgboye Kehinde, Marc Bohnet, and analytical team members of DBFZ and Likat for their commitments to the analyses of the biomass fuels and synthesized catalysts.

References of Chapter 6

1. Yu, D.-G.; He, L.-N. Introduction to CO₂ utilisation. *Green Chem.* **2021**, *23*, 3499–3501. <https://doi.org/10.1039/D1GC90036F>.
2. Garba, M.D.; Usman, M.; Khan, S.; Shehzad, F.; Galadima, A.; Ehsan, M.F.; Ghanem, A.S.; Humayun, M. CO₂ towards fuels: A review of catalytic conversion of carbon dioxide to HCs. *J. Environ. Chem. Eng.* **2021**, *9*, 104756. <https://doi.org/10.1016/j.jece.2020.104756>.

3. Ghosh, S.; Majumdar, D.; Jain, M.C. Methane and nitrous oxide emissions from an irrigated rice of North India. *Chemosphere* **2003**, *51*, 181–195. [https://doi.org/10.1016/S0045-6535\(02\)00822-6](https://doi.org/10.1016/S0045-6535(02)00822-6).
4. Bronson, K.F.; Mosier, A.R. Suppression of methane oxidation in aerobic soil by nitrogen fertilizers, nitrification inhibitors, and urease inhibitors. *Biol. Fert. Soils* **1994**, *17*, 263–268. <https://doi.org/10.1007/BF00383979>.
5. Malyan, S.K.; Bhatia, A.; Kumar, A.; Gupta, D.K.; Singh, R.; Kumar, S.S.; Tomer, R.; Kumar, O.; Jain, N. Methane production, oxidation and mitigation: A mechanistic understanding and comprehensive evaluation of influencing factors. *Sci. Total Env.* **2016**, *572*, 874–896. <https://doi.org/10.1016/j.scitotenv.2016.07.182>.
6. United Nations Framework Convention on Climate Change. Adoption of the Paris Agreement: Proposal by the President. In Proceedings of the Paris Climate Change, Paris, France, 30 November–11 December 2015.
7. African Climate Policy Centre. Overview of the ClimDev Africa Programme. Available online: <http://www.climdev-africa.org/afrian-climate-policy-center> (accessed on 10 August 2022.).
8. Philander, S. (Ed.) *Encyclopedia of Global Warming and Climate Change*; SAGE Publications, Inc.: Thousand Oaks, CA, USA, 2008.
9. Baldwin, T.R.; Burch, R. Catalytic combustion of methane over supported palladium catalysts. *Appl. Catal.* **1990**, *66*, 337–358. [https://doi.org/10.1016/S0166-9834\(00\)81648-6](https://doi.org/10.1016/S0166-9834(00)81648-6).
10. Xiao, L.-H.; Sun, K.-P.; Xu, X.-L.; Li, X.-N. Low-temperature catalytic combustion of methane over Pd/CeO₂ prepared by deposition–precipitation method. *Catal. Commun.* **2005**, *6*, 796–801. <https://doi.org/10.1016/j.catcom.2005.07.015>.
11. Tang, Z.; Zhang, T.; Luo, D.; Wang, Y.; Hu, Z.; Yang, R.T. Catalytic Combustion of Methane: From Mechanism and Materials Properties to Catalytic Performance. *ACS Catal.* **2022**, *12*, 13457–13474. <https://doi.org/10.1021/acscatal.2c03321>.
12. Ismagilov, Z.R.; Kerzhentsev, M.A.; Susharina, T.L. Catalytic methods for lowering the amount of nitrogen oxides in exhaust gases on combustion of fuel. *Russ. Chem. Rev.* **1990**, *59*, 973–988. <https://doi.org/10.1070/RC1990v059n10ABEH003570>.
13. Zheng, T.; He, J.; Zhao, Y.; Xia, W.; He, J. Precious metal-support interaction in automotive exhaust catalysts. *J. Rare Earths* **2014**, *32*, 97–107. [https://doi.org/10.1016/S1002-0721\(14\)60038-7](https://doi.org/10.1016/S1002-0721(14)60038-7).

14. Takigawa, A.; Matsunami, A.; Arai, N. Methane emission from automobile equipped with three-way catalytic converter while driving. *Energy* **2005**, *30*, 461–473. <https://doi.org/10.1016/j.energy.2004.04.016>.
15. Senanayake, S.D.; Rodriguez, J.A.; Weaver, J.F. Low Temperature Activation of Methane on Metal-Oxides and Complex Interfaces: Insights from Surface Science. *Acc. Chem. Res.* **2020**, *53*, 1488–1497. <https://doi.org/10.1021/acs.accounts.0c00194>.
16. Epling, W.S.; Hoflund, G.B. Catalytic Oxidation of Methane over ZrO₂-Supported Pd Catalysts. *J. Catal.* **1999**, *182*, 5–12. <https://doi.org/10.1006/jcat.1998.2341>.
17. Ciuparu, D.; Lyubovsky, M.R.; Altman, E.; Pfefferle, L.D.; Datye, A. Catalytic combustion of methane over palladium-based catalysts. *Catal. Rev.* **2002**, *44*, 593–649. <https://doi.org/10.1081/CR-120015482>.
18. Hasnan, N.S.N.; Timmiati, S.N.; Lim, K.L.; Yaakob, Z.; Kamaruddin, N.H.N.; Teh, L.P. Recent developments in methane decomposition over heterogeneous catalysts: An overview. *Mater. Renew. Sustain. Energy* **2020**, *9*, 1259. <https://doi.org/10.1007/s40243-020-00167-5>.
19. Valdebenito, G.; González-Carvajal, M.; Santibañez, L.; Cancino, P. Metal–Organic Frameworks (MOFs) and Materials Derived from MOFs as Catalysts for the Development of Green Processes. *Catalysts* **2022**, *12*, 136. <https://doi.org/10.3390/catal12020136>.
20. Yuvaraja, R.; Nanthakumar, K.; Dhasahinamoorthi, G. Development and Performance Analysis of New Catalytic Converter. *Aust. J. Basic & Appl. Sci.*, *9(27)*: 471-478, 2015.
21. Leman, A.M.; Jajuli, A.; Feriyanto, D.; Rahman, F.; Zakaria, S. Advanced Catalytic Converter in Gasoline Engine Emission Control: A Review. In *MATEC Web of Conferences*; EDP Sciences: Les Ulis, France, 2017; Volume 87, p. 02020. <https://doi.org/10.1051/mateconf/20178702020>.
22. Choudhary, T.V.; Goodman, D.W. Methane activation on Ni and Ru model catalysts. *J. Mol. Catal. A Chem.* **2000**, *163*, 9–18. [https://doi.org/10.1016/s1381-1169\(00\)00395-2](https://doi.org/10.1016/s1381-1169(00)00395-2).
23. Raynes, S.; Shah, M.A.; Taylor, R.A. Direct conversion of methane to methanol with zeolites: Towards understanding the role of extra-framework d-block metal and zeolite framework type. *Dalton Trans.* **2019**, *48*, 10364–10384. <https://doi.org/10.1039/c9dt00922a>.
24. Narui, K.; Furuta, K.; Yata, H.; Nishida, A.; Kohtoku, Y.; Matsuzaki, T. Catalytic activity of PdO/ZrO₂ catalyst for methane combustion. *Catal. Today* **1998**, *45*, 173–178. [https://doi.org/10.1016/S0920-5861\(98\)00274-0](https://doi.org/10.1016/S0920-5861(98)00274-0).

25. Widjaja, H.; Sekizawa, K.; Eguchi, K.; Arai, H. Oxidation of methane over Pd/mixed oxides for catalytic combustion. *Catal. Today* **1999**, *47*, 95–101. [https://doi.org/10.1016/S0920-5861\(98\)00286-7](https://doi.org/10.1016/S0920-5861(98)00286-7).
26. Hicks, R. Structure sensitivity of methane oxidation over platinum and palladium. *J. Catal.* **1990**, *122*, 280–294. [https://doi.org/10.1016/0021-9517\(90\)90282-O](https://doi.org/10.1016/0021-9517(90)90282-O).
27. Persson, K.; Thevenin, P.O.; Jansson, K.; Agrell, J.; Järås, S.G.; Pettersson, L.J. Preparation of alumina-supported palladium catalysts for complete oxidation of methane. *Appl. Catal. A Gen.* **2003**, *249*, 165–174. [https://doi.org/10.1016/S0926-860X\(03\)00193-5](https://doi.org/10.1016/S0926-860X(03)00193-5).
28. Enke, D.; Gläser, R.; Tallarek, U. Sol-Gel and Porous Glass-Based Silica Monoliths with Hierarchical Pore Structure for Solid-Liquid Catalysis. *Chem. Ing. Tech.* **2016**, *88*, 1561–1585. <https://doi.org/10.1002/cite.201600049>.
29. Sekizawa, K.; Widjaja, H.; Maeda, S.; Ozawa, Y.; Eguchi, K. Low temperature oxidation of methane over Pd/SnO₂ catalyst. *Appl. Catal. A Gen.* **2000**, *200*, 211–217. [https://doi.org/10.1016/S0926-860X\(00\)00634-7](https://doi.org/10.1016/S0926-860X(00)00634-7).
30. Eguchi, K.; Arai, H. Low temperature oxidation of methane over Pd-based catalysts—Effect of support oxide on the combustion activity. *Appl. Catal. A Gen.* **2001**, *222*, 359–367. [https://doi.org/10.1016/S0926-860X\(01\)00843-2](https://doi.org/10.1016/S0926-860X(01)00843-2).
31. Du, J.; Guo, M.; Zhang, A.; Zhao, H.; Zhao, D.; Wang, C.; Zheng, T.; Zhao, Y.; Luo, Y. Performance, structure and kinetics of Pd catalyst supported in Ba modified γ -Al₂O₃ for low temperature wet methane oxidation. *Chem. Eng. J.* **2022**, *430*, 133113. <https://doi.org/10.1016/j.cej.2021.133113>.
32. Burch, R.; Urbano, F.; Loader, P. Methane combustion over palladium catalysts: The effect of carbon dioxide and water on activity. *Appl. Catal. A Gen.* **1995**, *123*, 173–184. [https://doi.org/10.1016/0926-860X\(94\)00251-7](https://doi.org/10.1016/0926-860X(94)00251-7).
33. Nomura, K.; Noro, K.; Nakamura, Y.; Yazawa, Y.; Yoshida, H.; Satsuma, A.; Hattori, T. Pd–Pt bimetallic catalyst supported on SAPO-5 for catalytic combustion of diluted methane in the presence of water vapour. *Catal. Lett.* **1998**, *53*, 167–169. <https://doi.org/10.1023/A:1019082611978>.
34. Persson, K.; Ersson, A.; Jansson, K.; Fierro, J.; Jaras, S. Influence of molar ratio on Pd–Pt catalysts for methane combustion. *J. Catal.* **2006**, *243*, 14–24. <https://doi.org/10.1016/j.jcat.2006.06.019>.
35. Goodman, E.D.; Dai, S.; Yang, A.-C.; Wrasman, C.J.; Gallo, A.; Bare, S.R.; Hoffman, A.S.; Jaramillo, T.F.; Graham, G.W.; Pan, X.; et al. Uniform Pt/Pd Bimetallic

- Nanocrystals Demonstrate Platinum Effect on Palladium Methane Combustion Activity and Stability. *ACS Catal.* **2017**, *7*, 4372–4380. <https://doi.org/10.1021/acscatal.7b00393>.
36. Al Mohamadi, H.; Smith, K.J. The Impact of CeO₂ Loading on the Activity and Stability of PdO/γ-AlOOH/γ-Al₂O₃ Monolith Catalysts for CH₄ Oxidation. *Catalysts* **2019**, *9*, 557. <https://doi.org/10.3390/catal9060557>.
37. Peng, R.; Li, S.; Sun, X.; Ren, Q.; Chen, L.; Fu, M.; Wu, J.; Ye, D. Size effect of Pt nanoparticles on the catalytic oxidation of toluene over Pt/CeO₂ catalysts. *Appl. Catal. B Environ.* **2018**, *220*, 462–470. <https://doi.org/10.1016/j.apcatb.2017.07.048>.
38. Hoffmann, M.; Kreft, S.; Georgi, G.; Fulda, G.; Pohl, M.-M.; Seeburg, D.; Berger-Karin, C.; Kondratenko, E.V.; Wohlrab, S. Improved catalytic methane combustion of Pd/CeO₂ catalysts via porous glass integration. *Appl. Catal. B Environ.* **2015**, *179*, 313–320. <https://doi.org/10.1016/j.apcatb.2015.05.028>.
39. Liu, D.; Seeburg, D.; Kreft, S.; Bindig, R.; Hartmann, I.; Schneider, D.; Enke, D.; Wohlrab, S. Rice Husk Derived Porous Silica as Support for Pd and CeO₂ for Low Temperature Catalytic Methane Combustion. *Catalysts* **2019**, *9*, 26. <https://doi.org/10.3390/catal9010026>.
40. Vassalini, I.; Alessandri, I. Switchable Stimuli-Responsive Heterogeneous Catalysis. *Catalysts* **2018**, *8*, 569. <https://doi.org/10.3390/catal8120569>.
41. Prempeh, C.O.; Formann, S.; Schliermann, T.; Dizaji, H.B.; Nelles, M. Extraction and Characterization of Biogenic Silica Obtained from Selected Agro-Waste in Africa. *Appl. Sci.* **2021**, *11*, 10363. <https://doi.org/10.3390/app112110363>.
42. Prempeh, C.O.; Formann, S.; Hartmann, I.; Nelles, M. An improved method for the production of biogenic silica from cornhusk using sol–gel polymeric route. *Biomass Conv. Bioref.* **2022**, *4*, 107. <https://doi.org/10.1007/s13399-022-03615-6>.
43. Owens, G.J.; Singh, R.K.; Foroutan, F.; Alqaysi, M.; Han, C.-M.; Mahapatra, C.; Kim, H.-W.; Knowles, J.C. Sol–gel based materials for biomedical applications. *Prog. Mater. Sci.* **2016**, *77* (Suppl. S2), 1–79. <https://doi.org/10.1016/j.pmatsci.2015.12.001>.
44. Maseko NN, Enke D, Iwarere SA, Oluwafemi OS, Pocock J. Synthesis of Low Density and High Purity Silica Xerogels from South African Sugarcane Leaves without the Usage of a Surfactant. *Sustainability* **2023**;15(5):4626. <https://doi.org/10.3390/su15054626>.
45. Schwarz, J.A.; Contescu, C.; Contescu, A. Methods for Preparation of Catalytic Materials. *Chem. Rev.* **1995**, *95*, 477–510. <https://doi.org/10.1021/cr00035a002>.

46. Beidaghy Dizaji, H.; Zeng, T.; Hölzig, H.; Bauer, J.; Klöß, G.; Enke, D. Ash transformation mechanism during combustion of rice husk and rice straw. *Fuel* **2022**, *307*, 121768. <https://doi.org/10.1016/j.fuel.2021.121768>.
47. Brunauer, S.; Emmett, P.H.; Teller, E. Adsorption of Gases in Multimolecular Layers. *J. Am. Chem. Soc.* **1938**, *60*, 309–319. <https://doi.org/10.1021/ja01269a023>.
48. Scherrer, P. Bestimmung der inneren Struktur und der Größe von Kolloidteilchen mittels Röntgenstrahlen. In *Kolloidchemie Ein Lehrbuch*; Zsigmondy, R., Ed.; Springer: Berlin/Heidelberg, Germany, 1912; pp. 387–409.
49. Johansson, E.M. Controlling the Pore Size and Morphology of Mesoporous Silica. Ph.D. Dissertation, Linköping University, Linköping, 2010. Available online: <http://urn.kb.se/resolve?urn=urn:nbn:se:liu:diva-70405> (Last accessed on 23 April 2023).
50. Moncada, E.; Quijada, R.; Retuert, J. Nanoparticles prepared by the sol–gel method and their use in the formation of nanocomposites with polypropylene. *Nanotechnology* **2007**, *18*, 335606. <https://doi.org/10.1088/0957-4484/18/33/335606>.
51. Lopez Goerne, T.; Gomez, R.; Navarrete, J.; Gonzalez, R.D. Preparation of high-surface area sol-gel Pd/SiO₂ catalysts. *J. Mater. Synth. Process.* **1994**, *2*, 305–314.
52. El Rassy, H.; Pierre, A.C. NMR and IR spectroscopy of silica aerogels with different hydrophobic characteristics. *J. Non-Cryst. Solids* **2005**, *351*, 1603–1610. <https://doi.org/10.1016/j.jnoncrysol.2005.03.048>.
53. Feng, Q.; Chen, K.; Ma, D.; Lin, H.; Liu, Z.; Qin, S.; Luo, Y. Synthesis of high specific surface area silica aerogel from rice husk ash via ambient pressure drying. *Colloids Surf. A Physicochem. Eng. Asp.* **2018**, *539*, 399–406. <https://doi.org/10.1016/j.colsurfa.2017.12.025>.
54. Brinker, C.J.; Keefer, K.D.; Schaefer, D.W.; Ashley, C.S. Sol-gel transition in simple silicates. *J. Non-Cryst. Solids* **1982**, *48*, 47–64. [https://doi.org/10.1016/0022-3093\(82\)90245-9](https://doi.org/10.1016/0022-3093(82)90245-9).
55. Yang, H.; Yan, R.; Chen, H.; Lee, D.H.; Zheng, C. Characteristics of hemicellulose, cellulose and lignin pyrolysis. *Fuel* **2007**, *86*, 1781–1788. <https://doi.org/10.1016/j.fuel.2006.12.013>.
56. Singh, G.; Dizaji, H.B.; Puttuswamy, H.; Sharma, S. Biogenic Nanosilica Synthesis Employing Agro-Waste Rice Straw and Its Application Study in Photocatalytic Degradation of Cationic Dye. *Sustainability* **2022**, *14*, 539. <https://doi.org/10.3390/su14010539>.

57. Nakamoto, K. *Infrared and Raman Spectra of Inorganic and Coordination Compounds*; John Wiley & Sons, Inc.: Hoboken, NJ, USA, 2008.
58. Radu, D.R. *Mesoporous Silica Nanomaterials for Applications in Catalysis, Sensing, Drug Delivery and Gene Transfection*; Iowa State University: Ames, IA, USA, 2004. <https://doi.org/10.2172/837277>.
59. Singh, S.A.; Vishwanath, K.; Madras, G. Role of Hydrogen and Oxygen Activation over Pt and Pd-Doped Composites for Catalytic Hydrogen Combustion. *ACS Appl. Mater. Interfaces* **2017**, *9*, 19380–19388. <https://doi.org/10.1021/acsami.6b08019>.
60. Proctor, A. X-ray diffraction and scanning electron microscope studies of processed rice hull silica. *J. Am. Oil Chem. Soc.* **1990**, *67*, 576–584. <https://doi.org/10.1007/BF02540770>.
61. Muto, K.-I.; Katada, N.; Niwa, M. Complete oxidation of methane on supported palladium catalyst: Support effect. *Appl. Catal. A Gen.* **1996**, *134*, 203–215. [https://doi.org/10.1016/0926-860X\(95\)00189-1](https://doi.org/10.1016/0926-860X(95)00189-1).
62. Ferrer, V.; Moronta, A.; Sánchez, J.; Solano, R.; Bernal, S.; Finol, D. Effect of the reduction temperature on the catalytic activity of Pd-supported catalysts. *Catal. Today* **2005**, *107*, 487–492. <https://doi.org/10.1016/j.cattod.2005.07.059>.
63. de Leitenburg, C.; Trovarelli, A.; Kašpar, J. A Temperature-Programmed and Transient Kinetic Study of CO₂ Activation and Methanation over CeO₂ Supported Noble Metals. *J. Catal.* **1997**, *166*, 98–107.
64. Granger, P. Challenges and breakthroughs in post-combustion catalysis: How to match future stringent regulations. *Catal. Sci. Technol.* **2017**, *7*, 5195–5211. <https://doi.org/10.1039/C7CY00983F>.
65. Chen, J.; Arandiyana, H.; Gao, X.; Li, J. Recent Advances in Catalysts for Methane Combustion. *Catal. Surv. Asia* **2015**, *19*, 140–171. <https://doi.org/10.1007/s10563-015-9191-5>.
66. Ferri, D.; Elsener, M.; Kröcher, O. Methane oxidation over a honeycomb Pd-only three-way catalyst under static and periodic operation. *Appl. Catal. B Environ.* **2018**, *220*, 67–77. <https://doi.org/10.1016/j.apcatb.2017.07.070>.
67. Lou, Y.; Ma, J.; Hu, W.; Dai, Q.; Wang, L.; Zhan, W.; Guo, Y.; Cao, X.-M.; Guo, Y.; Hu, P.; et al. Low-Temperature Methane Combustion over Pd/H-ZSM-5: Active Pd Sites with Specific Electronic Properties Modulated by Acidic Sites of H-ZSM-5. *ACS Catal.* **2016**, *6*, 8127–8139. <https://doi.org/10.1021/acscatal.6b01801>.

68. Xie, S.; Liu, Y.; Deng, J.; Zhao, X.; Yang, J.; Zhang, K.; Han, Z.; Dai, H. Three-dimensionally ordered macroporous CeO₂-supported Pd@Co nanoparticles: Highly active catalysts for methane oxidation. *J. Catal.* **2016**, *342*, 17–26. <https://doi.org/10.1016/j.jcat.2016.07.003>.
69. Chen, J.; Wu, Y.; Hu, W.; Qu, P.; Zhang, G.; Jiao, Y.; Zhong, L.; Chen, Y.-Q. Evolution of Pd Species for the Conversion of Methane under Operation Conditions. *Ind. Eng. Chem. Res.* **2019**, *58*, 6255–6265. <https://doi.org/10.1021/acs.iecr.8b06226>.
70. van Giezen, J.C.; van den Berg, F.R.; Kleinen, J.L.; van Dillen, A.J.; Geus, J.W. The effect of water on the activity of supported palladium catalysts in the catalytic combustion of methane. *Catal. Today* **1999**, *47*, 287–293. [https://doi.org/10.1016/S0920-5861\(98\)00309-5](https://doi.org/10.1016/S0920-5861(98)00309-5).
71. Toso, A.; Colussi, S.; Padigapaty, S.; de Leitenburg, C.; Trovarelli, A. High stability and activity of solution combustion synthesized Pd-based catalysts for methane combustion in presence of water. *Appl. Catal. B Environ.* **2018**, *230*, 237–245. <https://doi.org/10.1016/j.apcatb.2018.02.049>.
72. Zhang, M.; Wang, M.; Xu, B.; Ma, D. How to Measure the Reaction Performance of Heterogeneous Catalytic Reactions Reliably. *Joule* **2019**, *3*, 2876–2883. <https://doi.org/10.1016/j.joule.2019.11.005>.
73. Aguila, B.; Sun, Q.; Wang, X.; O'Rourke, E.; Al-Enizi, A.M.; Nafady, A.; Ma, S. Lower Activation Energy for Catalytic Reactions through Host-Guest Cooperation within Metal-Organic Frameworks. *Angew. Chem. Int. Ed. Engl.* **2018**, *57*, 10107–10111. <https://doi.org/10.1002/anie.201803081>.
74. Fu, G.; Xu, X.; Lu, X.; Wan, H. Mechanisms of methane activation and transformation on molybdenum oxide-based catalysts. *J. Am. Chem. Soc.* **2005**, *127*, 3989–3996. <https://doi.org/10.1021/ja0441099>.
75. Pengpanich, S.; Meeyoo, V.; Rirkksomboon, T.; Bunyakiat, K. Catalytic oxidation of methane over CeO₂-ZrO₂ mixed oxide solid solution catalysts prepared via urea hydrolysis. *Appl. Catal. A Gen.* **2002**, *234*, 221–233. [https://doi.org/10.1016/S0926-860X\(02\)00230-2](https://doi.org/10.1016/S0926-860X(02)00230-2).
76. Oh, S.H.; Mitchell, P.J.; Siewert, R.M. *Methane Oxidation over Noble Metal Catalysts as Related to Controlling Natural Gas Vehicle Exhaust Emissions*; American Chemical Society: Washington, DC, USA, 1992.

77. Ding, Y.; Wang, S.; Zhang, L.; Lv, L.; Xu, D.; Liu, W.; Wang, S. Investigation of supported palladium catalysts for combustion of methane: The activation effect caused by SO₂. *Chem. Eng. J.* **2020**, *382*, 122969. <https://doi.org/10.1016/j.cej.2019.122969>.
78. Zimmerman, J. Physical chemistry for the biosciences: Chang, Raymond. *Biochem. Mol. Biol. Educ.* **2005**, *33*, 382. <https://doi.org/10.1002/bmb.2005.49403305383>.
79. Laidler, K.J. *IUPAC Standards Online*; De Gruyter: Berlin, Germany, 2016. <https://doi.org/10.1515/iupac.68.0011>.
80. Yang, L.; Fan, C.; Luo, L.; Chen, Y.; Wu, Z.; Qin, Z.; Dong, M.; Fan, W.; Wang, J. Preparation of Pd/SiO₂ Catalysts by a Simple Dry Ball-Milling Method for Lean Methane Oxidation and Probe of the State of Active Pd Species. *Catalysts* **2021**, *11*, 725. <https://doi.org/10.3390/catal11060725>.

Chapter 7

7 Summary, Conclusions, and Future Work

In this section, the primary findings of the thesis are briefly outlined regarding their impact on the set objectives, and conclusions are derived. In addition, detailed suggestions for future research endeavours are specified.

The initial goals of the study aimed to explore the extraction of high-quality biogenic silica from biomass residues, particularly from silicon-rich African agricultural residues. The objective was to prepare catalyst supports that could exhibit enhanced and stable catalytic activity in the context of low-temperature methane combustion. The results of the study have shown promising outcomes in line with the set objectives. Sustainable and environmentally-friendly procedures were successfully employed to extract biogenic silica from selected African biomass residues. Firstly, the investigation into chemical pretreatment and combustion techniques yielded significant insights into the efficient extraction and comprehensive characterization of the biogenic silica. Secondly, the study achieved success in improving the textural properties of the extracted biogenic silica. Post-treatment methods, including wet-chemistry-based synthesis routes such as the sol-gel polymeric process, enhanced the silica nanoparticles' quality beyond the initial ash material. This accomplishment marked a significant advancement toward obtaining high-quality silica with attributes suitable for advanced industrial applications. Lastly, the investigation into catalytic effectiveness yielded encouraging results. Metal catalysts supported on biogenic silica exhibited promising performance in the low-temperature catalytic combustion of methane. This achievement is particularly noteworthy, as it addresses the critical challenge of developing efficient catalyst supports for environmentally-friendly methane combustion, contributing to energy efficiency and reduced emissions.

Comparing these findings in the dissertation to the state-of-the-art in science and technology, the study has made substantial contributions. In brief, the novel use of agricultural waste materials as catalyst supports, the innovative extraction techniques, and the enhanced catalytic properties of the biogenic silica align with the ongoing drive toward sustainable practices in various industries. The approach of this study is unique and extends the current understanding of biomass-derived materials for catalysis. The following points reveal how the objectives and findings of the study build upon existing knowledge and introduce novel contributions:

- **Biogenic silica extraction:** The success of this study in extracting high-quality biogenic silica from biomass residues is aligned with the growing trend in sustainable materials research. The focus of this study on utilizing agricultural waste to obtain valuable materials resonates with state-of-the-art efforts to turn waste into valuable resources. The innovative application of systematic chemical pretreatment and combustion methods to extract and characterize biogenic silica is a significant contribution, providing a comprehensive understanding of the attributes of the material.
- **Catalyst support enhancement:** The utilization of wet-chemistry-based synthesis routes to improve the textural properties of biogenic silica builds upon existing methods to enhance catalyst supports. While previous research has explored similar routes, the study introduces a unique context— the utilization of biogenic silica derived from biomass residues. This adds an innovative layer to existing knowledge by showing the versatility of such approaches across different material origins.
- **Low-temperature catalytic methane combustion:** The investigation of the study into the catalytic effectiveness of biogenic silica-based catalysts for low-temperature methane combustion aligns with a crucial area of interest in catalysis research. The focus on promoting efficient combustion at lower temperatures aligns with the state-of-the-art drive to develop catalysts that enable clean and energy-efficient processes. The comparative performance of the biogenic silica-based catalysts against commercial supports demonstrates the potential for novel materials to outperform or match established ones.

The significance of the results of this study also extends well beyond the immediate scope of biogenic silica extraction and its catalytic applications. The findings bear broader implications for multiple facets of science, industry, and environmental sustainability. These include:

- **Contribution to environmental conservation:** The reduced reliance on conventional silica extraction methods, which often involve resource-intensive processes, aligns with global efforts to reduce the environmental footprint of

material production. By providing an eco-friendly route to valuable silica materials, the study contributes to minimizing ecological disruption.

- **Advancing sustainable practices:** The successful extraction of high-quality biogenic silica from biomass residues exemplifies a novel approach to utilizing abundant waste materials for valuable industrial applications. The repurposing of agricultural residues aligns with the principles of a circular economy, minimizing environmental impact and promoting resource efficiency.
- **Regional and global relevance:** The focus of the study on African biomass residues highlights the potential for regional self-sufficiency and economic development. By utilizing locally available waste materials, communities could tap into new avenues of resource utilization, creating opportunities for sustainable economic growth.

However, some limitations and unanswered questions exist, providing opportunities for further research and refinement of the findings. These include:

- **Optimization of synthesis methods:** The study succeeded in enhancing the textural properties of the extracted biogenic silica through post-treatment methods. However, there remains potential for optimizing these synthesis methods to elevate further the quality of the obtained silica nanoparticles. Investigating parameters such as reaction times, temperatures, and precursor concentrations could lead to even higher-quality silica with enhanced characteristics. This optimization process could involve systematically exploring the influence of these parameters on the final silica product, aiming to achieve specific attributes that cater to diverse applications.
- **Broader range of experimental conditions:** While the study addressed the catalytic effectiveness of metal catalysts supported on biogenic silica for low-temperature methane combustion, a broader range of experimental conditions and testing scenarios could offer a more comprehensive understanding of the versatility of the material. The performance of the catalysts could be tested under varying temperatures, pressures, and gas compositions to assess their robustness across different operating conditions. This broader scope of experimentation would provide insights into the stability and efficiency of

catalysts under a range of practical scenarios, making its applicability in real-world industrial settings more evident.

- **Long-term stability and durability:** An additional dimension to explore is the long-term stability and durability of the synthesized catalysts. Over extended periods of operation (beyond 10 h, as adopted in this study), catalysts can experience deactivation due to factors such as fouling, poisoning, or structural changes. Investigating the performance of the catalyst over extended time frames could shed light on its potential for sustained catalytic activity and resistance to deactivation mechanisms, which is crucial for industrial applications where catalyst lifespan significantly impacts operational efficiency and cost-effectiveness.
- **Impact of feedstock variability:** The study focused on specific African biomass residues for the extraction of biogenic silica. However, the inherent variability of biomass feedstocks within the selected type and across different sources could influence the extraction and catalytic performance. Exploring the impact of feedstock variability on the process outcomes could offer a comprehensive understanding of the feasibility and robustness of the developed methodologies.

In conclusion, while the achievements of this study represent significant strides toward sustainable and efficient catalyst supports, these limitations and unanswered questions highlight the dynamic nature of research. Addressing these aspects could lead to refined methodologies, enhanced materials, and a deeper understanding of the potential applications and challenges associated with biogenic silica extraction and utilization. More importantly, the originality of this study emanates from its pioneering approach to extracting and utilizing biogenic silica from biomass residues, innovative methods for improving material properties, and interdisciplinary integration. The work presented in this dissertation opens doors to novel solutions, fosters sustainable practices, and contributes to the ongoing transformation of scientific research into tangible contributions with real-world impact.

Appendix A: Supplementary Data

Comparative Study of Commercial Silica and Sol–Gel-Derived Porous Silica from Cornhusk for Low-Temperature Catalytic Methane Combustion

Clement Owusu Prempeh ^{1,2,*}, Ingo Hartmann ^{1,*}, Steffi Formann ¹, Manfred Eiden ¹, Katja Neubauer ³,
Hanan Atia ³, Alexander Wotzka ³, Sebastian Wohlrab ³ and Michael Nelles ^{1,2}

¹ Department of Thermochemical Conversion, DBFZ—Deutsches Biomasseforschungszentrum Gemeinnützige GmbH, Torgauer Straße 116, 04347 Leipzig, Germany; steffi.formann@dbfz.de (S.F.); manfred.eiden@dbfz.de (M.E.); michael.nelles@dbfz.de (M.N.)

² Department of Agriculture and Environmental Science, University of Rostock, Justus-von-Liebig-Weg 6, 18059 Rostock, Germany

³ Leibniz-Institute for Catalysis e.V. (LIKAT), Albert-Einstein-Str. 29a, 18059 Rostock, Germany; katja.neubauer@catalysis.de (K.N.); hanan.atia@catalysis.de (H.A.); alexander.wotzka@catalysis.de (A.W.); sebastian.wohrlab@catalysis.de (S.W.)

* Correspondence: clement.owusuprempeh@dbfz.de (C.O.P.); ingo.hartmann@dbfz.de (I.H.); Tel.: +49-(0)341-2434-523 (C.O.P.)

Table S3. Bulk elemental compositions measured by ICP-OES of the prepared silica xerogel support (SX) obtained from the cornhusk ash and commercial silica

Elements	Cornhusk support (sol-gel)	Commercial Support
SiO ₂	99.69	99.89
P ₂ O ₅	0.15	0.01
SO ₃	0.09	0.05
Fe ₂ O ₃	0.03	0.01
MgO	0.02	0.00
Na ₂ O	0.01	0.00
TiO ₂	0.01	0.03

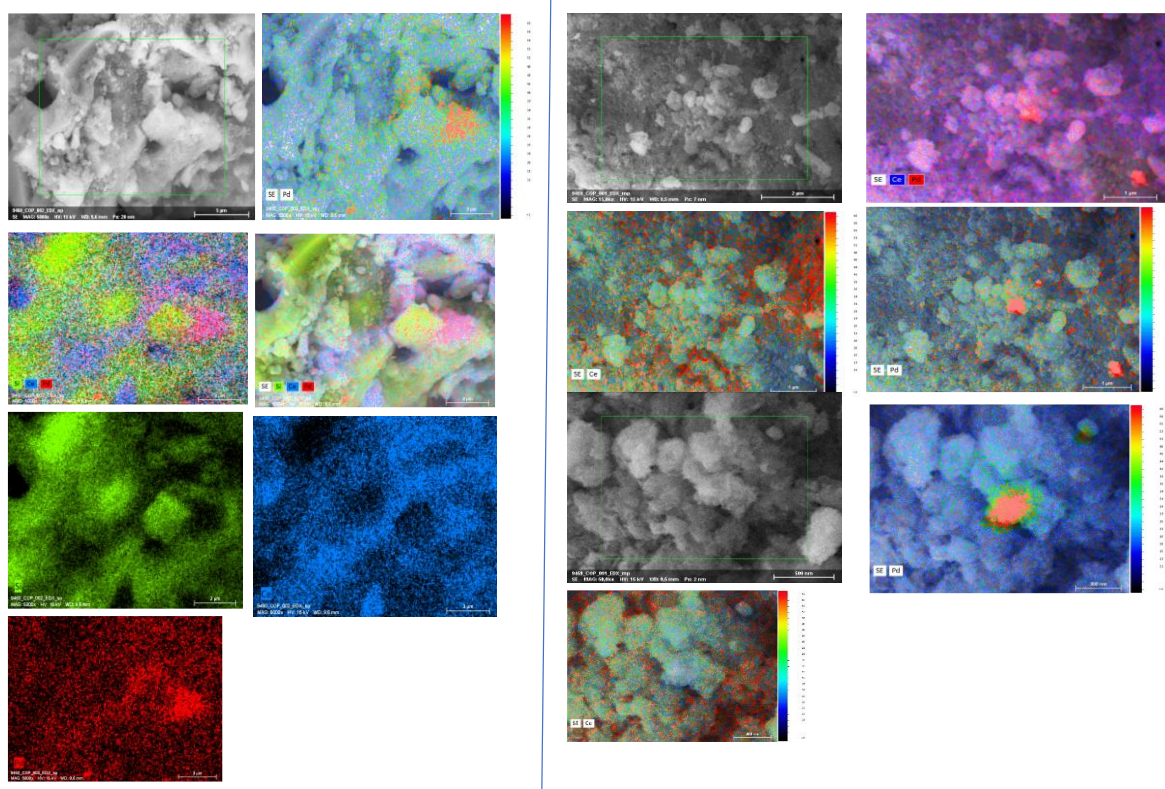
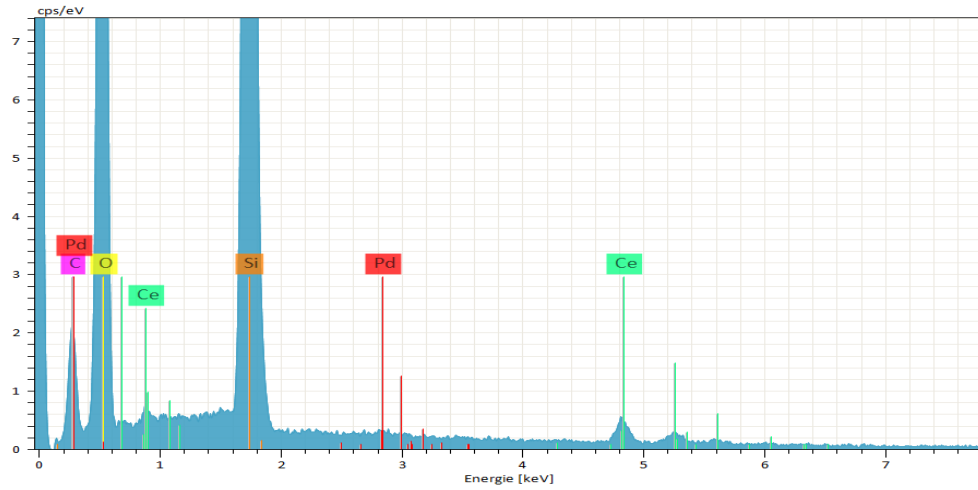
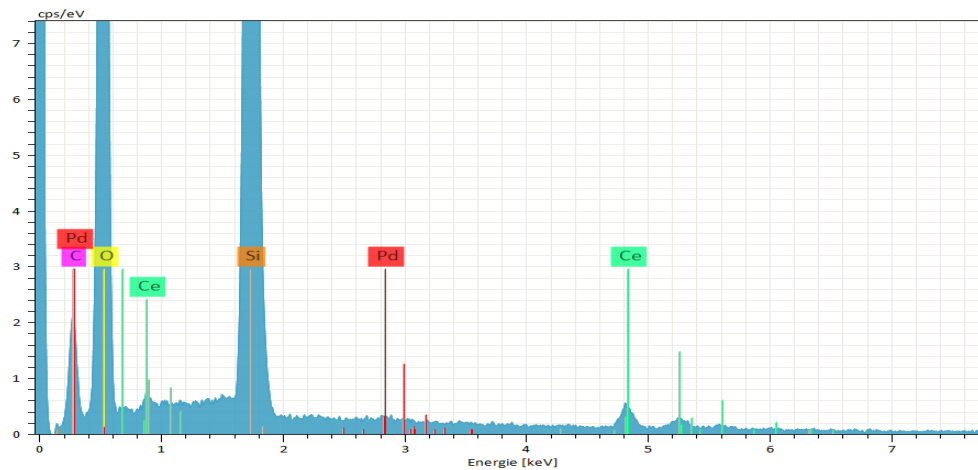


Figure S1. SEM/EDX mappings of Pd/CeO₂/CHSiO₂ (left side) and Pd/CeO₂/commercial catalyst (right side)

- EDX mapping at 2 different spots of the catalyst samples
- Clear separation of Pd and Ce can be seen



Element	Ord. Z	Net	Wt (%)	Norm mass (%)	Atom (%)	Abs. error (1 sigma)	Rel. error (1 sigma)
Oxygen	8	75596	56.28	54.49	66.89	6.47	11.50
Silicon	14	144844	37.30	36.12	25.26	1.58	4.23
Carbon	6	1613	4.50	4.36	7.13	0.92	20.52
Ce	56	3857	4.84	4.69	0.66	0.19	3.94
Pd	46	542	0.35	0.34	0.06	0.05	13.13
		Sum	103.27	100	100		



Element	Ord. Z	Net	Wt (%)	Norm mass (%)	Atom (%)	Abs. error (1 sigma)	Rel. error (1 sigma)
Oxygen	8	50605	31.30	32.96	55.11	3.71	11.86

Silicon	14	106555	33.02	34.78	33.12	1.40	4.24
Carbon	6	1462	2.60	2.74	6.10	0.56	21.42
Ce	58	27702	27.45	28.91	5.52	0.83	3.04
Pd	46	1061	0.58	0.61	0.15	0.05	9.17
		Sum	103.27	100	100		

Figure S2. Details of the two EDX spectra values of Pd/CeO₂/CHSiO₂ (top) and Pd/CeO₂/commercial (bottom) catalysts in atomic wt%.

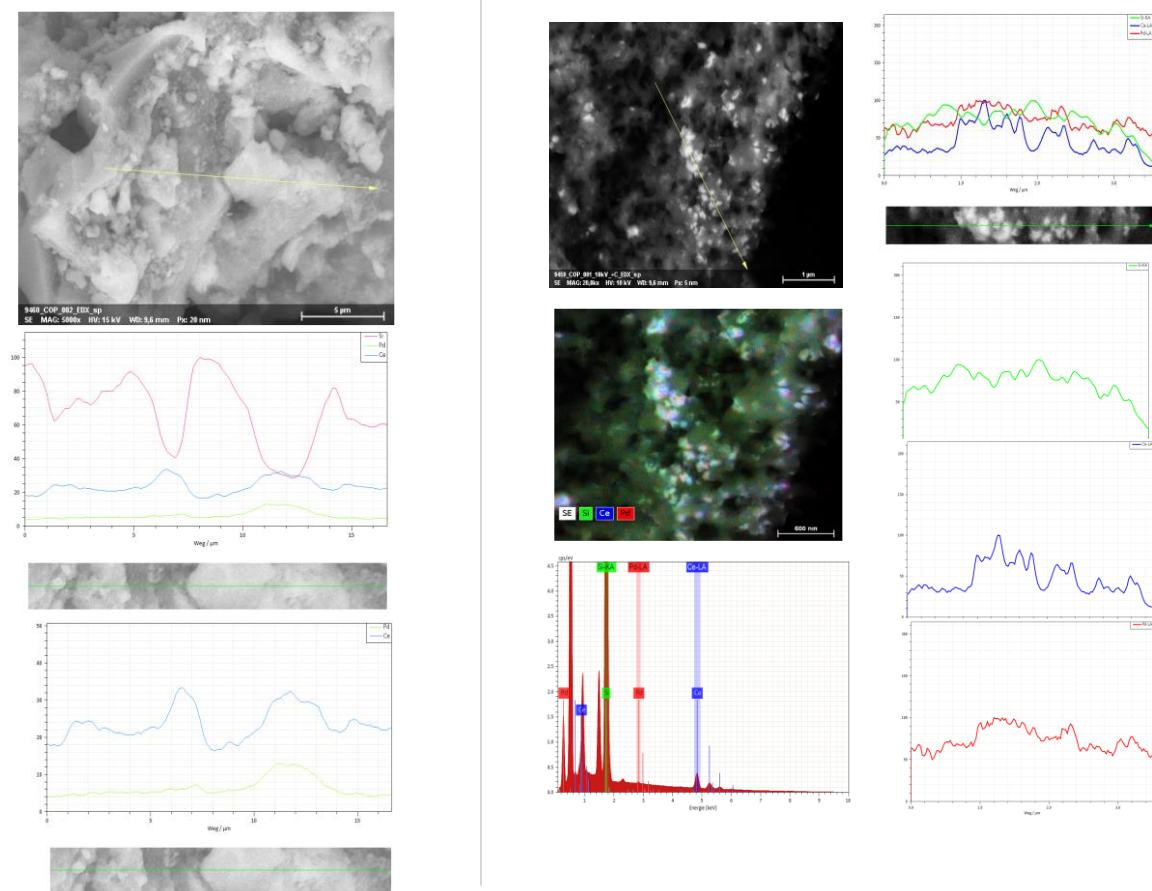


Figure S3. Analysis with BSE (back scattered electrons) detector and line scan for Pd/CeO₂/CHSiO₂ (left side) and Pd/CeO₂/commercial (right side) catalysts.

- The Line scan indicates a certain proximity between Ce and Pd
- heavier elements are made more visible by the BSE detector (glow brighter)
- Bright spots indicate areas with Ce and Pd loading

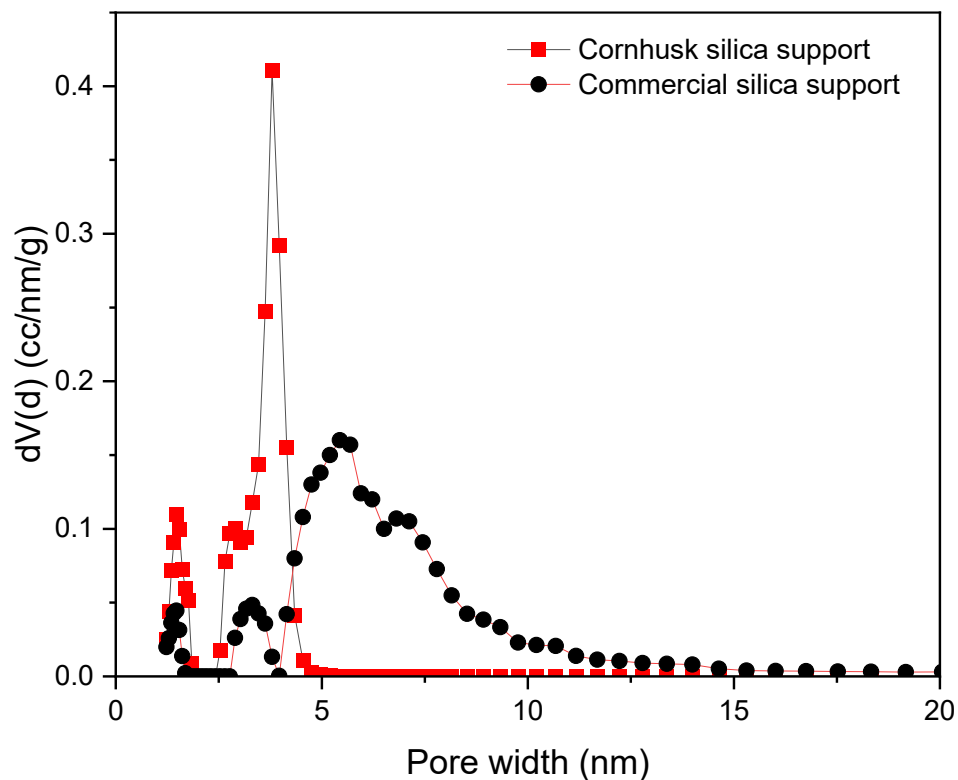


Figure S4. Pore size distribution of cornhusk support and commercial silica support determined by applying a dedicated NLDFT adsorption branch kernel on the adsorption branch of the N_2 (77 K) isotherm

For the cornhusk silica support:

$$V_{micro} = 0.123 \text{ cm}^3/\text{g}$$

$$S_{micro} = 210.841 \text{ m}^2/\text{g}$$

For the commercial silica support:

$$V_{micro} = 0 \text{ cm}^3/\text{g}$$

$$S_{micro} = 0 \text{ m}^2/\text{g}$$

Appendix B: Procedures and Standards

Fuels and sample preparation

The acquisition of fuel samples investigated in this study, each approximately 2 kg in weight, was conducted systematically by collecting samples from various levels and positions within each of the large storage bags received from Ghana. Subsequently, the gathered samples underwent a preparation phase to enhance their uniformity and consistency. The collected fuel samples, were subjected to a shredding process with a mesh size of less than 5 mm. This size specification ensured that the resulting particles were suitably uniform for subsequent processing. Following the chopping phase, the samples were introduced into a mixer for a duration of 15 minutes. to homogenize the resulting material, which served as the initial material for the leaching experiments.



Visual image of shredded and homogenized biomass fuels before leaching and combustion processes

Sample preparation for ICP-OES analysis of the fuels and ashes

The investigation of elemental composition within solid samples, specifically biomass fuels and ashes, was conducted through the utilization of optical emission spectroscopy with inductively coupled plasma (ICP-OES). The preparatory steps involved meticulous sample handling and digestion procedures.

For each solid fuel, an aliquot ranging from 100 to 500 mg was subjected to digestion in a composite mixture comprising 8 ml of nitric acid (65%), 2 ml of hydrofluoric acid (48%), and 6 ml of hydrogen peroxide (30%). Subsequently, these solutions underwent controlled microwave heating within pressurized vessels, reaching temperatures of up to 210

°C, maintained for a duration of 45 minutes. Following the cooling phase, boric acid (20 ml) was introduced to neutralize the acidic solutions. The vessels were once again subjected to microwave-assisted heating, this time at 150 °C for 15 minutes. Post-cooling, the solutions were subjected to a dilution process, with ultra-pure water employed at a ratio of 1:10 (1 ml solution to 9 ml ultra-pure water) for subsequent introduction into the auto-sampler (CETAC, ASX-520, Omaha, Nebraska, USA) of the ICP-OES instrument. Due to elevated silicon (Si) concentrations in the diluted samples, an additional dilution step (1:50, 0.2 ml solution, and 9.8 ml ultra-pure water) was performed.

Calibration procedures were undertaken employing a two-point calibration method with a blank solution and a high standard solution, both characterized by an acidic matrix. To ensure precision, each digestion was executed twice, and the resultant average values were reported.

Furthermore, solutions derived from chemical fractionation (CF) underwent filtration prior to ICP-OES analysis. Subsequent to the addition of nitric acid (HNO₃) in a dropwise manner to adjust the pH to below 7, transforming them into acid solutions, these were introduced into the auto-sampler (CETAC, ASX-520, Omaha, Nebraska, USA) of the ICP-OES instrument. Analogous to the solid sample preparations, a two-point calibration strategy was implemented using a blank solution and a high standard solution, both featuring an acidic matrix. The digestion process was duplicated to uphold data accuracy, with the resulting average values being reported for each iteration.

Appendix B: Curriculum Vitae

PROFILE



M. Eng. Clement Owusu Prempeh

Process engineer, Scientific researcher & PhD candidate

DBFZ - German Biomass Research Center gGmbH
|Thermochemical conversion Department |Catalytic Emission Control

D.O.B: 01.12.1989 | Kumasi, Ghana

OBJECTIVE:

Use my technical expertise, in contribution to developing Bioenergy and Environmentally Friendly Chemical Processes

EMAIL:

clement.owusuprempeh@dbfz.de
Tel: (+49) 0-1763-5604-168
Address: Torgauer str. 116, 04347, Leipzig

EDUCATION

PhD in Environmental Engineering Sciences

University of Rostock, Faculty of Agriculture and Environmental Science, Rostock, Germany (2020-to date).

Masters of Chemical Engineering

University of Stellenbosch, Process Engineering Department, Stellenbosch, South Africa (2015 – 2017).

Bachelor of Science Petrochemical Engineering

Kwame Nkrumah University of Science and Technology, Chemical Engineering Department, Kumasi, Ghana, (2009 – 2013).

WORK EXPERIENCE

Jan 2020 to date: **Scientific Researcher**, Thermo-chemical Conversion Department, Deutsches Biomasseforschungszentrum (DBFZ).

2021 to date: **Reviewer**, Waste and Biomass Valorization, Springer.

2021 to date: **Reviewer**, Biomass Conversion and Biorefinery, Springer.

2023 to date, **Reviewer**, Hybrid Wave

Jan 2021-2023 **Supervisor**, 2 Master's students' theses

May 2019 - Nov 2019: **Part-Time Research Fellow**, Department of Conservation and Entomology, Stellenbosch University.

“Education is the great engine of personal development. It is through education that the daughter of a peasant can become a doctor, that the son of a mineworker can become the head of the mine, that a child of farm workers can become the president of a great nation. It is what we make out of what we have, not what we are given, that separates one person from another. -Nelson Mandela, Long Walk to Freedom.

